NISTIR 7080

Verification and Validation of CFAST, A Model of Fire Growth and Smoke Spread

Walter W. Jones
Richard D. Peacock
Glenn P. Forney
Paul A. Reneke

National Institute of Standards and Technology
Technology Administration, U.S. Department of Commerce

NISTIR 7080

Verification and Validation of CFAST, A Model of Fire Growth and Smoke Spread

Walter W. Jones
Richard D. Peacock
Glenn P. Forney
Paul A. Reneke

Building and Fire Research Laboratory

February, 2004

U.S. DEPARTMENT OF COMMERCE
Donald L. Evans, Secretary
TECHNOLOGY ADMINISTRATION
Phillip J. Bond, Under Secretary of Commerce for Technology
NATIONAL INSTITUTE OF STANDARDS AND TECHNOLOGY
Arden L. Bement, Jr., Director

Bibliographic Information

Abstract

CFAST is a zone model capable of predicting the environment in a multi-compartment structure subjected to a fire. It calculates the time evolving distribution of smoke and fire gases and the temperature throughout a building during a user-specified fire. This report describes the equations which constitute the model, the physical basis for these equations, data which are used by the model, and details of the operation of the computer program implementing the model.

This paper is an assessment of the model following the template set forth in ASTM 1355, "Standard Guide for Evaluating the Predictive Capability of Deterministic Fire Models." We include in this paper a set of comparisons between the model and a range of real-scale fire experiments is presented as the validation exercise require by the standard. In addition, we have developed a means to do a quantitative comparison between the time series represented by these predictions and those found in experiments.

Keywords

Model assessment, validation, verification, fire growth, smoke transport, computer models; fire models; fire research; hazard assessment; toxicity

Ordering Information

National Institute of Standards and Technology
Internal Report 7080
Natl. Inst. Stand. Technol.
Internal Report 7080
180 pages (February 2004)

U.S. Government Printing Office
Washington: 2004

For sale by the Superintendent of Documents
U.S. Government Printing Office
Washington, DC 20402

DISCLAIMER

The U. S. Department of Commerce makes no warranty, expressed or implied, to users of - CFAST and associated computer programs, and accepts no responsibility for its use. Users of CFAST assume sole responsibility under Federal law for determining the appropriateness of its use in any particular application; for any conclusions drawn from the results of its use; and for any actions taken or not taken as a result of analyzes performed using these tools.

Users are warned that CFAST is intended for use only by those competent in the field of fire safety and is intended only to supplement the informed judgment of the qualified user. The software package is a computer model which may or may not have predictive value when applied to a specific set of factual circumstances. Lack of accurate predictions by the model could lead to erroneous conclusions with regard to fire safety. All results should be evaluated by an informed user.

INTENT AND USE

The algorithms, procedures, and computer programs described in this report constitute a methodology for predicting some of the consequences resulting from a specified fire. They have been compiled from the best knowledge and understanding currently available, but have important limitations that must be understood and considered by the user. The program is intended for use by persons competent in the field of fire safety and with some familiarity with personal computers. It is intended as an aid in the fire safety decision-making process.

Table of Contents

Figures and Tables

Nomenclature

A Surface area of an object: the subscript denotes the application (m^2)
A_d duct surface area (m^2)
A_o area of the inlet, outlet, duct, contraction, or expansion joint, coil, damper, bend, filter, and so on in a mechanical ventilation system. (m^2)
A_{room} floor area of a room (m^2)
A_s surface area (m^2)
A_{slab} cross-sectional area for horizontal flow (m^2)
A_v area of ceiling or floor vent (m^2)
A_w wall surface area (m^2)
b_i coefficients for adsorption and desorption of HCl
C flow coefficient for horizontal flow of gas through a vertical vent
C_{LOL} Lower oxygen limit (fraction, not percent)
C_o characteristic flow coefficient
C_w wind coefficient – dot product of the wind vector and vent direction
CO/CO_2 mass ratio of carbon monoxide to carbon dioxide in the pyrolysis of the fuel
CO_2/C ratio of the mass of carbon dioxide to carbon in the pyrolysis of the fuel
c specific heat
c_k heat sources for the k'th wall segment (W)
c_p heat capacity of air at constant pressure (J/kg K)
c_v heat capacity of air at constant volume (J/kg K)
D effective diameter of ceiling or floor vent (m)
D_e effective duct diameter (m)
d_{HCl} rate of deposition of HCl onto a wall surface (kg/s)
E_i internal energy in layer i (W)
F friction factor
F_{k-j} configuration factor
g gravitational constant (9.8 $m/s^{2)}$
G conductance
Gr Grashof number (dimensionless)
H_c heat of combustion of the fuel (J/kg)
h_c convective heat transfer coefficient (J/m^2 K)
$\dot{h}_i$ rate of addition of enthalpy into layer i (W)
h_l convective heat transfer coefficient in ceiling boundary layer (J/m^2 K)
h convective heat transfer coefficient (W/m^2 K)
H height of the ceiling above a fire source (m)
H/C ratio of the mass of hydrogen to the mass of carbon in the pyrolysis of the fuel
H_2O/H ratio of the mass of water to the mass of hydrogen in the pyrolysis of the fuel
HCl/C ratio of the mass of hydrogen chloride to the mass of carbon in the pyrolysis of the fuel
HCl/f ratio of the mass of hydrogen chloride to the total mass of the fuel
HCN/C mass ratio of hydrogen cyanide to carbon in the pyrolysis of the fuel
HCN/f mass ratio of hydrogen cyanide to the fuel

k	equivalent thermal conductivity of air (W/m K)
k	with subscripts c,e and s: mass transfer coefficients for HCl deposition defined in text
L, l	characteristic length of the geometry (m) - specific use as a length for convection
m_i	total mass in layer i (kg)
$m_{i,j}$	mass flow from node i to node j in a mechanical ventilation system (kg/s)
$\dot{m}_b$	burning rate of the fuel (perhaps constrained by available oxygen) (kg/s)
$\dot{m}_c$	production rate of carbon during combustion (kg/s)
m_d	mass flow in duct (kg/s)
$\dot{m}_e$	rate of entrainment of air into the fire plume (kg/s)
$\dot{m}_f$	pyrolysis rate of the fuel (before being constrained by available oxygen) (kg/s)
$\dot{m}_i$	rate of addition of mass into layer i (kg/s)
Nu	Nusselt number (dimensionless)
O/C	ratio of the mass of oxygen to the mass of carbon in the pyrolysis of the fuel
P	pressure (Pa)
P_{ref}	reference pressure (Pa)
Pr	Prandtl number (dimensionless)
$\dot{Q}''$	heat release rate per unit area (W/m^2)
$\dot{q}''_f$	flux per unit area from the flame
$\dot{Q}_c$	total convective heat transfer (W)
$\dot{Q}_{eq}$	dimensionless plume strength at layer interface
$\dot{Q}_f$	total heat release rate of the fire (W)
$\dot{Q}_H$	dimensionless plume strength at the ceiling
$\dot{Q}_r$	total radiative heat transfer (W)
Q''_{TOT}	total heat per unit area
r	radial distance from point source fire (m)
R	universal gas constant (J/kg K)
Ra	Rayleigh number (dimensionless)
R_e	Reynolds number (dimensionless)
S	vent shape factor for vertical flow
S/C	ratio of the mass of soot to the mass of carbon in the pyrolysis of the fuel
t	time (s)
T_{amb}	ambient temperature (K)
T_d	duct temperature (K)
T_e	temperature of gas entrainment into the fire plume (K)
T_f	film temperature (K)
T_g	bulk gas temperature (K)
T_{layer}	temperature of adjacent gas layer - used in convection and radiation calculations

T_s surface temperature (K)
$T_{s,min}$ minimum temperature at which lateral flame spread occurs.
T_i temperature of layer i (K)
T_{ig} surface ignition temperature (K)
T_{in} duct inlet temperature (K)
T_k temperature of the k'th wall segment (K)
T_{out} duct outlet temperature (K)
T_p temperature of the plume as it intersects the upper layer (K)
T_s surface temperature
T_w wall temperature (K)
v gas velocity (m/s)
V volume; subscript indicates usage (m^3)
V_d duct volume (m^3)
V_i volume of layer i (m^3)
x_b burnout front position in the opposed flow direction.
x_p pyrolysis front position in the opposed flow direction.
Y mass fraction of a species in a layer
Y_{LOL} lower oxygen limit for oxygen constrained burning, expressed as a mass fraction
y_b burnout front position in the wind aided direction.
y_f flame tip position.
y_p pyrolysis front position in the wind aided direction.
z height over which entrainment takes place (m)
Z general height (m)

α thermal diffusivity in conduction (m^2/s), absorption coefficient for gas radiation (m^{-1})
β expansion coefficient, $1/T_f$ (K^{-1})
ΔP pressure offset from reference pressure, $P - P_{ref}$ (Pa)
ΔL effective heat of gasification
γ ratio of c_p/c_v
ϵ_k emissivity of the k'th wall segment
κ thermal conductivity (J/m s K)
ν kinematic viscosity (m^2/s)
Φ Lateral flame spread parameter
ρ_d density of gas in a duct (kg/m^3)
ρ_i density of gas in layer i (kg/m^3)
σ Stefan-Boltzman constant (5.67×10^{-8} W/m^2K^4)
τ transmissivity (factor)
χ_c fraction of the heat release rate of the fire which goes into convection
χ_r fraction of the heat release rate of the fire which goes into radiation

Verification and Validation of CFAST, A Model of Fire Growth and Smoke Spread

Walter W. Jones, Richard D. Peacock, Glenn P. Forney, and Paul A. Reneke
National Institute of Standards and Technology

1 Introduction

The process of model evaluation is critical to establishing both the acceptable uses and limitations of fire models. It is not possible to evaluate a model in total; instead, available guides such as ASTM E 1355 are intended to provide a methodology for evaluating the predictive capabilities for a specific use [1]. Validation for one application or scenario does not imply validation for different scenarios. Several alternatives are provided for performing the evaluation process including: comparison of predictions against standard fire tests, full-scale fire experiments, field experience, published literature, or previously evaluated models.

The use of fire models currently extends beyond the fire research laboratory and into the engineering, fire service and legal communities. Sufficient evaluation of fire models is necessary to ensure that those using the models can judge the adequacy of the scientific and technical basis for the models, select models appropriate for a desired use, and understand the level of confidence which can be placed on the results predicted by the models. Adequate evaluation will help prevent the unintentional misuse of fire models.

The definitions as commonly used are

> - Validation is the process of determining the degree to which a calculation method is an accurate representation of the real world from the perspective of the intended uses of the calculation method. The fundamental strategy of validation is the identification and quantification of error and uncertainty in the implementation of the computational models.
>
> - Verification is the process of determining that a calculation method implementation accurately represents the developer's conceptual description of the calculation method and the solution to the calculation method. The fundamental strategy of verification of computational models is the identification and quantification of error in the computational model and its solution.

We use these terms together to perform a model assessment. The more general term, “model assessment,” encompasses both verification and validation of a computer model.

In order to use a model properly, it is important to know the circumstances under which it is expected to provide acceptably good predictions. At a minimum, this would include a statement of the stated uses, limitations, and results of the model, the type of model, that is the general

basis in terms of finite element, control volume, Lagrangian, etc., the assumptions inherent in the model and the governing equations included in the model formulation, the numerical techniques employed to solve the equations, and the method by which individual solutions are coupled. This latter point concerns the issues in disparate time and space scales, graininess of the various sub-models and similar implementation issues.

In assessing a model one must be cognizant of the wide range of possible errors which are inherent or can be inadvertently introduced. An evaluation should address these problems, including the multiple sources of potential error in the design and use of predictive tools.

Such an assessment ought to include insuring correct model inputs appropriate to the scenarios to be modeled, correct selection of a model appropriate to the scenarios to be modeled, correct calculations by the model chosen, and correct interpretation of the results of the model calculation.

In general, this document follows the ASTM 1355 guide for model assessment. provides a model assessment for the zone fire model CFAST. The guide provides four areas of evaluation for predictive fire models:

- Defining the model and scenarios for which the evaluation is to be conducted,
- Assessing the appropriateness of the theoretical basis and assumptions used in the model,
- Assessing the mathematical and numerical robustness of the model, and
- Quantifying the uncertainty and accuracy of the model results in predicting the course of events in similar fire scenarios.

2 Model and Scenario Definition

Analytical models for predicting fire behavior have been evolving since the 1960's. Over the past decade, the completeness of the models has grown considerably. In the beginning, the focus of these efforts was to describe in mathematical language the various phenomena which were observed in fire growth and spread. These separate representations have typically described only a small part of a fire. When combined though, they can create a complex computational model intended to give an estimate of the expected course of a fire based upon given input parameters. These analytical models have progressed to the point of providing predictions of fire behavior with an accuracy suitable for most engineering applications. In a recent international survey [2], 36 actively supported models were identified. Of these, 20 predict the fire driven environment (mainly temperature) and 19 predict smoke movement in some way. Six calculate fire growth rate, nine predict fire endurance, four address detector or sprinkler response, and two calculate evacuation times. The computer models now available vary considerably in scope, complexity, and purpose. Simple "compartment filling" models such as the Available Safe Egress Time (ASET) model [3] run quickly on almost any computer, and provide good estimates of a few parameters of interest for a fire in a single compartment. A special purpose model can provide a single function. For example, COMPF2 [4] calculates post-flashover compartment temperatures and LAVENT [5] includes the interaction of ceiling jets with fusible links in a compartment containing ceiling vents and draft curtains.

In addition to the single-compartment models mentioned above, there are a smaller number of multi-compartment models which have been developed. These include the BRI [6] transport model, FAST [7], CCFM [8] and the CFAST model discussed below [9].

Although the papers are several years old, Mitler [10] and Jones [11] reviewed the underlying physics in several of the fire models in detail. The models fall into two categories: those that start with the principles of conservation of mass, momentum, and energy such as CFAST; and those that typically are curve fits to particular experiments or series of experiments, used in order to discern the underlying relationship among some parameters. In both cases, errors arise in those instances where a mathematical short cut was taken, a simplifying assumption was made, or something important was not well enough characterized to be included.

Once a mathematical representation of the underlying science has been developed, the conservation equations can be re-cast into predictive equations for temperature, smoke and gas concentration and other parameters of interest, and coded into a computer for solution.

The environment in a fire is constantly changing. Thus the equations are usually in the form of *differential equations*. A complete set of equations can compute the conditions produced by the fire at a given time in a specified volume of air. Referred to as a *control volume*, the model assumes that the predicted conditions within this volume are uniform at any time. Thus, the control volume has one temperature, smoke density, gas concentration, *etc*.

Different models divide the building into different numbers of control volumes depending on the desired level of detail. The most common fire model, known as a *zone model*, generally uses two control volumes to describe a compartment – an upper layer and a lower layer. In the compartment with the fire, additional control volumes for the fire plume or the ceiling jet may be included to improve the accuracy of the prediction (see Figure 1). Additional zones can be added as necessity arises to cover extensions.

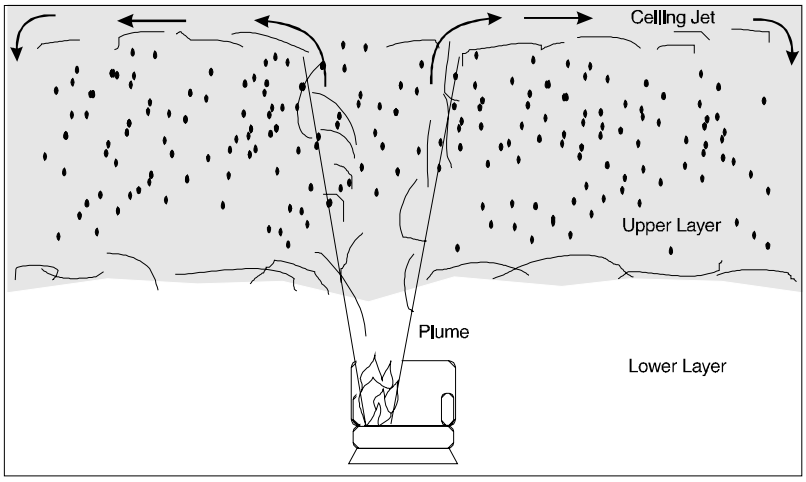

Figure 1. Zone model terms.

This two-layer approach has evolved from observation of such layering in real-scale fire experiments. Hot gases collect at the ceiling and fill the compartment from the top. While these experiments show some variation in conditions within the layer, these are small compared to the differences between the layers. Thus, the zone model can produce a fairly realistic simulation under most conditions.

Other types of models include *network models* and *field models*. Network models use one control volume per compartment and are used to predict conditions in spaces far removed from the fire compartment where temperatures are near ambient and layering does not occur. The field model goes to the other extreme, dividing the compartment into thousands or even a million or more control volumes. Such models can predict the variation in conditions within the layers, but typically require far longer run times than zone models. Thus, they are used when highly detailed calculations are essential.

2.1 Overview of the CFAST fire model

CFAST is a zone model used to calculate the evolving distribution of smoke, fire gases and temperature throughout a constructed facility during a fire. In CFAST, each compartment is divided into two layers.

The modeling equations used in CFAST take the mathematical form of an initial value problem for a system of ordinary differential equations (ODE). These equations are derived using the conservation of mass, the conservation of energy (equivalently the first law of thermodynamics), the ideal gas law and relations for density and internal energy. These equations predict as functions of time quantities such as pressure, layer heights and temperatures given the accumulation of mass and enthalpy in the two layers. The CFAST model then consists of a set of ODEs to compute the environment in each compartment and a collection of algorithms to compute the mass and enthalpy source terms required by the ODEs.

2.2 Implementation of the Conceptual Model

This section discusses each of the sub-models in CFAST. In general, the sections are similar to the way the model itself is structured. The sub-sections which follow discuss the way the actual phenomena are implemented numerically.

2.2.1 Fires

A fire in CFAST is implemented as a source of fuel which is released at a specified rate. This fuel is converted into enthalpy (the conversion factor is the heat of combustion) and mass (the conversion factor is the yield of a particular species) as it burns. A fire in CFAST is constrained if the enthalpy conversion depends on the oxygen concentration otherwise it is unconstrained. Burning can take place in the portion of the plume in the lower layer (if any), in the upper layer, or in a door jet. For an unconstrained fire, it is assumed that the burning will occur within the fire plume. For a constrained fire, burning will take place where there is sufficient oxygen. When insufficient oxygen is entrained into the fire plume, unburned fuel will successively move into and burn in: the upper layer of the fire compartment, the plume in the doorway to the next compartment, the upper layer of the next compartment, the plume in the doorway to the third compartment, and so forth until it is consumed or gets to the outside.

The model includes the ability to track, independently, multiple fires in one or more compartments of the building. These fires are treated as totally separate entities, i.e., with no interaction of the plumes or radiative exchange between fires in a compartment. These fires are generally referred to as “objects” and can be ignited at a specified time, temperature or heat flux.

It does not include a pyrolysis model to predict fire growth. Rather pyrolysis rates for each fire modeled define the fire history. The similarity of that input to the real fire problem of interest will determine the accuracy of the resulting calculation.

2.2.2 Plumes and Layers

A plume is formed above any burning object. It acts as a pump transferring mass and enthalpy from the lower layer into the upper layer. A correlation is used to predict the amount of mass and enthalpy that is transferred. A more complete plume model would predict plume entrainment by creating a separate zone and solving the appropriate equations.

Two sources exist for moving enthalpy and mass between the layers within and between compartments. Within the compartment, the fire plume provides one source. The other source of mixing between the layers occurs at vents such as doors or windows. Here, there is mixing at the boundary of the opposing flows moving into and out of the compartment. The degree of mixing is based on an empirically-derived mixing relation. Both the outflow and inflow entrain air from the surrounding layers. The flow at vents is also modeled as a plume (called the door plume or jet), and uses the same equations as the fire plume, with two differences. First, an offset is calculated to account for entrainment within the doorway and second, the equations are modified to account for the rectangular geometry of vents compared to the round geometry of fire plumes. All plumes within the simulation entrain air from their surroundings according to an empirically-derived entrainment relation. Entrainment of relatively cool, non-smoke laden air adds oxygen to the plume and allows burning of the fuel. It also causes it to expand as the plume moves upward in the shape of an inverted cone. The entrainment in a vent is caused by bi-directional flow and results from vortices formed near a shear layer. This phenomenon called the Kelvin-Helmholtz instability. It is not exactly the same as a normal plume, so some error arises when this entrainment is approximated by a normal plume entrainment algorithm.

While experiments show that there is very little mixing between the layers at their interface, sources of convection such as radiators or diffusers of heating and air conditioning systems, and the downward flows of gases caused by cooling at walls, will cause such mixing. These are examples of phenomena which are not included because the theories are still under development. Also, the plumes are *assumed* not to be affected by other flows which may occur. For example, if the burning object is near the door the strong inflow of air will cause the plume axis to lean away from the door and affect entrainment of gases into the plume. Such effects are not included in the model.

As discussed above, each compartment is divided into an upper and lower layer. At the start of the simulation, the layers in each compartment are initialized at ambient conditions and by default, the upper layer volume set to 0.001 of the compartment volume (an arbitrary, small value set to avoid the potential mathematical problems associated with dividing by zero). Other values can be set. As enthalpy and mass are pumped into the upper layer by the fire plume, the upper layer expands in volume causing the lower layer to decrease in volume and the interface to move downward. If the door to the next compartment has a soffit, there can be no flow through the vent from the upper layer until the interface reaches the bottom of that soffit. Thus in the early stages the expanding upper layer will push down on the lower layer air and force it into the next compartment through the vent by expansion.

Once the interface reaches the soffit level, a door plume forms and flow from the fire compartment to the next compartment is initiated. As smoke flow from the fire compartment fills the second compartment, the lower layer of air in the second compartment is pushed down. As a result, some of this air flows into the fire compartment through the lower part of the connecting doorway (or vent). Thus, a vent between the fire compartment and connecting compartments can have simultaneous, opposing flows of air. All flows are driven by pressure and density differences that result from temperature differences and layer depths. The key to getting the correct flow is to distribute correctly the fire and plume's mass and enthalpy between the layers.

2.2.3 Vent Flow

Flow through vents is a dominant component of any fire model because it is sensitive to small changes in pressure and transfers the greatest amount of enthalpy on an instantaneous basis of all the source terms (except of course for the fire and plume). Its sensitivity to environmental changes arises through its dependence on the pressure difference between compartments which can change rapidly.

CFAST models two types of vent flow, horizontal flow through vertical vents (ceiling holes, hatches *etc.*) and vertical flow through horizontal vents (doors, windows *etc.*). Horizontal flow is the flow which is normally thought of when discussing fires. Vertical flow is particularly important in two disparate situations: a ship, and the role of fire fighters doing roof venting.

Horizontal vent flow is determined using the pressure difference across a vent. Flow at a given elevation may be computed using Bernoulli's law by first computing the pressure difference at that elevation. The pressure on each side of the vent is computed using the pressure at the floor, the height of the floor and the density.

Atmospheric pressure is about 100 000 Pa, fires produce pressure changes from 1 Pa to 1000 Pa and mechanical ventilation systems typically involve pressure differentials of about 1 Pa to 100 Pa. The pressure variables are solved to a higher accuracy than other solution variables because of the subtraction (with resulting loss of precision) needed to calculate vent flows from pressure differences.

2.2.4 Heat Transfer

Gas layers exchange energy with their surroundings via convective and radiative heat transfer. Different material properties can be used for the ceiling, floor, and walls of each compartment (although all the walls of a compartment must be the same). Additionally, CFAST allows each surface to be composed of up to three distinct materials. This allows the user to deal naturally with the actual building construction. Material thermophysical properties are *assumed* to be constant, although we know that they actually vary with temperature. This assumption is made because data over the required temperature range is scarce even for common materials. However the user should recognize that the mechanical properties of some materials may change with temperature. These effects are not modeled.

Radiative transfer occurs among the fire(s), gas layers and compartment surfaces (ceiling, walls and floor). This transfer is a function of the temperature differences and the emissivity of the gas layers as well as the compartment surfaces. For the fire and typical surfaces, emissivity values only vary over a small range. For the gas layers, however, the emissivity is a function of the concentration of species which are strong radiators: predominately smoke particulates, carbon dioxide, and water. Thus errors in the species concentrations can give rise to errors in the distribution of enthalpy among the layers, which results in errors in temperatures, resulting in errors in the flows. This illustrates just how tightly coupled the predictions made by CFAST can be.

2.2.5 Species Concentration and Deposition

When the layers are initialized at the start of the simulation, they are set to ambient conditions. These are the initial temperatures specified by the user, and 23 % by mass (20.8 % by volume) oxygen, 77 % by mass (79 % by volume) nitrogen, a mass concentration of water specified by the user as a relative humidity, and a zero concentration of all other species. As fuel is pyrolyzed, the various species are produced in direct relation to the mass of fuel burned (this relation is the species yield specified by the user for the fuel burning). Since oxygen is consumed rather than produced by the burning, the "yield" of oxygen is negative, and is set internally to correspond to the amount of oxygen needed to burn the fuel. Also, hydrogen cyanide and hydrogen chloride are assumed to be products of pyrolysis whereas carbon dioxide, carbon monoxide, water, and soot are products of combustion.

Each unit mass of a species produced is carried in the flow to the various compartments and accumulates in the layers. The model keeps track of the mass of each species in each layer, and knows the volume of each layer as a function of time. The mass divided by the volume is the mass concentration, which along with the molecular weight gives the concentration in volume % or parts per million as appropriate.

CFAST uses a combustion chemistry scheme based on a carbon-hydrogen-oxygen balance. The scheme is applied in three places. The first is burning in the portion of the plume which is in the lower layer of the compartment of fire origin. The second is the portion in the upper layer, also in the compartment of origin. The third is in the vent flow which entrains air from a lower layer into an upper layer in an adjacent compartment. This is equivalent to solving the conservation equations for each species independently.

3 Predictive Equations Used by the CFAST Model

Appropriately detailed documentation of the model allows the model user to understand the underlying theory behind the model implementation and thus be able to assess the application of the model to specific problems. This section presents a derivation of the predictive equations for zone fire models and explains in detail the ones used in CFAST [7], [9]. The zone fire model used in CFAST takes the form of an initial value problem for a mixed system of differential and algebraic equations. These equations are derived from the conservation of mass and energy. Subsidiary equations are the ideal gas law and definitions of density and internal energy (for example, see [12]). These conservation laws are invoked for each zone or control volume. For further information on the numerical implications of these choices please see reference [13].

The basic element of the model is a zone. The basic assumption of a zone model is that properties such as temperature can be approximated throughout the zone by some uniform function. The usual approximation is that temperature, density and so on are uniform within a zone. The assumption of uniform properties is reasonable and yields good agreement with experiment. In general, these zones are grouped within compartments.

There are two reasonable conjectures which dramatically improve the ease of solving these equations. Momentum is ignored within a compartment. The momentum of the interface has no significance in the present context. However, at boundaries such as windows, doors and so on, the Euler equation is integrated explicitly to yield the Bernoulli equation. This is solved implicitly in the equations which are discussed below. The other approximation is that the pressure is approximately uniform within a compartment. The argument is that a change in pressure of a few tens of Pascals over the height of the compartment is negligible in comparison with atmospheric pressure. Once again, this is applied to the basic conservation equations. This is consistent with the point source view of finite element models. Volume is merely one of the dependent variables. However, the hydrostatic variation in pressure *is* taken into account in calculating pressure differences between compartments.

Many formulations based upon these assumptions can be derived. Several of these are discussed later. One formulation can be converted into another using the definitions of density, internal energy and the ideal gas law. Though equivalent analytically, these formulations differ in their numerical properties. Also, until the development of FAST [7], all models of this type assumed that the pressure equilibrated instantaneously, and thus the dP/dt term could be set to zero. However, as has been shown [14], it is better to solve these equations in the differential rather than the algebraic form if the proper solver is used.

As discussed in references [13] and [15], the zone fire modeling differential equations (ODE's) are stiff. The term stiff means that multiple time scales are present in the ODE solution. In our problem, pressures adjust to changing conditions much quicker than other quantities such as layer temperatures or interface heights. Special solvers are required in general to solve zone fire modeling ODE's because of this stiffness. Runge-Kutta methods or predictor-corrector methods

such as Adams-Bashforth require prohibitively small time steps in order to track the short-time scale phenomena (pressure in our case). Methods that calculate the Jacobian (or at least approximate it) have a much larger stability region for stiff problems and are thus more successful at their solution.

Each formulation can be expressed in terms of mass and enthalpy flow. These rates represent the exchange of mass and enthalpy between zones due to physical phenomena such as plumes, natural and forced ventilation, convective and radiative heat transfer, and so on. For example, a vent exchanges mass and enthalpy between zones in connected rooms, a fire plume typically adds heat to the upper layer and transfers entrained mass and enthalpy from the lower to the upper layer, and convection transfers enthalpy from the gas layers to the surrounding walls.

We use the formalism that the mass flow to the upper and lower layers is denoted $\dot{m}_U$ and $\dot{m}_L$ and the enthalpy flow to the upper and lower layers is denoted $\dot{s}_U$ and $\dot{s}_L$. It is tacitly assumed that these rates may be computed in terms of zone properties such as temperature and density. These rates represent the net sum of all possible sources of mass and enthalpy due to phenomena such as those listed above. The numerical characteristics of the various formulations are easier to identify if the underlying physical phenomena are decoupled in this way.

Many approximations are necessary when developing physical sub-models for the mass and enthalpy terms. For example, most fire models assume that 1) the specific heat terms c_p and c_v are constant even though they depend upon temperature, 2) hydrostatic terms can be ignored in the equation of state (the ideal gas law) relating density of a layer with its temperature. However, the derivations which follow are all based on the basic conservation laws.

3.1 Derivation of Equations for a Two-Layer Model

A compartment is divided into two control volumes, a relatively hot upper layer and a relatively cooler lower layer, as illustrated in Figure 2. The gas in each layer has attributes of mass, internal energy, density, temperature, and volume denoted respectively by m_i, E_i, ρ_i, T_i, and V_i where $i=L$ for the lower layer and $i=U$ for the upper layer. The compartment as a whole has the attribute of pressure P. These 11 variables are related by means of the following seven constraints

$$\rho_i = \frac{m_i}{V_i} \qquad \text{(density)} \tag{1}$$

$$E_i = c_v m_i T_i \qquad \text{(internal energy)} \tag{2}$$

$$P = R\rho_i T_i \qquad \text{(ideal gas law)} \tag{3}$$

$$V = V_L + V_U \qquad \text{(total volume)} \tag{4}$$

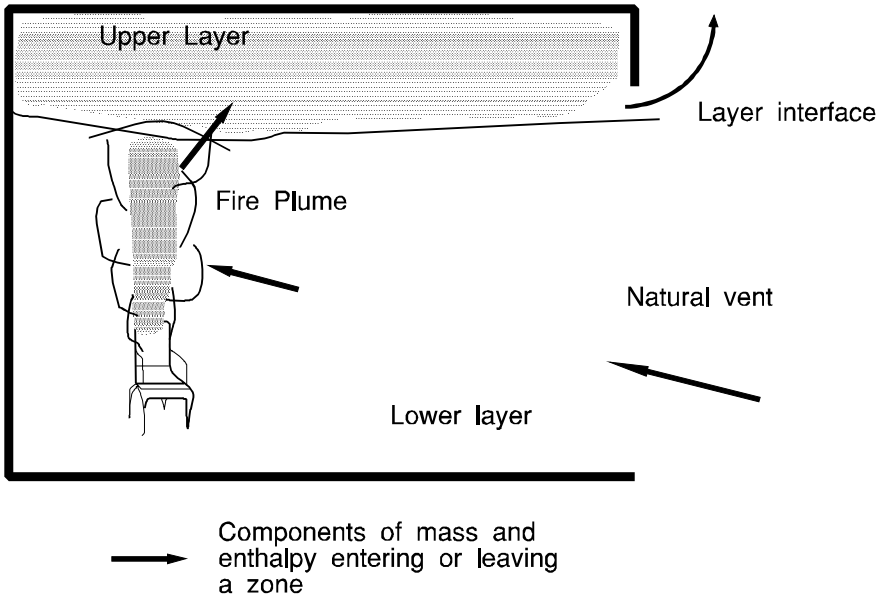

Figure 2. Schematic of control volumes in a two-layer zone model.

We get seven by counting density, internal energy and the ideal gas law twice (once for each layer). The specific heat at constant volume and at constant pressure c_v and c_p, the universal gas constant, R, and the ratio of specific heats, γ, are related by $\gamma = c_p / c_v$ and $R = c_p - c_v$. For air, $c_p \approx 1000$ kJ/kg/K and $\gamma = 1.4$. Four additional equations obtained from conservation of mass and energy for each layer are required to complete the equation set. The differential equations for mass in each layer are

$$\begin{aligned} \frac{dm_L}{dt} &= \dot{m}_L \\ \frac{dm_U}{dt} &= \dot{m}_U \end{aligned} \tag{5}$$

The first law of thermodynamics states that the rate of increase of internal energy plus the rate at which the layer does work by expansion is equal to the rate at which enthalpy is added to the gas. In differential form this is

$$\underbrace{\text{internal energy}}_{\frac{dE_i}{dt}} + \underbrace{\text{work}}_{P\frac{dV_i}{dt}} = \underbrace{\text{enthalpy}}_{\dot{s}_i} \tag{6}$$

where c_v is taken as constant, $c_p/c_v=\gamma$ and $c_p-c_v=R$. A differential equation for pressure can be derived by adding the upper and lower layer versions of eq (6), noting that $dV_U/dt = -dV_L/dt$, and substituting the differential form of eq (2) to yield

$$\frac{dP}{dt} = \frac{\gamma - 1}{V}\left(\dot{s}_L + \dot{s}_U\right). \tag{7}$$

Differential equations for the layer volumes can be obtained by substituting the differential form of eq (2) into eq (6) to obtain

$$\frac{dV_i}{dt} = \frac{1}{P\gamma}\left((\gamma - 1)\,\dot{s}_i - V_i\,\frac{dP}{dt}\right). \tag{8}$$

Equation (6) can be rewritten using eq (8) to eliminate dV/dt to obtain

$$\frac{dE_i}{dt} = \frac{1}{\gamma}\left(\dot{s}_i + V_i\frac{dP}{dt}\right) . \tag{9}$$

A differential equation for density can be derived by applying the quotient rule to $\frac{d\rho_i}{dt} = \frac{d}{dt}\left(\frac{m_i}{V_i}\right)$ and using eq (8) to eliminate dV_i/dt to obtain

$$\frac{d\rho_i}{dt} = -\frac{1}{c_p T_i V_i}\left(\left(\dot{s}_i - c_p\dot{m}_i T_i\right) - \frac{V_i}{\gamma - 1}\frac{dP}{dt}\right). \tag{10}$$

Temperature differential equations can be obtained from the equation of state by applying the quotient rule to $\frac{dT_i}{dt} = \frac{d}{dt}\left(\frac{P}{R\rho_i}\right)$ and using eq (10) to eliminate $d\rho/dt$ to obtain

$$\frac{dT_i}{dt} = \frac{1}{c_p\rho_i V_i}\left(\left(\dot{s}_i - c_p\dot{m}_i T_i\right) + V_i\frac{dP}{dt}\right). \tag{11}$$

These equations for each of the eleven variables are summarized in table 1. The time evolution of these solution variables can be computed by solving the corresponding differential equations together with appropriate initial conditions. The remaining seven variables can be determined from the four solution variables using eqs (1) to (4).

There are, however, many possible differential equation formulations. Indeed, there are 330 different ways to select four variables from eleven. Many of these systems are incomplete due to the relationships that exist between the variables given in eqs (1) to (4). For example the variables, ρ_U, V_U, m_U, and P form a dependent set since $\rho_U = m_U / V_U$. Table 2 shows the solution variable selection made by several zone fire models[2],[7],[9],[10],[11].

The number of differential equation formulations can be considerably reduced by not mixing variable types between layers; that is, if upper layer mass is chosen as a solution variable, then lower layer mass must also be chosen. For example, for two of the solution variables choose m_L and m_U, or ρ_L and ρ_U, or T_L and T_U. For the other two solution variables pick E_L and E_U or P and V_L or P and V_U. This reduces the number of distinct formulations to nine. Since the numerical properties of the upper layer volume equation are the same as a lower layer one, the number of distinct formulations can be reduced to six.

Table 1. Conservative zone model equations

Equation Type	Differential Equation
i'th layer mass	$\frac{dm_i}{dt} = \dot{m}_i$
pressure	$\frac{dP}{dt} = \frac{\gamma - 1}{V}\left(\dot{s}_L + \dot{s}_U\right)$
i'th layer energy	$\frac{dE_i}{dt} = \frac{1}{\gamma}\left(\dot{s}_i + V_i\frac{dP}{dt}\right)$
i'th layer volume	$\frac{dV_i}{dt} = \frac{1}{\gamma P}\left((\gamma - 1)\dot{s}_i - V_i\frac{dP}{dt}\right)$
i'th layer density	$\frac{d\rho_i}{dt} = -\frac{1}{c_p T_i V_i}\left(\left(\dot{s}_i - c_p\dot{m}_i T_i\right) - \frac{V_i}{\gamma - 1}\frac{dP}{dt}\right)$
i'th layer temperature	$\frac{dT_i}{dt} = \frac{1}{c_p \rho_i V_i}\left(\left(\dot{s}_i - c_p\dot{m}_i T_i\right) + V_i\frac{dP}{dt}\right)$

Table 2. Conservative zone model equation selections

Zone Fire Model	Equations	Substitutions
FAST	$\frac{d\Delta P}{dt}$, $\frac{dV_L}{dt}$, $\frac{dT_U}{dt}$, $\frac{dT_L}{dt}$	$\Delta P = P - P_{ref}$
CCFM.HOLE	$\frac{d\Delta P}{dt}$, $\frac{dy}{dt}$, $\frac{d\rho_U}{dt}$, $\frac{d\rho_L}{dt}$	$\Delta P = P - P_{ref}$ $y = V_L / A_{room}$
CCFM.VENTS	$\frac{d\Delta P}{dt}$, $\frac{dy}{dt}$, $\frac{dm_U}{dt}$, $\frac{dm_L}{dt}$	$\Delta P = P - P_{ref}$ $y = V_L / A_{room}$
FIRST, HARVARD	$\frac{dE_U}{dt}$, $\frac{dE_L}{dt}$, $\frac{dm_U}{dt}$, $\frac{dm_L}{dt}$	

3.2 Equation Set Used in CFAST

The current version of CFAST is set up to use the equation set for layer temperature, layer volume, and pressure as shown below. However, the internal structure of the model is such that it will allow any of the formulations above to be substituted with relative ease.

$$P = P_{ref} + \Delta P \tag{12}$$

$$\frac{dP}{dt} = \frac{\gamma - 1}{V}\left(\dot{s}_L + \dot{s}_U\right) \tag{13}$$

$$\frac{dV_U}{dt} = \frac{1}{\gamma P}\left((\gamma - 1)\dot{s}_U - V_U\frac{dP}{dt}\right) \tag{14}$$

$$\frac{dT_U}{dt} = \frac{1}{c_p \rho_U V_U}\left(\left(\dot{s}_U - c_p \dot{m}_U T_U\right) + V_U \frac{dP}{dt}\right) \tag{15}$$

$$\frac{dT_L}{dt} = \frac{1}{c_p \rho_L V_L}\left(\left(\dot{s}_L - c_p \dot{m}_L T_L\right) + V_L \frac{dP}{dt}\right) \tag{16}$$

3.3 Source Terms for the CFAST Model

The conserved quantities in each compartment are described by the set of predictive equations above. The form of the equations is such that the physical phenomena are source terms[1] on the right-hand-side of these equations. Such a formulation makes the addition and deletion of physical phenomena and changing the form of algorithms a *relatively* simple matter. For each of the phenomena discussed below, the physical basis for the model is discussed first, followed by a brief presentation of the implementation within CFAST. For all of the phenomena, there are basically two parts to the implementation: the physical interface routine (which is the interface between the CFAST model and the algorithm) and the actual physical routine(s) which implement the physics. This implementation allows the physics to remain independent of the structure of CFAST and allows easier insertion of new phenomena.

3.3.1 The Fire

3.3.1.1 Specified Fire (Fire Types 1 and 2)

A specified fire is one for which the time dependent characteristics are specified as a function of time. The specified fire can be unconstrained (type 1) or constrained (type 2). The heat release rate for a constrained fire may be reduced below its specified value based upon the concentration of fuel or oxygen available for combustion. Combustion chemistry is not calculated for type 1 fires. The pyrolysis rate for both fire types is specified as $\dot{m}_f$, the burning rate as $\dot{m}_b$ and the heat of combustion as H_c so that the heat release rate, Q_f, is

$$\dot{Q}_f = H_c \dot{m}_b - c_p \left(T_u - T_v\right) \dot{m}_b . \tag{17}$$

For the unconstrained fire, $\dot{m}_b = \dot{m}_f$, whereas for the constrained fire, $\dot{m}_b < \dot{m}_f$, or equivalently the burning rate may be less than the pyrolysis rate. Models of specified fires generally use an effective heat of combustion which is obtained from an experimental apparatus such as the cone calorimeter [16]. A shortcoming of this approach is that it does not account for increased pyrolysis due to radiative feedback from the flame or compartment. In an actual fire, this is an important consideration, and the specification used should match the experimental conditions as closely as possible.

The enthalpy which is released goes into radiation and convection

$$\begin{aligned} \dot{Q}_r(\mathit{fire}) &= \chi_R \dot{Q}_f \\ \dot{Q}_c(\mathit{fire}) &= \left(1 - \chi_R\right) \dot{Q}_f . \end{aligned} \tag{18}$$

where, χ_R , is the fraction of the fire's heat release rate given off as radiation. The convective heat release rate, $\dot{Q}_c(\mathit{fire})$ then becomes the driving term in the plume flow. For a specified fire

---

*The $\dot{m}$ and $\dot{s}$ in eqs (13) to (16)

there is radiation to both the upper and lower layers, whereas the convective part contributes only to the upper layer.

3.3.1.2 Combustion Chemistry (Fire Type 2)

Two types of fires can be selected. The first generates heat as described above. The second type of fire is constrained by the amount of available oxygen. The latter scheme is applied in three places. The first is burning in the portion of the plume which is in the lower layer of the room of fire origin (region #1). The second is the portion of the plume in the upper layer, also in the room of origin (region #2). The third is in the vent flow which entrains air from a lower layer into an upper layer in an adjacent compartment (region #3).These are shown schematically in Figure 3.

The species which are affected by this scheme are O_2, CO_2, CO, H_2O, unburned hydrocarbons (TUHC), and soot (OD). Nitrogen is carried as a gas, but only acts as a diluent. There are at present no nitrogen reactions. In a chemical equation, the individual atoms on the left and right hand sides must balance. This is true regardless of whether the reaction is considered to be stoichiometric (complete). We apply this idea to the combination of fuel and oxygen to yield a balance of number density (#/volume). In terms of the "regions," (Figure 3), we have

$\dot{m}_f$ = pyrolysis rate of the source (kg/sec) (region #1)

or

$\dot{m}_f = \dot{m}_{tuhc}$ from a previous region (kg/sec) (region #2 and #3).

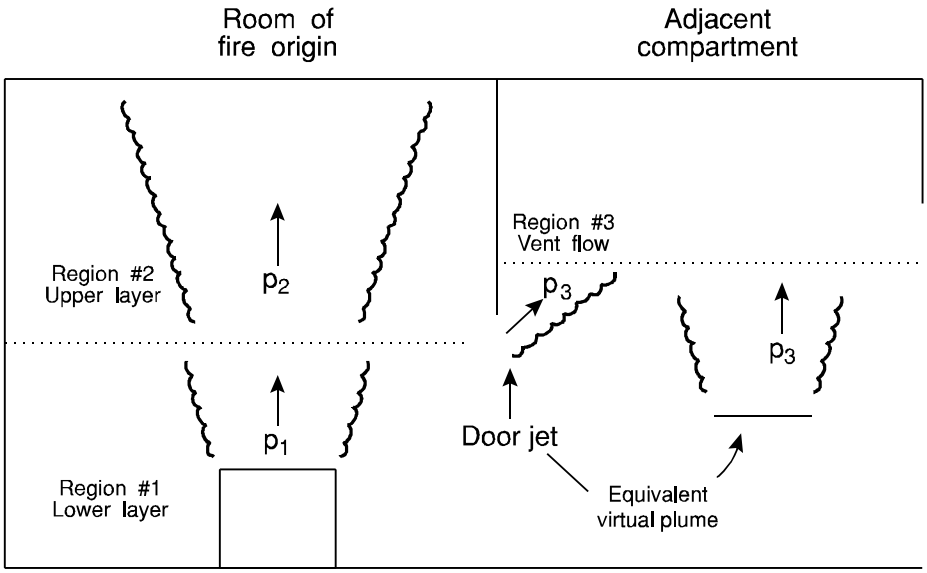

Figure 3. Schematic of entrainment and burning regions.

and

$$\dot{m}_{tuhc} = \dot{m}_f - \dot{m}_b$$

where *tuhc* stands for total un-burned hydrocarbons.

The simplest form of energy release is made by specifying a heat release rate, together with a consistent mass release rate. This would simulate the fire that occurs in an unconfined space. As soon as one is constrained by the confines of a compartment, then the nature of the fire changes. In particular the available oxygen may not be sufficient to allow complete combustion. However, it is not consistent to try to account for the oxygen alone. All pertinent species must be followed.

The essence of the species production scheme which we now utilize is to allow as realistic fuel composition as possible, i.e., include oxygen, carbon, hydrogen and chlorine as part of the fuel. Carbon monoxide, carbon dioxide, soot, water, hydrogen cyanide and hydrogen chloride are the products of combustion. The fuel properties are specified as H/C, HCl/C, HCN/C and O/C which are mass ratios of hydrogen, hydrochloric acid, hydrogen cyanide and oxygen to carbon respectively. The production properties are HCl/f, HCN/f, CO/CO_2, and S/CO_2 which again are mass ratios. The chemical symbols used here have their usual meaning, except for soot. The subscript "S" is used to designate soot, and we assume it consists primarily of carbon, at least by mass.

The fuel burning rate in terms of the carbon production is

$$\dot{m}_f = \{-\} \times \dot{m}_c \tag{19}$$

where {—} is the multiplier in the fuel production defined as

$$\{-\} = \left(1 + \frac{H}{C} + \frac{HCl}{C} + \frac{HCN}{C} + \frac{O}{C}\right) \equiv f/C. \tag{20}$$

In order to avoid detailed chemical kinetics, we use the oxygen consumption concept [17], [18] to relate the mass loss to the heat release rate. The following derivation is for the heat release rate as a function of the fuel burning rate, and the heat release rate based on oxygen consumption. H/C, HCl/C, HCN/C and O/C are the ratio of mass of that species to carbon in the fuel. Thus H/C is for the mass of hydrogen to the mass of carbon produced in pyrolysis. This is a very useful way to characterize the fuel. This is in terms of the elemental composition of the fuel, and not elemental molecules, such as H_2. These are the ratios for the fuel, and the material which comes from it. For the products of the combustion process, we have CO_2/C, CO/C, H_2O/C and S/C. These ratios are in terms of molecules, generally gaseous.

The first step is to limit the actual burning which takes place in the combustion zone. In each combustion zone, there is a quantity of fuel available. At the source this results from the pyrolysis of the material, m_f. In other situations such as a plume or door jet, it is the net unburned fuel available, m_{TUHC}. In each case, the fuel which is available but not burned is then deposited into the "m_{TUHC}" category. This provides a consistent notation. In the discussion below, m_f is the amount of fuel burned. This value is initialized to the available fuel, and then reduced if there is insufficient oxygen to support complete combustion. Subsequently, the available fuel, m_{TUHC}, is reduced by the final value of m_f. Thus we have a consistent description in each burning region, with an algorithm that can be invoked independent of the region being analyzed.

$$\dot{Q} = \dot{m}_f \times H_c \ , \tag{21}$$

with the mass of oxygen required to achieve this energy release rate (based on the oxygen consumption principle [19][2]) of

$$\dot{m}_O = \frac{\dot{Q}}{1.32\times10^7} = \dot{m}_f \times \frac{H_c}{1.32\times10^7} \ . \tag{22}$$

If the fuel contains oxygen (available for combustion), the oxygen needed to achieve full combustion is less than this value

$$\dot{m}_O(\text{needed}) = \dot{m}_O - \dot{m}_O(\text{in the fuel}) \tag{23}$$

If sufficient oxygen is available, then it is fully burned. However, if the oxygen concentration is low enough, it will constrain the burning and impose a limit on the amount of fuel actually burned, as opposed to the amount pyrolyzed. The actual limitation is discussed below and is presented as eq (38).

$$\dot{m}_O(\text{actual}) = \text{minimum of} \left\{ \dot{m}_O(\text{available}), \dot{m}_O(\text{needed}) \right\}, \tag{24}$$

$$\dot{m}_f(\text{actual}) = \dot{m}_O(\text{actual}) \times \frac{1.32\,x\,10^7}{H_c} \tag{25}$$

Essentially, we limit the amount of fuel that is burned, as opposed to the amount that is pyrolyzed, to the lesser of the amount pyrolyzed and that required to consume the *available* oxygen. The $\dot{m}_O$(actual) and $\dot{m}_f$(actual) are the quantities used below. By way of explanation, eq (21) tells us how much energy would be released by the available fuel if there were no constraint (free burn). Equation (22) then tells us the mass of oxygen required to achieve this energy release rate. Equation (23) yields the amount needed based on the required amount less the

---

** The units for oxygen consumption calorimetry are Joules/kg. The value $1.37x10^7$ is used (see reference 19) and implies these units.

oxygen available in the fuel. Solid propellant would yield a value of zero at this point. Equation (24) limits the amount used and eq (25) then yields the amount of fuel actually burned, as opposed to the amount pyrolyzed.

We begin with the mass balance equation. The mass consumed as pyrolyzate plus oxygen must reappear as product.

$$\begin{aligned} \dot{m}_f + \dot{m}_O &= \dot{m}_f + \dot{m}_f \times \frac{H_c}{1.32\times10^7} - \frac{\dot{m}_f}{\{-\}} \times \left(\frac{O}{C}\right) \\ &= \dot{m}_{CO_2} + \dot{m}_{CO} + \dot{m}_S + \dot{m}_{H_2O} + \dot{m}_{HCl} + \dot{m}_{HCN} \end{aligned} \tag{26}$$

We then substitute the following definitions of mass produced of each species based on the amount of carbon (ala. fuel) consumed as

$$\dot{m}_{HCl} = \left(\frac{HCl}{C}\right) \times \dot{m}_C \rightarrow \left(\frac{HCl}{f}\right) \times \dot{m}_f \tag{27}$$

$$\dot{m}_{HCN} = \left(\frac{HCN}{C}\right) \times \dot{m}_C \rightarrow \left(\frac{HCN}{f}\right) \times \dot{m}_f \tag{28}$$

$$\dot{m}_{H_2O} = \frac{1}{2}\left(\frac{H_2O}{H}\right) \times \left(\frac{H}{C}\right) \times \dot{m}_C = 9 \times \left(\frac{H}{C}\right) \times \dot{m}_C \rightarrow 9 \times \left(\frac{H}{C}\right) \times \frac{\dot{m}_f}{\{-\}} \tag{29}$$

$$\dot{m}_{CO_2} = \left(\frac{CO_2}{C}\right) \times \dot{m}_C \tag{30}$$

$$\dot{m}_S = \left(\frac{S}{C}\right) \times \dot{m}_C = \left(\frac{CO_2}{C}\right) \times \left(\frac{S}{CO_2}\right) \times \dot{m}_C \rightarrow \left(\frac{S}{CO_2}\right) \times \dot{m}_{CO_2} \tag{31}$$

$$\dot{m}_{CO} = \left(\frac{CO}{C}\right) \times \dot{m}_C = \left(\frac{CO_2}{C}\right) \times \left(\frac{CO}{CO_2}\right) \times \dot{m}_C \rightarrow \left(\frac{CO}{CO_2}\right) \times \dot{m}_{CO_2} \tag{32}$$

Substituting the above definitions into the mass balance equation yields:

$$\left(\frac{CO_2}{C}\right) = \frac{\{-\} \times \left(1 + \frac{H_c}{1.32\times10^7} - \frac{O/C}{\{-\}}\right) - \left(\frac{HCl}{C} + \frac{HCN}{C} + 9\frac{H}{C}\right)}{\left(1 + \frac{S}{CO_2} + \frac{CO}{CO_2}\right)} \tag{33}$$

With these definitions, we can substitute back into the equation for carbon dioxide production, which yields

$$\dot{m}_{CO_2} = \dot{m}_f \times \frac{\left(1 + \frac{h_c}{1.32\times10^7} - \frac{O/C}{\{-\}}\right) - \frac{\left(\frac{HCl}{C} + \frac{HCN}{C} + 9\frac{H}{C}\right)}{\{-\}}}{\left(1 + \frac{S}{CO_2} + \frac{CO}{CO_2}\right)}. \tag{34}$$

and the remainder follow explicitly.

The form in which we cast these equations evolves naturally from the properties of combustion. Hydrogen, carbon and bound oxygen are properties of the fuel. They can be measured experimentally independent of the combustion process. Thus we use these ratios as the basis of the scheme. In a similar sense, hydrogen chloride and hydrogen cyanide are properties of the pyrolysis process. So hydrogen chloride and hydrogen cyanide production are specified with respect to the fuel pyrolysis. Normally this is how they are measured, for example with the cone calorimeter, so we can use the measured quantities directly. Other than the cyanide, chloride and water production, hydrogen does not play a role. In general, hydrogen has a much greater affinity for oxygen than carbon, so almost all of the hydrogen will be utilized. This dictates our next choice, which is that soot is essentially all carbon. On a mass basis, this is certainly true. On a molecular basis, however, it may not be so simple. Carbon dioxide is a direct product of combustion, and the assumption is that most carbon will end up here. Carbon monoxide and soot are functions of incomplete combustion. Thus they depend on the environment in which the burning takes place. They are in no case a function of the pyrolysis process itself. Thus the production of these products is specified with respect to the carbon dioxide. At present, we must rely on measured ratios, but this is beginning to change as we gain a better understanding of the combustion process. So, in the present model, carbon goes to one of three final species, carbon dioxide, carbon monoxide or soot, with the particular branching ratio depending on the chemistry active at the time.

Eqs (29) through (34) are used in terms of the carbon production. We now need to recast HCl and HCN in terms of fuel production rather than carbon production, since that is how they are measured. Since HCl and HCN are similar, we will just make the argument for one, and then

assume that the derivation is the same for the other. One simplification will be possible for the HCN though, and that is that its production rate is *always* much less than the pyrolysis rate.

Since {—} is just f/C,

$$\left(\frac{HCl}{C}\right) = \left(\frac{HCl}{f}\right) \times \left(1 + \frac{H}{C} + \frac{HCl}{C} + \frac{HCN}{C} + \frac{O}{C}\right). \tag{35}$$

Therefore

$$\left(\frac{HCl}{C}\right) = \left(\frac{HCl}{f}\right) \times \left(\frac{1 + \frac{H}{C} + \frac{O}{C}}{1 - \left(\frac{HCl}{f}\right)}\right), \tag{36}$$

and for hydrogen cyanide we have

$$\left(\frac{HCN}{C}\right) = \left(\frac{HCN}{f}\right) \times \left(1 + \frac{H}{C} + \frac{HCl}{C} + \frac{O}{C}\right). \tag{37}$$

In this latter case, we assume that the cyanide ratio (*HCN/C*) is small compared to unity. It is the *HCl/C* and *HCN/C* ratios which are used by the model.

The relationship between oxygen and fuel concentration defines a range where burning will take place. The rich limit is where, for a given ratio of O_2 to N_2 (generally the ratio in air), there is too much fuel for combustion. At the other end, there is the lean flammability limit, where there is too little fuel for combustion. In the CFAST model, the rich limit is incorporated by limiting the burning rate as the oxygen level decreases until a "lower oxygen limit" (LOL) is reached. The lower oxygen limit is incorporated through a smooth decrease in the burning rate near the limit:

$$\dot{m}_o(available) = \dot{m}_e Y_{O_2} C_{LOL} \tag{38}$$

where m_e is the mass entrainment flow rate and the lower oxygen limit coefficient, C_{LOL}, is the fraction of the available fuel which can be burned with the available oxygen and varies from 0 at the limit to 1 above the limit. The functional form provides a smooth cutoff of the burning over a narrow range above the limit.

$$C_{LOL} = \frac{\tanh\left(800\left(Y_{O_2} - Y_{LOL}\right) - 4\right) + 1}{2} \tag{39}$$

For the lean flammability limit, an ignition temperature criterion is included, below which no burning takes place.

As stated, the burning rate simply decreases as the oxygen level decreases. We know that there is an oxygen concentration below which fuel will not oxidize. This is referred to as the "rich flammability" limit. In the present context we refer to this point as the lower oxygen limit (LOL). At the other end, there is a "lean flammability" limit. The fuel oxidation rate is limited at both ends. At present, we have incorporated only the rich flammability limit. We do not have sufficient theoretical underpinnings, nor sufficient experimental data, to include temperature dependence or the lean flammability limit. In the lean flammability limit, we use only a temperature criterion below which we assume no burning takes place.

In summary, we can predict the formation of some of the products of combustion, carbon dioxide, carbon monoxide, soot, water, hydrogen cyanide, and hydrogen chloride given the branching ratios CO/CO_2, $S(soot)/CO_2$, the composition of the fuel, H/C, O/C, HCl/f and HCN/f and the flammability limit. At present, in practice we use experimental values, such as those from Morehart *et al.*[20]. The composition of the fuel is a measurable quantity, although it is complicated somewhat by physical effects. The complication arises in that materials such as wood will yield methane in the early stages of burning, and carbon rich products at later times. Thus the H/C and O/C ratios are functions of time. Finally, the production ratios of CO/CO_2, $S(soot)/CO_2$ are based on the kinetics which in turn is a function of the ambient environment.

In earlier versions of CFAST, the chemistry routine was called once. However, a recent test case pointed out a long standing problem in the way CFAST coordinates plume entrainment with fire size. Before the fix outlined here, CFAST calculated plume entrainment via a two step process:

1) Determine the plume entrainment using McCaffrey's method using the fire size unconstrained by the available oxygen.

2) Once the actual fire size is calculated from the available oxygen, a new estimate for the plume entrainment is determined by a simple linear correction of

$$\dot{m}_{e,actual} = \dot{m}_{e,unconstrained} \frac{\dot{Q}_{actual}}{\dot{Q}_{unconstrained}} \tag{40}$$

Since the plume entrainment is not a linear function of the fire size and the fire size depends on the oxygen entrained, this simple process can lead to an inconsistency between the fire size (calculated from the unconstrained plume entrainment) and the new estimate of the plume entrainment. For very large fires where the fire size is limited by the amount of oxygen entrained, this can lead to significant differences between the calculated fire size and the amount of oxygen actually available for the combustion.

The fix is a simple one: when the fire is limited by the available oxygen entrained into the plume, the plume entrainment and fire size are both re-calculated by calling the plume sub-model and chemistry sub-model a second time to get a better estimate of the actual oxygen available (and thus the actual fire size).

3.3.2 Plumes

Buoyancy generated by the combustion processes in a fire causes the formation of a plume. Such a plume can transport mass and enthalpy from the fire into the lower or upper layer of a compartment. In the present implementation, we assume that both mass and enthalpy from the fire are deposited only into the upper layer. In addition the plume entrains mass from the lower layer and transports it into the upper layer. This yields a net enthalpy transfer between the two layers.

A fire generates energy at a rate $\dot{Q}$. Some fraction, χ_R, will exit the fire as radiation. The remainder, χ_C, will then be deposited in the layers as convective energy or heat additional fuel so that it pyrolyzes. We can use the work of McCaffrey [21] to estimate the mass entrained by the fire/plume from the lower into the upper layer. This correlation divides the flame/plume into three regions as given in eq(41). This prescription agrees with the work of Cetegen *et al*. [22] in the intermittent regions but yields greater entrainment in the other two regions. This difference is particularly important for the initial fire since the upper layer is far removed from the fire.

$$\begin{aligned}
&\text{flaming:} && \frac{\dot{m}_e}{\dot{Q}} = 0.011 \left(\frac{z}{\dot{Q}^{2/5}} \right)^{0.566} && 0.00 \le \left(\frac{z}{\dot{Q}^{2/5}} \right) < 0.08 \\
&\text{intermittent:} && \frac{\dot{m}_e}{\dot{Q}} = 0.026 \left(\frac{z}{\dot{Q}^{2/5}} \right)^{0.909} && 0.08 \le \left(\frac{z}{\dot{Q}^{2/5}} \right) < 0.20 \\
&\text{plume:} && \frac{\dot{m}_e}{\dot{Q}} = 0.124 \left(\frac{z}{\dot{Q}^{2/5}} \right)^{1.895} && 0.20 \le \left(\frac{z}{\dot{Q}^{2/5}} \right)
\end{aligned} \qquad (41)$$

McCaffrey's correlation is an extension of the common point source plume model, with a different set of coefficients for each region. These coefficients are experimental correlations.

Within CFAST, the radiative fraction defaults to 0.30 [23]; i.e., 30 % of the fires energy is released via radiation. For other fuels, the work or Tewarson [24], McCaffrey [25], or Koseki [26] is available for reference. These place the typical range for the radiative fraction from about 0.15 to 0.5.

In CFAST, there is a constraint on the quantity of gas which can be entrained by a plume arising from a fire. The constraint arises from the physical fact that a plume can rise only so high for a given size of a heat source. In the earlier versions of this model (FAST version 17 and earlier), the plume was not treated as a separate zone. Rather we assumed that the upper layer was connected immediately to the fire by the plume. The implication is that the plume is formed instantaneously and stretches from the fire to the upper layer or ceiling. Consequently, early in a fire, when the energy flux was very small and the plume length very long, the entrainment was

over predicted. This resulted in the interface falling more rapidly than was seen in experiments. Also the initial temperature was too low and the rate of rise too fast, whereas the asymptotic temperature was correct. The latter occurred when these early effects were no longer important.

The correct sequence of events is for a small fire to generate a plume which does not reach the ceiling or upper layer initially. The plume entrains enough cool gas to decrease the buoyancy to the point where it no longer rises. When there is sufficient energy present in the plume, it will penetrate the upper layer. The effect is two-fold: first, the interface will take longer to fall and second, the rate of rise of the upper layer temperature will not be as great. To this end the following prescription has been incorporated: for a given size fire, a limit is placed on the amount of mass which can be entrained, such that no more is entrained than would allow the plume to reach the layer interface. The result is that the interface falls at about the correct rate, although it starts a little too soon, and the upper layer temperature is over predicted, but follows experimental data after the initial phase.

For the plume to be able to penetrate the inversion formed by a hot gas layer over a cooler gas layer, the density of the gas in the plume at the point of intersection must be less than the density of the gas in the upper layer. In practice, this places a maximum on the air entrained into the plume. From conservation of mass and enthalpy, we have

$$\dot{m}_p = \dot{m}_f + \dot{m}_e \tag{42}$$

$$\dot{m}_p c_p T_p = \dot{m}_f c_p T_f + \dot{m}_e c_p T_l \tag{43}$$

where the subscripts *p*, *f*, *e*, and *l* refer to the plume, fire, entrained air, and lower layer, respectively.

The criterion that the density in the plume region be lower than the upper layer implies that $T_u < T_p$. Solving eq (43) for T_p and eliminating $\dot{m}_p$ using eq (42) yields

$$T_p = \frac{T_f \dot{m}_f + T_l \dot{m}_e}{\dot{m}_f + \dot{m}_e} > T_u \tag{44}$$

or

$$\dot{m}_e < \left(\frac{T_f - T_u}{T_u - T_l} \right) \dot{m}_f < \frac{T_f}{T_u - T_l} \dot{m}_f \tag{45}$$

Substituting the convective energy released by the fire,

$$\dot{Q}_c(fire)=\dot{m}_f c_p T_f \ , \tag{46}$$

Substituting eq (46) into eq (45) yields the final form of the entrainment limit used in the CFAST model:

$$\dot{m}_e < \frac{\dot{Q}_c(fire)}{c_p\left(T_u - T_l\right)} \tag{47}$$

which is incorporated into the model. It should be noted that both the plume and layers are assumed to be well mixed with negligible mixing and transport time for the plume and layers.

3.3.3 Vent Flow

Mass flow (in the remainder of this section, the term "flow" will be used to mean mass flow) is the dominant source term for the predictive equations because it fluctuates most rapidly and transfers the greatest amount of enthalpy on an instantaneous basis of all the source terms (except of course the fire). Also, it is most sensitive to changes in the environment. CFAST models horizontal flow through vertical vents and vertical flow through horizontal vents. Horizontal flow encompasses flow through doors, windows and so on. Horizontal flow is discussed in section 3.3.3.1. Vertical flow occurs in ceiling vents. It is important in two separate situations: on a ship with open hatches and in house fires with roof venting. Vertical flow is discussed in section 3.3.3.2.

3.3.3.1 Horizontal Flow Through Vertical Vents

Flow through normal vents such as windows and doors is governed by the pressure difference across a vent. A momentum equation for the zone boundaries is not solved directly. Instead momentum transfer at the zone boundaries is included by using an integrated form of Euler's equation, namely Bernoulli's solution for the velocity equation. This solution is augmented for restricted openings by using flow coefficients [27] to allow for constriction from finite size doors. The flow (or orifice) coefficient is an empirical term which addresses the problem of constriction of velocity streamlines at an orifice.

Bernoulli's equation is the integral of the Euler equation and applies to general initial and final velocities and pressures. The implication of using this equation for a zone model is that the initial velocity in the doorway is the quantity sought, and the final velocity in the target compartment vanishes. That is, the flow velocity vanishes where the final pressure is measured. Thus, the pressure at a stagnation point is used. This is consistent with the concept of uniform zones which are completely mixed and have no internal flow. The general form for the velocity of the mass flow is given by

$$v = C\left(\frac{2\Delta P}{\rho}\right)^{1/2} \tag{48}$$

where C is the constriction (or flow) coefficient ($\approx$0.7), ρ is the gas density on the source side, and ΔP is the pressure across the interface. (Note: at present we use a constant C for all gas temperatures)

The simplest means to define the limits of integration is with neutral planes, that is the height at which flow reversal occurs, and physical boundaries such as sills and soffits. By breaking the integral into intervals defined by flow reversal, a soffit, a sill, or a zone interface, the flow equation can be integrated piecewise analytically and then summed.

The approach to calculating the flow field is of some interest. The flow calculations are performed as follows. The vent opening is partitioned into at most six slabs where each slab is bounded by a layer height, neutral plane, or vent boundary such as a soffit or sill. The most general case is illustrated in Figure 4.

The mass flow for each slab can be determined from

$$\dot{m}_{i\to o} = \frac{1}{3}C(8\rho)A_{slab}\left(\frac{x^2 + xy + y^2}{x+y}\right) \tag{49}$$

where $x = |P_t|^{1/2}$, and $y = |P_b|^{1/2}$. P_t and P_b are the cross-vent pressure differential at the top and bottom of the slab respectively and A_{slab} is the cross-sectional area of the slab. The value of the density, ρ, is taken from the source compartment.

A mixing phenomenon occurs at vents which is similar to entrainment in plumes. As hot gases from one compartment leave that compartment and flow into an adjacent compartment a door jet can exist which is analogous to a normal plume. Mixing of this type occurs for $\dot{m}_{13} > 0$ as shown in Figure 5. To calculate the entrainment ($\dot{m}_{43}$ in this example), once again we use a plume description, but with an extended point source. The estimate for the point source extension is given by Cetegen *et al*. [22]. This virtual point source is chosen so that the flow at the door opening would correspond to a plume with the heating (with respect to the lower layer) given by

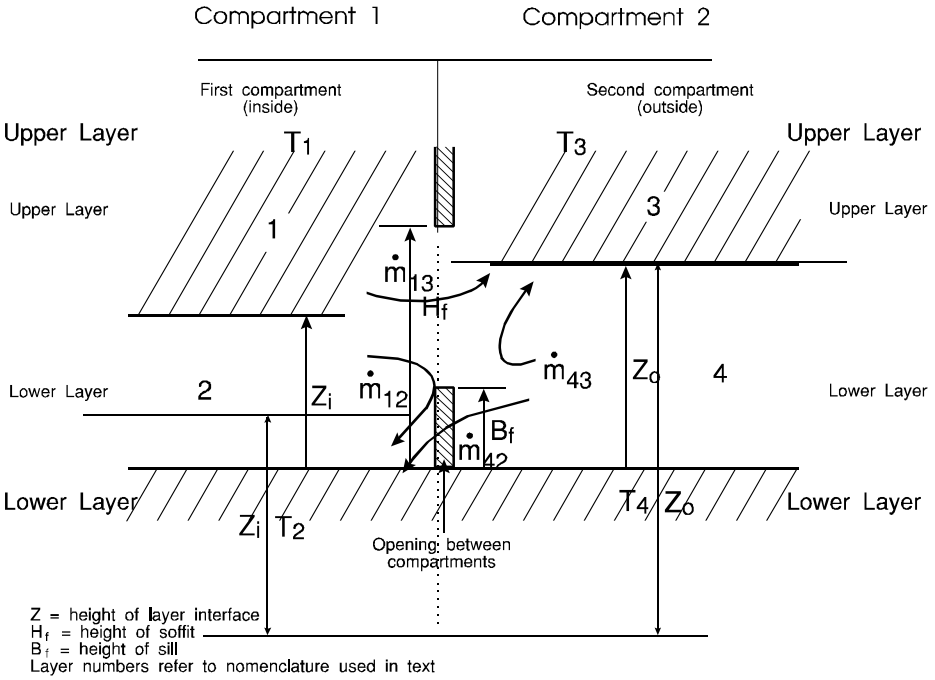

Figure 4. Notation conventions for two-layer model in two compartments with a connecting vent.

Figure 5. Flow patterns and layer numbering convention.

$$\dot{Q} = c_p \left(T_l - T_4\right) \dot{m}_{13} \tag{50}$$

The concept of the virtual source is that the enthalpy flux from the virtual point source should equal the actual enthalpy flux in the door jet at the point of exit from the vent using the same prescription. Thus the entrainment is calculated the same way as was done for a normal plume. The height, z_p, of the plume is

$$z_p = \frac{z_{13}}{\dot{Q}_{eq}^{2/5}} + v_p \tag{51}$$

where v_p, the virtual point source, is defined by inverting the entrainment process to yield

$$
\begin{aligned}
v_p &= \left(\frac{90.9\dot{m}}{\dot{Q}_{eq}} \right)^{1.76} && \text{if } 0.00 < v_p \le 0.08 \\
v_p &= \left(\frac{38.5\dot{m}}{\dot{Q}_{eq}} \right)^{1.001} && \text{if } 0.08 < v_p \le 0.20 \\
v_p &= \left(\frac{8.10\dot{m}}{\dot{Q}_{eq}} \right)^{0.528} && \text{if } 0.20 < v_p
\end{aligned}
\qquad (52)
$$

The units of this height, z_p and of v_p, are not length, but rather the reduced notation of McCaffrey [21]. That is, the z_p defined here is the term $z/Q^{2/5}$ used earlier. Although outside of the normal range of validity of the plume model, a level of agreement with experiment is apparent (see section 6). Since a door jet forms a flat plume whereas a normal fire plume will be approximately circular, strong agreement is not expected.

The other type of mixing is much like an inverse plume and causes contamination of the lower layer. It occurs when there is flow of the type $\dot{m}_{42} > 0$. The shear flow causes vortex shedding into the lower layer and thus some of the particulates end up in the lower layer. The actual amount of mass or energy transferred is usually not large, but its effect can be large. For example, even minute amounts of carbon can change the radiative properties of the gas layer, from negligible to something finite. It changes the rate of radiation absorption by orders of magnitude and invalidates the simplification of an ambient temperature lower layer. This term is predicated on the Kelvin-Helmholz flow instability and requires shear flow between two separate fluids. The mixing is enhanced for greater density differences between the two layers. However, the amount of mixing has never been well characterized. Quintiere *et al* [27]. discuss this phenomena for the case of crib fires in a single room, but their correlation does not yield good agreement with experimental data in the general case [28]. In the CFAST model, it is assumed that the incoming cold plume behaves like the inverse of the usual door jet between adjacent hot layers; thus we have a descending plume. It is possible that the entrainment is overestimated in this case, since buoyancy, which is the driving force, is not nearly as strong as for the usually upright plume.

3.3.3.2 Vertical Flow Through Horizontal Vents

Flow through a ceiling or floor vent can be somewhat more complicated than through door or window vents. The simplest form is uni-directional flow, driven solely by a pressure difference. This is analogous to flow in the horizontal direction driven by a piston effect of expanding gases. Once again, it can be calculated based on the Bernoulli equation, and presents little difficulty. However, in general we must deal with more complex situations that must be modeled in order to have a proper understanding of smoke movement. The first is an occurrence of puffing. When a fire exists in a compartment in which there is only one hole in the ceiling, the fire will

burn until the oxygen has been depleted, pushing gas out the hole. Eventually the fire will die down. At this point ambient air will rush back in, enable combustion to increase, and the process will be repeated. Combustion is thus tightly coupled to the flow. The other case is exchange flow which occurs when the fluid configuration across the vent is unstable (such as a hotter gas layer underneath a cooler gas layer). Both of these pressure regimes require a calculation of the onset of the flow reversal mechanism.

Normally a non-zero cross vent pressure difference tends to drive unidirectional flow from the higher to the lower pressure side. An unstable fluid density configuration occurs when the pressure alone would dictate stable stratification, but the fluid densities are reversed. That is, the hotter gas is underneath the cooler gas. Flow induced by such an unstable fluid density configuration tends to lead to bi-directional flow, with the fluid in the lower compartment rising into the upper compartment. This situation might arise in a real fire if the room of origin suddenly had a hole punched in the ceiling. We make no pretense of being able to do this instability calculation analytically. We use Cooper's algorithm [29] for computing mass flow through ceiling and floor vents. It is based on correlations to model the unsteady component of the flow. What is surprising is that we can find a correlation at all for such a complex phenomenon. There are two components to the flow. The first is a net flow dictated by a pressure difference. The second is an exchange flow based on the relative densities of the gases. The overall flow is given by [29]

$$\dot{m} = C f(\gamma,\varepsilon)\left(\frac{\delta P}{\bar{\rho}}\right)^{1/2} A_v \tag{53}$$

where $\gamma = c_p/c_v$ is the ratio of specific heats and

$$C = 0.68 + 0.17\varepsilon, \tag{54}$$

$$\varepsilon = \frac{\delta P}{P}, \tag{55}$$

and f is a weak function of both γ and ε. In the situation where we have an instability, we use Cooper's correlations. The algorithm for this exchange flow is given by

$$\dot{m}_{ex} = 0.1\left(\frac{g\,\delta\rho\,A_v^{5/2}}{\rho_{av}}\right)\left(1.0 - \frac{2\,A_v^2\,\delta\rho}{S^2\,g\,\delta\rho\,D^5}\right) \tag{56}$$

where

$$D = 2\sqrt{\frac{A_v}{\pi}} \tag{57}$$

and S is 0.754 or 0.942 for round or square openings, respectively.

3.3.3.3 Forced Flow

Fan-duct systems are commonly used in buildings for heating, ventilation, air conditioning, pressurization, and exhaust. Figure 6(a) shows smoke management by an exhaust fan at the top of an atrium, and Figure 6(b) illustrates a kitchen exhaust. Cross ventilation, shown in Figure 6(c), is occasionally used without heating or cooling. Generally systems that maintain comfort conditions have either one or two fans. Residences often have a systems with a single fan as shown in Figure 6 and 7(a). In this system return air from the living quarters is drawn in at one location, flows through filter, fan and coils, and is distributed back to the residence. This system does not have the capability of providing fresh outside air. These systems are intended for applications where there is sufficient natural air leakage through cracks in walls and around windows and doors for odor control. Further information about these systems is presented in Klote and Milke [30] and the American Society of Heating, Refrigerating and Air Conditioning Engineers [31].

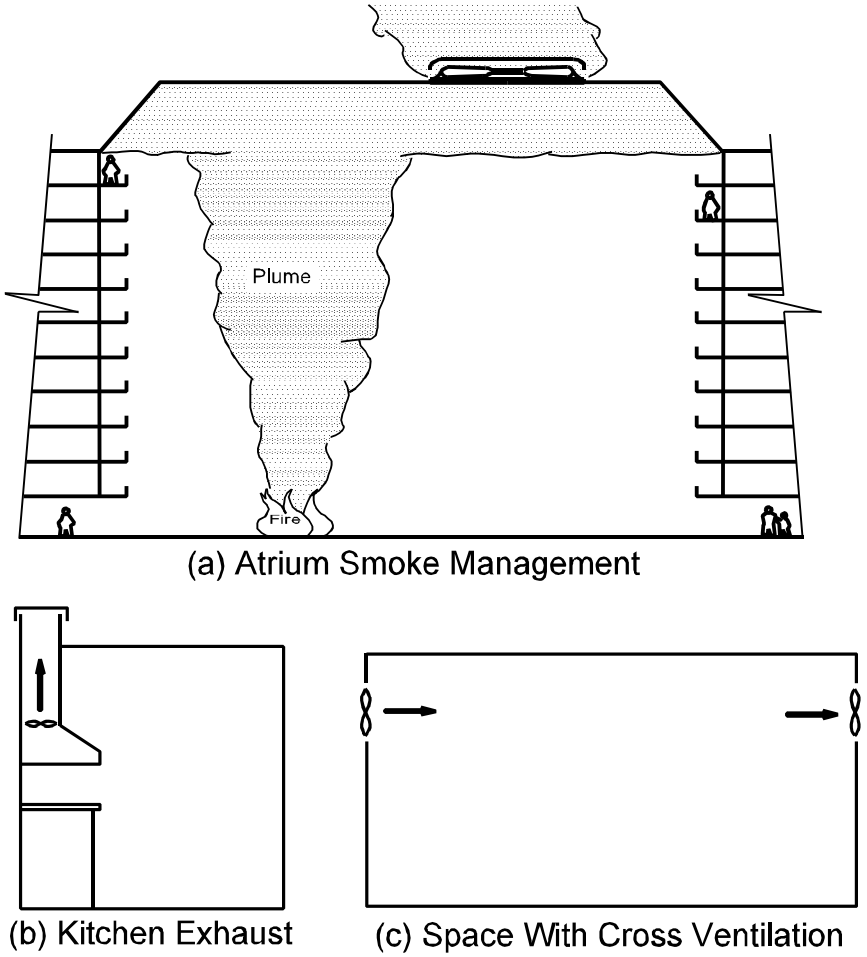

Figure 6. Some simple fan-duct systems.

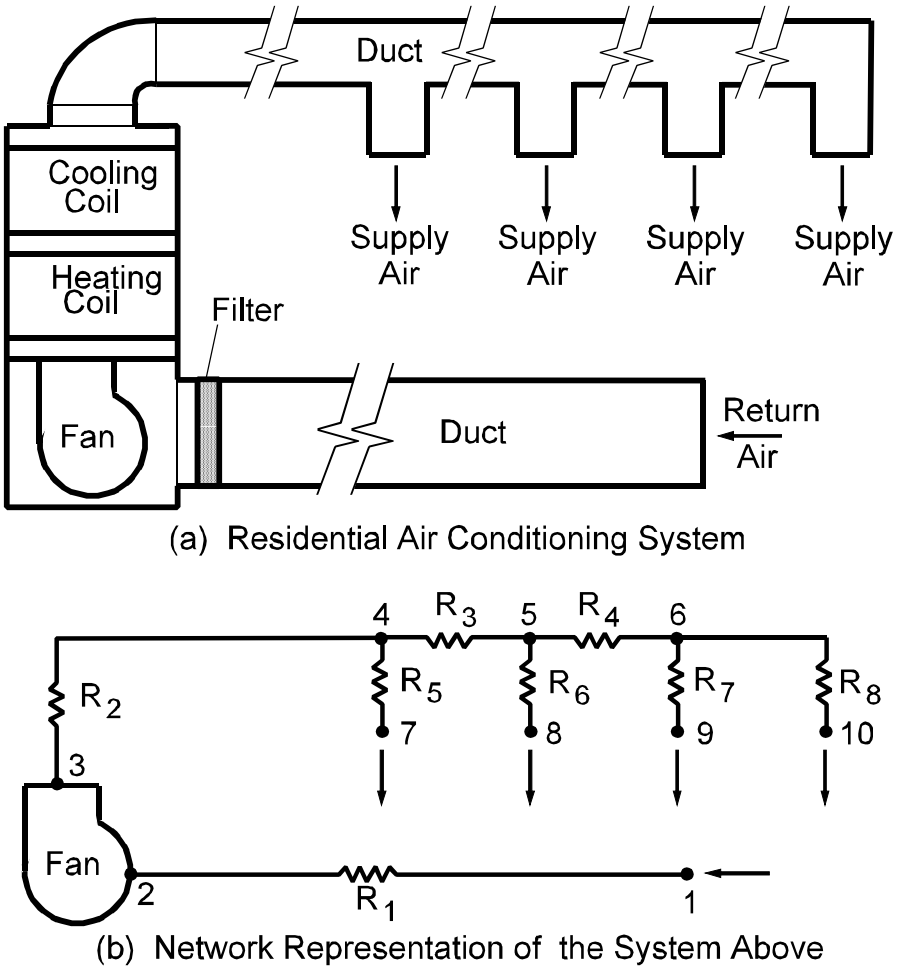

Figure 7. Network representation of a residential system

The model for mechanical ventilation used in CFAST is based on the theory of networks and is based on the model developed by Klote [32]. This is a simplified form of Kirchoff's law which says that flow into a node must be balanced by flow out of the node. Adapting Ohm's law,

$$\text{voltage} = \text{current} \times \text{resistance},$$

to HVAC flow, we have

$$\text{pressure change} = \text{mass flow} \times \text{resistance}$$

which can then be written equivalently

$$\text{mass flow} = \text{conductance} \times (\text{pressure drop across a resistance})^{1/2}.$$

For each node, this flow must sum to zero. There are several assumptions which are made in computing this flow in ducts, fans, elbow, *etc*. First, we assume unidirectional flow. Given the usual size of ducts, and the nominal presence of fans, this is quite reasonable. Also, the particular implementation used here [32] does not allow for reverse flow in the fans. The difficulty lies in describing how a fan behaves in such a case.

Each fan-duct system is represented as a network of nodes, each at a specific temperature and pressure. The nodes may be connected by fans, ducts, fittings and other components. Except for fans, air flows through these components from nodes of higher pressure to nodes of lower pressure. For example, the residential system illustrated in 7(a) is represented in 7(b) as a network of a fan, eight resistances and ten nodes. These resistances incorporate all the resistance to flow between nodes. For instance, the equivalent resistance, R_1, between nodes 1 and 2 accounts for resistances of the inlet, duct, filter and connection to the fan.

Given that we can describe mass flow in terms of pressure differences and conductance, the conservation equation for each node is

$$f_i(P_1,P_2,\ ...)=\sum_j \dot{m}_{i,j} \ = \ 0. \tag{58}$$

The index "*j*" is a summation over connections to a node, and there is an equation "*i*" for each node. The remaining problem is to specify the boundary conditions. At each connection to a compartment, the pressure is specified. Then, given that flow at each connection is unidirectional (at a given instant of time, the flow is either all into or all out of a given connection), the mass and enthalpy flow into or out of a room can be calculated explicitly. Thus we end up with a set of equations of the form

$$\begin{aligned} f_1(P_1,P_2,\ ...) \ &= \ 0 \\ &\vdots \\ f_i(P_1,P_2,\ ...) \ &= \ 0 \\ &\vdots \\ f_n(P_1,P_2,\ ...) \ &= \ 0. \end{aligned} \tag{59}$$

This is an algebraic set of equations that is solved simultaneously with the equations for flow in the compartments.

The equations describe the relationship between the pressure drop across a duct, the resistance of a duct, and the mass flow. The pressure can be changed by conditions in a compartment, or a fan in line in the duct system. Resistance arises from the finite size of ducts, roughness on surfaces, bends and joints. To carry the electrical analog a little further, fans act like constant voltage sources. The analogy breaks down in this case because the pressure (voltage) is proportional to the square of the velocity (current) rather than linearly related as in the electrical case. Since we

are using the current form of the conservation equation to balance the system, the flow can be recast in terms of a conductance

$$\dot{m} = G\sqrt{\Delta P}. \tag{60}$$

The conductance can be expressed generally as

$$G = \sqrt{\frac{2\rho}{C_0}}\, A_0 \tag{61}$$

where C_0 is the flow coefficient, and A_0 is the area of the inlet, outlet, duct, contraction or expansion joint, coil, damper, bend, filter, and so on. Their values for the most common of these items are tabulated in the ASHRAE Handbook [33].

The mechanical ventilation system is partitioned into one or more independent systems. Differential equations for species for each of these systems are derived by lumping all ducts in a system into one pseudo tank. This set of equations is then solved at each time step. Previously the mechanical ventilation computations in CFAST were performed as a side calculation using time splitting. This could cause problems since time-splitting methods require that the split phenomenon (the pressures and temperatures in this case) change slowly compared to other phenomenon such as room pressures, layer heights *etc*. The pressures at each internal node and the temperatures in each branch (duct, fan) are now determined explicitly by the solver, once again using conservation of mass and energy discussed in this section.

3.3.3.3.1 Ducts.

Ducts are long pipes through which gases can flow. They have been studied much more extensively than other types of connections. For this reason, eq (61) can be put into a form which allows one to characterize the conductance in more detail, depending on the type of duct (e.g., oval, round, or square) and is given by

$$G = \sqrt{\frac{FL}{2\rho D_e A_0^2}}\,, \tag{62}$$

where F is the friction factor, L and D_e are the length and effective diameter of the duct respectively. The temperature for each duct d is determined using the following differential equation:

accumulated heat = (heat in - heat out) - convective losses through duct walls

$$c_v \rho_d V_d \frac{dT_d}{dt} = c_p m_d (T_{in} - T_{out}) - h_d A_d (T_d - T_{amb}) \quad (63)$$

where c_v, c_p are the constant volume/pressure specific heats; V_d is the duct volume, ρ_d is the duct gas density, dT_d/dt is the time rate of change of the duct gas temperature, m_d is the mass flow rate, T_{in} and T_{out} are the gas temperatures going into and out of the duct, c_d, A_d are the convective heat transfer coefficient and surface area for duct d and T_{amb} is the ambient temperature. The first term on the right hand side of eq (63) represents the net gain of energy due to gas transported into or out of the duct. The second term represents heat transferred to the duct walls due to convection. In version 1.6, the loss coefficient is set to zero. We retain the form for future work. The differential and algebraic (DAE) solver used by CFAST solves eq (63) exactly as written. A normal ordinary differential equation solver would require that this equation be solved for dT/dt. By writing it this way, the duct volumes can be zero which is the case for fans.

3.3.3.3.2 Fans.

This section provides background information about fan performance. For more information about fans, readers are referred to Jorgensen (1983) and ASHRAE (1992). Normal fan operating range is represented by the line segment *AB* in Figure 8. In this figure, Δp_f is the static pressure of the fan, and $\dot{V}_f$ is the volumetric flow of the fan. The point *B* represents a margin of safety selected by the fan manufacturer in order to avoid unstable flow.

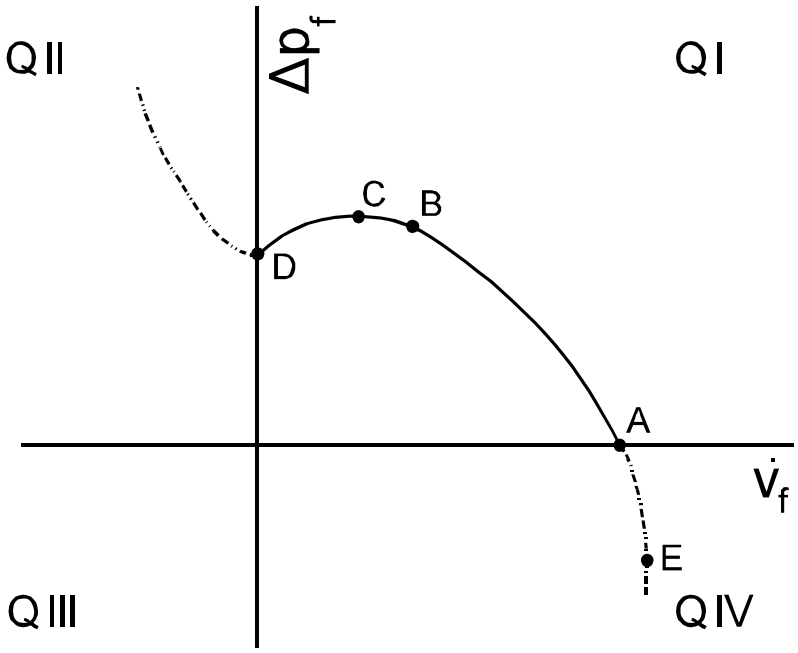

Figure 8. Typical fan performance at constant speed.

Fans operating in the positively sloping portion (*CD* of Figure 8) of the fan curve exhibit unstable behavior called surging or pulsing. Unstable flow consists of violent flow reversals accompanied by significant changes in pressure, power and noise. There is little information about how long a fan can operate in the unstable region before it is destroyed.

Backward flow through a fan occurs when the static pressure is greater than that at point *D*. This is also called second quadrant flow. Quadrant terminology is customarily used in description of fan performance. The horizontal axis and the vertical axis divide a plane into four quadrants which for convenience are labeled Q I, Q II, Q III and Q IV on Figure 8. Backward flow can be exhibited by all types of fans. The wind blowing into the outlet of a propeller fan can result in backflow, and pressures produced by fires could also produce backflow. Fourth quadrant flow is probably representative of all fans. As Δp_f becomes negative, the flow increases with decreasing Δp_f until a choking condition develops at point *E*.

It is common practice in the engineering community and fan industry to represent fan performance with Δp_f on the vertical axis and $\dot{V}_f$ on the horizontal axis. Probably the reason is that $\dot{V}_f$ can be thought of as a single valued function of Δp_f for flow in the first and second quadrants. Fan manufacturers generally supply flow-pressure data for the normal operating range, and they often supply data for the rest of the fan curve in the first quadrant. Specific data is not available for either second or fourth quadrant flow. No approach has been developed for simulation of unstable fan operation, and numerical modeling of unstable flow would be a complicated effort requiring research.

Numerical Approximation of Fan Performance: Figure 9 illustrates four approaches that can be used to approximate fan performance without simulation of unstable flow. For all of these approaches, the fan curve is used for the normal operating range of *AB*. Also for all of the approaches, flows above the normal operating range are approximated by a straight line tangent to the fan curve at point *A*. This results in fourth quadrant flow that is similar to the expected flow provided that Δp_f is not overly far below the horizontal axis. In Figure 9(a), flows below the normal range are approximated by a linear curve tangent to the fan curve at point *B*. This avoids simulation of unstable flows, but the approximated flow is higher than expected in the first quadrant and lower than expected for much of the fourth quadrant.

The approach of Figure 9(b) reduces the approximated flow in the first quadrant. In this approach, the fan curve is also used for the range *BF*, and flows above the normal operating range are approximated by a straight line tangent to the fan curve at point *F*. To increase the flow in the second quadrant, Figure 9(c) uses a line passing through point *D* with the slope of the fan curve at point *A*. Both of the modification of Figure 9(b) and Figure 9(c) are combined in the approach of Figure 9(d).

Fan manufacturer data is routinely either in tabular or graphical form. As indicated by Jorgensen [34], the use of a polynomial form of fan curve is common within the industry.

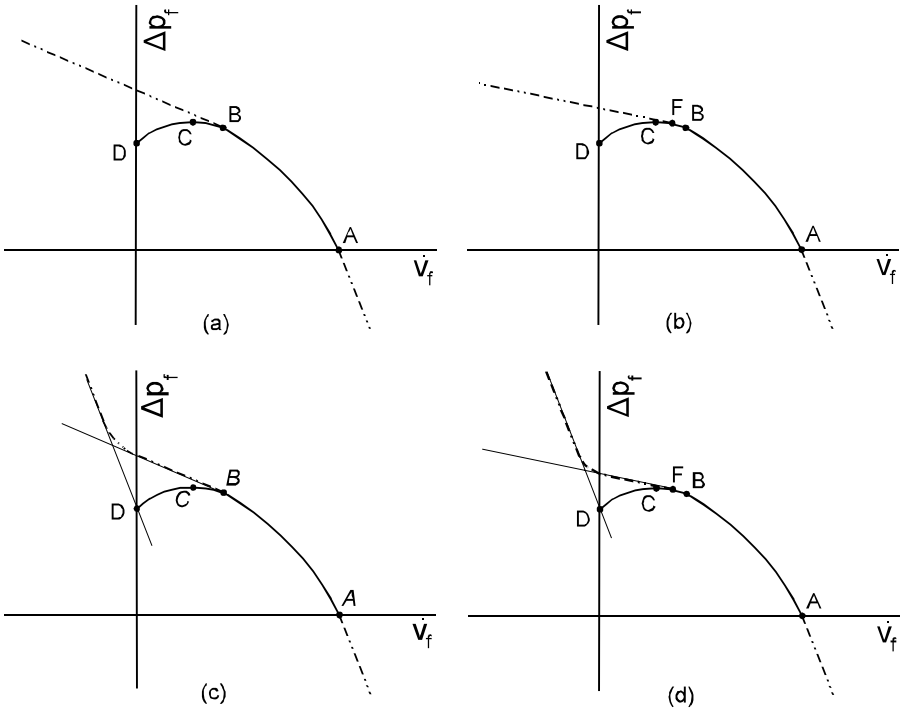

Figure 9. Some approaches to approximation of fan performance for computer simulation

$$\dot{V}_f = B_1 + B_2 \Delta p_f + B_3 (\Delta p_f)^2 + \cdots + B_n (\Delta p_f)^{n-1} \tag{64}$$

The units for $\dot{V}_f$ and Δp_f in CFAST are m^3/s and Pa respectively. Therefor the units for the coefficients B_i (i=1, ... , 5) are $m^3/(s\ Pa^{i-1})$. The coefficients can be entered as data or calculated by least squares regression from flow and pressure data. For constant volumetric flow applications, the only non-zero coefficient in eq (64) is B_1 (n = 1). For incompressible fluids, eq (64) is independent of temperature and pressure. For fan data at 20 °C, compressibility effects amount to an error of about 6 % at a temperature of 200 °C.

3.3.3.3.3 Effective Resistance.

The resistance, R, of a flow element can be defined as

$$R = \frac{\sqrt{\Delta p}}{\dot{m}} \tag{65}$$

where Δp is the pressure loss through the element corresponding to a mass flow rate, $\dot{m}$. The effective resistance between two nodes is always positive, however, sometimes one of the resistances between nodes can be negative as will be explained later. To account for this, $R = K^{½}$ can be substituted into eq (65) to give

$$\Delta p = K\dot{m}^2 \tag{66}$$

The total pressure loss, Δp_t, from one node to the next is the sum of the losses, Δp_i, through each flow element, i, between the nodes.

$$\Delta p_t = \sum_i \Delta p_i \tag{67}$$

The effective value, K_e, relates the total pressure loss to the mass flow rate as $\Delta p_t = K_e\dot{m}^2$, and K_i relates the pressure loss through element i as $\Delta p_i = K_i\dot{m}^2$. These pressure losses can be substituted into eq (67), and canceling like terms yields

$$K_e = \sum_i K_i \tag{68}$$

Values of K_i can be calculated for each element using equations developed later, and K_e can be calculated by eq (68).

Resistance of Ducts: For a straight section of duct with constant cross sectional area, the Bernoulli equation incorporating pressure loss, Δp_{fr}, due to friction is commonly written

$$p_1 - p_2 = \Delta p_{fr} + \rho g(Z_1 - Z_2) \tag{69}$$

where the subscripts 1 and 2 refer to the duct inlet and outlet respectively, p is pressure, Z is elevation, g is the acceleration due to gravity, and ρ is the density of the gas. The pressure loss due to friction is expressed by the Darcy equation in most elementary treatments of flow in pipes and ducts [35], [36], [37].

$$\Delta p_{fr} = f\frac{L}{D_e}\frac{\rho U^2}{2} \tag{70}$$

where f is the friction factor, L is the duct length, D_e is the effective diameter of the duct and U is the average velocity in the duct ($\dot{m} = \rho UA$ where A is the cross-sectional area of the duct). For a circular duct, the effective diameter is the duct diameter. For rectangular duct, Huebscher [38] developed the relationship

$$D_e = 1.30\frac{(ab)^{0.625}}{(a+b)^{0.250}} \tag{71}$$

where a is the length of one side of the duct, and b is the length of the adjacent side. For flat oval duct, Heyt and Diaz [39] developed the relationship

$$D_e = \frac{1.55A^{0.625}}{P^{0.200}} \tag{72}$$

where A and P are the cross-sectional area and the perimeter of the flat oval duct. The area of a flat oval duct is

$$A = (\pi b^2/4) + b(a - b) \tag{73}$$

and the perimeter of a flat oval duct is

$$P = \pi b + 2(a - b) \tag{74}$$

where a is the major dimension of the flat oval duct, and b is the minor dimension of the duct. Combining eqs 65 and 69 results in

$$\dot{m}_{ij} = \frac{1}{R}\sqrt{p_j - p_i + \rho g(Z_j - Z_i)} \tag{75}$$

Combining eqs 66 and 70 results in

$$K = \frac{fL}{2D_e\rho A^2} \tag{76}$$

where A is the cross sectional area of the duct. Colebrook developed the following equation for the friction factor [40].

$$\frac{1}{\sqrt{f}} = -2Log_{10}\left(\frac{\varepsilon}{3.7D_e} + \frac{2.51}{R_e\sqrt{f}}\right) \tag{77}$$

where R_e is the Reynolds number (UD_e/υ where υ is the kinematic viscosity) and ε is the roughness of the inside surface of the duct. Data on roughness of duct materials are listed in Table 3. A graphical presentation of the Colebrook equation developed by Moody [41] was used for decades to calculate friction factors. However, today it is practical to solve the Colebrook equation with computers.

Table 3. Absolute roughness values for common duct materials

Duct Material	Roughness Category	Absolute Roughness, ε	
		mm	ft
Uncoated Carbon Steel, Clean. PVC Plastic Pipe. Aluminum.	Smooth	0.03	0.0001
Galvanized Steel, Longitudinal Seams, 1200 mm Joints. Galvanized Steel, Continuously Rolled, Spiral Seams, 3000 mm Joints. Galvanized Steel, Spiral Seam with 1, 2 and 3 Ribs, 3600 mm Joints.	Medium Smooth	0.09	0.0003
Galvanized Steel, Longitudinal Seams, 760 mm Joints.	Average	0.15	0.0005
Fibrous Glass Duct, Rigid. Fibrous Glass Duct Liner, Air Side With Facing Material.	Medium Rough	0.9	0.003
Fibrous Glass Duct Liner, Air Side Spray Coated. Flexible Duct, Metallic. Flexible Duct, All Types of Fabric and Wire. Concrete.	Rough	3.0	0.01

Local Loss Resistances: The pressure loss, Δp, through many other elements can be expressed as

$$\Delta p = C_o \frac{\rho U_o^2}{2} \tag{78}$$

where U_o is the average velocity at cross section o within the element, and C_o is a local loss coefficient. This equation is commonly used for inlets, outlets, duct contractions and expansions, heating and cooling coils, dampers, bends and many filters. For a large number of these elements, values of C_o have been empirically determined and are tabulated frequently as functions of geometry in handbooks [10 - 12]. Manufacturers literature also contains some values of C_o. The value of K for these resistances is

$$K = \frac{C_o}{2\rho A_o^2}$$

where A_o is the area at cross section *o*.

3.3.4 Corridor Flow

A standard assumption in zone fire modeling is that once hot smoke enters a compartment, a well defined upper layer forms instantly throughout the compartment. This assumption breaks down in large compartments and long corridors due to the time required to fill these spaces. A simple procedure is described for accounting for the formation delay of an upper layer in a long corridor by using correlations developed from numerical experiments generated with the NIST fire model Large Eddy Simulation Model (LES) [42], which is now the Fire Dynamic Simulation Model (FDS) [43]. FDS is a computational fluid dynamics model capable of simulating fire flow velocities and temperatures with high (~0.1m) resolution. Two parameters related to corridor flow are then estimated, the time required for a ceiling jet to travel in a corridor and the temperature distribution down the corridor. These estimates are then used in CFAST by delaying flow into compartments connected to corridors until the ceiling jet has passed these compartments.

FDS is used to estimate ceiling jet characteristics by running a number of cases for various inlet layer depths and temperatures. The vent flow algorithm in CFAST then uses this information to compute mass and enthalpy flow between the corridor and adjacent compartments. This is accomplished by presenting the vent algorithm with a one layer environment (the lower layer) before the ceiling jet reaches the vent and a two layer environment afterwards. Estimated ceiling jet temperatures and depths are used to define upper layer properties.

The problem is to estimate the ceiling jet temperature and depth as a function of time until it reaches the end of the corridor. The approach used here is to run a field model as a pre-processing step and to summarize the results as correlations describing the ceiling jet's temperatures and velocities. An outline of this process is given by

1. Model corridor flow for a range of inlet ceiling jet temperatures and depths. Inlet velocities are derived from the inlet temperatures and depths.

2. For each model run calculate average ceiling jet temperature and velocity as a function of distance down the corridor.

3. Correlate the temperature and velocity distribution down the hall.

The zone fire model then uses these correlations to estimate conditions in the corridor. An outline of the steps involved is given by

1. Estimate the inlet temperature, depth and velocity of the ceiling jet. If the corridor is the fire room then use a standard correlation. If the source of the ceiling jet is another room then calculate the inlet ceiling jet flow using Bernoulli's law for the vent connecting the source room and the corridor.

2. Use correlations in 3. above to estimate the ceiling jet arrival time at each vent.

3. For each vent in the corridor use lower layer properties to compute vent flow before the ceiling jet arrives at the vent and lower/upper layer properties afterwards.

3.3.4.1 Assumptions

The assumptions made in order to develop the correlations are:

- The time scale of interest is the time required for a ceiling jet to traverse the length of the corridor. For example, for a 100 m corridor with 1 m/s flow, the characteristic time period would be 100 s.

- Cooling of the ceiling jet due to mixing with adjacent cool air is large compared to cooling due to heat loss to walls. Equivalently, we assume that walls are adiabatic. This assumption is conservative. An adiabatic corridor model predicts more severe conditions downstream in a corridor than a model that accounts for heat transfer to walls, since cooler ceiling jets travel slower and not as far.

- We do not account for the fact that ceiling jets that are sufficiently cooled will stagnate. Similar to the previous assumption, this assumption is conservative and results in over predictions of conditions in compartments connected to corridors (since the model predicts that a ceiling jet may arrive at a compartment when in fact it may have stagnated before reaching it).

- Ceiling jet flow is buoyancy driven and behaves like a gravity current. The inlet velocity of the ceiling jet is related to its temperature and depth.

- Ceiling jet flow lost to compartments adjacent to the corridor is not considered when estimating ceiling jet temperatures and depths. Similarly, a ceiling jet in a corridor is assumed to have only one source.

- The temperature and velocity at the corridor inlet is constant in time.

- The corridor height and width do not effect a ceiling jet's characteristics. Two ceiling jets with the same inlet temperature, depth and velocity behave the same when flowing in corridors with different widths or heights as long as the ratio of inlet widths to corridor width are equal.

- Flow entering the corridor enters at or near the ceiling. The inlet ceiling jet velocity is reduced from the vent inlet velocity by a factor of w_{vent}/w_{room} where w_{vent} and w_{room} are the width of the vent and room, respectively.

3.3.4.2 Corridor Jet Flow Characteristics

Ceiling jet flow in a corridor can be characterized as a one dimensional gravity current. We will summarize the algorithm, but for a detailed description, please see Appendix A - Corridor Flow.

To a first approximation, the velocity of the current depends on the difference between the density of the gas located at the leading edge of the current and the gas in the adjacent ambient air. The velocity also depends on the depth of the current below the ceiling. A simple formula for the gravity current velocity may be derived by equating the potential energy of the current, $mgd_0/2$, measured at the half-height $d_0/2$ with its kinetic energy, $mU^2/2$ to obtain

$$U=\sqrt{gd_0}$$

where m is mass, g is the acceleration of gravity, d_0 is the height of the gravity current and U is the velocity. When the density difference, between the current and the ambient fluid is small, the velocity U is proportional to $\sqrt{gd_0\Delta\rho/\rho_{cj}}=\sqrt{gd_0\Delta T/T_{amb}}$ where ρ_{amb}, T_{amb} are the ambient density and temperature and ρ_{cj}, T_{cj} are the density and temperature of the ceiling jet and $\Delta T = T_{cj} - T_{amb}$ is the temperature difference. Here use has been made of the ideal gas law, $\rho_{amb}T_{amb} \approx \rho_{cj}T_{cj}$ This can be shown using terms defined in Figure 10 by using an integrated form of Bernoulli's law noting that the pressure drop at the bottom of the ceiling jet is $P_b = 0$, the pressure drop at the top is $P_t=gd_0(\rho_{cj}-\rho_{amb})$ and using a vent coefficient c_{vent} of 0.74, to obtain

$$\begin{aligned} U_0 &= c_{vent}\frac{\sqrt{8}}{3}\frac{1}{\sqrt{\rho_{cj}}}\frac{P_t+\sqrt{P_tP_b}+P_b}{\sqrt{P_t}+\sqrt{P_b}} \\ &= c_{vent}\frac{\sqrt{8}}{3}\sqrt{P_t/\rho_{cj}} \\ &= c_{vent}\frac{\sqrt{8}}{3}\sqrt{gd_0\frac{\rho_{amb}-\rho_{cj}}{\rho_{cj}}} \\ &\approx 0.7\sqrt{gd_0\frac{\Delta T}{T_{amb}}} \end{aligned} \qquad (81)$$

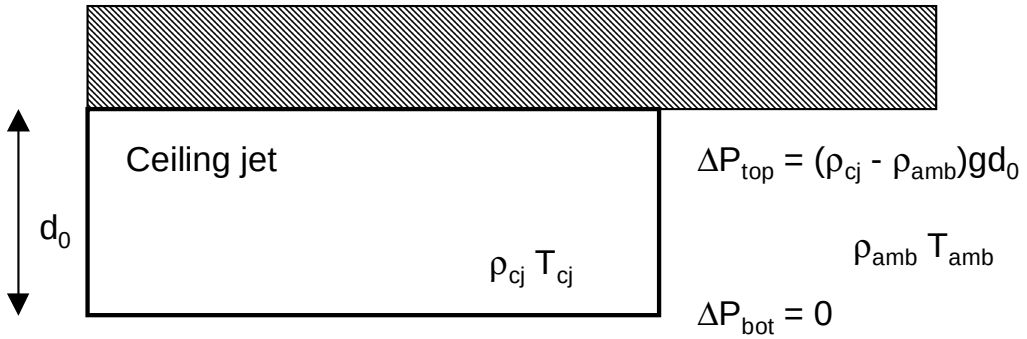

Figure 10 Schematic of a gravity current defining terms used to estimate its inlet velocity

Formulas of the form of the above equation lead one to conclude that a ceiling jet's characteristics in a corridor depend on its depth, d_0, and relative temperature difference, $\Delta T/T_{amb}$. Therefore, as the jet cools, it slows down. If no heat transfer occurs between the ceiling jet and the surrounding walls, then the only mechanism for cooling is mixing with surrounding cool air.

Twenty numerical experiments were performed using FDS in order to better understand the effects of the inlet ceiling jet temperature and depth on ceiling jet characteristics downstream in a corridor. These cases were run with five different inlet depths and four different inlet temperatures. The inlet ceiling jet temperature rise, ΔT_0, and depth, d_0, were used to define an inlet velocity, U_0 using eq(81). The inlet ceiling jet depths, d_0, used in the parameter study are 0.15 m, 0.30 m, 0.45 m, 0.60 m and 0.75 m. The inlet ceiling jet temperature rises, T_0, used in the parameter study are 100 °C, 200 °C, 300 °C and 400 °C.

3.3.4.3 Correlations

Ceiling jet functions were plotted as a function of distance down a corridor for each of the twenty test cases. These results are shown in Figure 11. Note that all but the 0.15 m ceiling jet data lies on essentially the same line.

The best fit line is given in the form of

$$\log\frac{\Delta T}{\Delta T_0} = a + bx.$$

This is equivalent to

$$\frac{\Delta T}{\Delta T_0} = C_1 10^{bx} = C_1\left(\frac{1}{2}\right)^{x/h_{1/2}}$$

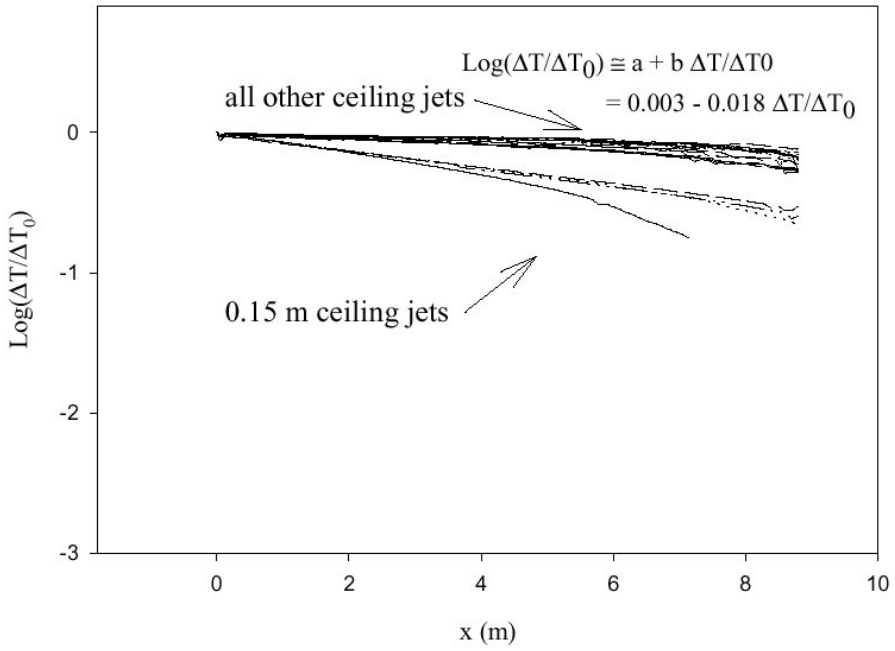

Figure 11. Log_{10} of the relative temperature excess downstream in a corridor using an adiabatic temperature boundary condition for several inlet depths and inlet temperature boundary condition for several inlet depths and inlet temperature rises. The inlet velocity, U_0, is given by equation (4).

where $C_1 = 10^a$ and $h_{1/2}$= - log(2)/b. The parameter $h_{1/2}$ has a physical interpretation. It is the distance down the corridor where the temperature rise T , falls off to 50 per cent of its original value or equivalently, $T(x + h_{1/2}) = T(x)/2$.

The half-distance, $h_{1/2}$, can be approximated by $h_{1/2}$ = log(2)/0.018 = 16.7 m where b = -0.018 is given in Figure 11. Similarly, the coefficients C_1 is approximated by $C_1 = 10^a = 10^{-0.003} \approx 1$ where a is also given in Figure 11. Therefore the temperature rise, ΔT , may be approximated by

$$\Delta T = \Delta T_0 \left(\frac{1}{2}\right)^{\frac{x}{16.7}}$$

The numerical experiments with IFS demonstrated that for the cases simulated, ceiling jet characteristics depend on the relative inlet temperature rise and not the inlet depth. Flow in long corridors (greater than 10 m) need to be better characterized due to the flow stagnation which may occur because of the ceiling jet's temperature decay.

3.3.5 Heat Transfer

This section discusses radiation, convection and conduction, the three mechanisms by which heat is transferred between the gas layers and the enclosing compartment walls. This section also discusses heat transfer algorithms for calculating target temperatures.

3.3.5.1 Radiation

Objects such as walls, gases and fires radiate as well as absorb radiation. Each object has its own properties, such as temperature and emissivity. As we are solving the enthalpy equation for the gas temperature, the primary focus is in finding out how much enthalpy is gained or lost by the gas layers due to radiation. To calculate the radiation absorbed in a zone, a heat balance must be done which includes all surfaces which radiate to and absorb radiation from a zone. The form of the terms which contribute heat to an absorbing layer are the same for all layers. Essentially we assume that all zones in these models are similar so we can discuss them in terms of a general layer contribution. For this calculation to be done in a time commensurate with the other sources, some approximations are necessary.

Radiation can leave a layer by going to another layer, by going to the walls, by exiting through a vent, by heating an object, or by changing the pyrolysis rate of the fuel source. Similarly, a layer can be heated by absorption of radiation from these surfaces and objects as well as from the fire itself. The formalism which we employ for the geometry and view factor calculation is that of Siegel and Howell [45]. Although the radiation could be done with a great deal of generality, we have assumed that the zones and surfaces radiate and absorb like a grey body.

Radiation is an important mechanism for heat exchange in compartments subject to fires. It is important in the present application because it can affect the temperature distribution within a compartment, and thus the buoyancy forces. In the present implementation the fire is assumed to be a point source; it is assumed that plumes do not radiate. We use a simplified geometrical equivalent of the compartment in order to calculate the radiative transfer between the ceiling, floor and layer(s). The original paper which described FAST pointed out that there was an inconsistency in the interaction between the two wall radiation and the four wall conduction algorithms used to transfer heat between the gas layers and the walls. A four wall radiation heat transfer algorithm fixes this problem. A radiative heat transfer calculation could easily dominate the computation in any fire model. This is because radiation exchange is a global phenomena. Each portion of an enclosure interacts radiatively with every other portion that it “sees.” Therefore, it is important to construct algorithms for radiative heat transfer that are both accurate and efficient [44].

This is a “next step” algorithm for computing radiative heat transfer between the bounding surfaces of a compartment containing upper and lower layer gases and point source fires. The two-wall radiation model used has been enhanced to treat lower layer heating and to treat radiative heat exchange with the upper and lower walls independently of the floor and ceiling. We refer to this as the four wall model.

The original radiation algorithm used the extended floor and ceiling concept for computing radiative heat exchange. For the purposes of this calculation, the room is assumed to consist of two wall segments: an extended ceiling and an extended floor. The extended ceiling consisted of the ceiling plus the upper wall segments. Similarly, the extended floor consisted of the floor plus the lower wall segments. The upper layer was modeled as a sphere equal in volume to the volume of the upper layer. Radiative heat transfer to and from the lower layer was ignored. This algorithm is inconsistent with the way heat conduction is handled, since we solve up to four heat conduction problems for each room: the ceiling, the upper wall, the lower wall and the floor. The purpose of the new radiation algorithm then is to enhance the radiative module to allow the ceiling, the upper wall segments, the lower wall segments and the floor to transfer radiant heat independently and consistently.

The four wall algorithm for computing radiative heat exchange is based upon the equations developed in Siegel and Howell [45] which in turn is based on the work of Hottel [46]. Siegel and Howell model an enclosure with N wall segments and an interior gas. A radiation algorithm for a two layer zone fire model requires treatment of an enclosure with two uniform gases. Hottel and Cohen [47] developed a method where the enclosure is divided into a number of wall and gas volume elements. An energy balance is written for each element. Each balance includes interactions with all other elements. Treatment of the fire and the interaction of the fire and gas layers with the walls is based upon the work of Yamada and Cooper [48]. They model fires as point heat sources radiating uniformly in all directions and use the Lambert-Beer law to model the interaction between heat emitting elements (fires, walls, gas layers) and the gas layers. The original formulation is for an N-wall configuration. Although this approach would allow arbitrary specification of compartment surfaces (glass window walls, for example), the computational requirements are significant.

Even the more modest approach of a four wall configuration for computing radiative heat transfer is more sophisticated than was used previously. By implementing a four wall rather than an N wall model, significant algorithmic speed increases were achieved. This was done by exploiting the simpler structure and symmetry of the four wall problem.

The radiation exchange at the k'th surface is shown schematically in Figure 12. For each wall segment k from 1 to N, we must find a net heat flux, $\Delta q_k''$, such that

$$A_k \epsilon_k \sigma_k T_k^4 + (1-\epsilon_k) q_k^{in} = q_k^{in} + A_k \Delta q_k'' \quad (k = 1,..N). \tag{85}$$

Radiation exchange at each wall segment has emitted, reflected, incoming and net radiation terms. Equation (85) then represents a system of linear equations that must be solved for $\Delta q''$ to determine the net fluxes given off by each surface. The setup and solution of this linear system is the bulk of the work required to implement the net radiation method of Siegel and Howell. Equation (86) derived by Siegel and Howell [45] and listed there as eqs 17 to 20, is called the net radiation equation,

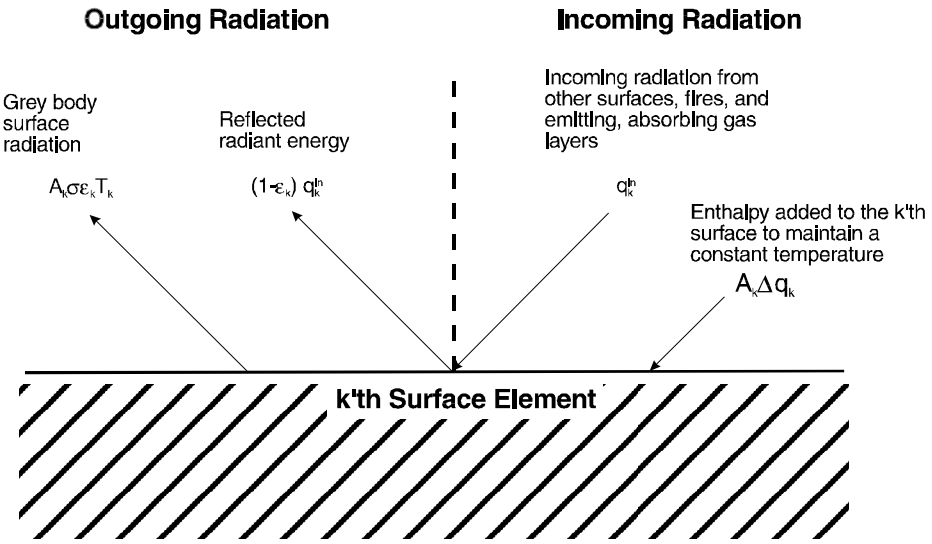

Figure 12. Radiation exchange in a two-zone fire model.

$$\frac{\Delta q_k''}{\epsilon_k} - \sum_{J=1}^{N} \frac{1-\epsilon}{\epsilon_j} \Delta q_j'' F_{k-j} \tau_{j-k} = \sigma T_k^{\,4} - \sum_{j=1}^{N} \sigma T_j^{\,4} F_{k-j} \tau_{j-k} - \frac{c_k}{A_k}. \tag{86}$$

where σ is the Stefan-Boltzman constant, ε_k is the emissivity of the k'th wall segment, T_k is the temperature of the k'th wall segment, F_{k-j} a configuration factor, and τ is a transmissivity factor. This latter is the fraction of energy passing unimpeded through a gas along a path from surface j to k. The parameters c_k represent the various sources of heat, namely the fire itself and the gas layers. In the form shown, the view factor of the k'th element is included in the parameter c_k.

The actual implementation uses a slightly modified form of eq (86), namely

$$\Delta \hat{q}_k'' - \sum_{j=1}^{N} (1-\epsilon_j) \Delta \hat{q}_j'' F_{k-j} \tau_{j-k} = \sigma T_k^{\,4} - \sum_{j=1}^{N} \sigma T_j^{\,4} F_{k-j} \tau_{j-k} - \frac{c_k}{A_k}, \text{ where} \tag{87}$$

$$\Delta q_k'' = \epsilon_k \Delta \hat{q}_k''. \tag{88}$$

There are two reasons for solving eq (87) rather than eq (86). First, since ε_k does not occur in the denominator, radiation exchange can be calculated when some of the wall segments have zero emissivity. Second and more importantly, the matrix corresponding to the linear system of eq () is diagonally dominant [44]. Iterative algorithms can be used to solve such systems more efficiently than direct methods such as Gaussian elimination. The more diagonally dominant a matrix (the closer the emissivities are to unity), the quicker the convergence when using iterative

methods. Typical values of the emissivity for walls subject to a fire environment are in the range of $0.85 < \varepsilon < 0.95$, so this is a reasonable approximation. The computation of, $F_{k\text{-}j}$, $\tau_{j\text{-}k}$ and c_k is discussed by Forney [44]. It is shown how it is possible to use the symmetries present in the four wall segment problem to minimize the number of direct configuration factor calculations required. In earlier versions of CFAST, the gas transmittance per unit length was assumed constant. In this new version, is calculated from the properties of the gas layers. Appendix B provides details of the gas transmittance calculation.

For rooms containing a fire, CFAST models the temperature of four wall segments independently. A two wall model for radiation exchange can break down when the temperatures of the ceiling and upper walls differ significantly. This typically happens in the room of fire origin when different wall materials are used as boundaries for the ceiling, walls and floor.

To demonstrate this consider the following example. To simplify the comparison between the two and four wall segment models, assume that the wall segments are black bodies (the emissivities of all wall segments are one) and the gas layers are transparent (the gas absorptivities are zero). This is legitimate since for this example we are only interested in comparing how a two wall and a four wall radiation algorithm transfer heat to the wall segments. Let the room dimensions be (4×4×4) m, the temperature of the floor and the lower and upper walls be 300 K. Let the ceiling temperature vary from 300 K to 600 K.

Figure 13 shows a plot of the heat flux to the ceiling and upper wall as a function of the ceiling temperature [44], [49]. The two wall model predicts that the extended ceiling (a surface formed by combining the ceiling and upper wall into one wall segment) cools, while the four wall model predicts that the ceiling cools and the upper wall warms. The four-wall model moderates temperature differences that may exist between the ceiling and upper wall (or floor and lower wall) by allowing heat transfer to occur between the ceiling and upper wall. The two wall model is unable to predict heat transfer between the ceiling and the upper wall since it models them both as one wall segment.

3.3.5.2 Convection

Convection is one of the mechanisms by which the gas layers lose or gain energy to walls, objects or through openings. Conduction is a process which is intimately associated with convection; but as it does not show up directly as a term for heat gain or loss, it will be discussed separately. Convective heating describes the energy transfer between solids and gases. The enthalpy transfer associated with flow through openings was discussed in the section on flow through vents.

Convective heat flow is enthalpy transfer across a thin boundary layer. The thickness of this layer is determined by the temperature difference between the gas zone and the wall or object being heated [50]. In general, convective heat transfer, $\dot{q}$, is defined as

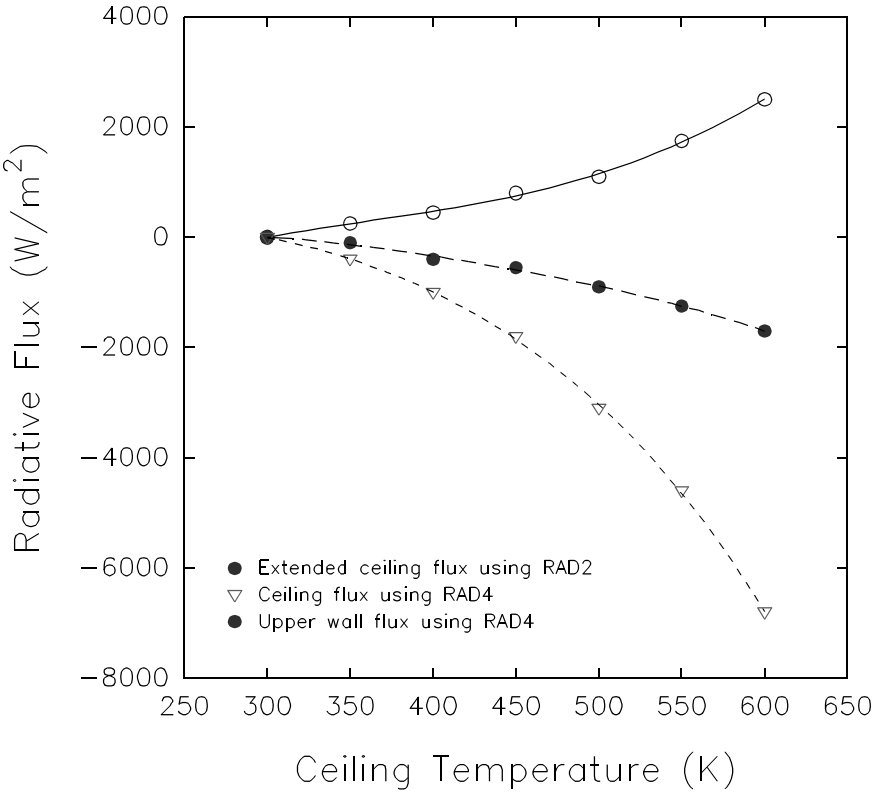

Figure 13. An example of two-wall and four-wall calculations for radiation exchange on a ceiling and wall surface.

$$\dot{q} = hA_s\left(T_g - T_s\right) . \tag{89}$$

The convective heat transfer coefficient, *h*, is defined in terms of the Nusselt number, a dimensionless temperature gradient at the surface, which is defined via correlations of the form

$$h = \frac{Nu_L k}{L} = CRa_L^n \tag{90}$$

where the Rayleigh number,

$$Ra_L = Gr_L Pr = \frac{g\beta\left(T_s - T_g\right)L^3}{\nu\alpha} \tag{91}$$

is based on a characteristic length, *L*, of the geometry. The power *n* is typically 1/4 and 1/3 for laminar and turbulent flow, respectively. All properties are evaluated at the film temperature, T_f

$= (T_s+T_g)/2$. The typical correlations applicable to the problem at hand are available in the literature [51]:

Geometry	Correlation	Restrictions
Walls	$Nu_L = \left(0.825 + \frac{0.387 Ra_L^{1/6}}{\left(1 + (0.492/Pr)^{9/16}\right)^{8/27}} \right)^2 \approx 0.12\ Ra_L^{1/3}$	none
Ceilings and floors (hot surface up or cold surface down)	$Nu_L = 0.13\ Ra_L^{1/3}$	$2 \cdot 10^8 \le Ra_L \le 10^{11}$
Ceilings and floors (cold surface up or hot surface down)	$Nu_L = 0.16\ Ra_L^{1/3}$	$10^8 \le Ra_L \le 10^{10}$

The thermal diffusivity, α, and thermal conductivity, k, of air are defined as a function of the film temperature from data in reference [51].

$$\alpha = 1.0\times10^{-9}\ T_f^{7/4}$$
$$k = \left(\frac{0.0209+2.33\times10^{-5}T_f}{1-0.000267T_f} \right) \qquad (92)$$

Implementation: The algorithm is implemented as described above in the routine CONVEC in CFAST. The values of the correlation coefficients have changed in the new algorithm. In the old implementation, these were 0.21 and 0.012 for hot surface up and hot surface down respectively. In the new implementation, these are 0.16 and 0.13. The new values come from currently accepted engineering literature pertaining to this general area. As an example of the effect of the new algorithm, Figure 14 shows layer and wall temperatures for a single room test case with a relatively small 100 kW fire. Only minor differences are seen in the temperatures. For larger fires, the effect should be even less pronounced since convection will play a lesser role as the temperatures rise. A major advantage in the new algorithm should be a speed increase due to the closer correlation coefficients and smooth transition for cases where the surfaces are cooling – a point where the existing code tends to slow dramatically.

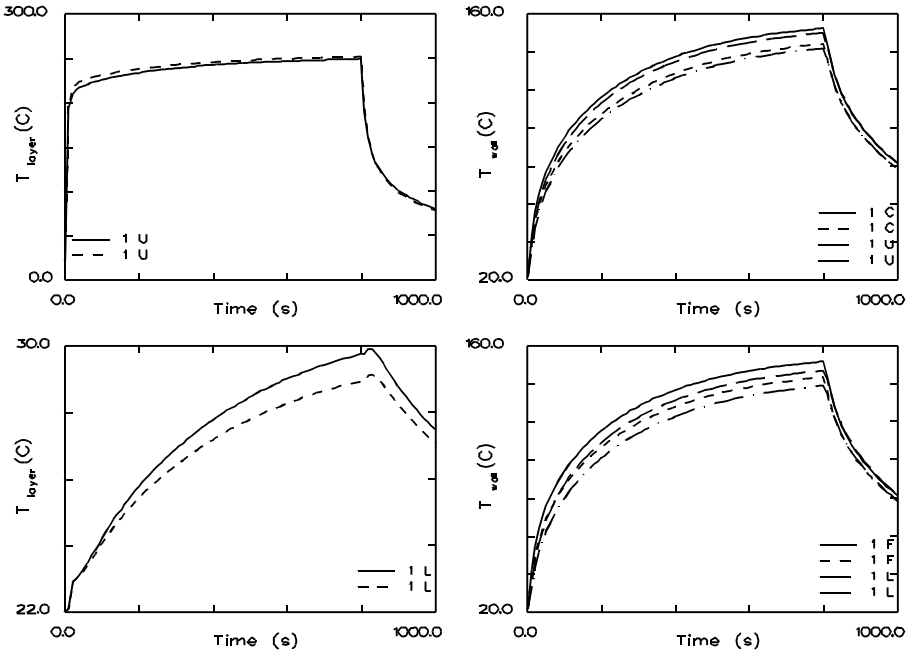

Figure 14. Effects on layer and wall temperatures of modifications to the convection algorithm in CFAST.

3.3.5.3 Conduction

Heat loss or gain between a wall and a gas layer is due to convection or radiation not conduction. Conduction transfers heat within the wall. Therefore, source terms for conduction do not appear in the gas layer ordinary differential equations. However, convection and radiative heat transfer calculations provide the boundary conditions for the conduction algorithm discussed below.

The partial differential equation which governs the heat transfer in solids is

$$\frac{\partial T}{\partial t} = \frac{k}{\rho c}\nabla^2 T \tag{93}$$

It must be solved by a different technique than is used for the ordinary differential equations used to model gas layer quantities. We assume that the coefficients k, ρ and c are independent of temperature throughout the material. This may not be the case, especially for some materials such as gypsum for which the value of k may vary by a factor of two or more. However, to the accuracy that we know most of the thermal properties, it is a reasonable approximation.

Procedures for solving 1-d heat conduction problems are well known. For finite difference methods such as backward difference (fully implicit), forward difference (fully explicit) or Crank-Nicolson, see [52]. For finite element methods see [53].

A finite difference approach [54] using a non-uniform spatial mesh is used to advance the wall temperature solution. The heat equation is discretized using a second order central difference for the spatial derivative and a backward differences for the time derivative. The resulting tri-diagonal system of equations is then solved to advance the temperature solution to time $t+\Delta T$. This process is repeated , using the work of Moss and Forney [54], until the heat flux striking the wall (calculated from the convection and radiation algorithms) is consistent with the wall temperature gradient at the surface via Fourier's law

$$q'' = -K\frac{dT}{dx}$$

where K is the thermal conductivity. This solution strategy requires a differential algebraic (DAE) solver that can simultaneously solve both differential (gas ODE's) and algebraic equations (Fourier's law). With this method, only one or two extra equations are required per wall segment (two if both the interior and exterior wall segment surface temperatures are computed). This solution strategy is more efficient than the method of lines since fewer equations need to be solved. Wall segment temperature profiles, however, still have to be stored so there is no decrease in storage requirements. Conduction is then coupled to the room conditions by temperatures supplied at the interior boundary by the differential equation solver. The exterior boundary condition types (constant flux, insulated, or constant temperature) are specified in the configuration of CFAST.

A non-uniform mesh scheme was chosen to allow breakpoints to cluster near the interior and exterior wall segment surfaces. This is where the temperature gradients are the steepest. A breakpoint x_b was defined by $x_b=MIN(x_p,W/2)$,where $x_p = 2(\alpha t_{final})^{\frac{1}{2}}\ \mathrm{erfc}^{-1}(.05)$ and erfc^{-1} denotes the inverse of the complementary error function. The value x_p is the location in a semi-infinite wall where the temperature rise is 5 % after t_{final} seconds and is sometimes called the penetration depth. Eighty % of the breakpoints were placed on the interior side of x_b and the remaining 20 % were placed on the exterior side.

To illustrate the method, consider a one room case with one active wall. There will be four gas equations (pressure, upper layer volume, upper layer temperature, and lower layer temperature) and one wall temperature equation. Implementation of the gradient matching method requires that storage be allocated for the temperature profile at the previous time, t, and at the next time, $t + \delta t$. Given the profile at time t and values for the five unknowns at time $t + \delta t$ (initial guess by the solver), the temperature profile is advanced from time t to time $t + \delta t$. The temperature profile gradient at $x = 0$ is computed followed by the residuals for the five equations. The DAE solver adjusts the solution variables and the time step until the residuals for all the equations are

below an error tolerance. Once the solver has completed the step, the array storing the temperature profile for the previous time is updated, and the DAE solver is ready to take its next step.

One limitation of our implementation of conduction is that it serves only as a loss term for enthalpy. Heat lost from a compartment by conduction is assumed to be lost to the outside ambient. In reality, compartments adjacent to the room which contains the fire can be heated, possibly catastrophically, by conducted energy not accounted for in the model. Although solving the conduction equations for this situation is not difficult, the geometrical specification is. For this reason, we have chosen to assume that the outside of a boundary is always the ambient. A means to connect compartments physically so that heat can be transported by conduction is under active study.

3.3.5.4 Inter-compartment Heat Transfer

Heat transfer between vertically connected compartments is modeled by merging the connected surfaces for the ceiling and floor compartments or for the connected horizontal compartments. A heat conduction problem is solved for the merged walls using a temperature boundary condition for both the near and far wall. As before, temperatures are determined by the DAE solver so that the heat flux striking the wall surface (both interior and exterior) is consistent with the temperature gradient at that surface. This option is implemented with the CFCON (for vertical heat transfer) and the HHEAT (for horizontal heat transfer) keywords.

For horizontal heat transfer between compartments, the connections can be between partial wall surfaces, expressed as a fraction of the wall surface. CFAST first estimates conduction fractions analogous to radiative configuration factors. For example, a conduction fraction between a rear wall in room 1 and a front wall room 2 is the heat flux fraction from the room 2 wall that strikes contributes to room 1's wall heat transfer. Alternatively, these fractions can be specified on the HHEAT keyword line. Once these fractions are determined, an average flux, q_{avg}, is calculated using

$$q_{avg} = \sum_{walls} F_{ij} q_{wall_j}$$

where F_{ij} is the fraction of flux from wall i that contributes to wall j, q_{wallj} is the flux striking wall j.

3.3.5.5 Heating of Targets

The target calculation is similar to the heat conduction through boundaries. The net flux striking a target can be used as a boundary condition for an associated heat conduction problem in order to compute the surface temperature of the target. This temperature can then be used to estimate the conditions at the target, ie whether the target will ignite. Alternatively, if the target is assumed to be thin, then its temperature quickly rises to a level where the net heat flux striking the target is zero, ie to a steady state. The calculation is done using the concept of net heat flux,

which literally implies a Kirchoff law for the radiation. While this should be obvious, it has not always been done this way in fire modeling.

The net heat flux, $\Delta''q_t$, striking a target t is given by

$$\Delta'' q_t = q''_{rad}(in) + q''_{convec} - q''_{rad}(out) \tag{95}$$

where $q''_{rad}(in)$ is the incoming radiative flux, q''_{convec} is the convective flux and $q''_{rad}(out)$ is the outgoing radiative flux, Figure 15. The incoming radiative flux can be split into components from each fire, $q''_{f,t}$, each wall segment, $q''_{w,t}$ and each gas layer, $q''_{g,t}$. The incoming radiative flux, $q''_{rad}(in)$ is obtained by summing over all fires, wall segments, and gas layers to obtain

$$q_{rad}(in) = \sum_f q''_{f,t} + \sum_w q''_{w,t} + \sum_g q''_{g,t} \tag{96}$$

The outgoing radiative flux, $q''_{rad}(out)$, has contributions due to target emission or emissive power, $\epsilon_t \sigma T^4_t$, and a fraction, $1-\epsilon_t$, of the incoming radiative flux that is reflected at the target surface. It is given by

$$q''^{out}_{rad} = (1-\epsilon_t) q''^{in}_{rad} + \epsilon_t \sigma T_t^4 \tag{97}$$

where ϵ_t is the emittance of the target and σ is the Stefan-Boltzman constant. Substituting eqs (96) and (97) into (95) we obtain

$$\Delta'' q_t = \epsilon_t q''_{rad}(in) + q''_{convec} - \epsilon_t \sigma T_t^4 = \epsilon_t \left(\sum_f q''_{f,t} + \sum_w q''_{w,t} + \sum_i q''_{g,t} \right) + q''_{convec} - \epsilon_t \sigma T_t^4 \tag{98}$$

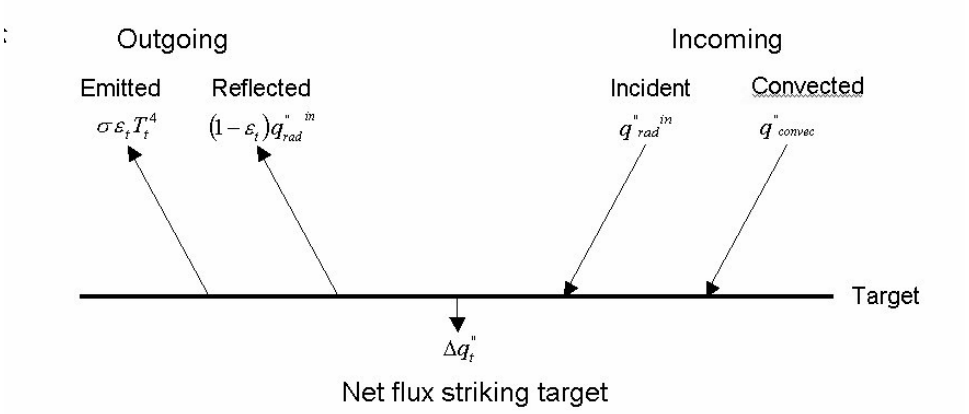

Figure 15. Radiative and convective heat transfer at a target.

The heat flux, $\Delta''q_t$, specified by eq(98) can be used in one of two ways: to estimate the surface temperature of the target or as a boundary condition to solve the heat conduction problem

$$\frac{\partial T}{\partial t}(x,t) = \frac{k}{\rho C}\frac{\partial^2 T}{\partial x^2}(x,t) \tag{99}$$

$$T(x,0) = T_0(x) \tag{100}$$

$$-k\frac{\partial T}{\partial x}(0,t) = \Delta'' q_t \tag{101}$$

$$-k\frac{\partial T}{\partial x}(L,t) = 0 \tag{102}$$

for the target temperature profile T where k, ρ and C are the thermal conductivity, density and heat capacity of the target, L is the thickness of the target and T_0 is the target's initial temperature profile.

Alternatively, we can assume that the target temperature is always at steady state, *i.e.* that $\Delta''q_t = 0$. A temperature, T_t, can then be found using Newton's method that will satisfy $\Delta''q_t = 0$. To illustrate, suppose that the convective flux is given by $q''_{convec} = c(T_g - T_t)$ where c is a convective heat transfer coefficient and T_g is the gas temperature adjacent to the target. Then, eq(98) can be simplified to

$$f(T_t) = \epsilon_t \sigma T_t^4 - c(T_g - T_t) - \epsilon_t q''_{rad}(in) = -\Delta'' q_t \tag{103}$$

We wish to find a temperature T_t satisfying $f(T_t) = -\Delta''q_t = 0$. The non-linear eq(103) can be solved using Newton's method. There are three steps necessary to complete this calculation: 1) calculate the heat transfer through the compartment; 2) calculate the heat flux to the target or object; and finally 3) compute the target temperature. In order to calculate the radiation heat transfer from fires, gas layers and wall surfaces to targets we must be able to calculate configuration factors, gas layer transmissivity and absorptance.

Configuration Factors: Figure 16 illustrates the definition of a configuration factor between two finite areas. A configuration factor between two finite areas 1 and 2 denoted F_{1-2} is the fraction of radiant energy given off by surface 1 that is intercepted by surface 2. The following terms are needed to define a configuration factor mathematically. Vectors n_1 and n_2 are unit vectors perpendicular to surfaces 1 and 2. s is a vector with origin on surface 1 and destination on

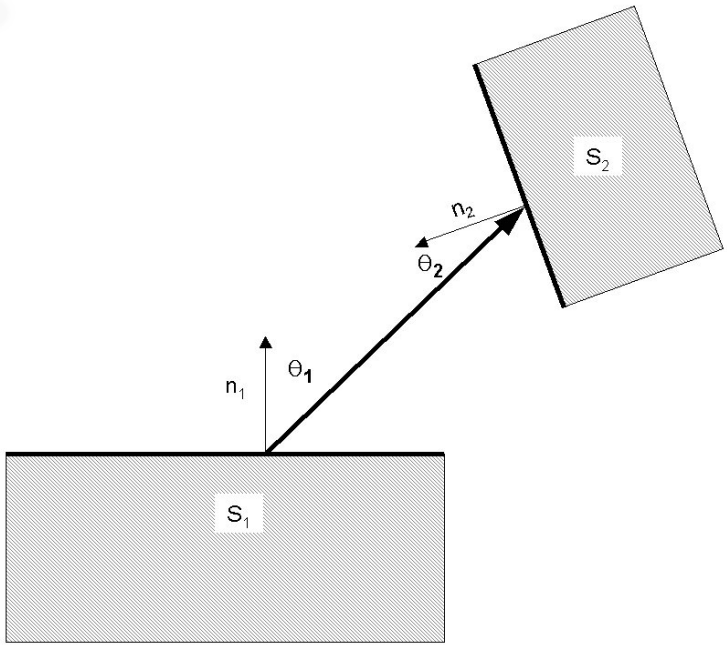

Figure 16. Setup for a configuration factor calculation
between two arbitrarily oriented finite areas

surface 2. $S = \|s\|$ is the length of this vector. The angle between n_1 and s is θ_1. Similarly the angle between the vector n_2 and $-s$ is θ_2. The sign is reversed because the origin of s is on surface 1 not 2. The cosines of angles θ_1 and θ_2 are

$$\cos(\theta_1) = \frac{n_1 \cdot s}{\|s\|} \tag{104}$$

The configuration factor, $F_{1\text{-}2}$ is then given by

$$F_{1-2} = \frac{1}{A_1} \int_{A_1} \int_{A_2} \frac{\cos(\theta_1) \cdot \cos(\theta_2)}{\pi S^2} dA_1 dA_2 \tag{105}$$

When the surfaces A_1 and A_2 are far apart relative to their surface area, eq(105) can be approximated by assuming that θ_1, θ_2 and S are constant over the region of integration to obtain

$$F_{1-2} \approx \frac{\cos(\theta_1)\cos(\theta_2)}{\pi S^2} A_2 \tag{106}$$

The dot product form of the cosine defined in eqs (104) and ? can be substituted into the previous equation to obtain

$$F_{1-2} \approx -\frac{(n_1 \cdot s)(n_2 \cdot s)}{\pi S^4} A_2 \ . \tag{107}$$

A simpler, though less accurate, approximation for the configuration factor can be made using the following observation. Suppose that surface 1 is a differential element at the center of a base of a hemisphere with area A_H and surface 2 is a region on this hemisphere with area A_2, then $F_{1-2} = A_2/A_H$. Therefore, if surface 1 is a differential element (*i.e.* our target) in a compartment and surface 2 is a wall in this compartment, then F_{1-2} can be approximated by

$$F_{1-2} \approx A_2/A_{total} \tag{108}$$

where A_2 is the area of the wall and A_{total} is the total area of the surfaces 'seen' by the target. The above equation rather than eq(107) is used to approximate the configuration factors.

Transmissivity: The transmissivity of a gas volume is the fraction of radiant energy that will pass through it unimpeded and is given by

$$\tau(y) = e^{-ay} \tag{109}$$

where *a* is the absorptance per unit length of the gas volume and *y* is a characteristic path length.

In a two layer zone model, a path between an object (fire, wall segment, *etc.*) and a target may traverse through both layers. In this case, the length of the path in the lower layer, y_L, can be computed given the total distance *S* between the object and target, and the elevations of the target, y_t, object, y_o and layer, y_{lay}, to be

$$y_L = \begin{Bmatrix} 0, & y_{lay} < y_{\min} \\ \dfrac{y_{lay} - y_{\min}}{y_{\max} - y_{\min}} S, & y_{\min} \le y_{lay} \le y_{\max} \\ S, & y_{lay} \ge y_{\max} \end{Bmatrix} \tag{110}$$

where

$$\begin{aligned} y_{\min} &= \min(y_0, y_t) \\ y_{\max} &= \max(y_0, y_t) \ , \end{aligned} \tag{111}$$

the path length in the upper layer is $y_U = S - y_L$, and the transmittance of the lower (upper) layer is denoted τ_L (τ_U).

Absorptivity: The absorptivity, α, of a gas volume is the fraction of radiant energy absorbed by that volume. For a grey gas $\alpha + \tau = 1$. The absorptivity of the lower (upper) layer is denoted α_L (α_U).

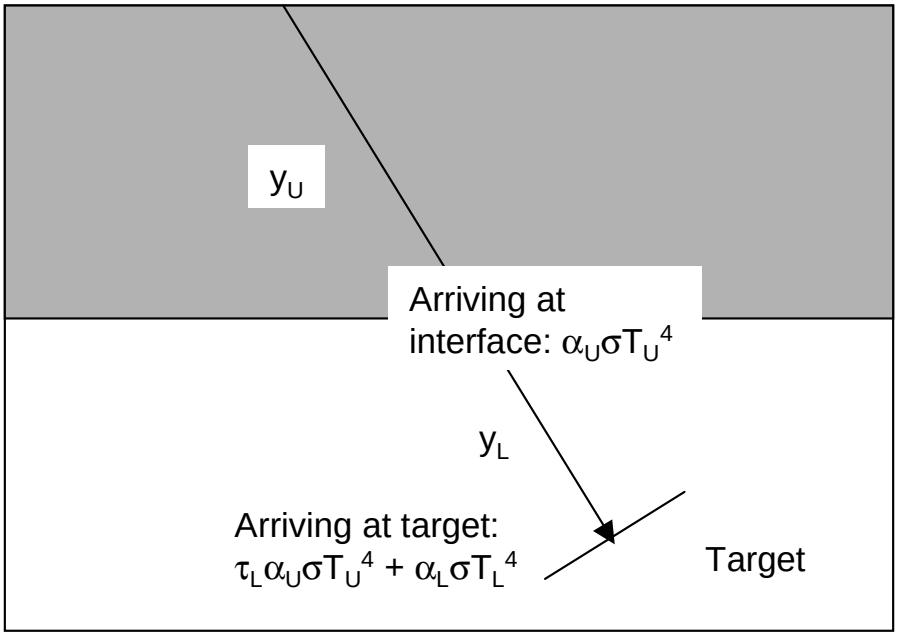

$\alpha_U = 1 - \exp(-a_U y_U)$ = emittance of upper layer

$\alpha_L = 1 - \exp(-a_L y_L)$ = emittance of lower layer

$\tau_L = \exp(-a_L y_L)$ = transmittance of lower layer

Figure 17. Radiative heat transfer from a wall surface in the upper layer to a target in the lower layer.

3.3.5.6 Computing the Heat Flux to a Target

There are four components of heat flux to a target: fires, walls, gas layer radiation and gas layer convection.

Heat Flux from a Fire to a Target: Figure 18 illustrates terms used to compute heat flux from a fire to a target. Let n_t be a unit vector perpendicular to the target and θ_t be the angle between the vectors -s and n_t.

Using the definition that q_f is the radiative portion of the energy release rate of the fire, then the heat flux on a sphere of radius S due to this fire is $q_f/(4\pi S^2)$. Correcting for the orientation of the target and accounting for heat transfer through the gas layers, the heat flux to the target is

$$q''_{f,t} = \frac{q_f}{4\pi S^2}\cos(\theta_t)\tau_U(y_u)\tau_L(y_L) = -q_f\frac{n_t S}{4\pi S^3}\tau_U(y_u)\tau_L(y_L) \qquad (112)$$

Radiative Heat Flux from a Wall Segment to a Target: Figure 17 illustrates terms used to compute heat flux from a wall segment to a target. The flux, $q''_{w,t}$, from a wall segment to a target can then be computed using

$$q''_{w,t} = \frac{A_w q''_w(out) F_{w-t}}{A_t}\tau_U(y_U)\tau_L(y_L) \qquad (113)$$

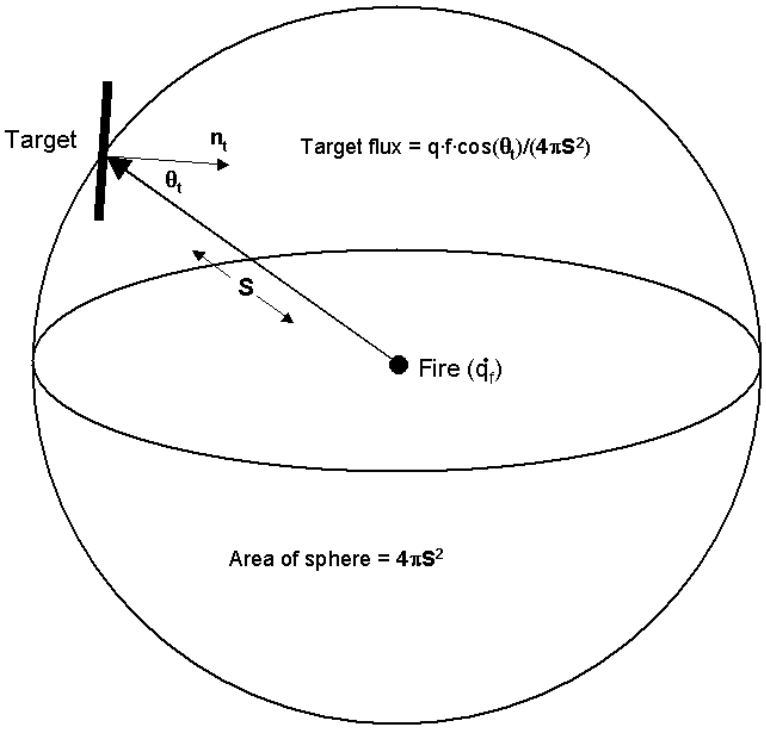

Figure 18. Radiative heat transfer from a point source fire to a target.

where $q''_w(out)$ is the flux leaving the wall segment, A_w, A_t are the areas of the wall segment and target respectively, F_{w-t} is the fraction of radiant energy given off by the wall segment that is intercepted by the target (*i.e.* a configuration factor) and $\tau_U(y_U)$ and $\tau_L(y_L)$ are defined as before.

Equation (112) can be simplified using the symmetry relation $A_w F_{w-t} = A_t F_{t-w}$ (see [55], eq(7-25) or [56]) to obtain

$$q''_{w,t} = q''_w(out) F_{t-w} \tau_U(y_U) \tau_L(y_L) \tag{114}$$

where

$$q''_w(out) = \sigma T_w^4 - (1 - \epsilon_w) \frac{\Delta q''_w}{\epsilon_w} \tag{115}$$

(see [55, eq (17-15)]) and $\sigma = 5.67^{-8}$ $W/(m^2K^4)$, T_w is the temperature of the wall segment, ϵ_w is the emissivity of the wall segment and $\Delta q_w''$ is the net flux striking the wall segment.

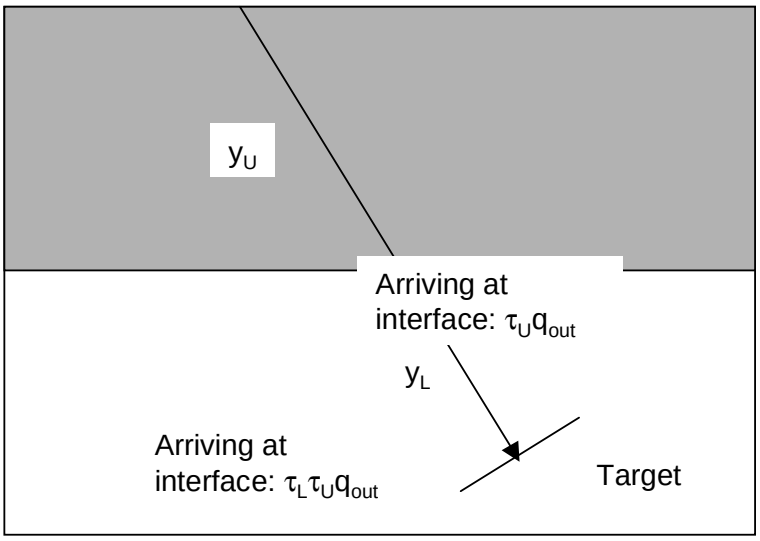

$\tau_U = \exp(-a_U y_U)$ = transmittance of upper layer

$\tau_L = \exp(-a_L y_L)$ = transmittance of lower layer

Figure 19. Radiative heat transfer from the upper and lower layer gas layers to a target in the lower layer.

Radiation from the Gas Layer to the Target: Figure 19 illustrates the setup for calculating the heat flux from the gas layers to the target. The upper and lower gas layers in a room contribute to the heat flux striking the target if the layer absorptances is non-zero. Heat transfer does not occur to the target when there are no fires and conditions are isothermal, i.e., target, wall segments and gas layers are at the same temperature. Therefore, substituting $q''_{f,t}=0$ into eq (98) we must have

$$\Delta'' q_t \;=\; 0 \;=\; \epsilon_t\left(\sum_w q''_{w,t} + \sum_i q''_{q,t} - \sigma T_t^4\right) \;+\; q''_{convec} \tag{116}$$

whenever $T_t = T_g = T_w$ for each wall segment and each gas layer.

Let $q''_{w,t}(gas)$ denote the flux striking the target due to the gas g in the direction of wall segment w. Then

$$q''_{w,t}(gas) \;=\; \begin{Bmatrix} \sigma F_{t-w}(T_L^4 \alpha_L \tau_U \;+\; T_U^4 \alpha_U)\, w \;\; is \; in the \;\; lower \;\; layer \\ \sigma F_{t-w}(T_U^4 \alpha_U \tau_L \;+\; T_L^4 \alpha_L) \;\; w \;\; is \;\; in \;\; the \;\; upper \;\; layer \end{Bmatrix} \tag{117}$$

The total target flux due to the gas (upper or lower layer) is obtained by summing eq (117) over each wall segment or

$$q''_{g,t} \;=\; \sum_w q''_{w,t}(gas). \tag{118}$$

The procedure expressed in eqs (117) and (118) for computing heat flux to the target from the gas layers satisfies the iso-thermal condition, eq (116), that no heat transfer occurs when all material have the same temperature. To see this, assume that $T_t = T_w = T_g$ and substitute eqs (114), (117) and (118) into eq (116) . Then $q''_{convec}=0$ and

$$\begin{aligned} \sum_w q''_{w,t} + \sum_i q''_{g,t} \;=\; & \sum_{w_{upper}} F_{t-w}\left(q''_w(out)\tau_U \tau_L + \sigma\left(T_t^4 \alpha_U \tau_L + T_t^4 \alpha_L\right)\right) \;+ \\ & \sum_{w_{lower}} F_{t-w}\left(q''_w(out)\tau_L \tau_U + \sigma\left(T_t^4 \alpha_L \tau_U + T_t^4 \alpha_U\right)\right) \\ =\; & \sigma T_t^4 \sum_{w_{upper}} F_{t-w}\left(\tau_U \tau_L + \alpha_U \tau_L + \alpha_L\right) \;+ \\ & \sigma T_t^4 \sum_{w_{lower}} F_{t-w}\left(\tau_L \tau_U + \alpha_L \tau_U + \alpha_U\right) \\ =\; & \sigma T_t^4 \sum_w F_{t-w} \;=\; \sigma t_t^4 \end{aligned} \tag{119}$$

since $\tau_L\tau_U + \alpha_L\tau_U + \alpha_U = 1 = \tau_U\tau_L + \alpha_U\tau_U + \alpha_L$, $q_w''(\text{out}) = \sigma T_t^4$ ($\Delta q''_w$ in eq (118) is zero when conditions are iso-thermal) and $\Sigma_w F_{t-w} = 1$.

Convective Heat Transfer from a Gas Layer to a Target: The convective heat transfer from an adjoining gas layer to the target can be computed using existing CFAST routines. These routines require the orientation of the target, i.e., whether it is horizontal or vertical.

3.3.5.7 Computing the Target Temperature

The steady state target temperature, T_t can be found by solving the equation $f(T_t) = 0$ where $f(T_t)$ is defined in eq (103). This can be done by using the Newton iteration

$$T_{new} = T_{old} - \frac{f(T_{old})}{f'(T_{old})} \tag{120}$$

where

$$\begin{aligned} f(T_t) &= \epsilon_t \sigma T_t^4 - c(T_g - T_t) - \epsilon_t q''_{rad}(in) \\ f'(T_t) &= \frac{d}{dT_t}\left(\epsilon_t \sigma T_t^4 - q''_{convec}\right) = 4\epsilon_t \sigma T_t^3 + c - \frac{dc}{dT_t}(T_g - T_t) \end{aligned} \tag{121}$$

Note that $q''_{rad}(in)$ does not depend on the target temperature T_t so that $d/dT_t(q''_{rad}(in)) = 0$. If the convective heat transfer coefficient, c, in the above equation is independent of T_t then $d/dT_t(q''_{convec}) = -c$, otherwise (e.g. in the case of CFAST) this derivative may be evaluated numerically using finite differences. Equation (120) is iterated until the difference $T_{new} - T_{old}$ is sufficiently small.

3.3.6 Ceiling Jet

Relatively early in the development of a fire, fire-driven ceiling jets and gas-to-ceiling convective heat transfer can play a significant role in room-to-room smoke spread and in the response of near-ceiling mounted detection hardware. Cooper [57] details a model and computer algorithm to predict the instantaneous rate of convective heat transfer from fire plume gases to the overhead ceiling surface in a room of fire origin. The room is assumed to be a rectangular parallelopiped and, at times of interest, ceiling temperatures are simulated as being uniform. Also presented is an estimate of the convective heat transfer due to ceiling-jet driven wall flows. The effect on the heat transfer of the location of the fire within the room is taken into account. This algorithm has been incorporated into the CFAST model. In this section, we provide an overview of the model. Complete details are available in reference [57].

A schematic of a fire, fire plume, and ceiling jet is shown in Figure 20 The buoyant fire plume rises from the height Z_{fire} toward the ceiling. When the fire is below the layer interface, its mass and enthalpy flow are assumed to be deposited into the upper layer at height Z_{layer}. Having penetrated the interface, a portion of the plume typically continues to rise toward the ceiling. As it impinges on the ceiling surface, the plume gases turn and form a relatively high temperature, high velocity, turbulent ceiling jet which flows radially outward along the ceiling and transfers heat to the relatively cool ceiling surface. The convective heat transfer rate is a strong function

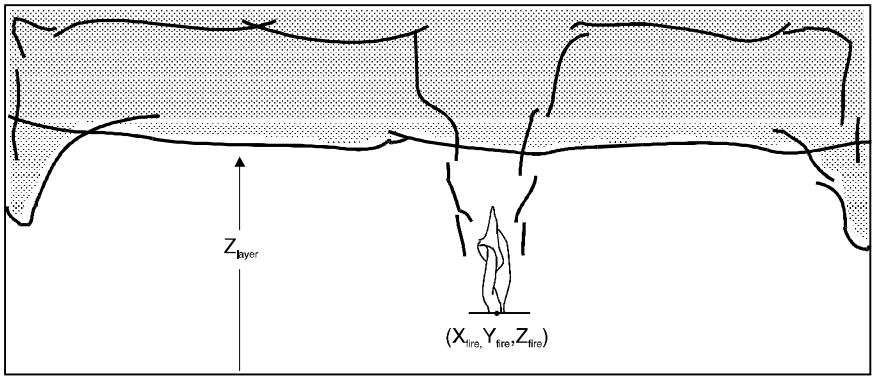

Figure 20. Convective heat transfer to ceiling and wall surfaces via the ceiling jet.

of the radial distance from the point of impingement, reducing rapidly with increasing radius. Eventually, the relatively high temperature ceiling jet is blocked by the relatively cool wall surfaces [58]. The ceiling jet then turns downward and outward in a complicated flow along the vertical wall surfaces [59], [60]. The descent of the wall flows and the heat transfer from them are eventually stopped by upward buoyant forces. They are then buoyed back upward and mix with the upper layer.

The average convective heat flux from the ceiling jet gases to the ceiling surface, Q_{ceil}, can be expressed in integral form as

$$\dot{Q}_{ceil} = \int_0^{X_{wall}} \int_0^{Y_{wall}} \dot{q}''_{ceil}(x,y)\, dxdy \tag{122}$$

The instantaneous convective heat flux, $q''_{ceil}(X,Y)$ can be determined as derived by Cooper [57]:

$$\dot{q}''_{ceil}(x,y) = h_l \left(T_{ad} - T_{ceil}\right) \tag{123}$$

where T_{ad}, a characteristic ceiling jet temperature, is the temperature that would be measured adjacent to an adiabatic lower ceiling surface, and h_l is a heat transfer coefficient. h_l and T_{ad} are given by

$$\frac{h_l}{\tilde{h}} = \begin{cases} 8.82 Re_H^{-1/2} Pr^{-2/3} \left(1 - \left(5 - 0.284 Re_H^{2/5}\right) \frac{r}{H} \right) & 0 \le \frac{r}{H} < 0.2 \\ 0.283 Re_H^{0.3} Pr^{-2/3} \left(\frac{r}{H} \right)^{-1.2} \frac{\frac{r}{H} - 0.0771}{\frac{r}{H} + 0.279} & 0.2 \le \frac{r}{H} \end{cases} \tag{124}$$

$$\frac{T_{ad} - T_u}{T_u Q_H^{*2/3}} = \begin{cases} 10.22 - 14.9 \frac{r}{H} & 0 \le \frac{r}{H} < 0.2 \\ 8.39 f\left(\frac{r}{H}\right) & 0.2 \le \frac{r}{H} \end{cases} \tag{125}$$

where

$$f\left(\frac{r}{H}\right) = \frac{1 - 1.10\left(\frac{r}{H}\right)^{0.8} + 0.808\left(\frac{r}{H}\right)^{1.6}}{1 - 1.10\left(\frac{r}{H}\right)^{0.8} + 2.20\left(\frac{r}{H}\right)^{1.6} + 0.690\left(\frac{r}{H}\right)^{2.4}} \tag{126}$$

$$r = \left(\left(X - X_{fire}\right)^2 + \left(Y - Y_{fire}\right)^2 \right)^{\frac{1}{2}} \tag{127}$$

$$\tilde{h} = \rho_u c_p g^{1/2} H^{1/2} \dot{Q}_H^{*1/3}; \qquad Re_H = \frac{g^{1/2} H^{3/2} \dot{Q}_H^{*1/3}}{\nu_u}; \qquad \dot{Q}_H^* = \frac{\dot{Q}'}{\rho_u c_p T_u (gH)^{1/2} H^2} \tag{128}$$

$$\dot{Q}' = \begin{cases} \dot{Q}_{fc} \frac{\sigma \dot{M}^*}{1+\sigma} & Z_{fire} < Z_{layer} < Z_{ceil} \\ \dot{Q}_{fc} & \begin{matrix} Z_{fire} \ge Z_{layer} \\ Z_{layer} = Z_{ceil} \end{matrix} \end{cases} \qquad \dot{M}^* = \begin{cases} 0 & -1 < \sigma \le 0 \\ \frac{1.04599\sigma + 0.360391\sigma^2}{1 + 1.37748\sigma + 0.360391\sigma^2} & \sigma > 0 \end{cases} \tag{129}$$

$$\sigma = \frac{1 - \frac{T_u}{T_l} + C_T \dot{Q}_{EQ}^{*2/3}}{\frac{T_u}{T_l}}; \qquad C_T = 9.115 \tag{130}$$

$$\dot{Q}_{EQ}^* = \left(\frac{0.21 \dot{Q}_{fc}}{c_p T_l \dot{m}_p} \right)^{3/2} \tag{131}$$

In the above, H is the distance from the (presumed) point source fire and the ceiling, X_{fire} and Y_{fire} are the position of the fire in the room, Pr is the Prandtl number (taken to be 0.7) and ν_u is the kinematic viscosity of the upper layer gas which is assumed to have the properties of air and can be estimated from $\nu_u = 0.04128(10^7)T_u^{5/2}/(T_u+110.4)$. Q_H^* and Q_{EQ}^* are dimensionless numbers and are measures of the strength of the plume at the ceiling and the layer interface, respectively.

When the ceiling jet is blocked by the wall surfaces, the rate of heat transfer to the surface increases. Reference [57] provides details of the calculation of wall surface area and convective heat flux for the wall surfaces.

3.4 Detection

Detection is modeled using temperatures obtained from the ceiling jet[61]. Rooms without fires do not have ceiling jets. Sensors in these types of rooms use gas layer temperatures instead of ceiling jet temperatures. The characteristic smoke detector temperature is simply the temperature of the ceiling jet (at the location of the smoke detector). The characteristic heat detector temperature is modeled using the differential equation[62]

$$\frac{dT_L}{dt} = \frac{\sqrt{S(t)}}{RTI}\left(T_g(t) - T_L(t)\right) \tag{132}$$

$$T_L(0) = T_g(0) \tag{133}$$

where T_L, T_g are the link and gas temperatures, S is the flow speed of the gas and RTI (response time index) is a measure of the sensor's sensitivity to temperature change (thermal inertia). The heat detector differential eq (132) may be rewritten to

$$\frac{dT(t)}{dt} = a(t) - b(t)T(t) \tag{134}$$

$$T(t_0) = T_0$$

where

$$a(t) = \frac{\sqrt{S(t)}\,T(t)}{RTI}, \qquad b(t) = \frac{\sqrt{S(t)}}{RTI} \tag{136}$$

Equation (134) may be solved using the trapezoidal rule to obtain

$$\frac{T_{i+1}-T_i}{\Delta t} = \frac{1}{2}\left(\left(a_i - b_i T_i\right) + \left(a_{i+1} - b_{i+1} T_{i+1}\right)\right) \tag{137}$$

where the subscript i denotes time at t_i. Equation (137) may be simplified to

$$T_{i+1} = A_{i+1} - b_{i+1} T_{i+1} \tag{138}$$

$$A_{i+1} = T_i + \frac{\Delta t}{2}\left(a_i - b_i T_i + a_{i+1}\right) \tag{139}$$

$$B_{i+1} = \frac{\Delta t}{2} b_{i+1} \tag{140}$$

which has a solution

$$T_{i+1} = \frac{A_{i+1}}{1+B_{i+1}} = \frac{1-\frac{\Delta t}{2} b_i}{1+\frac{\Delta t}{2} b_{i+1}} T_i + \frac{\Delta t}{1+\frac{\Delta t}{2} b_{i+1}}\left(\frac{a_i + a_{i+1}}{2}\right) \tag{141}$$

Equation (141) reduces to the trapezoidal rule for integration when $b(t) = 0$. When $a(t)$ and $b(t)$ are constant (the gas temperature, T_g, and gas velocity, S are not changing), eq (132) has the solution

$$T(t) = \frac{a}{b} + \frac{e^{-b(t-t_0)}(b T_0 - a)}{b} = T_g + e^{-\sqrt{S(t)}(t-t_0)/RTI}\left(T_0 - T_g\right) \tag{142}$$

3.5 Suppression

For suppression, the sprinkler is modeled using a simple model [63] generalized for varying sprinkler spray densities [64]. Fire suppression in CFAST is then modeled by attenuating all fires in the room where the sensor activated by a term of the form $e^{-(t-tact)/trate}$ where t_{act} is the time when the sensor activated and t_{rate} is a constant determining how quickly the fire attenuates. The term

t_{rate} can be related to spray density of a sprinkler using a correlation developed in [64]. The suppression correlation was developed by modifying the heat release rate of a fire. For $t>t_{act}$ the heat release is given by

$$\dot{q}_{fire}(t) = e^{-(t-t_{act})/3.0\dot{q}_{spray}^{-1.8}}\dot{q}(t_{act})$$

where q_{spray} is the spray density of a sprinkler. Note that decay rate can be formulated in terms of either the attenuation rate or the spray density. Both options are available. t_{rate} can be expressed in terms of q_{spray} as

$$t_{rate} = 3.0\dot{q}_{spray}^{-1.8} \tag{144}$$

$$t_{50\%} = 3\ln(2)\dot{q}_{spray}^{-1.8} \tag{145}$$

and the decay time (time to 50% attenuation) as the input line allows the specification of either the spray density of the sprinkler q_{spray} or the time required to reduce the fire release rate by 50%, $t_{50\%}$. The chemistry routine performs the combustion chemistry, making sure that the fuel burned is consistent with the available oxygen. If detection has occurred then the mass and energy release rates are attenuated by the term $e^{-(t-tact)}=t_{rate}$ to obtain

$$\dot{m}_{pyrols}(t) = e^{-(t-t_{act})/t_{rate}}\ \dot{m}_{pyrols}(t_{act}) \tag{146}$$

$$\dot{m}_{pyrols}(t) = e^{-(t-t_{act})/t_{rate}}\ \dot{m}_{pyrols}(t_{act}). \tag{147}$$

Another approach would be to calculated the $m_{pyrols}(t)$ mass production rate that would result in the desired constrained energy release rate computed in CHEMIE. This is not practical since the energy release rate $q_{chemie}(t)$ is a non-linear function (via the plume entrainment function) of the pyrolis rate $m_{pyrols}(t)$.

There are assumptions and limitations in this approach. Its main deficiency is that it assumes that sufficient water is applied to the fire to cause a decrease in the rate of heat release. This suppression model cannot handle the case when the fire overwhelms the sprinkler. The suppression model as implemented does not include the effect of a second sprinkler. Detection of all sprinklers are noted but their activation does not make the fire go out any faster. Further, multiple fires in a room imply multiple ceiling jets. It is not clear how this should be handled, ie how two ceiling jets should interact. When there is more than one fire, the detection algorithm

uses the fire that results in the worst conditions (usually the closest fire) in order to calculate the fire sensor temperatures. The ceiling jet algorithm that we use results in temperature predictions that are too warm (as compared to ceiling jet full scale experiments of Madrzykowski[65]). This has not been resolved.

3.6 Species Concentration and Deposition

3.6.1 Species Transport

The species transport in CFAST is really a matter of bookkeeping to track individual species mass as it is generated by a fire, transported through vents, or mixed between layers in a compartment. When the layers are initialized at the start of the simulation, they are set to ambient conditions. These are the initial temperature specified by the user, and 23 % by mass (21 % by volume) oxygen, 77 % by mass (79 % by volume) nitrogen, a mass concentration of water specified by the user as a relative humidity, and a zero concentration of all other species. As fuel is burned, the various species are produced in direct relation to the mass of fuel burned (this relation is the species yield specified by the user for the fuel burning). Since oxygen is consumed rather than produced by the burning, the "yield" of oxygen is negative, and is set internally to correspond to the amount of oxygen used to burn the fuel (within the constraint of available oxygen limits discussed in sec. 3.3.1.2).

Each unit mass of a species produced is carried in the flow to the various rooms and accumulates in the layers. The model keeps track of the mass of each species in each layer, and knows the volume of each layer as a function of time. The mass divided by the volume is the mass concentration, which along with the molecular weight gives the concentration in volume % or ppm as appropriate.

For soot, the input for C/CO_2 is used to calculate a "soot" yield from the fire (assuming all the carbon goes to soot). This soot generation is then transported as a species to yield a soot mass concentration to use in the optical density calculation based on the work of Seader and Einhorn[66].

3.6.2 HCl Deposition

Hydrogen chloride produced in a fire can produce a strong irritant reaction that can impair escape from the fire. It has been shown [67] that significant amounts of the substance can be removed by adsorption by surfaces which contact smoke. In our model, HCl production is treated in a manner similar to other species. However, an additional term is required to allow for deposition on, and subsequent absorption into, material surfaces.

The physical configuration that we are modeling is a gas layer adjacent to a surface (Figure 21). The gas layer is at some temperature T_g with a concomitant density of hydrogen chloride, ρ_{HCl}. The mass transport coefficient is calculated based on the Reynolds analogy with mass and heat transfer: that is, hydrogen chloride is mass being moved convectively in the boundary layer, and some of it simply sticks to the wall surface rather than completing the journey during the

convective roll-up associated with eddy diffusion in the boundary layer. The boundary layer at the wall is then in equilibrium with the wall. The latter is a statistical process and is determined by evaporation from the wall and stickiness of the wall for HCl molecules. This latter is greatly influenced by the concentration of water in the gas, in the boundary layer and on the wall itself.

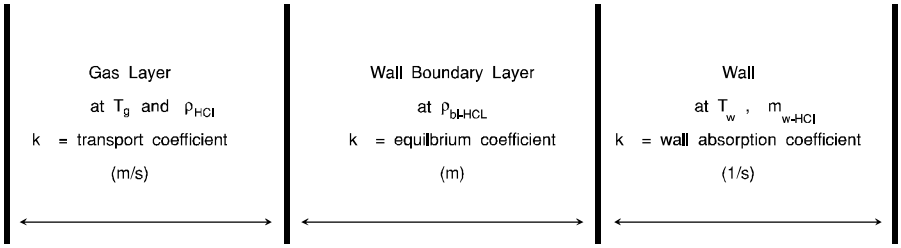

Figure 21. Schematic of hydrogen chloride deposition region.

The rate of addition of mass of hydrogen chloride to the gas layer is given by

$$\frac{d}{dt} m_{HCl} = source - k_c \times \left(\rho_{HCl} - \rho_{blHCl}\right) \times A_w \tag{148}$$

where source is the production rate from the burning object plus flow from other compartments.

For the wall concentration, the rate of addition is

$$\frac{d}{dt} d_{HCl,w} = k_c \times \left(\rho_{HCl} - \rho_{blHCl}\right) - k_s \times m_{HCl,w} \tag{149}$$

where the concentration in the boundary layer, ρ_{blHCl}, is related to the wall surface concentration by the equilibrium constant k_e,

$$\rho_{blHCl} = d_{HCl,w} \; / \; k_e \; . \tag{150}$$

We never actually solve for the concentration in the boundary layer, but it is available, as is a boundary layer temperature if it were of interest. The transfer coefficients are

$$k_c = \frac{\dot{q}}{\Delta T \; \rho_g \; c_p} \tag{151}$$

$$k_e = \frac{b_1 \; e^{1500/T_w}}{1 + b_2 \; e^{1500/T_w} \; \rho_{hcl}} \left(1 + \frac{b_5 \left(\rho_{H_2O}\right)^{b6}}{\left(\rho_{H_2O,sat} - \rho_{H_2O,g}\right)^{b7}} \right) \tag{152}$$

$$k_s = b_3 \; e^{-\left(\frac{b_4}{R \; T_w}\right)} \; . \tag{153}$$

The only values currently available [68] for these quantities are shown in table 4. The "*b*" coefficients are parameters which are found by fitting experimental data to eqs (148) through (153). These coefficients reproduce the adsorption and absorption of HCl reasonably well. Note though that error bars for these coefficients have not been reported in the literature.

Table 4. Transfer coefficients for HCl deposition

Surface	b_1 (m)	b_2 (m^3/kg)	b_3 (s^{-1})	b_4 (J/g-mol)	b_5 (note a)	b_6 (note b)	b_7 (note c)
Painted Gypsum	0.0063	191.8	0.0587	7476.	193	1.021	0.431
PMMA	9.6×10^{-5}	0.0137	0.0205	7476.	29	1.0	0.431
Ceiling Tile	4.0×10^{-3}	0.0548	0.123	7476.	30[b]	1.0	0.431
Cement Block	1.8×10^{-2}	5.48	0.497	7476.	30[b]	1.0	0.431
Marinite®	1.9×10^{-2}	0.137	0.030	7476.	30[b]	1.0	0.431

a units of b_5 are $(m^3/kg)^{\wedge}(b_7-b_6)$
b very approximate value, insufficient data for high confidence value
c non-dimensional

The experimental basis for poly(methyl methacrylate) and gypsum cover a sufficiently wide range of conditions that they should be usable in a variety of practical situations. The parameters for the other surfaces do not have much experimental backing, and so their use should be limited to comparison purposes.

3.7 Flame Spread

The Quintiere-Cleary flame spread model incorporated into CFAST is based on five simple differential equations. One each for concurrent, eq (154), and opposed flow flame spread, eq (155). One each, eqs (157) and (156) for the two burnout fronts and the last one for burn out at the ignition point eq (158).

$$\frac{dy_p}{dt} = \frac{y_f - y_p}{\frac{\pi}{4} k\rho c \left[\frac{T_{ig} - T_s}{\dot{q}''_f}\right]^2} \tag{154}$$

$$\frac{dx_p}{dt} = \frac{\phi}{k\rho c (T_{ig} - T_s)^2}, \quad for \ T_s \geq T_{s,\min} \tag{155}$$

$$\frac{dy_b}{dt} = \frac{\dot{Q}''(y_p - y_b)}{Q''_{TOT}} \tag{156}$$

$$\frac{dx_b}{dt} = \frac{\dot{Q}''(x_p - x_b)}{Q''_{TOT}} \tag{157}$$

and

$$\frac{dQ''}{dt} = \frac{(\dot{q}''_f - \sigma T_{ig}^4 + \sigma T_{layer}^4)}{\Delta L} \Delta H \tag{158}$$

The equations describe the growth of two rectangles. At ignition a single rectangle, R_p, is defined and its growth is determined by eq (154) for spread up the wall and eq (155) for lateral spread as well as spread down the wall. When $Q'' \leq 0$ a second rectangle, R_b, the same size as R_p was originally starts growing. It is governed by eqs (157) and (156). After R_b starts to be tracked the pyrolysis area is $R_p - R_b$.

When a flame spread object is defined, CFAST adds five additional differential equations to the equation set. A target is also placed at the specified location on the specified wall surface and the maximum time step is set to be 1 s. This allows the temperature of the target to be tracked and the ignition temperature and time to be calculated,

Once a flame spread object ignites, its mass loss and heat release rate are calculated and then treated like any other object fire by CFAST.

3.8 Single Zone Approximation

A single zone approximation may be derived by using two-zone source terms and the substitutions:

$$\begin{aligned} \dot{m}_U^{new} &= \dot{m}_L + \dot{m}_U, \\ \dot{m}_L^{new} &= 0 \\ \dot{q}_U^{new} &= \dot{q}_L + \dot{q}_U, \\ \dot{q}_L^{new} &= 0. \end{aligned} \tag{159}$$

This is not a fundamental improvement, but rather is designed to fit in with the concept of single zone and network models that are being utilized currently.

3.9 Miscellaneous Phenomena

Several improvements have been incorporated into the fire model based on experience in using it. One was to include the calculation of the species oxygen in the basic equation set. As is discussed elsewhere, the basic equations are for the upper and lower layer temperatures, the upper layer volume and the pressure at the floor of the compartment. These equations are derived from fluid dynamics and are based on the conservation of mass, momentum and energy. They can form a set of stiff, ordinary differential equations. In general, however, it has been a common practice to assume that the phenomena that drive these flows happen either much more quickly or much more slowly than that characteristic of the fluid flow time scales. In the case of fires where lack of oxygen can limit the combustion, and therefore the driving force, the oxygen which flows into a fire is intimately coupled to the forcing of the fluid flow and therefor the set becomes stiff.

4 Mathematical and Numerical Robustness

In order to understand the meaning of accuracy and robustness, it is necessary to understand the means by which the numerical routines are structured. In this chapter, details of the implementation of the model are presented. These include

- an overview of the model formulation,
- the structure of the model including the major routines implementing the various physical phenomena included in the model,
- the organization of data initialization and data input used by the model,
- the structure of data used to formulate the differential equations solved by the model,
- a summary of the main control routines in the model that are used to control all input and output, initialize the model and solve the appropriate differential equation set for the problem to be solved.

4.1 Structure of the Numerical Routines

4.2 Subroutine Structure

The model can be split into distinct parts. There are routines for reading data, calculating results and reporting the results to a file or printer. The major routines for performing these functions are identified in Figure 22. These physical interface routines link the CFAST model to the actual routines which calculate quantities such as mass or energy flow at one particular point in time for a given environment.

The routines SOLVE, RESID and DASSL are the key to understanding how the physical equations are solved. SOLVE is the control program that oversees the general solution of the problem. It invokes the differential equation solver DASSL [69] which in turn calls RESID to solve the transport equations. The problem that these routines solve is as follows. Given a solution at time t, what is the solution at time $t + \Delta t$? The differential equations are of the form

$$\begin{aligned} \frac{dy}{dt} &= \mathrm{f}(y,t) \\ y(t_0) &= y_0 \end{aligned} \tag{160}$$

where y is a vector representing pressure, layer height, mass, *etc*. and f is a vector function that represents changes in these values with respect to time. The term y_0 is an initial condition at the initial time t_0. The subroutine RESID (see sec. 4.3) computes the right hand side of eq (160) and returns a set of residuals of that calculation to be compared to the values expected by DASSL. DASSL then checks for convergence. Once DASSL reaches an error limit (defined as convergence of the equations) for the solution at $t+\Delta t$, SOLVE then advances the solution of species concentration, wall temperature profiles, and mechanical ventilation for the same time interval.

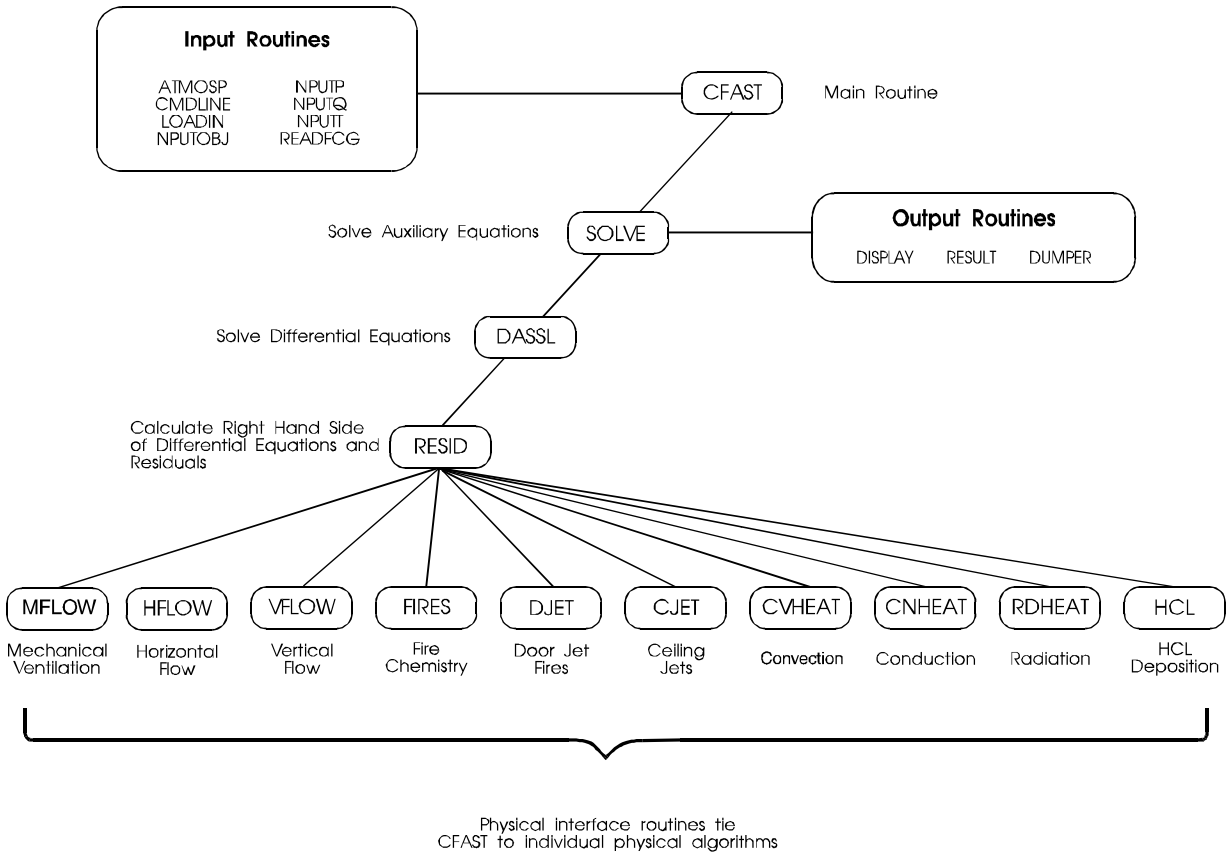

Figure 22. Subroutine structure for the CFAST Model.

Note that there are several distinct time scales that are involved in the solution of this type of problem. The fastest will be chemical kinetics. We avoid that scale by assuming that the chemistry is infinitely fast. The next larger time scale is that associated with the flow field. These are the equations which are cast into the form of ordinary differential equations. Then there is the time scale for mechanical ventilation, and finally, heat conduction through objects. By way of example, chemical kinetic times are typically on the order of milliseconds. The transport time scale will be on the order of 0.1 s. The mechanical ventilation and conduction time scales are typically several seconds, or even longer. Unlike earlier versions of the model, this new version dynamically adjusts the time step over the entire simulation to a value appropriate for the solution of the currently defined equation set. In addition to allowing a more correct solution to the pressure equation, very large time steps are possible if the problem being solved approaches steady-state.

4.3 The Control Programs (SOLVE and RESID)

As discussed above, the routine RESID controls most of the model calculations. SOLVE coordinates the solution and output, but the physical phenomena are accessed by RESID. This section provides an annotated overview of these two control programs.

4.3.1 SOLVE

Since much of the function of the control routine SOLVE is bookkeeping, the source code is not particularly illustrative. Rather, for this routine, we will provide an summary of the functioning of the routine below.

1. Initialize the print, history, and plot times to the user's input specifications.

2. By calling routine INITSOLN, determine a set of initial pressures consistent with the initial conditions (temperatures and vent sizes) of the problem to be solved. By solving a set of linear equations to determine appropriate steady-state initial conditions for the pressures, the differential equation solver is able to determine solutions for the always difficult first second of the solution several times faster than allowing the differential equation solver to find the initial solution.

3. Output results (or initial conditions at time t=0) of the calculation by printing (routine RESULT), writing a history file interval (routine DUMPER), or plotting (routine DISPLAYC) results if current time is appropriate for such output.

4. Call the differential equation solver, DASSL, to advance the solution in time. The length of the advance in time is chosen dynamically by DASSL. DASSL chooses the time step but reports back a solution based on the lesser of the print, display and dump intervals. DASSL call RESID to compute the actual solution, as well as the residuals.

5. Advance the solution for species not handled directly by the differential equation solver by calling routines RESID (again, but with different switches) and TOXIC.

6. Repeat steps 3-5 until the final time is reached.

Note that many of the defaults, switches, and tolerances can be changed in the initialization routine. SOLVE calls the initialization routine INITSLV. It has switches built in which can be redefined with the configuration file, SOLVER.INI. If this file is not present, then internal defaults are used which are the best available. However, for testing, turning off phenomena, alternative settings can be useful. See the appendices at the end for the format of this configuration file.

4.3.2 RESID

RESID is split into several parts. First, the current environment is copied from the form used by the differential equation solver into the environment common blocks for use by the physical routines in CFAST. Then the physical phenomena are calculated with calls to appropriate physical interface routines. Each physical interface routine returns its contribution to mass, enthalpy, and species flows into each layer in each room. These are then summed into total

mass, enthalpy, and species flows into each layer in each room. Finally, the differential equations are formed for each room, wall surface, and mechanical ventilation system in the problem.

This portion of the model is the real numerical implementation and is accessed many times per simulation run. Careful thought must be given to the form of the routines since the execution time is *very* sensitive to the coding of the software. What follows is an annotated form of the routine RESID. Extraneous comments have been left out to shorten the listing somewhat.

```
      SUBROUTINE RESID(TSEC,X,XPSOLVE,DELTA,IRES,RPAR,IPAR)
```

Common blocks go here to define the environment for CFAST use by all physical routines. Definition of temporary variables used to store the output of each physical routine are also included here. See section 4.4 for the format of each of these variables. The routine DATA-COPY is called to copy the environment from the form used by the differential equation solver into the environment common blocks for use by the physical routines in CFAST.

```
      XX0 = 0.0D0
      ND = 0
      NPROD = NLSPCT
      DT = TSEC - TOLD
C
      NIRM = NM1
C
      CALL DATACOPY(X,ODEVARA+ODEVARB)
```

The IPAR and RPAR parameters are passed from SOLVE to RESID via DASSL and are used to control the calculation of the residuals by RESID. For a call to RESID from the differential equation solver, DASSL, IPAR(2) is equal to the parameter SOME to indicate that the routine is to calculate the set of differential equations without including the species. Species are updated by SOLVE once DASSL has found an appropriate solution for the smaller equation set.

```
      IF (IPAR(2).EQ.SOME) THEN
        UPDATE = .FALSE.
      ELSE
        UPDATE = .TRUE.
      END IF
      EPSP = RPAR(1)
```

All of the physical phenomena included in the model are included here with calls to the physical interface routines for each phenomena. Each physical interface routine returns its contribution to mass, enthalpy, and species flows into each layer in each room.

```
C
C     CALCULATE FLOW THROUGH VENTS (HFLOW FOR HORIZONTAL FLOW
C     THROUGH VERTICAL VENTS, VFLOW FOR VERTICAL FLOW THROUGH
C     HORIZONTAL VENTS, AND MVENT FOR MECHANICAL VENTILATION)
C
      CALL HFLOW(TSEC,EPSP,NPROD,FLWNVNT,QLPQUV)
      CALL VFLOW(FLWHVNT,QLPQUH)
      CALL MVENT(X(NOFPMV+1),X(NOFTMV+1),XPSOLVE(NOFTMV+1),FLWMV,
     +     DELTA(NOFPMV+1),DELTA(NOFTMV+1),XPRIME(NOFHVPR+1),NPROD)
C
C     CALCULATE HEAT AND MASS FLOWS DUE TO FIRES
C
      CALL FIRES(TSEC,FLWF,QLPQUF,NFIRE,IFROOM,XFIRE)
```

```
      CALL SORTFR(NFIRE,IFROOM,XFIRE,IFRPNT)
      CALL DJET(NFIRE,FLWDJF,XFIRE)
C
C     CALCULATE FLOW AND FLUX DUE TO HEAT TRANSFER (CEILING JETS,
C     CONVECTION AND RADIATION
C
      CALL CJET(IFRPNT,XFIRE,ND,XD,YD,ZD,FLWCJET,FLXCJET,TD,VD)
      CALL CVHEAT(IFRPNT,FLWCV,FLXCV)
      CALL RDHEAT(IFRPNT,XFIRE,FLWRAD,FLXRAD)
C
C     CALCULATE HCL DEPOSITION TO WALLS
C
      CALL HCL(FLWHCL,FLXHCL)
```

The flows returned from each physical interface routine are then summed into total mass, enthalpy, and species flows into each layer in each room. The form of each of these flows is discussed in section 4.4. In general, the array FLWTOT(room,species,layer) contains the total flow of each species into each layer of each room in the simulation. For ease of definition, mass and enthalpy are included in this array as pseudo-species (1 & 2) and summed along with the actual species (3 to 2+lsp). Heat flux to surfaces is included in a similar manner for used by the conduction routine.

```
C
C     SUM FLOW FOR INSIDE ROOMS
C
      DO 50 IROOM = 1, NIRM
        QLPQUR(IROOM) = QLPQUV(IROOM) + QLPQUH(IROOM) + QLPQUF(IROOM) +
     +      FLWCV(IROOM,LL) + FLWCV(IROOM,UU) + FLWRAD(IROOM,LL) +
     +      FLWRAD(IROOM,UU) + FLWCJET(IROOM,LL) + FLWCJET(IROOM,UU) +
     +      FLWDJF(IROOM,Q,LL) + FLWDJF(IROOM,Q,UU) +
     +      FLWMV(IROOM,Q,LL) + FLWMV(IROOM,Q,UU)
        DO 40 IPROD = 1, NPROD + 2
          IP = IZPMAP(IPROD)
          FLWTOT(IROOM,IPROD,LL) = FLWNVNT(IROOM,IPROD,LL) +
     +        FLWMV(IROOM,IP,LL) + FLWF(IROOM,IP,LL) +
     +        FLWDJF(IROOM,IP,LL) + FLWHVNT(IROOM,IP,LL)
          FLWTOT(IROOM,IPROD,UU) = FLWNVNT(IROOM,IPROD,UU) +
     +        FLWMV(IROOM,IP,UU) + FLWF(IROOM,IP,UU) +
     +        FLWDJF(IROOM,IP,UU) + FLWHVNT(IROOM,IP,UU)
   40   CONTINUE
C
C     ADD IN HCL CONTRIBUTION TO FLWTOT
C
        IF (ACTIVS(6)) THEN
          FLWTOT(IROOM,1,LL) = FLWTOT(IROOM,1,LL) + FLWHCL(IROOM,1,LL)
          FLWTOT(IROOM,1,UU) = FLWTOT(IROOM,1,UU) + FLWHCL(IROOM,1,UU)
          FLWTOT(IROOM,8,LL) = FLWTOT(IROOM,8,LL) + FLWHCL(IROOM,8,LL)
          FLWTOT(IROOM,8,UU) = FLWTOT(IROOM,8,UU) + FLWHCL(IROOM,8,UU)
        END IF
C
        FLWTOT(IROOM,Q,LL) = FLWTOT(IROOM,Q,LL) + FLWCV(IROOM,LL) +
     +      FLWRAD(IROOM,LL) + FLWCJET(IROOM,LL)
        FLWTOT(IROOM,Q,UU) = FLWTOT(IROOM,Q,UU) + FLWCV(IROOM,UU) +
     +      FLWRAD(IROOM,UU) + FLWCJET(IROOM,UU)
C
   50 CONTINUE
C
C     SUM FLUX FOR INSIDE ROOMS
C
      DO 70 IROOM = 1, NIRM
        DO 60 IWALL = 1, NWAL
          IF (SWITCH(IWALL,IROOM)) THEN
            FLXTOT(IROOM,IWALL) = FLXCV(IROOM,IWALL) +
     +          FLXRAD(IROOM,IWALL) + FLXCJET(IROOM,IWALL)
          END IF
   60   CONTINUE
   70 CONTINUE
```

The differential equations are formed for each room, wall surface, and mechanical ventilation system in the problem. These follow directly from the derivation in section 3.2.

```
      DO 80 IROOM = 1, NIRM
        AROOM = AR(IROOM)
        HCEIL = HR(IROOM)
        PABS = ZZPABS(IROOM)
        HINTER = ZZHLAY(IROOM,LL)
        QL = FLWTOT(IROOM,Q,LL)
        QU = FLWTOT(IROOM,Q,UU)
        TMU = FLWTOT(IROOM,M,UU)
        TML = FLWTOT(IROOM,M,LL)
        QLPQU = QLPQUR(IROOM)
C
C     PRESSURE EQUATION
C
        PDOT = (GAMMA-1.0D0) * QLPQU / (AROOM*HCEIL)
        XPRIME(IROOM) = PDOT
C
C     UPPER LAYER TEMPERATURE EQUATION
C
        TLAYDU = (QU-CP*TMU*ZZTEMP(IROOM,UU)) / (CP*ZZMASS(IROOM,UU))
        IF (OPTION(FODE).EQ.ON) THEN
          TLAYDU = TLAYDU + PDOT / (CP*ZZRHO(IROOM,UU))
        END IF
        XPRIME(IROOM+NOFTU) = TLAYDU
C
C     UPPER LAYER VOLUME EQUATION
C
        VLAYD = (GAMMA-1.0D0) * QU / (GAMMA*PABS)
        IF (OPTION(FODE).EQ.ON) THEN
          VLAYD = VLAYD - ZZVOL(IROOM,UU) * PDOT / (GAMMA*PABS)
        END IF
        XPRIME(IROOM+NOFVU) = VLAYD
C
C     LOWER LAYER TEMPERATURE EQUATION
C
        TLAYDL = (QL-CP*TML*ZZTEMP(IROOM,LL)) / (CP*ZZMASS(IROOM,LL))
        IF (OPTION(FODE).EQ.ON) THEN
          TLAYDL = TLAYDL + PDOT / (CP*ZZRHO(IROOM,LL))
        END IF
        XPRIME(IROOM+NOFTL) = TLAYDL
   80 CONTINUE
```

The species are only calculated once DASSL has an acceptable solution for the equation set not including the species. We presume that the species production rates occur on a time scale similar to the total mass production which is solved directly.

```
      IF (NPROD.GT.0.AND.IPAR(2).EQ.ALL) THEN
        IPRODU = NOFPRD - 1
        DO 100 IPROD = 1, NPROD
          DO 90 IROOM = 1, NM1
            HCEIL = HR(IROOM)
            HINTER = ZZHLAY(IROOM,LL)
            IPRODU = IPRODU + 2
            IPRODL = IPRODU + 1
            IF (HINTER.LT.HCEIL) THEN
              XPRIME(IPRODU) = FLWTOT(IROOM,IPROD+2,UU)
            ELSE IF (HINTER.GE.HCEIL.AND.FLWTOT(IROOM,IP,UU).LT.XX0)
     +          THEN
              XPRIME(IPRODU) = FLWTOT(IROOM,IPROD+2,UU)
            ELSE
              XPRIME(IPRODU) = XX0
            END IF
            IF (HINTER.GT.XX0) THEN
              XPRIME(IPRODL) = FLWTOT(IROOM,IPROD+2,LL)
            ELSE IF (HINTER.LE.XX0.AND.FLWTOT(IROOM,IP,LL).GT.XX0) THEN
              XPRIME(IPRODL) = FLWTOT(IROOM,IPROD+2,LL)
            ELSE
```

```
              XPRIME(IPRODL) = XX0
            END IF
   90     CONTINUE
  100   CONTINUE
      END IF
```

Finally, the residuals are calculated. These are simply the difference between the solution vector calculated by RESID and that passed to RESID by the differential equation solver. This is done in several parts to correspond with the layout of the solution vector.

```
C
C     RESIDUALS FOR PRESSURE, LAYER VOLUME, AND LAYER TEMPERATURES
C
      DO 110 I = NOFP + 1, NOFP + NM1
        DELTA(I) = XPRIME(I) - XPSOLVE(I)
  110 CONTINUE
      DO 120 I = NOFTU + 1, NOFTU + 3 * NM1
        DELTA(I) = XPRIME(I) - XPSOLVE(I)
  120 CONTINUE
C
C     CONDUCTION RESIDUAL
C
      CALL CNHEAT(UPDATE,DT,FLXTOT,DELTA)
C
C     RESIDUALS FOR GAS LAYER SPECIES, NOTE THAT DASSL IS NOT SOLVING FOR
C     SPECIES NOW, THIS IS DONE IN SOLVE
C
      DO 130 I = NOFPRD + 1, NOFPRD + 2 * NPROD * NM1
        DELTA(I) = XPRIME(I) - XPSOLVE(I)
  130 CONTINUE
C
C     RESIDUAL FOR HVAC SPECIES
C
      IF (NPROD.NE.0) THEN
        DO 140 I = NOFHVPR + 1, NOFHVPR + NLSPCT * NHVSYS
          DELTA(I) = XPRIME(I) - XPSOLVE(I)
  140   CONTINUE
      END IF
      IF (IPAR(2).EQ.SOME) THEN
        NPROD = NPRODSV
      END IF
      RETURN
      END
```

4.4 Interface to the CFAST Physical Interface Routines

Each physical interface routine calculates flow and/or flux terms as appropriate for all rooms and/or surfaces of the simulation being modeled. These flow and flux terms are the effect of the phenomenon on each of the layers and/or surfaces and includes flows due to mass, enthalpy and products of combustion. Rather than using multiple variables for each room, these are organized into a single array for each phenomenon. This structure is shown in Figure 23. To illustrate the organization of the physical interface routines, the following outlines the steps in calculating one of the phenomena.

The physical interface routine, FIRES, calculates the rates of addition of mass, enthalpy, and species into all layers in all rooms from all fires in a simulation. For each fire, the following scheme is employed:

1. Initialize the fire data structure, FLWF, to zero.

2. For each specified fire, the routine PYROLS (for the main fire) or OBJINT (for object fires) calculates time dependent quantities for the time of interest by interpolating between the time points specified by the user. The routine DOFIRE calculates the plume entrainment rate.

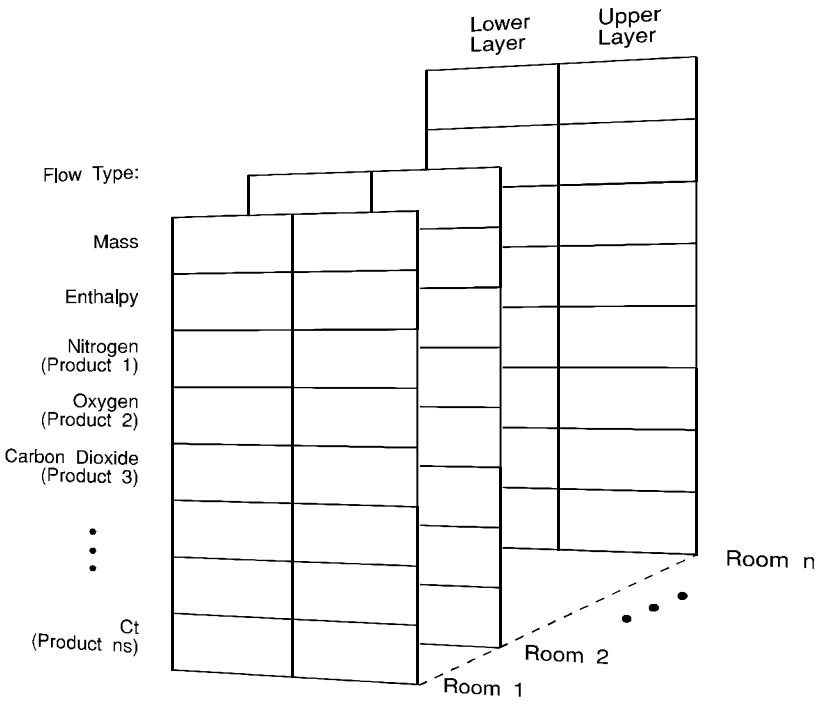

Figure 23. Data structure for flow and/or flux terms returned from physical interface routines to the control routine RESID.

3. For a type 1 (unconstrained) fire, the routine DOFIRE sets the burning rate to the pyrolysis rate. The heat release rate is found by multiplying the burning rate by the heat of combustion.

4. For a type 2 (constrained) fire, the prescribed chemistry scheme, discussed above, is used to constrain the burning rate based on *both* the fuel and oxygen available. This chemistry scheme is implemented in the routine CHEMIE. This calculation is done for both the lower layer (from the mass entrained by the plume) and for burning in the upper layer (with oxygen and fuel available in the layer).

5. Sum the contributions from all fires into the fire data structure for return to the control routine. The following code fragment is typical of those in all of the physical interface routines:

```
FLWF(LFBO,M,UPPER) = FLWF(LFBO,M,UPPER) + EMS(LFBO)
FLWF(LFBO,M,LOWER) = FLWF(LFBO,M,LOWER) - EME(LFBO)
FLWF(LFBO,Q,UPPER) = FLWF(LFBO,Q,UPPER) + QF(LFBO) + QEME + QEMP
FLWF(LFBO,Q,LOWER) = FLWF(LFBO,Q,LOWER)           - QEME
QLPQUF(LFBO)       = QLPQUF(LFBO)       + QF(LFBO)       + QEMP
```

```
      DO 40 LSP = 1, NS
        FLWF(LFBO,LSP+2,UPPER) = FLWF(LFBO,LSP+2,UPPER) +
     +       XNTMS(UPPER,LSP)
        FLWF(LFBO,LSP+2,LOWER) = FLWF(LFBO,LSP+2,LOWER) +
     +       XNTMS(LOWER,LSP)
40    CONTINUE
```

5 Sensitivity of the Model

Analytical models for predicting fire behavior have been evolving since the 1960's. During this time, the completeness of the models has grown. In the beginning, the focus of these efforts was to describe in mathematical language the various phenomena which were observed in fire growth and spread. These separate representations have typically described only parts of a fire. When combined though, they can create a complex computer code capable of giving an estimate of the expected effects of a fire based upon given input parameters. Analytical models have progressed to the point of providing predictions of fire behavior with an accuracy suitable for most engineering applications. Two obvious questions arise concerning the use of these models for engineering calculations:

- How good do the inputs to the model need to be (How do changes in the model inputs affect the model outputs)?
- How good is the output of model (How close are the actual conditions to those predicted by the model)?

To address the former question, this paper presents a discussion of the issues involved in conducting a sensitivity analysis of a complex room fire model. Examples using one fire model are provided. For the latter question, some examples are presented illustrating comparisons for both simple correlations and complex fire models. More complete investigations are available[70],[71],[79]. From the outset, it is important to note that this paper does not provide all the answers to the issues discussed. Rather, it is intended to highlight the strengths and weaknesses of the current level of understanding of evaluation of complex fire models and to promote further discussion of the topic.

5.1 Earlier Research

Although published literature is available which includes discussion of techniques for sensitivity analysis of predictive models[81], their primary focus is most often stochastic models of human behavior and rarely have been applied to deterministic fire models. This section provides a brief overview of some of the publications related to the evaluation of of fire models. It is not an exhaustive review. Rather, it is intended to give an appreciation for the current status of the topic as applied to fire modeling.

Clemson, et. al.[72] provide an overview of methods for sensitivity analysis of simulation models. Although not specific to fire modeling, they provide numerous references to additional research, present the advantages and disadvantages of different sampling techniques for experiment selection, and apply chosen methods to an example simulation model.

Khoudja[79] has studied the sensitivity of an early version of the FAST model with a fractional factorial design involving two levels of 16 different input parameters. The statistical design, taken from the texts by Box and Hunter[73], and Daniel[74] reduced the necessary model runs

from more than 65000 to 256 by studying the interactions of input parameters simultaneously. His choice of values for each input parameter represented a range for each parameter. His analysis of the FAST model (a precursor to the CFAST model used for this paper) showed a particular sensitivity to the inclusion of conduction in the calculations and lesser, though consistent sensitivities to the number of compartments included in a simulation and the ambient temperature. Without the inclusion of surface thermophysical properties, this model treats surfaces as adiabatic for conductive heat transfer. Thus, this consistent sensitivity should be expected. Sensitivity to changes in thermal properties of the surfaces were not explored.

Iman and Helton[75] studied the sensitivity of complex computer models developed to simulate the risk of severe nuclear accidents which may include fire and other risks. Three approaches to uncertainty and sensitivity analysis were explored:

- response surface methodology where the complex model is replaced by a series of simple linear models with inputs determined from a fractional factorial design,
- Latin hypercube sampling where carefully chosen random sampling is used to determine model inputs, and
- differential analysis used to evaluate sensitivity for small perturbations about a single set of model inputs.

These techniques were evaluated for three different models with respect to ease of implementation, flexibility, estimation of the cumulative distribution function of the output, and adaptability to different methods of sensitivity analysis. With respect to these criteria, the techniques using Latin hypercube sampling had the best overall performance. Programs to generate such samples are available [76],[77].

A sensitivity analysis is a study of how changes in model parameters affect the results generated by the model. Model predictions may be sensitive to uncertainties in input data, to the level of rigor employed in modeling the relevant physics and chemistry, and to the accuracy of numerical treatment. Among the purposes for conducting a sensitivity analysis are to determine:

- the important variables in the models,
- the computationally valid range of values for each input variable, and
- the sensitivity of output variables to variations in input data.

Conducting a sensitivity analysis of a complex fire model is a difficult task. Many models require extensive input data and generate predictions for numerous output variables over a period of simulated time. Several methods of sensitivity analysis have been applied to fire models, but most have had limited utility. These range from explicit evaluation of the equations used in simple models such as ASET[78] to pointwise evaluation of complex models from numerous computer runs of the model[79]. The technique chosen for use will be dependent on the objectives of the study, the required results, the resources available and the complexity of the model being analyzed.

Fire growth models are typically based on a system of ordinary differential equations of the form

$$\frac{dz}{d\tau} = f(z,p,\tau) \qquad z(\tau=0) = z_0 \tag{161}$$

where z (z_1, z_2, ..., z_m) is the solution vector for the system of equations (for example, mass, temperature, or volume) and p (p_1, p_2, ... p_n) is a vector of input parameters (for example, room area, room height, heat release rate) and τ is time[80]. The solutions to these equations are, in general, not known explicitly and must be determined numerically. To study the sensitivity of such a set of equations the partial derivatives of an output z_j with respect to an input p_i (for j=1,...,m and i=1,...,n) are examined.

Two basic approaches exist for obtaining sensitivity information:

- Local methods – produce sensitivity measures for a particular set of input parameters and must be repeated for a range of input parameters to obtain information on the overall model performance. Finite difference methods can be applied without modifying a model's equation set, but require careful selection of input parameters to obtain good estimates. Direct methods supplement the equation set solved by a model with sensitivity equations derived from the equation set solved by the model[81]. The sensitivity equations are then solved in conjunction with the model's system of equations to obtain the sensitivities. Direct methods must be incorporated into the design of a fire model and are not often available for already existing fire models.

- Global methods – produce sensitivity measures which are averaged over the entire range of input parameters. Global methods require knowledge of the probability density functions of the input parameters, which in the case of fire models, is generally unknown.

5.2 Sensitivity Analysis for More Complex Fire Models

For more complex fire models, obtaining an overall assessment of model sensitivity may become overly complex with numerous model inputs and outputs. Thus, more directed local sensitivity investigations are appropriate. Local methods produce sensitivity measures at a particular point of the parameter space of the model. There are several classes of local methods which are of interest. Using the nomenclature of equation (161), these are outlined below.

- Finite difference methods provide estimates of sensitivity functions by approximating the partial derivatives of an output z_i with respect to an input p_i as finite differences:

$$\frac{\partial z_j}{\partial p_m} = \frac{z_j(p_1,p_2,\ldots,p_m+\Delta p_m,\ldots,p_k) - z_j(p_1,p_2,\ldots,p_m,\ldots,p_k)}{\Delta p_m} \quad j=1,2,\ldots,n,\ m=1,2,\ldots,k \tag{162}$$

  This method is easy and straightforward to implement. However, as with any finite difference method, the choice of Δp_m is pivotal in obtaining good estimates. To determine the n x k first-order sensitivity equations requires k+1 runs of the model. These may be run sumultaneously as a larger system or in parallel.

- Direct methods derive the sensitivity differential equations from the model's system of ordinary differential equations

$$\frac{d}{dt}\frac{\partial z_j}{\partial p_m} = \frac{\partial f_j}{\partial p_m} + \sum_i \frac{\partial f_j}{\partial z_i}\frac{\partial z_i}{\partial p_m} \qquad j=1,2,....,n, \qquad m=1,2,....,k \tag{163}$$

  These equations are then solved in conjunction with the model's system of differential equations to obtain the sensitivities. To compute the n x k first-order sensitivities requires 1 model run. These may be incorporated directly into the model and solved as a single, coupled set of n+(n x k) differential equations[82] or decoupled solving the model equations and the sensitivity equations iteratively using the model's solution and an appropriate interpolation scheme[?]. This method was applied to the ASET earlier in this paper.

- Response surface methods fit an appropriate set of functions to selected model runs. The resulting functions are then assumed to behave in the same manner as the model. With appropriate choice for the set of functions (such that the sensitivity functions are easily calculable), the analysis of the behavior of the model is facilitated.

Even though it is possible to define the sensitivities and establish various methods for their computation, there are still difficulties associated with performing a sensitivity analysis. Iman and Helton[75] note some of the properties of complex computer models which make analysis difficult:

- There are many input and output variables.
- The model is time consuming to run on a computer.
- Alterations to the model are difficult and time consuming.
- It is difficult to reduce the model to a single system of equations.
- Discontinuities may exist in the behavior of the model.
- Correlations may exist among the input variables and the associated marginal probability distributions are often nonnormal.
- Model predictions are nonlinear, multivariate, time-dependent functions of the input variables.
- The relative importance of individual input variables is a function of time.

Many of these comments are applicable to current room fire models. In addition, the sensitivity equations have similar properties. For a given model output and a given model input, there may be regions of time where the model output is sensitive to the input and also regions where the model output is insensitive to the same parameter.

5.2.1 Selecting Inputs and Outputs for Sensitivity Analysis

At least two broad questions can be addressed with a sensitivity analysis of a fire model. First, the more general question, "How sensitive is the model to a specific input?" is an attempt to gain an overall appreciation of the importance of an input relative to all other inputs. For this

question, the range of model inputs could be chosen as broad as possible representing the range of applicability of the model. A subsequent analysis of model outputs for such broad changes would then provide insight into the relative importance of a given input variable on selected outputs. Such an analysis provides an overall picture of model behavior.

The second question, "How closely must a specific input be specified?" is more focused than the first question. Rather than understanding the overall behavior of the model, it is an effort to obtain an understanding of the effect on the model outputs of uncertainties in selected inputs. For this question, small perturbations in the inputs could be examined. If a specific scenario is of interest, perturbations of the inputs for this scenario could be examined.

For either question, several topics are of interest:

- What input and output variables are of interest?
- How should specific models runs be selected to study these variables?
- How can the results be quantified?

5.2.2 Model Inputs and Outputs

Current zone-type fire models have numerous inputs (Table 5) and outputs (Table 6) which may be of interest in a sensitivity analysis. The inputs and outputs for the CFAST model are typical of a complex zone-based room fire model.

Most studies of modeling related to fire hazard and fire reconstruction present a consistent set of variables of interest to the model user[83],[84],[85],[86]: gas temperature, gas species concentrations, and layer interface position. To assess the accuracy of the physical basis of the models, additional variables must be included. Pressure drives the movement of gases through openings. The pyrolysis rate, and heat release rate of the fire in turn, produces the gases of interest to be moved. For sensitivity analysis it is appropriate to consider all these variables for evaluation:

- upper and lower layer gas temperature,
- layer interface position,
- gas species concentration,
- fire pyrolysis and heat release rate,
- room pressure, and
- vent flow.

Although there are certainly other comparisons of interest, these will provide evidence of the sensitivity of the model to most model inputs.

Table 5. Typical Inputs for a Two-Zone Fire Model.

Ambient Conditions	Inside **temperature** and **pressure** Outside **temperature** and **pressure** Wind **speed** **Relative humidity** (0%-100%)
Building Geometry	**Compartment width**, **depth**, **height**, and surface material properties (**conductivity**, **heat capacity**, **density**, **thickness**) Horizontal Flow Vents: **Height of soffit above floor**, **height of sill above floor**, **width of vent**, **angle of wind to vent**, **time history of vent openings and closings** Vertical Flow Vents: **Area of vent**, shape of vent Mechanical Ventilation, Orientation of vent, **Center height of vent**, **area of vent**, **length of ducts**, **diameter of ducts**, **duct roughness**, **duct flow coefficients**, **fan flow characteristics**
Fire Specification	Fire room, **X, Y, Z position in room**, **fire area** Fire Chemistry: Molar Weight, **Lower oxygen limit**, **heat of combustion**, **initial fuel temperature**, **gaseous ignition temperature**, **radiative fraction** Fire History: **Mass loss rate**, **heat release rate**, species yields for **HCN, HCl, Ct, H/C, O_2/C, C/CO_2, CO/CO_2**

Items in **bold** are inputs that may vary due to error in measurements

Table 6. Typical Outputs for a Two-Zone Fire Model.

Compartment Environment	for each compartment	Compartment pressure and layer interface height
	for each layer and compartment	temperature, layer mass density, layer volume, heat release rate, gas concentrations (N_2, O_2, CO_2, CO, H_2O, HCl, HCN, soot optical density), radiative heat into layer, convective heat into layer, heat release rate in layer
	for each vent and layer	mass flow, entrainment, vent jet fire
	for each fire	heat release rate of fire, mass flow from plume to upper layer, plume entrainment, pyrolysis rate of fire
	for each compartment surface	surface temperatures
Tenability		Temperature Fractional Exposure Dose (FED)

Values are typically time histories

5.2.3 Selecting Specific Model Simulations

With a sensitivity analysis of any model, numerous scenarios must be tested with the model. Usually, this implies some sort of statistical design for the experiments to be conducted. Techniques are readily available[79,77] which can be used to select appropriate sets of model inputs and which have been applied to the analysis of fire models. With current computer capabilities, the efficiency of a particular design may not be as important as it has been in the past as considerably more model simulations can be conducted within a reasonable time frame.

Efficient choice of model inputs and outputs is further complicated by functional dependencies and redundancy in model inputs and outputs. For example, suppose two parameters, say *a* and *b*, occur in an unsimplified form of a model, always as the product $a \cdot b$. Comparing outputs of calculations which double the parameter *a* while halving the parameter *b* will produce the same result as the base case in which both are unchanged. For example, Cooper[4] simplified the ASET model from twelve dimensional physical parameters to four dimensionless parameters. In addition, even these can be further simplified to only two dimensionless groups[78]. Choice of inputs to vary such a set of core parameters over the entire range of applicability of the inputs provides for a more complete assessment of the model's behavior.

5.3 Calculating and Interpreting Sensitivity Functions for a Complex Fire Model

In this section, some examples of model sensitivity are presented using the CFAST model[9] for the simulations. Although numerous scenarios could be chosen for study, a single one was used in this paper to illustrate the analysis of a complex fire model. To obtain a complete picture of a model's sensitivity, a number of scenarios representing the entire range of the model would have to be studied. The scenario chosen includes a range of phenomena which can be simulated with this model. The building geometry (figure 24) includes four rooms on two floors with horizontal, vertical, and mechanical vents connecting the rooms and venting to the outdoors. The fire source in one of the rooms on the lower floor is a medium growth rate t^2 fire [87] chosen to simulate a mattress fire [88] (figure 25).

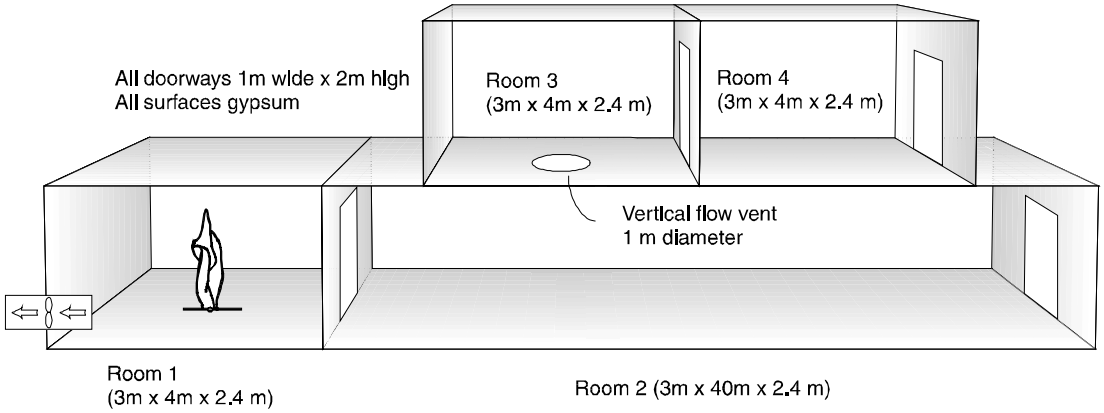

Figure 24. Building geometry for base case scenario.

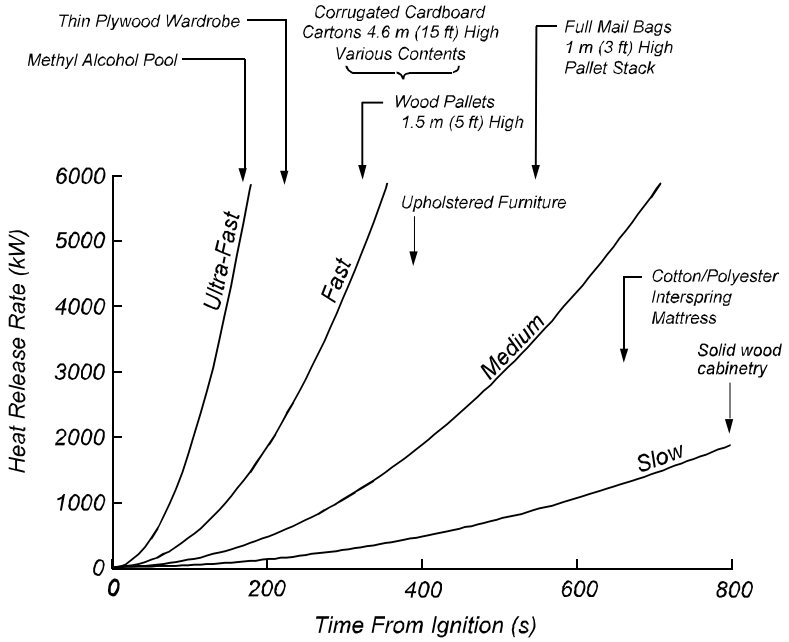

Figure 25. Characterization of heat release rate of growing fires as t^2 fires.

5.3.1 Sensitivity to small changes in model inputs

To investigate the sensitivity of the model, a number of simulations were conducted varying the input parameters for CFAST about this base scenario. Both small (±10%) and larger (up to an order of magnitude) variations for selected inputs were studied. Varying most of the inputs by small amounts had little effect on the model outputs. Figure 26 presents and example of the time dependent sensitivity of several outputs to a 10% change in room volume for the fire compartment in the scenario described above. For example, the pair of dotted-line curves labeled "Upper Layer Volume" were created by comparing the base case scenario with a scenario whose compartment volume was increased and decreased by 10%. The resulting curves presented on the graph are the releative difference between the variant cases and the base case defined by *(Variant value - Base value) / Base value* for each time point. The graph shows that temperature and pressure are insensitive to changes in the volume of the fire room since the 10% change in room volume led to smaller relative changes in layer temperature and room pressure for all times. Upper layer volume can be considered neutrally sensitive (a 10% change in room volume led to about a 10% change in layer volume). Further, this implies that there is negligible effect on layer interface height. This is consistent with both experimental observations in open compartment room fires[89] and analytical solutions for single compartment steady-state fires[90]. In essence, this implies that reasonable uncertainties in room dimensions would have little effect on the results predicted by the model for this scenario.

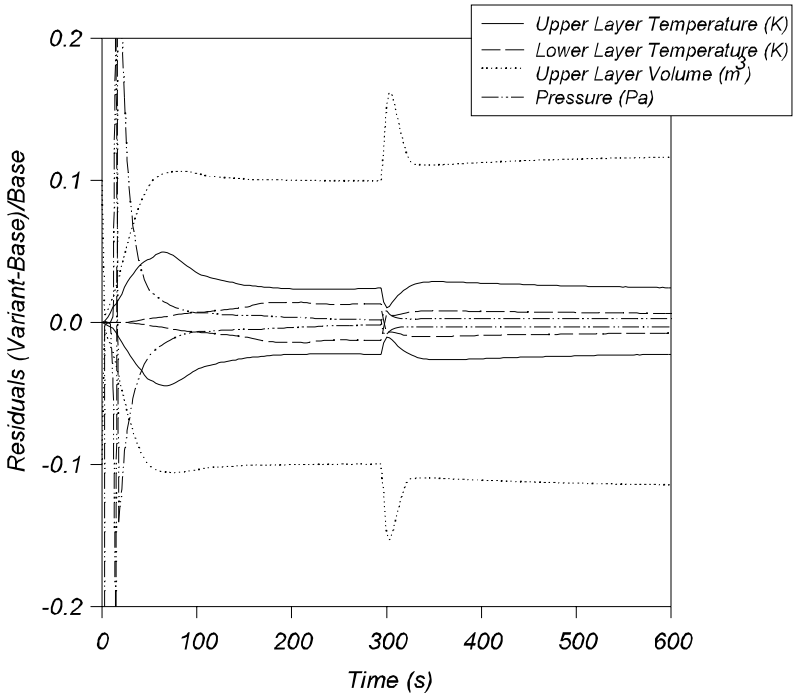

Figure 26. An example of time dependent sensitivity of fire model outputs to a 10% change in room volume for a single room fire scenario

In addition, figure 26 shows a somewhat constant relative difference for the changes as a function of time. As suggested by Iman and Helton [75], an average relative difference could thus be used to characterize the model sensitivity for comparing individual inputs and outputs.

5.3.2 Sensitivity to larger changes in model inputs

To investigate the effects of much larger changes in the inputs, a series of simulations where the inputs were varied from 0.1 to 4.0 times the base value was conducted. Simulations changing the heat release rate (HRR) inputs are shown in figure 27.

Each set appears as families of curves with similar functional forms. This indicates that multiples of the HRR have a simple monotonic effect on the layer temperatures. Again, it may be possible to describe the sensitivity with a single characteristic number. The choice of heat release is particularly interesting since it appears to be one of the inputs to the model which has a greater effect on the model outputs than other inputs. In the majority of fire cases, the most crucial question that can be asked by the person responsible for fire protection is: "How big is the fire?" Put in quantitative terms, this translates to: "What is the HRR of this fire?" Recently the

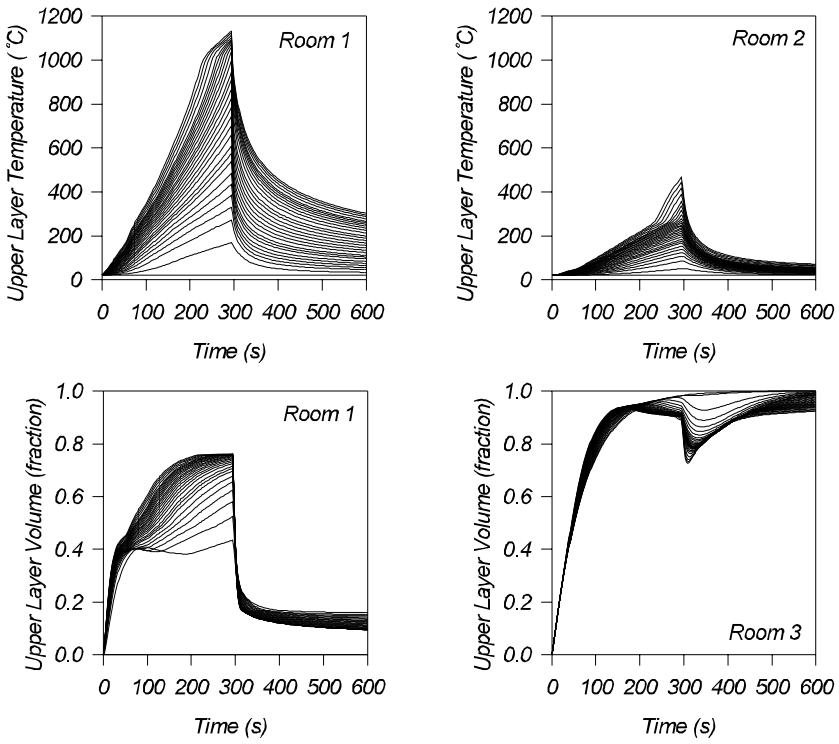

Figure 27. Layer temperatures and volumes in several rooms resulting from variation in heat release rate for a four-room growing fire scenario.

National Institute of Standards and Technology (NIST) examined the pivotal nature of HRR measurements in detail[91]. Not only is HRR seen as the key indicator of real-scale fire performance of a material or construction, HRR is, in fact, the single most important variable in characterizing the “flammability” of products and their consequent fire hazard. Much of the remainder of this paper focuses on HRR as an example for examining sensitivity analysis.

5.3.3 Simple "response-surface” correlations

A next step beyond the simple plots presented in figure 27 is a cross-plot of outputs of interest against HRR. Figure 28 presents plots of the upper (presented in figure 27) and lower layer temperatures plotted against the heat release rate for all the simulations. The shaded areas on figure 28 shows the locus of all the individual data points representing all the layer temperature time points for all the simulations shown in figure 27. For each room, a regression fit to the data for each room overlays the locus. The temperature curves for both upper and lower layer temperature in all four rooms (figure 28) show a strong functional dependence on HRR. Even for the wide variation in inputs, the HRR provides a simple predictor of the temperature in the rooms. In addition, this relationship allows calculation of the sensitivity of the temperature outputs to the HRR inputs as a simple slope of the resulting correlation between HRR and temperature.

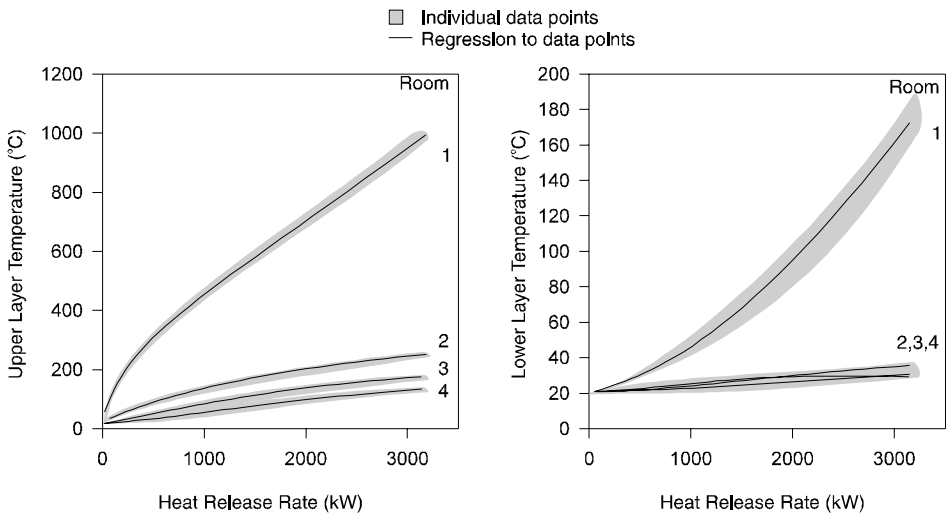

Figure 28. Comparison of heat release rate and layer temperature in several rooms for a four-room growing fire scenario.

Figure 29, simply a plot of the slope of the curves in figure 28, shows this sensitivity, $\partial(T)/\partial(HRR)$, for the four-room scenarios studied and represents all time points in all the simulations in which the peak HRR was varied from 0.1 to 4.0 times the base value. Except for relatively low HRR, the upper layer temperature sensitivity is less than 1 K/kW and usually below 0.2 K/kW. Not surprisingly, the layer that the fire feeds directly is most sensitive to changes. The lower layer in the fire room and all layers in other rooms have sensitivities less than 0.2 K/kW. This implies, for example, that if the HRR for a 1 MW fire is known to within 100 kW, the resulting uncertainty in the calculation of upper layer temperature in the fire room is about ±30 K.

For upper layer volumes (figure 30) of both rooms 1 and 2, it is again a simple correlation between HRR and volume fraction (upper layer volume expressed as a fraction of the total room volume). The correlations for the upper layer volumes of room one and room two could also be differentiated as was done for the temperature correlations to obtain sensitivities for the upper layer volume. For rooms 3 and 4, the relationship is not as clear. The flow into the layers of these rooms is more complicated than for rooms 1 and 2, resulting from flow from the first floor through a vent in the floor of room 3 and from a vent to the outside in room 4. However, even these rooms approach a constant value for higher HRR values, implying near zero sensitivity for high HRR.

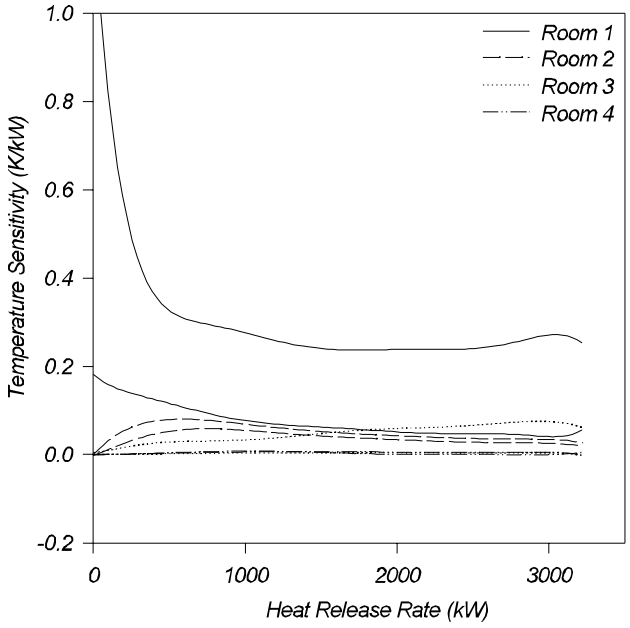

Figure 29. Sensitivity of temperature to heat release rate for a four-room growing fire scenario.

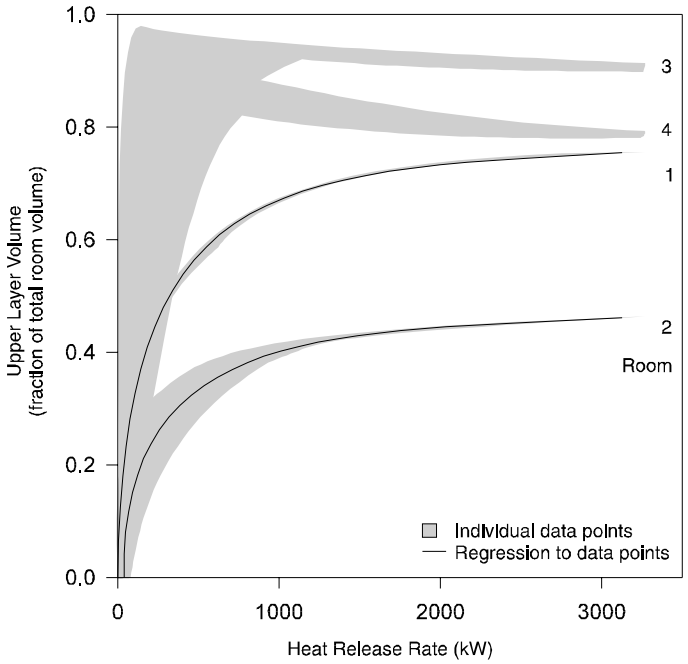

Figure 30. Comparison of heat release rate and upper layer volume in several rooms for a four-room growing fire scenario.

5.3.4 Evaluating sensitivity by single values

Many phenomena of interest in fire modeling are transient events that are best represented as time history curves. Examples are HRR, gas temperature, smoke density, and CO concentration. To evaluate the sensitivity of multiple outputs, it would be desirable to have a single number to characterize each output. For the example scenario used in this paper, several choices are available. From figure 26, an average relative difference could be used. From figure 29, the average sensitivity calculated from a simpler model (in this case, a simple correlation) could be used. Other possibilities include time to critical events (for example, flashover), average value, or peak value. Figure 31 shows the peak HRR and peak upper layer temperature normalized relative to the values at corresponding times from the base scenario for the base scenario and ±50% of the base HRR.

Although there is some scatter in the data, most of this comes at early times in the fire. From figure 31, it is apparent that choosing a single temperature. For ease of discussion and obvious interest, we will focus on peak values for HRR and temperature.

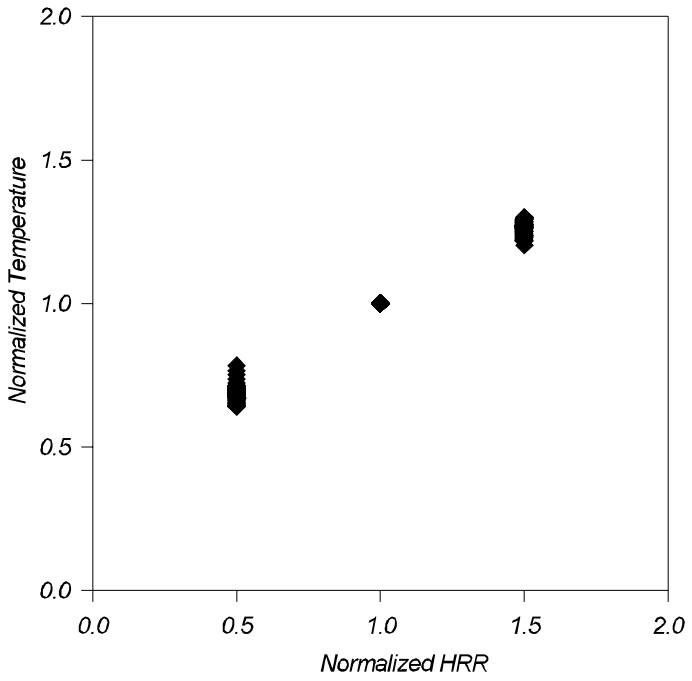

Figure 31. Comparison of normalized peak temperature to normalized heat release rate for a series of four-room growing fire scenarios.

Figure 32 presents the effect of both peak HRR and vent opening (in the fire room) on the peak upper layer temperature. In this figure, actual model calculations, normalized to the base scenario values are indicated by circles overlaid on a surface grid generated by a spline interpolation between the data points. At high HRR and small vent openings, the fire becomes oxygen limited and the temperature trails off accordingly, but for the most part, the behavior of the model is monotonic in nature. Although more laborious, the approaches used to calculate sensitivities for single variable dependencies illustrated earlier are thus equally applicable to multivariate analyses.

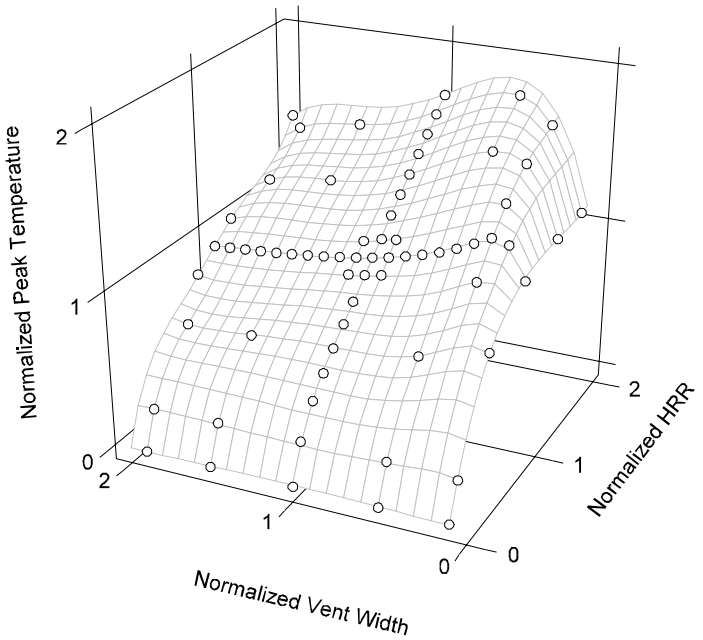

Figure 32. Effect of both heat release rate and vent opening size on upper layer temperature for a four-room growing fire scenario.

From the surface, it is clear that HRR has more of an effect on the peak temperature than does the vent width. Until the fire becomes oxygen limited, the trends evident in the surface are consistent with expectations – temperature goes up with rising HRR and down with rising vent width. The effects are not, of course, linear with either HRR or vent opening. Plume theory and typically used calculations for estimating upper layer temperature in a single room with a fire[92],[93] suggest that the dependence is on the order of $\dot{q}^{2/3}$ for HRR and $A\sqrt{h}$ for the vent opening where A is the area of the vent and h is the height of the vent. Although these correlations are based on a simple analysis of a single room fire, the dependence suggested is similar to that illustrated in figure 32.

In the past, sensitivity analysis has been applied with limited success to fire models. In this paper, both analytical and numerical techniques were applied to obtain limited estimates of model sensitivity. Several areas which need additional research are apparent in order to be able to perform broader analyses:

- *Presenting the results of a sensitivity analysis* – For a complex fire model with m inputs and n outputs, a complete sensitivity analysis will result in a matrix of $m * n$ time series.

  It is unlikely that this much information will be of general use. It may be appropriate to develop threshold values for important outputs to alert the model user of particularly sensitive effects for a given test case.

- *Range of applicabilty for fire model inputs* – little guidance is available in documentation for any of the current generation of room fire models on the range of applicability of the inputs to the models. For example, for different scenarios of interest, compartment size could range from small residential rooms to large industrial plants. Such information is important in order to obtain an overall picture of model performance and allow the models to be studied over the entire range of applicability.

- *Selecting specific model inputs for study* – With a sensitivity analysis of any model, numerous scenarios must be tested with the model. Although current computer capabilities allow far more simulations to be conducted than in earlier studies, the scope of room fire models continues to expand. Suitability of particular statistical designs to the selection of specific scenarios to be simulated should be included in future studies of fire model sensitivity.

- *Calculating sensitivity functions for a complex fire model* – In order to apply analytical techniques for sensitivity analysis of a complex fire model, the sensitivity equations need to be included in the equation set solved directly by the model. Even though it is desirable to obtain an overall picture of model performance, the broad range of application of current models demonstrates that whatever range of study is chosen, applications outside this envisioned range will continue to be of interest.

Comparisons of model predictions with experimental measurements to date have been largely subjective in nature. Areas of additional research which would address the need for more qunatitative comparisons include:

- *Statistical treatment of the data* – presentation of the differences between model predictions and experimental data in this paper are intentionally simple. With a significant base of data to study, appropriate statistical techniques to provide a true measure of the "goodness of fit" should be investigated.

- *Experimental measurements* – measurement of leakage rates, room pressure, or profiles of gas concentration are atypical in experimental data. These measurements are critical to assessing the accuracy of the underlying physics of the models or of the models ability to predict toxic gas hazard.

- *Uncertainty* – uncertainty in model predictions can be estimated by a sensitivity analysis. Estimation of uncertainty in experimental measurements by performing replicate experiments is uncommon in real-scale fire experiments. Such estimates for both model and experiment would place the resulting comparisons in better context.

6 Validation of the Model

6.1 Methods of validating a model

There are two ways of comparing predictive capability with actual events. The first is simply graphing the time series curves of model results with measured values of sensible variables such as temperature. Another approach is to consider the time to critical conditions such as flashover.

Making direct comparisons between theory and experiment gives a good sense of whether predictions are reasonable. In addition to direct comparisons, we want to quantify what is meant by a goodness of fit. That is, in the same sense that one can say two point measurements are identical if they are within a standard deviation of each other in a statistical sense, we would like to be able to make a similar statement about the closeness of two time series.

6.2 Available Experimental Data

Several systematic test series have been undertaken specifically to provide data for comparison with model predictions. In other cases, tests in which fire properties have been systematically varied (for various reasons) have been modeled using current computer fire simulations. In the first group are the study of Alpert et al. [94] for a single room connected to a short, open corridor, and those of Cooper et al. [95] and Peacock et al. [4] for gas burner fires in a room-corridor-room configuration. Although the second group is large, the works of Quintiere and McCaffrey [96], and Heskestad and Hill [97] are particularly detailed.

Cooper et al. [95] reported an experimental study of the dynamics of smoke filling in realistic, full-scale, multi-room fire scenarios. A major goal of the study was to generate an experimental database for use in the verification of mathematical fire simulation models. The test space involved 2 or 3 rooms, connected by open doorways. During the study, the areas were partitioned to yield four different configurations. One of the rooms was a burn room containing a methane burner which produced either a constant heat release rate of 25, 100, or 225 kW or a time-varying heat release rate which increased linearly with time from zero at ignition to 300 kW in 600 s. An artificial smoke source near the ceiling of the burn room provided a means for visualizing the descent of the hot layer and the dynamics of the smoke filling process in the various spaces. The development of the hot stratified layers in the various spaces was monitored by vertical arrays of thermocouples and photometers. A layer interface was identified and its position as a function of time was determined. An analysis and discussion of the results including layer interface position, temperature, and doorway pressure differentials is presented. These data were later used by Rockett et al. [98], [99] for comparison to a modern predictive fire model [100].

Quintiere and McCaffrey [96] described a series of experiments designed to provide a measure of the behavior of cellular plastics in burning conditions related to real life. They experimentally determined the effects of fire size, fuel type, and natural ventilation conditions on the resulting room fire variables, such as temperature, radiant heat flux to room surfaces, burning rate, and air

flow rate. This was accomplished by burning up to four cribs made of sugar pine or of a rigid polyurethane foam to provide a range of fire sizes intended to simulate fires representative of small furnishings to chairs of moderate size. Although few replicates were included in the test series, fuel type and quantity, and the room door opening width were varied. The data from these experiments were analyzed with quantities averaged over the peak burning period to yield the conditions for flashover in terms of fuel type, fuel amount, and doorway width. The data collected were to serve as a basis for assessing the accuracy of a mathematical model of fire growth from burning cribs.

Heskestad and Hill [97] performed a series of 60 fire tests in a room/corridor configuration to establish accuracy assessment data for theoretical fire models of multi-room fire situations with particular emphasis on health care facilities. With steady state and growing fires from 56 kW to 2 MW, measurements of gas temperatures, ceiling temperatures, smoke optical densities, concentrations of CO, CO_2, and O_2, gas velocities, and pressure differentials were made. Various combinations of fire size, door opening size, window opening size, and ventilation were studied. To increase the number of combinations, only a few replicates of several of the individual test configurations were performed.

Except for the data of Cooper et al. [95] and Quintiere and McCaffrey [96] which are not available in machine readable form, the above data, along with other experimental results, have been reviewed by Peacock, Davis and Babrauskas [101]. They provide a single consistent form for the experimental data from several series of experiments. Five sets of experimental data which can be used to test the limits of a typical two-zone fire model are detailed. Availability of ancillary data (such as smaller-scale test results) is included. These descriptions, along with the data should allow comparisons between the experiment and model predictions. The base of experimental data ranges in complexity from one-room tests with individual furniture items to a series of tests conducted in a multiple-story hotel equipped with a zoned smoke control system. These data will be used as the set of experimental results for comparisons in this paper.

6.3 Previous Comparisons with Experimental Data

Several researchers have studied the level of agreement between computer fire models and real-scale fires. These comparisons fall into two broad categories: fire reconstruction and comparison with laboratory experiments. Both categories provide a level of verification for the models used. Fire reconstruction, although often more qualitative, provides a higher degree of confidence for the user when the models successfully simulate real-life conditions. Comparisons with laboratory experiments, however, can yield detailed comparisons that can point out weaknesses in the individual phenomena included in the models.

Fire reconstructions: Nelson [102] used simple computer fire models along with existing experimental data to develop an analysis of a large high-rise building fire. This analysis showed the value of available analytical calculations in reconstructing the events involved in a multiple-story fire. Bukowski [103] has applied the FAST model (an earlier version of the CFAST model) in a litigation against the United States Government. At the request of the Justice Department, the model was used to recreate a multiple-fatality fire in a residence. The analysis

reproduced many details of the fire including conditions consistent with damage patterns to the building, the successful escape of three older children, and three fatalities including the locations of the bodies and the autopsy results. Emmons applied computer fire modeling to the MGM Grand Hotel fire of 1980. This work, conducted during the litigation of this fire was only recently published [104]. Using the HARVARD 5 model, Prof. Emmons analyzed the relative contributions of booth seating, ceiling tiles, decorative beams, and the HVAC system on the outcome of the fire.

Comparisons with laboratory experiments: Rockett, Morita, and Cooper [99] used the HARVARD VI multi-room fire model to simulate the results of real-scale, multi-room fire experiments. These experiments can be characterized by fire sizes of several hundred kW and total compartment volume of about 1000 m^3. While the model was generally found to provide favorable simulations, several areas where improvements were needed were identified. They pointed out limitations in modeling of oxygen-limited burning, mixing of gases at vents, convective heat transfer, and plume entrainment.

Jones and Peacock [7] presented a limited set of comparisons between the FAST model and a multi-room fire test. The experiment involved a constant fire of about 100 kW in a three-compartment configuration of about 100 m^3. They noted "slight over-prediction" of the upper layer temperature and satisfactory prediction of the layer interface position. Again, convective heating and plume entrainment were seen to limit the accuracy of the predictions. A comparison of predicted and measured pressures in the rooms showed good agreement. Since pressure is the driving force for flow between compartments, this agreement was seen as important.

Levine and Nelson [105] used a combination of full-scale fire testing and modeling to simulate a fire in a residence. The 1987 fire in a first-floor kitchen resulted in the deaths of three persons in an upstairs bedroom, one with a reported blood carboxyhemoglobin content of 91 percent. Considerable physical evidence remained. The fire was successfully simulated at full scale in a fully-instrumented seven-room two-story test structure. The data collected during the test have been used to test the predictive abilities of two multiroom computer fire models: FAST and HARVARD VI. A coherent ceiling layer flow occurred during the full-scale test and quickly carried high concentrations of carbon monoxide to remote compartments. Such flow is not directly accounted for in either computer code. However, both codes predicted the carbon monoxide buildup in the room most remote from the fire. Prediction of the pre-flashover temperature rise was also good. Prediction of temperatures after flashover that occurred in the room of fire origin was less good. Other predictions of conditions throughout the seven test rooms varied from good approximations to significant deviations from test data. Some of these deviations are believed to be due to phenomena not considered in any computer models.

Deal [106] reviewed four computer fire models (CCFM [8], FIRST [6], FPETOOL [107] and FAST) to ascertain the relative performance of the models in simulating fire experiments in a small room (about 12 m^3 in volume) in which the vent and fuel effects were varied. Peak fire size in the experiments ranged up to 800 kW. All the models simulated the experimental conditions including temperature, species generation, and vent flows, quite satisfactorily. With a variety of conditions, including narrow and normal vent widths, plastic and wood fuels, and

flashover and sub-flashover fire temperatures, competence of the models at these room geometries was demonstrated.

Duong [108] studied the predictions of several computer fire models (CCFM, FAST, FIRST, and BRI [6]), comparing the models with one another and with large fires (4 to 36 MW) in an aircraft hanger (60,000 m^3). For the 4 MW fire size, he concluded that all the models are reasonably accurate. At 36 MW, however, none of the models did well. Limitations of the heat conduction and plume entrainment algorithms were seen to account for some of the inaccuracies.

6.4 A Direct Comparison Between Model and Measurement

Comparisons of model predictions with experimental measurements serves two purposes: 1) to determine, within limits, the accuracy of the predictions for those quantities of interest to the users of the models (usually those extensive variables related to hazard), and 2) to highlight the strengths and weaknesses of the underlying algorithms in the models to guide future improvements in the models. The predicted variables selected for comparison must deal with both of these purposes.

Most of the studies discussed above present a consistent set of variables of interest to the model user: gas temperature, gas species concentrations, and layer interface position. To assess the accuracy of the physical basis of the models, additional variables must be included. Pressure drives the movement of gases through openings. The pyrolysis rate, and heat release rate of the fire in turn, produces the gases of interest to be moved.

In this section, we will consider all these variables for comparison:

- upper and lower layer gas temperature,
- layer interface position,
- gas species concentration.
- fire pyrolysis and heat release rate,
- room pressure, and
- vent flow,

Although there are certainly other comparisons of interest, these will provide an indication of the match of the model to the experimental data.

6.4.1 Experimental Data Selected for Comparison

Peacock, et. al. [109] compared the performance of the CFAST model with experimental measurements for these variables. Using a range of laboratory tests, they presented comparisons of peak values, average values, and overall curve shape for a number of variables of interest to model users. A total of five different real-scale fire tests were selected for the current comparisons to represent a range of challenges for the CFAST model. These same tests and comparisons were used in this report to evaluate the new version of CFAST. Details of the

experimental measurements and procedure for model calculations are available in the original comparison paper [109].

1) A single-room test using upholstered furniture as the burning item was selected for its well-characterized and realistic fire source in a simple single-room geometry [110]. Heat release rate, mass loss rate, and species yields are available for the test. This should allow straightforward application of the model. Peak fire size was about 2.9 MW with a total room volume of 21 m^3.

2) Like the first test, this test is a single-room fire test using furniture as the fire source [111]. It expands upon that data set by adding the phenomenon of wall burning. Peak fire size was about 7 MW. Room size is similar to the first test.

3) This data set is actually an average of a series of 11 replicate tests in a three-room configuration with simple steady-state gas burner fires [4]. It provides a basic set of quantities that are predicted by current fire models for small to medium size fires. Since all fires were gas burner fires, simulation should be straightforward. It is of particular interest since it was undertaken as a part of a program to develop a methodology for the evaluation and accuracy assessment of fire models. Fire size was about 100 kW with a total volume of 100 m^3.

4) This data set is part a series of tests conducted in a multiple room configuration with more complex gas burner fires than the previous data set [97] , [112]. This study was included because it expands upon that data set by providing larger and time-varying gas burner fires in a room-corridor configuration. Fire size was about up to 1 MW with a total volume of 200 m^3.

5) By far the most complex test, this data set is part of a series of full-scale experiments conducted to evaluate zoned smoke control systems, with and without stairwell pressurization [113]. It was conducted in a seven story hotel with multiple rooms on each floor and a stairwell connecting to all floors. This data set was chosen because it would be considered beyond the scope of most current fire models. Measured temperatures and pressure differences between the rooms and floors of the building are extensive and consistent. Peak fire size was 3 MW with a total building volume of 140,000 m^3.

6.4.2 Discussion

All of the simulations were performed with the CFAST model on an MS-DOS compatible computer. For each of the data sets, the model data were developed from the building and fire descriptions provided in the original reports. Obtaining building geometry, construction materials, and room interconnections was straightforward. Usually, description of the fire source was more difficult. Where freeburn data were available, such data were used to describe the heat release rate, pyrolysis rate, and species yields. In other cases, estimates from tests of similar materials or textbook values were used to determine missing quantities.

How to best quantify the comparisons between model predictions and experiments is not obvious. The necessary and perceived level of agreement for any variable is dependent upon both the typical use of the variable in a given simulation (for instance, the user may be interested in the time it takes to reach a certain temperature in the room), the nature of the experiment (peak temperatures would be of little interest in an experiment which quickly reached steady state), and the context of the comparison in relation to other comparisons being made (a true validation of a model would involve proper statistical treatment of many compared variables).

Insufficient experimental data and understanding of how to compare the numerous variables in a complex fire model prevent a true validation of the model. Thus, the comparisons of the differences between model predictions and experimental data in this paper are intentionally simple and vary from test to test and from variable to variable due to the changing nature of the tests and typical use of different variables.

A recent paper by Pitts, et. al. [114] has shown that there are significant errors in analysis of the data from thermocouples. Once these measurement errors are compensated for, generally there is a significant improvement in the comparison of the model predictions with the corresponding data. These notions have not been incorporated into the following analysis. In general, the thermocouple junctions in the hot layer are really reading a higher temperature than previously thought, and those in the lower layer, lower than reported. Generally, this is due to the relative radiation between the hot and cold wires and the corresponding gas layers to which they are subjected.

6.4.3 Layer Temperature and Interface Position

Arguably the most frequent question asked about a fire is "How hot did it become?" Temperature in the rooms of a structure is an obvious indicator to answer this question. Peak temperature, time to peak temperature, or time to reach a chosen temperature tenability limit are typical values of interest. Quality of the prediction (or measurement) of layer interface position is more difficult to quantify. Although observed valid in a range of experiments, the two-layer assumption is in many ways just a convenience for modeling. From a standpoint of hazard, time of descent to a chosen level may be a reasonable criterion (assuming some in the room will then either be forced to crawl beneath the interface to breathe the "clean" atmosphere near the floor or be forced to breath the upper layer gases). Minimum values may also be used to indicate general agreement. For the single-room tests with furniture or wall-burning, these are appropriate indicators to judge the comparisons between model and experiment. For the more-closely steady-state three- and four-room tests with corridor or the multiple-story building tests, a steady-state average better characterizes the nature of the experiment.

Figures 33 – 35 and Tables 7 – 9 show the upper layer temperature, lower layer temperature, and interface position for the tests studied. Like all zone-based fire models, CFAST calculates conditions within each room as an upper and a lower volume (layer), each with uniform conditions throughout the volume at any instant of time. Thus, for the model, the temperature environment within a room can be described by an upper and lower layer temperature and by the position of the interface between these two layers. By contrast, experimental measurements

often take the form of a vertical array of measurement points describing a profile of temperature. Techniques for collapsing these profiles to data that can be compared to zone fire models are available [101] and are used here to facilitate the comparison.

For the single-room tests, predicted temperatures and layer interface position show obvious similarities to the measured values. Peak values occur at similar times with comparable rise and fall for most comparisons. Interface height for the single-room with wall-burning is a notable exception. Unlike the model prediction, the experimental measurement does not show the rise and fall in concert with the temperature measurement. Peak values are typically higher for upper layer temperature and lower for lower layer temperature and layer interface position. For all the tests, including the single-room tests, times to peak values and times to 100 °C predicted by the model average within 25 s of experimentally measured values.

Table 7. Comparison of experimental measurements and model predictions of upper layer temperature (°C) for several tests

Numbers in parentheses are model predictions	Peak Value (°C)	Time to Peak (s)	Time to 100°C (s)	Steady-State Value (°C)	Similar Shape?
Single-room furniture tests[a] (Tests 1 and 6)	790 (780) 920 (780)	500 (510) 450 (510)	290 (250) 290 (250)	--[b]	✓
	590 (660) 900 (660)	510 (520) 510 (520)	330 (260) 330 (260)	--	✓
Single-room tests with wall burning (Tests 1 and 2)	750 (620)	710 (230)	100 (140)	--	✓
	810 (1190)	520 (470)	100 (80)	--	✓
Three-room tests with corridor[c] (SET 4, 11 replicates)	--	--	100 (120) 830 (n.r.) n.r.	230 (215) 75 (90) 45 (50)	
Four-room tests with corridor[c] (Tests 19 and 21)	--	--	195 (195) n.r. n.r. n.r.	240 (370) 70 (90) 55 (35) 40 (35)	✓
	--	--	200 (195) n.r. (240) n.r. n.r.	260 (370) 80 (100) 65 (50) 50 (50)	
Multiple-story building (Test 7)	--	--	390 (180) 210 (390) n.r.	270 (340) 110 (110) 15 (15)	✓

[a] Two measurement positions within the room were available from the experimental data.
[b] Not appropriate for the experiment.
[c] Multiple entries indicate multiple comparable rooms in the test structure.

Table 8. Comparison of experimental measurements and model predictions of lower layer temperature (°C) for several tests

Numbers in parentheses are model predictions	Peak Value (°C)	Time to Peak (s)	Time to 100°C (s)	Steady-State Value (°C)	Similar Shape?
Single-room furniture tests[a]	570 (430) 590 (430)	500 (510) 420 (510)	370 (400) 390 (400)	--[b]	✓
	230 (230) 590 (230)	510 (520) 500 (520)	410 (460) 390 (460)	--	✓
Single-room tests with wall burning	710 (240)	710 (230)	240 (220)	--	✓
	700 (950)	520 (470)	290 (290)	--	✓
Three-room tests with corridor[c]	--	--	n.r. n.r. n.r.	70 (50) 30 (30) 23 (30)	
Four-room tests with corridor[c]	--	--	n.r. n.r. n.r.	75 (50) 21 (22) 21 (17)	✓
	--	--	n.r. n.r. n.r.	70 (52) 20 (22) 20 (17)	
Multiple-story building	--	--	520 (n.r.) n.r. n.r.	85 (95) 40 (45) 14 (16)	✓

See notes for Table 7.

Table 9. Comparison of experimental measurements and model predictions of layer interface position (m) for several tests

Numbers in parentheses are model predictions	Peak Value (m)	Time to Peak (s)	Time to 1 m (s)	Steady-State Value (m)	Similar Shape?
Single-room furniture tests[a]	0.8 (0.3) 0.8 (0.3)	420 (480) 450 (480)	400 (390) 380 (390)	--[b]	✓
	0.8 (0.5) 0.9 (0.5)	480 (510) 460 (510)	420 (430) 430 (430)	--	✓
Single-room tests with wall burning	0.2 (0.7)	710 (220)	120 (210)	--	✓
	0.1 (0.6)	500 (410)	80 (280)	--	✓
Three-room tests with corridor[c]	--	--	360 (n.r.) 1210 (n.r.) 90 (n.r.)	1.0 (1.7) 1.2 (1.6) 0.9 (1.3)	✓
Four-room tests with corridor[c]	--	--	n.a.	0.7 (1.7) 1.0 (1.8) 1.0 (1.7) 0.7 (1.7)	
	--	--	n.a.	0.8 (1.5) 0.9 (1.4) 0.8 (1.2) 0.6 (1.2)	
Multiple-story building	--	--	n.a.	0.3 (0.6) 0.8 (0.8) 1.8 (0.9)	

See notes for Table 7.

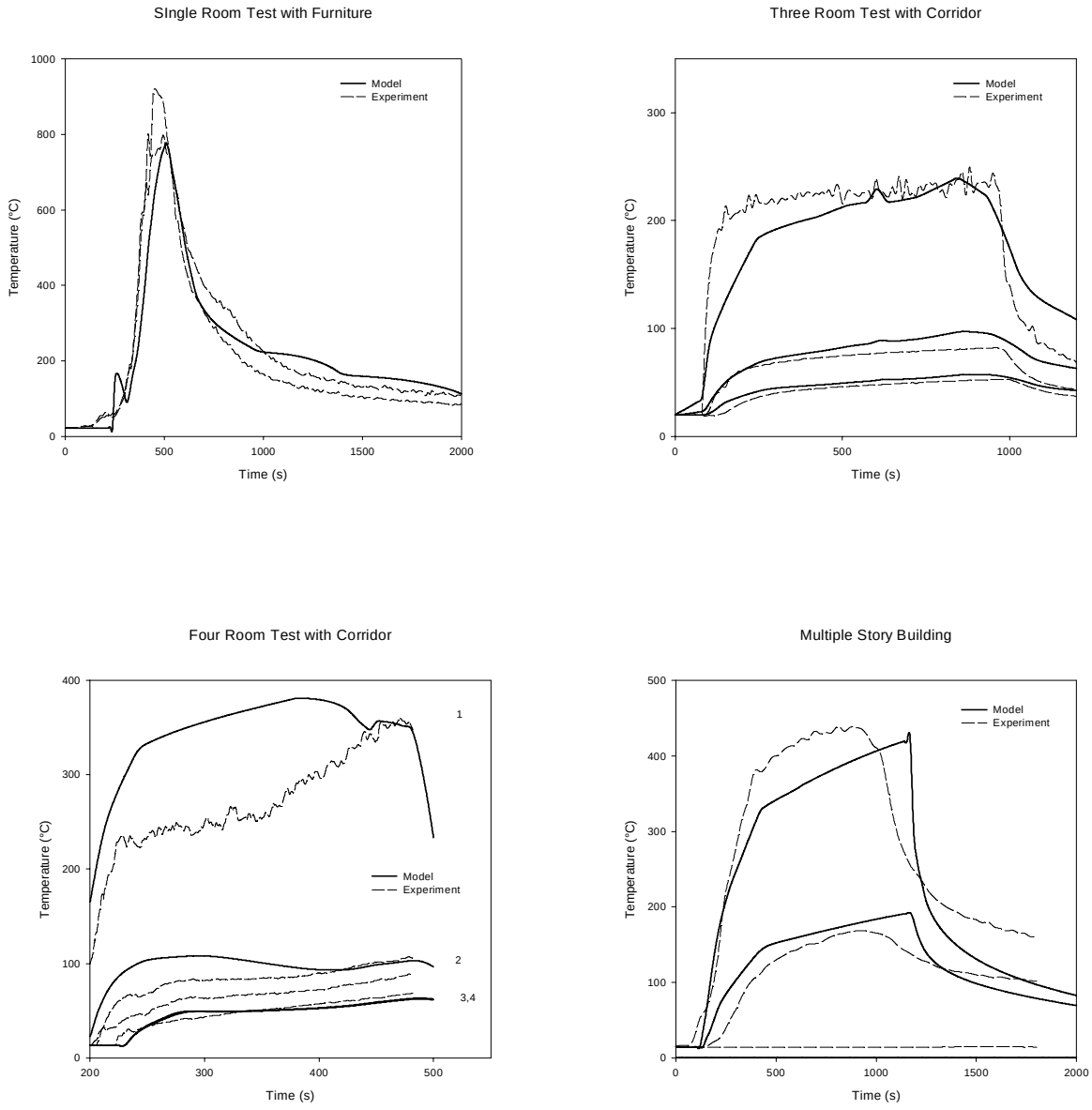

Figure 33. Comparison of measured and predicted upper layer temperatures for several tests. (Numbers indicate comparable rooms in the test structure.)

Systematic deviations exist for the remaining three data sets. Differences between model predictions and experimental measurements change monotonically over time (rising for the three-room test and falling for the four-rooms tests. Modeling of heat conduction (losing too much or too little heat to the surfaces) or lack of modeling of leakage (rooms are presumed

perfectly sealed unless vents are included to simulate leakage) may account for the trends. The comparison of interface position for the four-room test with corridor seems an anomaly. Although a nearly closed space, the roughly level interface position from the experiment seems more typical of a test more open to the ambient. The model calculations would appear to better represent the mixing which would occur in a closed volume. Again, leakage may be a factor. With some leakage in the space, lower temperatures for both the lower and upper layer and higher (and more uniform) interface position would be calculated.

In general, upper layer temperature and interface position predicted by the model are somewhat higher than experimental measurements [95], with the differences ranging from -140 to 380 °C for the temperature and -0.5 to 0.8 m for the interface position. Conversely, the lower layer temperature is somewhat lower for the model than for the experiments (-470 to 250 °C). Presuming conservation of energy (an underlying assumption in *all* fire models), these three observations are consistent. A higher interface position gives rise to a smaller upper volume (and larger lower volume) within a room. With the same enthalpy in a smaller upper volume, higher temperatures result. This lends credence to the assumption of enthalpy conservation. Layer interface position is primarily affected by entrainment by the fire or at vents. Plume entrainment in CFAST is based on the work of McCaffrey [21] on circular plumes in relatively small spaces. For large fires in small spaces where the fire impinges on the ceiling (such as the single room tests with wall burning) or very small fires in large spaces (such as atria), these correlations may not be as valid.

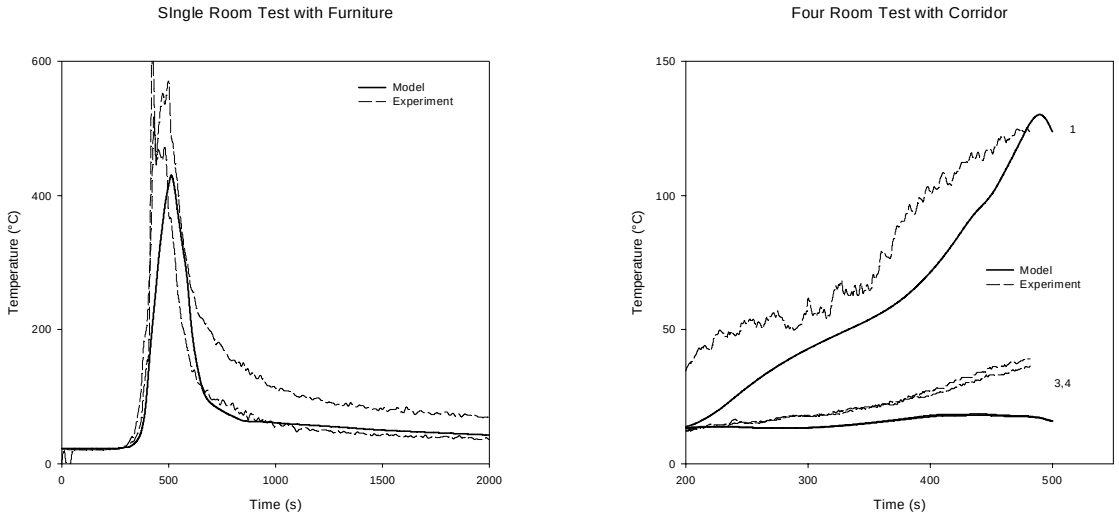

Figure 34. Comparison of measured and predicted lower layer temperatures for several tests. (Numbers indicate comparable rooms in the test structure.)

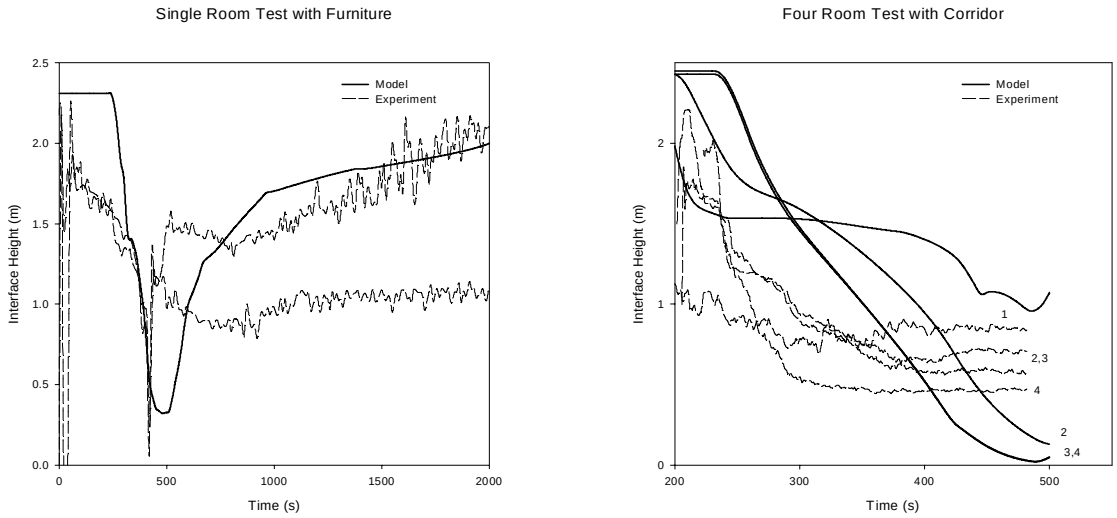

Figure 35. Comparison of measured and predicted layer interface position for several tests. (Numbers indicate comparable rooms in the test structure.)

6.4.4 Gas Species

The fire chemistry scheme in CFAST is essentially a species balance from user-specified species yields and the oxygen available for combustion. Once generated, it is a matter of bookkeeping to track the mass of species throughout the various control volumes in a simulated building. It does, however, provide another check of the flow algorithms within the model. Since the major species (CO and CO_2) are generated only by the fire, the relative accuracy of the predicted values throughout multiple rooms of a structure should be comparable. Figure 36 and table 10 show measured and predicted concentrations of O_2, CO_2, and CO in two of the tests studied.

For the single-room tests with furniture, the predicted concentrations are lower than those measured experimentally (averaging 5 percent low). This is probably due to the treatment of oxygen limited burning. In CFAST, the burning rate simply decreases as the oxygen level decreases. A user specified lower limit determines the point below which burning will not take place. This parameter could be finessed to provide better agreement with the experiment. For the present comparisons, it was always left at the default value.

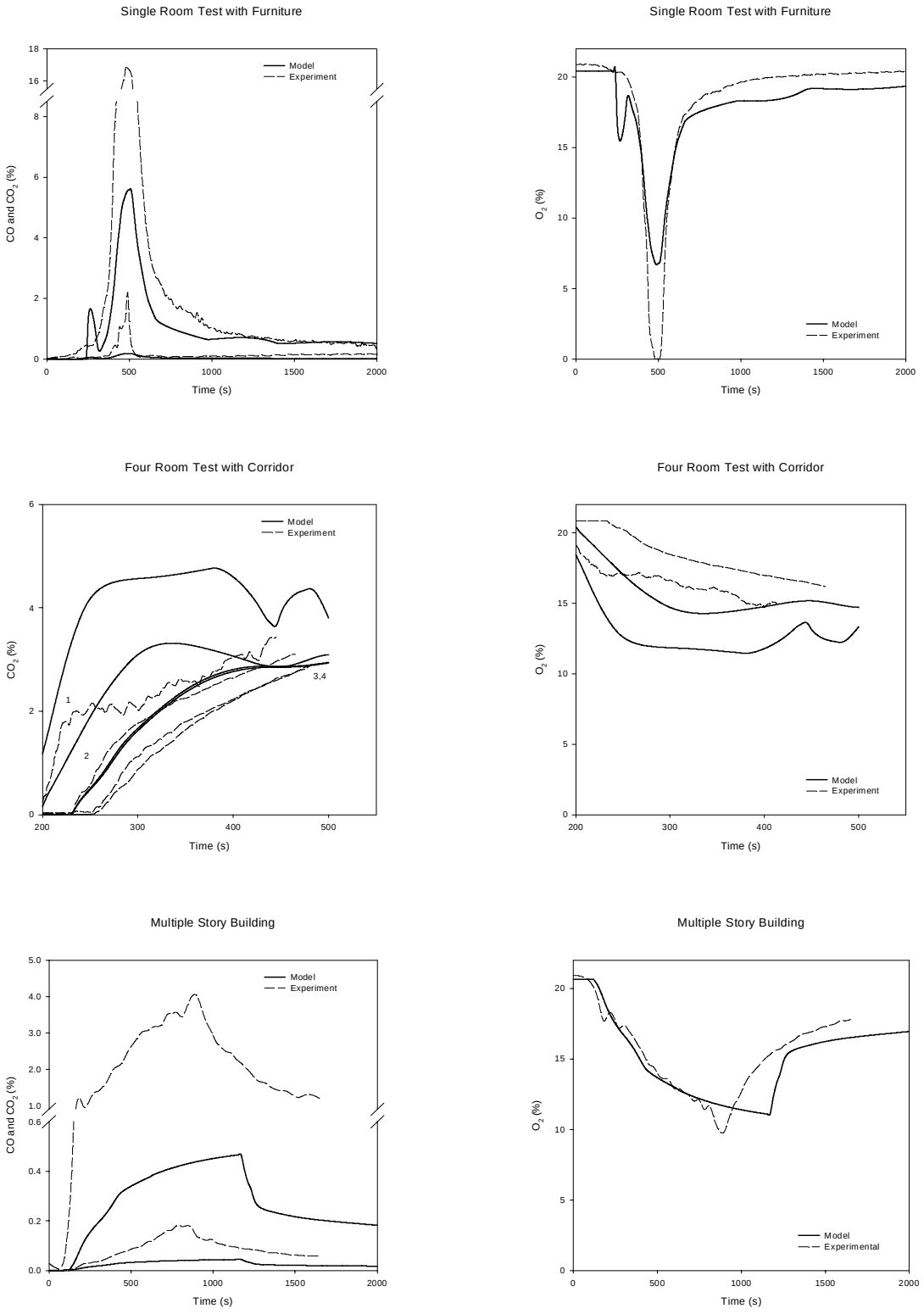

Figure 36. Comparison of measured and predicted gas species concentration for several tests. (Numbers indicate comparable rooms in the test structure.)

Table 10. Comparison of experimental measurements and model predictions of oxygen concentration for several tests

Oxygen Concentration

Numbers in parentheses are model predictions	Peak Value (%)	Time to Peak (s)	Steady-State Value (%)	Similar Shape?
Single-room furniture fire tests	0.01 (6.7)	510 (490)	--[a]	✓
	6.9 (10.6)	490 (510)	--	✓
Four-room tests with corridor[b]	--	--	17.9 (12.8) 18.0 (15.4)	✓
	--	--	16.1 (11.8) 18.1 (16.5)	✓
Multiple-story building test[b]	--	--	15.5 (11.1) 20.9 (20.3)	

Carbon Dioxide Concentration

Single-room furniture fire tests	17.0 (5.6)	480 (510)	--[a]	✓
	10.6 (4.1)	490 (510)	--	✓
Four-room tests with corridor[b]	--	--	2.3 (4.1)	✓
	--	--	2.4 (4.8)	✓
Multiple-story building test[b]	--	--	2.0 (0.5)	

Carbon Monoxide Concentration

Single-room furniture fire tests	2.2 (0.2)	490 (510)	--[a]	✓
	0.6 (0.1)	440 (510)	--	✓
Multiple-story building test[b]	--	--	0.8 (0.04)	

[a] not appropriate for the test.
[b] multiple entries indicate comparable rooms in the test structure.

For the four room test with corridor, the asymptotic values of the gas concentrations agree quite well. At first glance, the model predictions reach this equilibrium more quickly. An appreciation of the differences between the modeled parameters and the experimental measurements put this in perspective. From figure 35, it takes about 100 s for the upper layer to descend to the level of the gas sampling port in the test. In addition, it is assumed than this point measurement is the bulk concentration of the entire upper layer. In reality, some vertical distribution not unlike the temperature profile (figure 35) exists for the gas concentration as well.

Since this measurement point is near the lower edge of the upper layer for a significant time, it should underestimate the bulk concentration until the layer is large in volume and well mixed.

For the multiple-story building test, predicted values for CO_2, CO, and O_2 are far lower than measured experimentally. Both the lower burning rate limit as well as leakage in the 100 year-old structure probably contribute to the differences between the experiments and model. In addition, values for species yields were simply literature values since no test data were available.

6.4.5 Heat Release and Fire Pyrolysis Rate

Heat release rate and its intimately related pyrolysis rate are key indicators of fire hazard [115]. Peak values and time to reach peak values are typical scalar estimates used to represent the time-variant heat release rate and fire pyrolysis rate. For the single-room tests with furniture or wall-burning, these are appropriate indicators to judge the comparisons between model and experiment. For the three- and four-room tests with corridor or the multiple-story building tests, a steady state average is more appropriate.

Table 11 and figure 37 compare measured and predicted heat release rates for the tests. In the CFAST model, the fire is specified as a series of straight line segments describing the pyrolysis rate, heat release rate, and species yields. Thus, the model predictions could be expected to agree quite well with experimental measurements. For tests where experimental data were available, the agreement is excellent – usually within 5 percent of the peak experimental values. Since this effectively just shows how well a series of line segments reproduces experimental measurement, this level of agreement is expected.

Times to peak values are always close. For two tests (the single-room with furniture and wall burning and the multiple-story building), the heat release rate in the room is limited by the available oxygen. Additional burning outside the room (seen in the single-room with furniture) accounts for the remainder of the heat released.

For the three-room test with corridor, multiple replicate tests put the agreement between the model and experiments in perspective. For all tests in the original study [4], the coefficients of variation (the standard deviation expressed as a percentage of the mean) ranged from 4 to 52 percent. In another study, precision to within 15 percent for fires of 2.5 MW was noted [110]. Thus, the simplification of specifying the fire growth as a series of straight lines is easily justified with the expected accuracy of experimental measurements.

Table 11. Comparison of experimental measurements and model predictions of heat release rate for several tests

Numbers in parentheses are model predictions	Peak Value (kW)	Time to Peak (s)	Steady-State Value (kW)	Similar Shape?
Single-room furniture fire tests	2450 (2200)	480 (480)	--[a]	✓
	2600 (2350)	500 (510)	--	✓
Single-room tests with wall-burning	2050 (2000)	230 (200)	--	✓
	4000 (3150)	420 (370)	--	✓
Three-room test with corridor	--	--	86 (87)	✓
Four-room tests with corridor	--	--	n.r.[b]	✓
	--	--	n.r	✓
Multiple-story building test	--	--	n.r	✓

[a] not appropriate for the test.
[b] not available from experimental data.

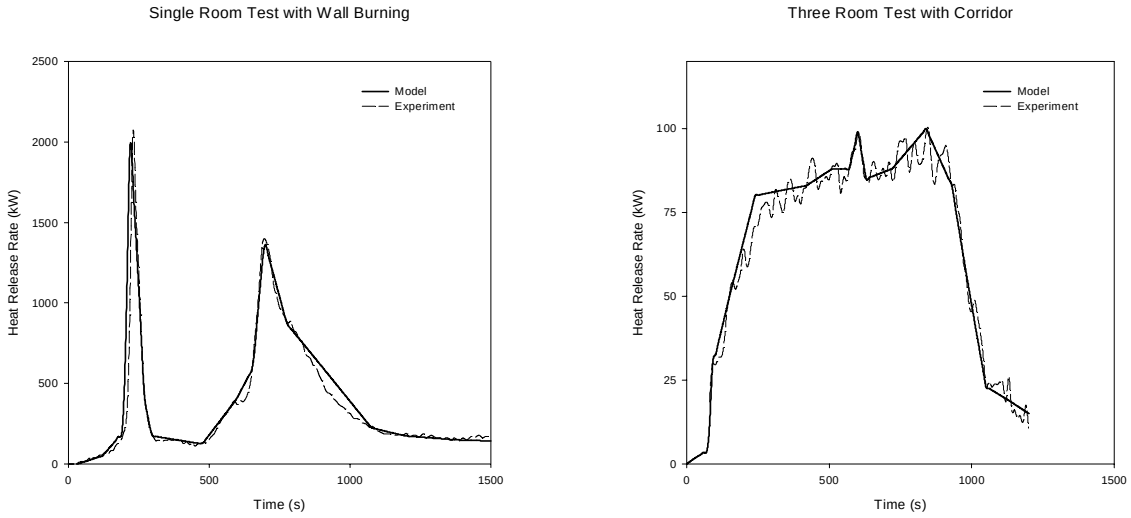

Figure 37. Comparison of measured and predicted heat release rates for two selected tests.

For the multiple-story building test, *no* pyrolysis rate or heat release rate data were available. Estimates of the "steady-state" burning rate, time to reach "steady-state," and duration of "steady-state" burning were made from available correlations for wood cribs [116], [117]. Although the comparisons for this test should be considered approximate, it was included since, if successful, the scope of the model is extended considerably to a large multiple-story building with mechanical ventilation.

6.4.6 Pressure

The differential pressure across an opening drives the flow through the opening. For each room, the CFAST model calculates a differential pressure at floor level, referenced to ambient. Noting that the ambient pressure is approximately 100 kPa, typical pressure drops across openings induced by fires are but a small fraction of the ambient pressure – typically from less than 1 Pa to perhaps a few hundred Pascals in well-sealed enclosures. The ability to model these extremely small differential pressures provides another check on the flow algorithms in the model. These are, however, expected to be difficult to model and measure accurately. Thus, agreement within a few pascals is often considered acceptable. In four of the five experimental test series, measurements (corrected to floor level) were available which could be compared to these predicted values (measurements were not available for the single room tests with furniture).

Figure 38 and table 12 show the comparisons. For most cases, the agreement is reasonable, with the difference between measured and predicted values typically less than 2 Pa and for some experiments, less than 0.5 Pa. Trends displayed in the experimental data are replicated by the model predictions. Some interesting exceptions are apparent however. In major part, these are due to quantities unknown in the experiments (leakage). Not all of the onus for agreement should be placed on the model, however. Only one of the test series included any estimate of leakage through cracks in the buildings. Logically, unless directed otherwise, the model assumes *no* leakage from any room. This leakage can have a dramatic effect on the results predicted by the model. Figure 39 illustrates the effect of leakage for a single room with a single doorway and an upholstered chair used as the fire source. Leakage areas from 0 to 100 percent of the vent area were simulated with a second vent of appropriate size and placed at floor level (much of the leakage in rooms take place at floor level). Both temperatures and pressures change by more than a factor of two (other variables can be expected to change with similar variation). Temperatures changes by about 20 percent with only a 10 percent leakage area. The effect on pressure is not quite as straightforward, but for larger leakages changes in concert with the temperature. For the four-room tests with corridor, leakage from the "well sealed rooms" was estimated via measurement at not more than 25 percent of the total vent area.

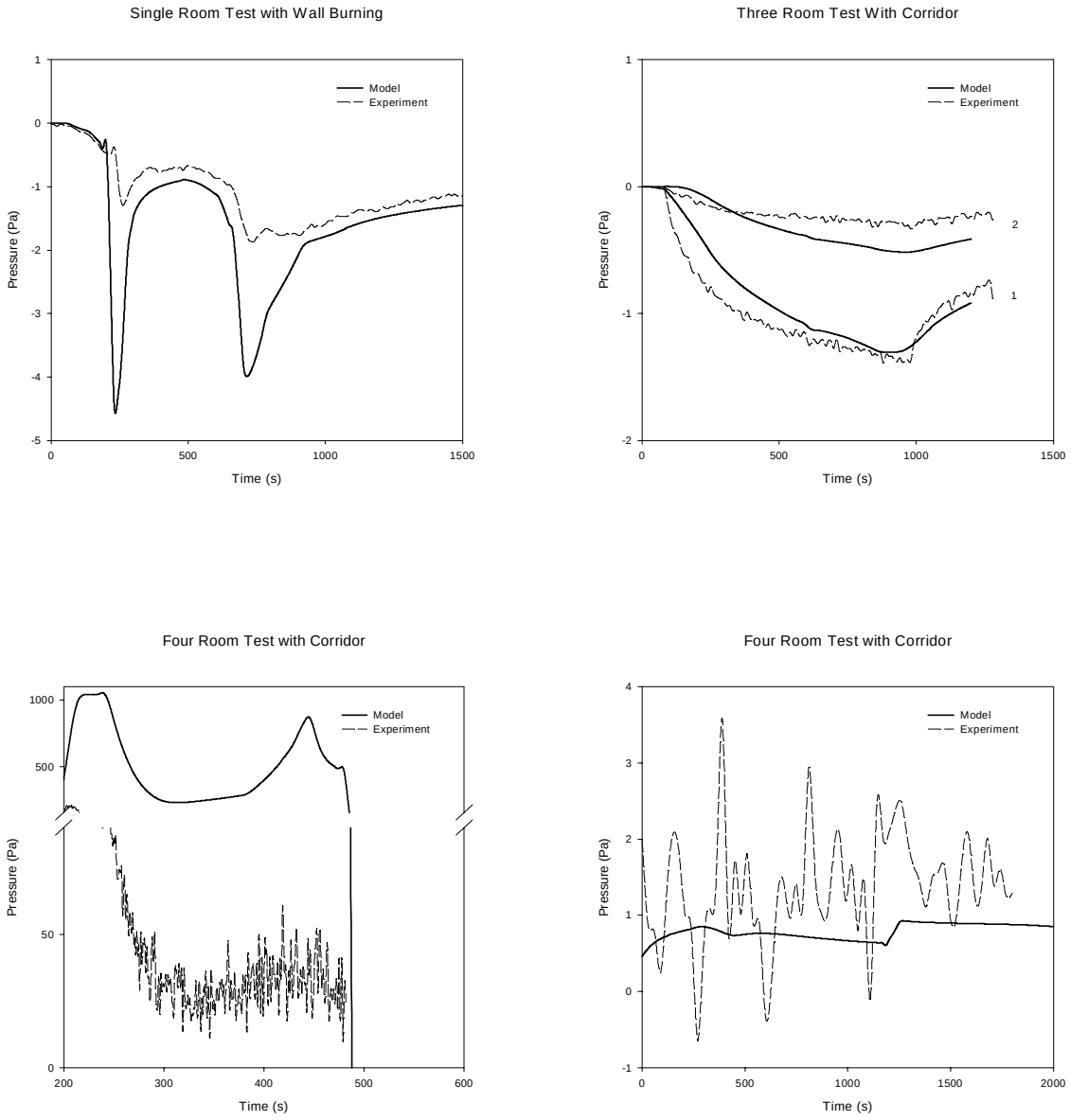

Figure 38. Comparison of measured and predicted pressures for several tests. (Numbers indicate comparable rooms in the test structure.)

Table 12. Comparison of experimental measurements and model predictions of room pressure for several tests

Numbers in parentheses are model predictions	Peak Value	Time to Peak	Steady-State Value	Similar Shape?
Single-room tests with wall-burning	-1.9 (-4.5)	730 (230)	--	✓
	-1.9 (-6.4)	520 (490)	--	✓
Three-room test with corridor	--	--	-1.1 (-0.6) -0.2 (-0.5)	✓
Four-room tests with corridor	--	--	-1.0 (-2.1)	✓
	--	--	36 (22)	
Multiple-story building test	--	--	2.4 (1.3)	✓

[a] not appropriate for the test.

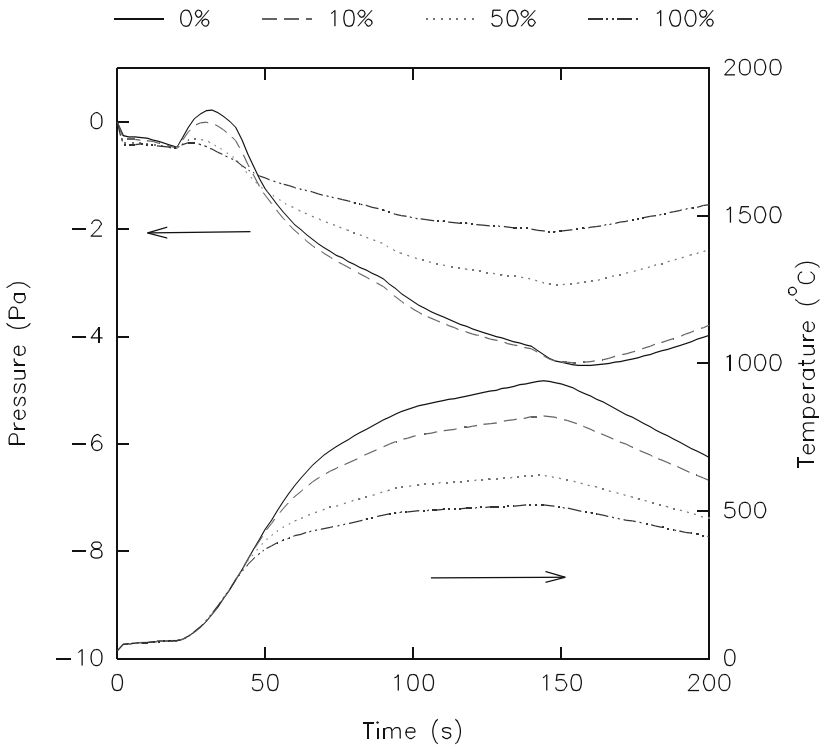

Figure 39. Effect of leakage in an arbitrary single-room fire.

6.4.7 Flow Through Openings

In the control volume approach, the differential form of the momentum equation for the zones is not solved directly. Rather, the momentum transfer at the zone boundaries is included by using Bernoulli's approximation for the velocity equation. This solution is augmented for restricted openings by using flow coefficients [27], [51] to allow for constriction in vents. The flow coefficients allow for an effective constriction of fluid flow which occurs for vents with sharp edges. In CFAST, these coefficients are for rectangular openings in walls whose surfaces are much larger than the opening.

Figure 40 and table 13 compare measured and predicted mass flows through doorways in two of the tests studied. For the three-room test with corridor, flow through two doorways of the same test are shown (one between the fire room and the corridor and one between the corridor and the outdoors). Not surprisingly, the flow is typically somewhat underpredicted by the model (averaging 0.1kg/s). The vent flow in CFAST includes mixing phenomena at the vents. As hot gases from one compartment leave that compartment and flow into an adjacent compartment, a door jet can exist which is analogous to a normal fire plume, but with an extended flat plume similar to a waterfall. This places its use outside the normal range of the plume model [21] and perhaps beyond its range of validity. However, no reliable correlation yet exists for the extended flat plume which occurs in vent flow. Examining the trends of prediction of upper layer temperature in tests with multiple rooms (Tables 1 and 2), the typical over-prediction in the room of fire origin is far greater than for other rooms in the structures. The under-prediction of the mass flows probably accounts for this as a cascading effect as you move away from the room of fire origin.

Table 13. Comparison of experimental measurements and model predictions of mass flow through openings for several tests

Numbers in parentheses are model predictions	Peak Value	Time to Peak	Steady-State Value	Similar Shape?
Single-room furniture fire tests	1.2 (1.3)	380 (410)	--[a]	✓
	1.9 (1.9)	560 (460)	--	✓
Three-room test with corridor	--	--	0.4 (0.3)	✓

[a] not appropriate for the test.

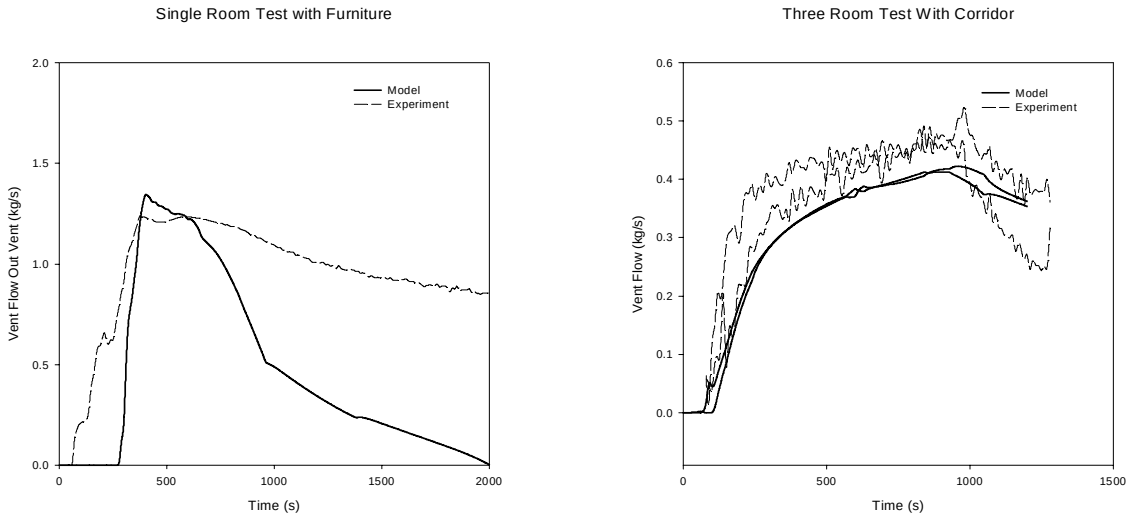

Figure 40. Comparison of measured and predicted mass flow through vents for several tests. (Numbers indicate comparable rooms in the test structure.)

6.4.8 Other comparisons

Arguably the most frequent question asked about a fire is "How hot did it become?" Temperature in the rooms of a structure is an obvious indicator to answer this question. Peak temperature, time to peak temperature, or time to reach a chosen temperature tenability limit are typical values of interest. Papers by Peacock, Jones, and Bukowski[118], Beard[119], Deal and Beyler[120], and Reneke *et.al*. [121] are illustrative.

Figure 41 shows a comparison of measured and predicted upper layer temperature for several tests studied[?]. For the single-room tests, predicted temperatures show obvious similarities to the measured values. Peak values occur at similar times with comparable rise and fall for most comparisons. Peak values are typically higher for upper layer temperature and lower for lower layer temperature and layer interface position. For all the tests, including the single-room tests, times to peak values and times to 100 °C predicted by the model average within 25 s of experimentally measured values.

Systematic deviations exist for the remaining three data sets. Differences between model predictions and experimental measurements change monotonically over time (rising for the three-room test and falling for the four-rooms tests. Modeling of heat conduction (losing too much or too little heat to the surfaces) or lack of modeling of leakage (rooms are presumed perfectly sealed unless vents are included to simulate leakage) may account for the trends.

In general, upper layer temperatures predicted by the model are higher than experimental measurements, with the differences ranging from -46 to 230 °C. Conversely, the lower layer temperature is somewhat lower for the model than for the experiments (-60 ˚C to 5 °C). Presuming conservation of energy (an underlying assumption in *all* fire models), these observations

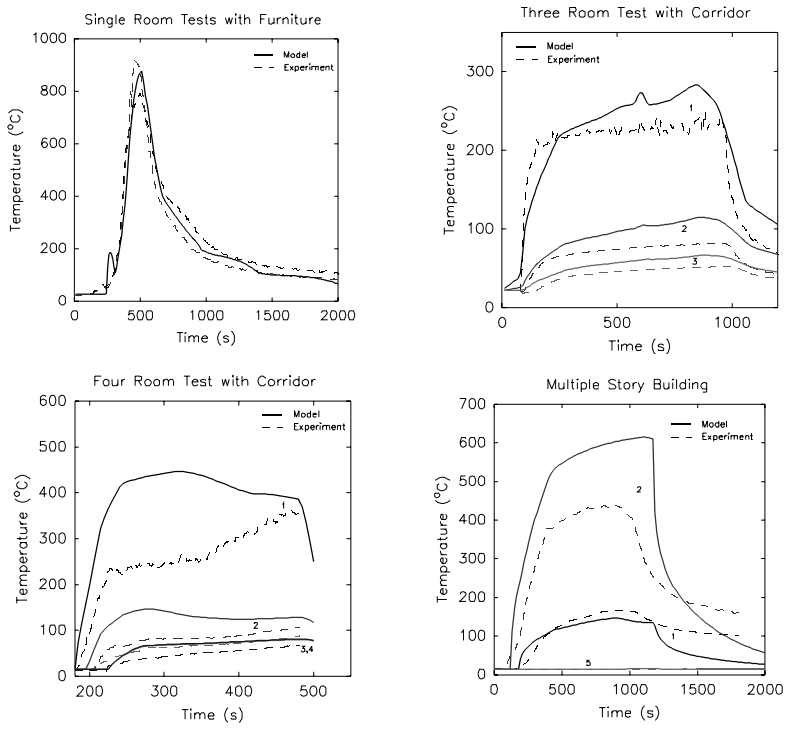

Figure 41. Comparison of measured and predicted upper layer temperatures for several tests. (Numbers indicate comparable rooms in the test structure.)

are consistent. Limitations inherent in the model also account partially for these trends. In the current version of CFAST, energy exchange in the lower layer is *only* by mixing or convection from surfaces. Adding radiative exchange to the lower layer would reduce the upper layer temperature and increase the lower layer temperature. Layer interface position is primarily affected by entrainment by the fire or at vents. Underestimation of the conduction would also account for the effect. Plume entrainment in CFAST is based on the work of McCaffrey on circular plumes in relatively small spaces. For large fires in small spaces where the fire impinges on the ceiling (such as the single room tests with wall burning) or very small fires in large spaces (such as atria), these correlations may not be as valid.

6.5 Prediction of flashover

A number of simple correlations and the CFAST model were used to simulate a range of geometries and fire conditions to predict the development of the fire up to the point of flashover. The simulation represent a range of compartment sizes from 8 m^3 to 1327 m^3, with ceiling height varying from 2.4 m to 12.2 m and vent openings from 10% to 100% of the length of the short wall (plus a "standard" door, 0.76 m in width). For most of the simulations, the surface lining material was gypsum wallboard, 12.7 mm in thickness, consistent with the values used in the correlations. A simple constant fire size was varied until the calculated upper layer temperature reached 600 ˚C at the end of the simulation. For some simulations, the surface linings ranged from aluminum to a highly insulating foam and the fire source diverged from the simple steady-state fire to more complex shapes.

The important test of all these prediction methods is in the comparison of the predictions with actual fire observations. Figure 42 presents estimates of the minimum energy required to achieve flashover for a range of room and vent sizes. This figure is an extension of the earlier work of Babrauskas[122] and includes additional experimental measurements from a variety of sources, most notably the work of Deal and Beyler[123]. In addition, it includes predictions from the CFAST model.

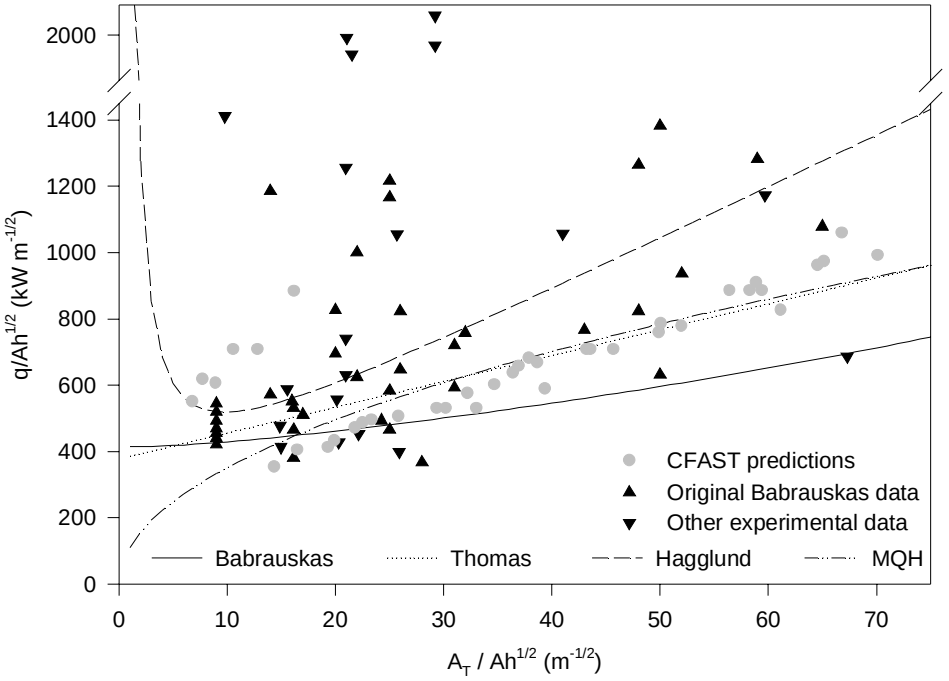

Figure 42. Comparison of correlations, CFAST predictions, and experimental data for the prediction of flashover in a compartment fire.

As with some of the experimental data defining flashover as an upper layer temperature reaching 600 °C, many experimental measures were reported as peak values rather than minimum values necessary to achieve flashover. Thus, ideally all the predictions should provide a lower bound for the experimental data. Indeed, this is consistent with the graph – the vast majority of the experimental observations lie above the correlations and model predictions. For a considerable range in the ratio $A_T/A\sqrt{h}$, the correlations of Babrauskas, Thomas, and McCaffrey, Quintiere, and Harkelroad provide nearly identical estimates of the minimum energy required to produce flashover. The estimates of Hägglund yields somewhat higher estimates for values of $A_T/A\sqrt{h}$ greater than 20.

The results from the CFAST model for this single compartment scenario provide similar results to the experiments and the correlations for most of the range of $A_T/A\sqrt{h}$. For small values of $A_T/A\sqrt{h}$, the CFAST values rise somewhat above the values from the correlations. These small values of $A_T/A\sqrt{h}$ result from either very small compartments (small A_T) or very large openings (large $A\sqrt{h}$), both of which stretch the limits of the assumptions inherent in the model. For very small compartments, radiation from the fire to the compartment surfaces becomes more important, enhancing the conductive heat losses through the walls. However, the basic two-zone assumption may break down as the room becomes very small. For very large openings, the calculation of vent flow via an orifice flow coefficient approach is likely inaccurate. Indeed, for such openings, this limitation has been observed experimentally[7]. Still, the estimates are close to the ranges provided by the correlations which also diverge at very small values of $A_T/A\sqrt{h}$.

Perhaps most significant in these comparisons is that all the simple correlations provide estimates similar to the CFAST model and all the models are consistent with a wide range of experimental data. For this simple scenario, little is gained with the use of the more complex models. For more complicated scenarios, the comparison may not be as simple.

6.6 Quantifying the Comparison of Model Predictions with Experimental Data

Using the same data as in the section 6.4, we can also apply the mathematics of functional analysis (see Appendix C) to provide a quantification of the closeness of the measured and predicted time series (*i.e.*, the time/temperature curve).

Table 14 presents the hybrid relative difference norm (eq 1) and cosine of the angle between the vectors of experimental data and model predictions for a selection of the data from these five tests. To better understand these quantified comparisons, Figures 43 to 46 present both the experimental data and model predictions for several of the variables included in Table 14.

Figure 43 shows a comparison of upper layer temperatures for a single room test. In this test, two measurement positions were available from the experimental data. The predicted temperatures show obvious similarities to the measured values. Peak values occur at similar times with comparable rise and fall for both measurement positions. For both positions, peak temperatures are higher than the model predictions, with one position somewhat higher than the other position. Both the relative difference norm and cosine reflect these trends. The relative difference norm is somewhat higher for one of the experimental positions (0.36 versus 0.31)

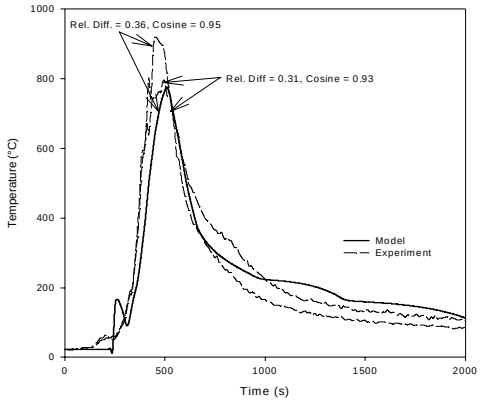

Figure 43. Comparison of Upper Layer Temperature for a Single-Room Test.

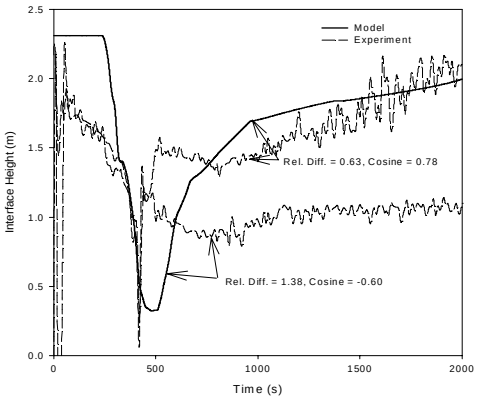

Figure 44. Comparison of Layer Interface Position for a Single-Room Test.

reflecting the higher temperature at this measurement position. With the shapes of all the curves similar, the cosine shows similar values for both curves (0.93 and 0.95).

The relative difference norm and cosine for the comparison of interface position for this same test also reflects trends in the data. Figure 44 shows the interface position calculated from experimental temperature profiles compared with that predicted by the model. For one of the measurement positions, the dip in the layer height from 2 m to 1 m at about 500 s is evident in both the experimental measurements and in the model prediction. The relative difference norm and cosine for this comparison is 0.63 and 0.78 respectively. For the other measurement position, the interface height drops to about a 1 m height and remains there for the duration of the test. A higher relative difference norm of 1.38 and negative value for the cosine of –0.60 reflects the poor comparison at this measurement position. For both positions, the cosine values are lower than those of the upper layer temperature comparisons due both to differences in the shapes of the curves and to high noise in the experimentally determined interface position.

Figure 45 shows a comparison of measured and predicted gas concentrations in the four-room test (set number 4). The relative difference norms show that there are significant differences in the magnitude of the measured and predicted O_2, CO, and CO_2 concentrations, ranging from 0.85 to 1.16. These differences are likely indicative of the production rates for the species used as input to the model. More consistent cosine values ranging from 0.53 to 0.63 reflects the similar functional form used by the model to calculate the concentration and flow of species throughout the compartments.

Figure 46 shows room pressure in two tests. In the single room test of figure 6(a), the functional form of the predicted pressure is somewhat similar to the experimental measurements, but the model predictions show deeper dips in the curves. For this comparison, a relative difference

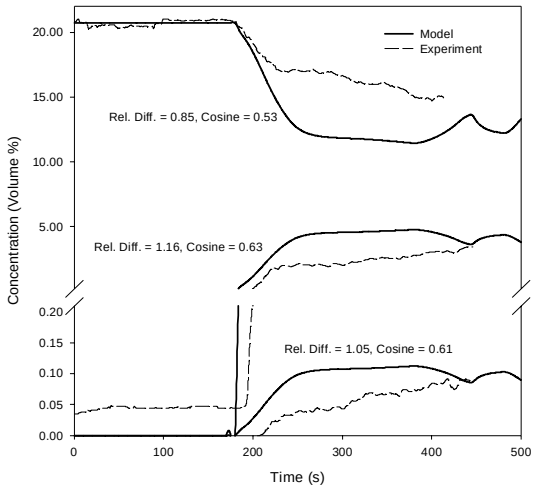

Figure 45. Comparison of Gas Concentrations in a Four-room Test.

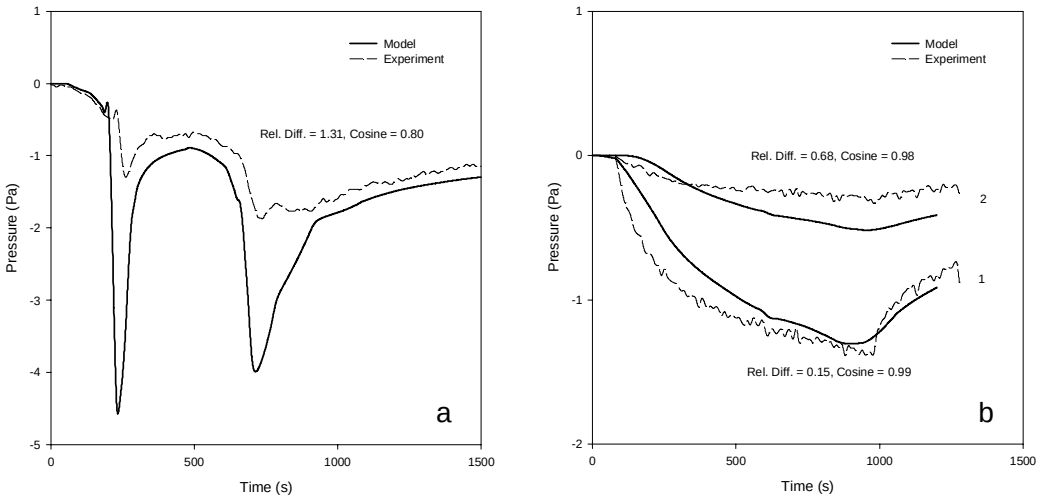

Figure 46. Comparison of Room Pressures for Two Tests.

norm of 1.31 and cosine of 0.80 reflect these trends. For the three-room test in figure 6(b), the similar functional form of the experimental measurements and model predictions is shown in the values of the cosine of 0.98 and 0.99. For compartment 1, the magnitude of the model predictions agrees quite well with the experiment with a relative difference norm of 0.15. For

compartment 2, the value is higher at 0.68 since the curves cross early in the test and remain different for the duration of the test.

6.7 A Summary of the Difference Between Direct and Quantified Comparisons

In the past, the comparison of experimental measurements with model predictions has been largely qualitative in nature. We now have techniques to quantify the differences between experimental measurements and model predictions in the context of zone fire modeling. For the experiments and models examined, the techniques provide the ability to quantify the comparison magnitude and functional form consistent with visual examination of the comparisons.

Table 14. Comparison between experimental measurements and predicted values for selected experiments. When no comparison is available, the table entry is (-).

	Compartment	Rel. Dif.	Cosine	Rel. Dif.	Cosine	Rel. Dif.	Cosine
Upper Layer Temperature and Interface Position							
		Upper Layer Temperature		**Lower Layer Temperature**		**Interface Position**	
Single compartment	1	0.31	0.95	0.47	0.92	1.38	-0.60
	2	0.36	0.93	0.63	0.78	0.63	0.78
Three compartments	1	0.25	0.97	–	–	–	–
	2	0.26	0.99	–	–	–	–
	3	0.26	0.98	–	–	–	–
Four compartments	1	0.51	0.93	0.33	0.95	2.26	0.06
	2	0.54	0.91	0.52	0.87	–	–
	3	0.36	0.97	0.78	0.86	–	–
	4	0.20	0.98	–	–	–	–
Multiple story	1	0.28	0.97	–	–	–	–
	2	0.27	0.96	–	–	–	–
	7	2.99	0.20	–	–	–	–
Gas Concentration							
		Oxygen		**Carbon Monoxide**		**Carbon Dioxide**	
Single compartment	1	0.48	0.90	0.93	0.66	0.69	0.93
Four compartments	1	0.85	0.53	1.05	0.61	1.16	0.63
	2	0.93	0.39	1.02	0.57	0.90	0.63
Multiple story	2	0.74	0.68	0.72	0.90	0.87	0.93
Heat Release, Pressure, and Vent Flow							
		HRR		**Pressure**		**Vent Flow**	
Single compartment		0.19	0.98	–	–	0.61	0.79
Wall burning		0.21	0.98	1.31	0.80	–	–
Three compartments	1	0.43	0.96	0.15	0.99	0.14	0.99

7 Acknowledgment

Preparation of this document was sponsored by the U.S. Nuclear Regulatory Commission.

8 References

[1] ASTM. Standard Guide for Evaluation the Predictive Capability of Deterministic Fire Models, ASTM E1355-97, West Conshohocken, PA (1998).

[2] Friedman, R., "Survey of Computer Models for Fire and Smoke," *Factory Mutual Research Corp.*, Norwood, MA, 02062 1990.

[3] Cooper, L.Y., "A Mathematical Model for Estimating Available Safe Egress Time in Fires," *Fire and Materials.* 1982, *6(4),* 135-144.

[4] Babrauskas, V., "COMPF2-A Program for Calculating Post-Flashover Fire Temperatures," *Natl. Bur. Stand. (U.S.)* 1979, *Tech. Note 991,* 76 p.

[5] Davis, W. D. and Cooper, L. Y., "Computer Model for Estimating the Response of Sprinkler Links to Compartment Fires With Draft Curtains and Fusible Link-Actuated Ceiling Vents," *Fire Technology* 1991, *27 (2),* 113-127.

[6] Tanaka, T., "A Model of Multiroom Fire Spread," *Nat. Bur. Stand. (U.S.)* 1983, *NBSIR 83-2718,* 175 p.

[7] Jones, W. W., A Multicompartment Model for the Spread of Fire, Smoke and Toxic Gases, Fire Safety Journal *9*, 55 (1985); Jones, W. W. and Peacock, R. D., Refinement and Experimental Verification of a Model for Fire Growth and Smoke Transport, Proceedings of the 2nd International Symposium on Fire Safety Science, Tokyo (1989).

[8] Forney, G. P. and Cooper, L. Y., The Consolidated Compartment Fire Model (CCFM) Computer Application CCFM.VENTS - Part II: Software Reference Guide, Nat. Inst. Stand. Technol., NISTIR 90-4343 (1990).

[9] Jones, W. W. and Forney, G. P. "A Programmer's Reference Manual for CFAST, the Unified Model of Fire Growth and Smoke Transport," *Natl. Inst. Stand. Technol.* 1990, *Tech. Note 1283*, 104 p.

[10] Mitler, H. E. "Comparison of Several Compartment Fire Models: An Interim Report," *Natl. Bur. Stand. (U.S.)* 1985, *NBSIR 85-3233*, 33 p.

[11] Jones, W. W. "A Review of Compartment Fire Models," *Natl. Bur. Stand. (U.S.)* 1983, *NBSIR 83-2684*, 41 p.

[12] Cooper L. Y. and Forney, G. P., The consolidated compartment fire model (CCFM) computer application CCFM-VENTS – part I: Physical reference guide. Natl. Inst. Stand. Technol., NISTIR 4342 (1990).

[13] Forney, G. P. and Moss, W. F., Analyzing and Exploiting Numerical Characteristics of Zone Fire Models, Natl. Inst. Stand. Technol., NISTIR 4763 (March 1992).

[14] Jones, W. W. and Bodart, X., Buoyancy Driven Flow as the Forcing Function of Smoke Transport Models, Natl. Bur. Stand. (U. S.), NBSIR 86-3329 (1986).

[15] Rehm, R. G. and Forney, G. P., “A Note on the Pressure Equations Used in Zone Fire Modeling,” Natl. Inst. Stand. Technol., NISTIR 4906 (1992).

[16] Babrauskas, V., "Development of the Cone Calorimeter - A Bench Scale Heat Release Rate Apparatus Based on Oxygen Consumption," *Fire and Materials 8,* 1984, p 81.

[17] Thornton, “The Relation of Oxygen to the Heat of Combustion of Organic Compounds,” Philosophical Magazine and J. of Science, **33** (1917).

[18] Huggett, C., “Estimation of the Rate of heat Release by Means of Oxygen Consumption,” J. of Fire and Flammability, **12**, pp. 61-65 (1980).

[19] Standard Test Method for Heat and Visible Smoke Release for Materials and Products Using and Oxygen Consumption Calorimeter, ASTM E1354-90, *American Society for Testing and Materials,* Philadelphia, PA 1990.

[20] Morehart, J. H., Zukowski, E. E. and Kubota, T., Characteristics of Large Diffusion Flames Burning in a Vitiated Atmosphere, Third International Symposium on Fire Safety Science, Edinburgh (1991).

[21] McCaffrey, B. J., "Momentum Implications for Buoyant Diffusion Flames," *Combustion and Flame 52*, 1983, p. 149.

[22] Cetegen, B. M., "Entrainment and Flame Geometry of Fire Plumes," Ph.D. Thesis, California Institute of Technology, Pasadena 1982.

[23] Drysdale, D., “An Introduction to Fire Dynamics,” John Wiley and Sons, New York, 143 p. (1985).

[24] Tewarson, A., Combustion of Methanol in a Horizontal Pool Configuration, Factory Mutual Research Corp., Norwood, MA, Report No. RC78-TP-55 (1978).

[25] McCaffrey, B. J., Entrainment and Heat Flux of Buoyant Diffusion Flames, Natl. Bur. Stand. (U. S.), NBSIR 82-2473, 35 p. (1982).

[26] Koseki, H., Combustion Properties of Large Liquid Pool Fires, Fire Technology, **25(3)**, 241-255 (1989).

[27] Quintiere, J. G., Steckler, K., and Corley, D., An Assessment of Fire Induced Flows in Compartments, Fire Science and Technology *4*, 1 (1984).

[28] Quintiere, J. G., Steckler, K. and McCaffrey, B. J., "A Model to Predict the Conditions in a Room Subject to Crib Fires," First Specialist Meeting (International) of the Combustion

Institute, Talence, France 1981.

[29] Cooper, L. Y., Calculation of the Flow Through a Horizontal Ceiling/Floor Vent, Natl. Inst. Stand. Technol., NISTIR 89-4052 (1989).

[30] Klote, J.K. and Milke, J.A., Design of Smoke Management Systems, American Society of Heating, Refrigerating and Air-conditioning Engineers, Atlanta, GA (1992).

[31] ASHRAE Handbook HVAC Systems and Equipment, American Society of Heating, Refrigerating and Air-Conditioning Engineers, Atlanta, GA (1992).

[32] Klote, J. H., A Computer Model of Smoke Movement by Air Conditioning Systems, NBSIR 87-3657 (1987).

[33] 1989 ASHRAE Handbook Fundamentals, American Society of Heating, Refrigeration and Air Condition Engineers, Inc., Atlanta, GA 1989.

[34] Jorgensen, R. 1983. Fan Engineering, Buffalo Forge Co., Buffalo, NY.

[35] ASHRAE. Handbook of Fundamentals, Chapter 32 Duct Design, American Society of Heating, Refrigerating and Air-Conditioning Engineers, Atlanta, GA (1993).

[36] Murdock, J.W., Mechanics of Fluids, Marks' Standard Handbook for Mechanical Engineers, 8th ed., Baumeister, *et al*. editors, McGraw, New York, NY (1978).

[37] Schlichting, H., Boundary Layer Theory, 4th ed., Kestin, J. Translator, McGraw, New York, NY (1960).

[38] Huebscher, R.G., Friction Equivalents for Round, Square and Rectangular Ducts, ASHVE Transactions (renamed ASHRAE Transactions), Vol. 54, pp 101-144 (1948).

[39] Heyt, J.W. and Diaz, J. M., Pressure Drop in Flat-Oval Spiral Air Duct, ASHRAE Transactions, Vol. 81, Part 2, p 221-230 (1975).

[40] Colebrook, C.F., Turbulent Flow in Pipes, With Particular Reference to the Transition Region Between the Smooth and Rough Pipe Laws, Journal of Institution of Civil Engineers (London, England), Vol 11, pp 133-156 (1938-1939).

[41] Moody, L.F., Friction Factors for Pipe Flow, Transactions of ASME, Vol 66, p 671-684 (1944).

[42] McGrattan, K. B., Baum, H. R., and Rehm, R. G., Large Eddy Simulations of Smoke Movement, Fire Safety J. **30** (2), pp 161-178 (1998).

[43] McGrattan, K. B.; Baum, H. R.; Rehm, R. G.; Hamins, A.;Forney, G. P.; Floyd, J. E.; Hostikka, S., Fire Dynamics Simulator (Version 2): Technical Reference Guide. NISTIR 6783 (November 2001).

[44] Forney, G. P., Computing Radiative Heat Transfer Occurring in a Zone Fire Model, Natl. Inst. Stand. Technol., NISTIR 4709 (1991).

[45] Siegel, R. and Howell, J. R., Thermal Radiation Heat Transfer, Hemisphere Publishing Corporation, New York, second ed. (1981).

[46] Hottel, H. C., Heat Transmission, McGraw-Hill Book Company, New York, third ed. (1954).

[47] Hottel, H. and Cohen, E., Radiant Heat Exchange in a Gas Filled Enclosure: Allowance for non-uniformity of Gas Temperature, American Institute of Chemical Engineering Journal *4*, 3 (1958).

[48] Yamada, T. and Cooper, L. Y., Algorithms for Calculating Radiative Heat Exchange Between the Surfaces of an Enclosure, the Smoke Layers and a Fire, Building and Fire Research Laboratory Research Colloquium, July 20, 1990.

[49] Jones, W. W. and Forney, G. P., Improvement in Predicting Smoke Movement in Compartmented Structures, Fire Safety J., **21**, pp 269-297 (1993).

[50] Schlichting, H., "Boundary Layer Theory," translated by J. Kestin, Pergammon Press, New York, 1955.

[51] Atreya, A., “Convection Heat Transfer,” Chapter 1-4 in SFPE Handbook of Fire Protection Engineering, DiNenno, P. J, Beyler, C. L., Custer, R. L. P., Walton, W. D., and Watts, J. M., eds., National Fire Protection Association, Quincy, MA (1988).

[52] Golub, G. H. and Ortega, J. M., Scientific Computing and Differential Equations, An Introduction to Numerical Methods. Academic Press, New York (1989).

[53] Strang, G. and Fix, G. J., An Analysis of the Finite Element Method. Prentice-Hall, Englewood Cliffs, New Jersey (1973).

[54] Moss, W. F. and Forney, G. P., “Implicitly coupling heat conduction into a zone fire model.” Natl. Inst. Stand. Technol., NISTIR 4886 (1992).

[55] Robert Siegel and John R. Howell. Thermal Radiation Heat Transfer. Hemisphere Publishing Corporation, New York, second edition, 1981.

[56] Glenn P. Forney. Computing radiative heat transfer occurring in a zone fire model. Internal Report 4709, National Institute of Standards and Technology, 1991.

[57] Cooper, L. Y., Fire-Plume-Generated Ceiling Jet Characteristics and Convective Heat Transfer to Ceiling and Wall Surfaces in a Two-Layer Zone-Type Fire Environment, Natl. Inst. Stand. Technol., NISTIR 4705, 57 p. (1991).

[58] Cooper, L. Y., Heat Transfer in Compartment Fires Near Regions of Ceiling-Jet Impingement on a Wall. J. Heat Trans., 111, pp. 455-460 (1990).

[59] Cooper, L. Y., Ceiling Jet-Driven Wall Flows in Compartment Fires. Combustion Sci. and Technol., 62, pp. 285-296 (1988).

[60] Jaluria, Y. and Cooper, L. Y., Negatively Buoyant Wall Flows Generated in Enclosure Fires. Progress in Energy and Combustion Science, 15, pp. 159-182 (1989).

[61] Leonard Y. Cooper. Fire-plume-generated ceiling jet characteristics and convective heat transfer to ceiling and wall surfaces in a two-layer zone-type fire environment: Uniform temperature and walls. Technical Report 4705, National Institute of Standards and Technology, 1991.

[62] Gunnar Heskestad and Herbert F. Smith. Investigation of a new sprinkler sensitivity approval test: The plunge test. Technical Report Serial No. 22485 2937, Factory Mutual Research Corporation, Norwood, MA, 1976. RC 76-T-50.

[63] D. Madrzykowski and R.L. Vettori. A sprinkler fire suppression algorithm for the gsa engineering fire assessment system. Technical Report 4833, National Institute of Standards and Technology, 1992.

[64] David D. Evans. Sprinkler fire suppression for hazard. Technical Report 5254, National Institute of Standards and Technology, 1993.

[65] Madrzykowski, D. Evaluation of Sprinkler Activation Prediction Methods. International Conference on Fire Science and Engineering, Interscience Communications Limited. ASIAFLAM (Kowloon, 1995).

[66] Seader, J., and Einhorn, I., “Some Physical, Chemical, Toxicological and Physiological Aspects of Fire Smokes,: *Sixteenth Symposium (International) on Combustion.* The Combustion Institute, Pittsburgh, PA 1976, pp. 1423-1445.

[67] Galloway, F. M., Hirschler, M. M., "A Model for the Spontaneous Removal of Airborne Hydrogen Chloride by Common Surfaces," *Fire Safety Journal 14,* 1989, pp. 251-268.

[68] Galloway, F. M., Hirschler, M. M., "Transport and Decay of Hydrogen Chloride: Use of a Model to Predict Hydrogen Chloride Concentrations in Fires Involving a Room-Corridor-Room Arrangement," *Fire Safety Journal 16,* 1990, pp. 33-52.

[69] Brenan, K. E., Campbell, S. L., and Petzold, L. R., Numerical Solution of Initial-Value Problems in Differential-Algebraic Equations, Elsevier Science Publishing, New York (1989).

[70] Peacock, R. D., Jones, W. W., and Bukowski, R. W., Verification of a Model of Fire and Smoke Transport, Fire Safety J. **21**, 89-129 (1993).

[71] Beard, A., Evaluation of Fire Models: Part I – Introduction. Fire Safety J. **19**, 295-306 (1992).

[72] Clemson, B., Tang, Y., Pyne, J., and Unal, R., "Efficient Methods for Sensitivity Analysis," System Dynamics Review, Vol. 11, No. 1, 31-49 (1995).

[73] Box, G. E. P., Hunter, W. G., and Hunter, J. S., Statistics for Experimenters, An Introduction to Design, Data Analysis and Model Building, John Wiley & Sons (1978).

[74] Daniel, C., Applications of Statistics to Industrial Experimentation, John Wiley & Sons (1976).

[75] Iman, R. L. and Helton, J. C., An Investigation of Uncertainty and Sensitivity Analysis Techniques for Computer Models, Risk Analysis, Vol. 8, No. 1, 71-90 (1988).

[76] Iman, R. L. and Conover, W. J., A Distribution-Free Approach to Inducing Rank Correlation Among Input Variables. Communications in Statistics **B11**(3), 331-334 (1982).

[77] Iman, R. L. and Shortencarier, A FORTRAN 77 Program and User's Guide for the Generation of Latin Hypercube and Random Samples for Use with Computer Models. NUREG/CR-3624, SAND83-2365, Sandia National Laboratories, Albuquerque, New Mexico (1984).

[78] Jarvis, J. P., Kostreva, M. M., Forney, C. L., Tools for Validation and Analysis of Fire Models, Combustion Institute/Eastern States Section. Chemical and Physical Processes in Combustion. 20th Fall Technical Meeting. Abstracts. November 2-5, 1987, Gaithersburg, MD, 103/1-4 pp. 1987.

[79] Khoudja, N., Procedures for Quantitative Sensitivity and Performance Validation of a Deterministic Fire Safety Model. Ph.D. Dissertation, Texas A&M University, NBS-GCR-88-544, Natl. Inst. Stand. Technol. 1988.

[80] Forney, G. P., and Moss, W. F., Analyzing and Exploiting Numerical Characteristics of Zone Fire Models. NISTIR 4763, Natl. Inst. Stand Technol. 1992.

[81] Wierzbicki, A., Models and Sensitivity of Control Systems, Wiley and Sons, New York, 1984.

[82] Dickinson, R. P. and Gelinas, R. J., Sensitivity Analysis of Ordinary Differential Equation Systems – A Direct Method, Journal of Comp. Physics, Vol. 21, 123-143 (1976).

[83] Nelson, H. E., "An Engineering View of the Fire of May 4, 1988 in the First Interstate Bank Building, Los Angeles, California," *Natl. Inst. Stand. Technol.* 1989, *NISTIR 89-4061*, 39 p.

[84] Emmons, H.W., "Why Fire Model? The MGM Fire and Toxicity Testing," *Fire Safety J.*, **13** 77-85 1988.

[85] Duong, D. Q., "The Accuracy of Computer Fire Models: Some Comparisons with Experimental Data from Australia," *Fire Safety J.* 1990, *16(6)*, 415-431.

[86] Beard, A., "Evaluation of Fire Models: Overview," Unit of Fire Safety Engineering, University of Edinburgh, Edinburgh, UK 1990.

[87] NFPA 72, National Fire Alarm Code, National Fire Protection Association, Quincy, Massachusetts (1993).

[88] Babrauskas, V. and Krasny J. F., Fire Behavior of Upholstered Furniture, Natl. Bur. Stand. (U. S.), Monograph 173 (1985).

[89] Peacock, R. D., Davis, S., and Babrauskas, V., Data for Room Fire Model Comparisons, J. Res. Natl. Inst. Stand. Technol. Vol. 96, 4, 411-462 (1991).

[90] Drysdale, D. An Introduction to Fire Dynamics, John Wiley and Sons, pp. 310 (1985).

[91] Babrauskas, V. and Peacock, R. D., Heat Release Rate: The Single Most Important Variable in Fire Hazard, *Fire Safety J.*, Vol. 18, No. 3, pp 255-272 (1992).

[92] McCaffrey, B. J., Quintiere, J. G., and Harkleroad, M. F., Estimating Room Temperatures and the Likelihood of Flashover Using Fire Tests Data Correlations, Fire Technology, Vol. 17, No. 2, 98-119 (1981).

[93] Babrauskas, V., Upholstered Furniture Room Fires – Measurements, Comparisons with Furniture Calorimeter Data, and Flashover Predictions, J. Fire Sci., Vol. 2, 5-19 (1984).

[94] Alpert, R. L., et al., "Influence of Enclosures on Fire Growth: Volume I: Test Data," *Factory Mutual Research Corp.*, Norwood MA. 1977, *FMRC No. OAOR2.BU-1 through 7*.

[95] Cooper, L. Y., Harkleroad, M., Quintiere, J. G., and Rinkinen, W. J., "An Experimental Study of Upper Hot Layer Stratification in Full-Scale Multiroom Fire Scenarios," *J. Heat Trans.* 1982, *104*, 741-749.

[96] Quintiere, J. G., and McCaffrey, B. J., "The Burning of Wood and Plastic Cribs in an Enclosure," 2 vols., *Nat. Bur. Stand. (U.S.)* 1980, *NBSIR 80-2054*.

[97] Heskestad, G., and Hill, J. P., "Experimental Fires in Multiroom / Corridor Enclosures," *Natl. Bur. Stand. (U.S.)* 1986, *NBSGCR 86-502, CIB W14/85/10 (USA)*.

[98] Rockett, J. A., Morita, M., and Cooper, L. Y., "Comparisons of NBS/Harvard VI Simulations and Full-scale Multi-room Fire Test Data," in *Proceedings of 2nd International Symposium of Fire Safety Science,* Tokyo, Japan. 1988, 481-490.

[99] Rockett, J. A., Morita, M., and Cooper, L. Y., "Comparisons of NBS/Harvard VI Simulations and Data from all Runs of a Full-scale Multi-room Fire Test Program," *Fire Safety J.* 1989, *15*, 115-169.

[100] Rockett, J. A., and Morita, M., "The NBS Harvard VI Multi-room Fire Simulation," *Fire Sci. Technol.* 1985, *5(2)*, 159-164.

[101] Peacock, R. D., Davis, S., and Babrauskas, V., Data for Room Fire Model Comparisons. J. Res. Natl. Inst. Stand. Technol. **96**, 411 (1991).

[102] Nelson, H. E., "An Engineering View of the Fire of May 4, 1988 in the First Interstate Bank Building, Los Angeles, California," *Natl. Inst. Stand. Technol.* 1989, *NISTIR 89-4061*, 39 p.

[103] Bukowski, R. W., "Reconstruction of a Fatal Residential Fire at Ft. Hood, Texas," *First HAZARD I Users' Conference,* Natl. Inst. Stand. Technol., Gaithersburg, MD, June 5-6, 1990.

[104] Emmons, H.W., "Why Fire Model? The MGM Fire and Toxicity Testing," *Fire Safety J.*, **13** 77-85 1988.

[105] Levine, R. S. and Nelson, H. E., "Full Scale Simulation of a Fatal Fire and Comparison of Results with Two Multiroom Models," *Natl. Inst. Stand. Technol.* 1990, *NISTIR 90-4268,* 105 p.

[106] Deal, S. "A Review of Four Compartment Fires with Four Compartment Fire Models," *Fire Safety Developments and Testing,* Proceedings of the Annual Meeting of the Fire Retardant Chemicals Association. October 21-24, 1990, *Ponte Verde Beach, Florida*, 33-51.

[107] Nelson, H. E., "FPETOOL: Fire Protection Engineering Tools for Hazard Estimation," *Natl. Inst. Stand. Technol.* 1990, *NISTIR 4380*, 120 p.

[108] Duong, D. Q., "The Accuracy of Computer Fire Models: Some Comparisons with Experimental Data from Australia," *Fire Safety J.* 1990, **16**, 415-431.

[109] Peacock, R. D., Jones, W. W., and Bukowski, R. W., "Verification of a Model of Fire and Smoke Transport," *Fire Safety J.* 1993, **21**, 89-129.

[110] Babrauskas, V., “Upholstered Furniture Room Fires -- Measurements, Comparison with Furniture Calorimeter Data, and Flashover Predictions,” *J. Fire Sci.* 1984, *4*, 5-19.

[111] Lee, B. T., Effect of Wall and Room Surfaces on the Rates of Heat, Smoke, and Carbon Monoxide Production in a Park Lodging Bedroom Fire, *Natl. Bur. Stand.* (U. S.), 1985, *NBSIR 85-2998,* 78 p.

[112] Heskestad, G., and Hill, J. P., “Propagation of Fire and Smoke in a Corridor,” *Proceedings of the 1987 ASME:JSME Thermal Engineering Joint Conference* 1987, *Honolulu, HI*, 371-379.

[113] Klote, J. H., “Fire Experiments of Zoned Smoke Control at the Plaza Hotel in Washington DC,” *Natl. Inst. Stand. Technol.* 1990, *NISTIR 90-4253,* 75 p.

[114] Pitts, W. M., Braun, E., Peacock, R. D., Mitler, H. E., Johnsson, E. L., Reneke, P. A., and Blevins, L. G., "Temperature Uncertainties for Bare-Bead and Aspirated Thermocouple Measurements in Fire Environments," Thermal Measurements: The Foundation of Fire Standards, ASTM STP 1427, L. A. Gritzo and N. J. Alvares, Eds., American Society for Testing and Materials, West Conshohocken, PA, 2002.

[115] Babrauskas, V. B. and Peacock, R. D., “Heat Release Rate: The Single Most Important Variable in Fire Hazard.” *Fire Safety J.* **18** (1992) 255-272.

[116] Quintiere, J. G., and McCaffrey, B. J., “The Burning of Wood and Plastic Cribs in an Enclosure,” *Natl. Bur. Stand. (U. S.)* 1980, *NBSIR 80-2954*, 2 vols.

[117] Delichatsios, M. A., “Fire Growth Rate in Wood Cribs,” *Combustion and Flame* 1976, *27*, 267-278.

[118] Peacock, R. D., Jones, W. W., and Bukowski, R. W., Verification of a Model of Fire and Smoke Transport, Fire Safety J. **21**, 89-129 (1993).

[119] Beard, A., Evaluation of Fire Models: Part I – Introduction. Fire Safety J. **19**, 295-306 (1992).

[120] Deal, S. and Beyler, C., Correlating Preflashover Room Fire Temperatures, J. of Fire. Prot. Engr., **2** (2), 33-48. 1990.

[121] Reneke, P. A., Peatross, M. J., Jones, W. W., Beyler, C. L., and Richards, B., A Comparison of CFAST Predictions to USCG Real-scale Fire Tests, to be published.

[122] Babrauskas, V., “COMPF2-A Program for Calculating Post-Flashover Fire Temperatures,” *Natl. Bur. Stand. (U.S.)* 1979, *Tech. Note 991,* 76 p.

[123] Deal, S. and Beyler, C., Correlating Preflashover Room Fire Temperatures, J. of Fire. Prot. Engr., **2** (2), 33-48. 1990.

Appendix A - Theory of Corridor Flow

This section outlines the procedure used for estimating a ceiling jet's temperature decay, depth, velocity and hence arrival time at each vent in a corridor. The vent flow algorithm in CFAST uses this information to compute mass and enthalpy flow between the corridor and adjacent compartments. This is accomplished by presenting the vent algorithm with a one layer environment (the lower layer) before the ceiling jet reaches the vent and a two layer environment afterwards. Estimated ceiling jet temperatures and depths are used to define upper layer properties. The fire model then uses these correlations to estimate conditions in the corridor.

Assumptions

The assumptions made in order to develop the correlations described in this note are:

o The time scale of interest is the time required for a ceiling jet to traverse the length of the corridor. For example, for a 100 m corridor with 1 m/s flow, the characteristic time period would be 100 seconds.

o Cooling of the ceiling jet due to mixing with adjacent cool air is large compared to cooling due to heat loss to walls. In addition, we assume that walls are adiabatic. This assumption is conservative. An adiabatic corridor model predicts more severe conditions downstream in a corridor than a model that accounts for heat transfer to walls, since cooler ceiling jets travel slower and not as far.

o We do not account for the fact that ceiling jets that are sufficiently cooled will stagnate. Similar to the previous assumption, this assumption is conservative and results in over predictions of conditions in compartments connected to corridors (since the model predicts that a ceiling jet may arrive at a compartment when in fact it may have stagnated before reaching it).

o Ceiling jet flow is buoyancy driven and behaves like a gravity current. The inlet velocity of the ceiling jet is related to its temperature and depth.

o Ceiling jet flow lost to compartments adjacent to the corridor is not considered when estimating ceiling jet temperatures and depths. Similarly, a ceiling jet in a corridor is assumed to have only one source.

o The temperature and velocity at the corridor inlet is constant in time.

o The corridor height and width do not effect a ceiling jet's characteristics. Two ceiling jets with the same inlet temperature, depth and velocity behave the same when flowing in corridors with different widths or heights as long as the inlet widths are the same fraction of the corridor width.

o Flow entering the corridor enters at or near the ceiling. The inlet ceiling jet velocity is reduced from the vent inlet velocity by a factor of w_{vent}/w_{room} where w_{vent} and w_{room} are the width of the vent and room respectively.

Ceiling Jet Characteristics

Compartments with Length Height Ratios Near One - Normal Rooms

In a normal compartment where the length to height ratio is near one, ceiling jet velocities can be estimated from correlations[1,2], or by solving the horizontal momentum equation in addition to the mass and energy conservation equations.

Smoke flow in a normal room is qualitatively different from smoke flow in a corridor in one important respect. Corridor smoke spreads in only one dimension, along the length of the corridor. Smoke spreads in a normal room on the other hand in two dimensions. In addition, assuming no friction or heat transfer to boundaries, ceiling velocities in corridors will be essentially constant while ceiling jet velocities in normal rooms will be approximately proportional to 1/r. This arises since the surface area at the exterior boundary is proportional to r, then the velocity must be proportional to 1/r so that the mass flow out remains equal to the mass flow in. As a result, these correlations are not valid for estimating ceiling jet velocities in corridors.

If the length to height ratio of the room of fire origin is near one then ceiling jet traversal times may be estimated using the velocity correlation for a steady state fire,

$$u(r) = \begin{pmatrix} 0.96\left(\dfrac{Q}{H}\right)^{1/3}, (r/H) < 0.15 \\ 0.198\dfrac{(Q/H)^{1/3}}{(r/H)^{5/6}}, (r/H) \geq 0.15 \end{pmatrix} \qquad (1)$$

found in [6] where H is the ceiling height (m), Q is the total energy release rate of the fire (W) and r is the distance from the plume centerline (m). The constants, 0.96 and 0.195 each have units of ($m^{4/3}/(W^{1/3}s)$. CFAST[3] estimates ceiling jet temperatures and velocities using a correlation derived by Cooper, given in [7].

The time, t(r), required for the jet to travel a distance r from the source can then be obtained from the velocity by integrating the quantity dr/u(r). Using the correlation given in [6] we obtain

$$t(r) = \int_0^r \frac{dr}{u(r)} \rightarrow \begin{Bmatrix} \dfrac{s}{6.4q} & r < 1 \\ \dfrac{1}{6.4q} + \dfrac{1}{11.6q}\left(s^{11/6} - 1\right), & r \geq 1 \end{Bmatrix} \qquad (2)$$

where s= r/(0.15H) and $q=(Q/H)^{1/3}$. The time t(r) corresponding to Cooper's velocity correlation must be integrated numerically[4]. The arrival time is approximately proportional to r^2, the distance squared. It will be shown later empirically that in a corridor the arrival time is proportional to the distance, r.

Compartments with Large Length Height Ratios - Corridors

The correlations defined by (1) and (2) are not appropriate in corridors. Ceiling jet flow in a corridor can be characterized as a one dimensional gravity current. To a first approximation, the velocity of the current depends on the difference of the density of the gas located at the leading edge of the current and the gas in the adjacent ambient air. The velocity also depends on the depth of the current below the ceiling. A simple formula for the gravity current velocity may be derived by equating the potential energy of the current, $mgd_0/2$, measured at the half-height $d_0/2$ with its kinetic energy, mU^2, to obtain

$$U = \sqrt{gd_0} \qquad (3)$$

where m is mass, g is the acceleration of gravity, H is the height of the gravity current and U is the velocity. When the density difference, $\Delta\rho=\rho_{amb} - r_{cj}$, between the current and the ambient fluid is small, the velocity U is proportional to

$$\sqrt{gd_0 \frac{\Delta\rho}{\rho_{cj}}} \rightarrow \sqrt{gd_0 \frac{\Delta T}{T_{amb}}} \qquad (4)$$

where ρ_{amb}, T_{amb} are the ambient density and temperature, ρ_{ci}, T_{ci} are the density and temperature of the ceiling jet, and $T = T_{cj} - T_{amb}$ is the temperature difference. Here use has been made of the ideal gas law, $\rho_{amb}T_{amb} \approx \rho_{ci}T_{ci}$.

This can be shown using terms defined in Figure 1 by using an integrated form of Bernoulli's law noting that the pressure drop at the bottom of the ceiling jet is Pb = 0, the pressure drop at the top is $P_t = gd_0(\rho_{cj} - \rho_{amb})$ and using a vent coefficient $c_{vent} = 0{:}74$, to obtain.

$$U_0 \approx 0.7\sqrt{gd_0 \frac{\Delta T}{T_{amb}}} \qquad (5)$$

Formulas of the form of equation (4) lead one to conclude that the characteristics of a ceiling jet in a corridor depends on its depth, d_0, and relative temperature difference, $\Delta T/T_{amb}$. Therefore, as the jet cools, it slows down, due to the factor $\Delta T/T_{amb}$. If no heat transfer occurs between the ceiling jet and the surrounding walls, then the only mechanism for cooling is mixing with surrounding cool air.

Numerical Experiments

In order to better understand the effects of the inlet ceiling jet temperature and depth on its characteristics downstream in a corridor, a number of numerical experiments were per-formed using the field model LES3D[5]. Twenty cases were run with five different inlet depths and four different inlet temperatures.

Boundary Conditions - corridor flow entrance

The inlet ceiling jet depths, d_0, used in the parameter study are 0.15 m, 0.30 m, 0.45 m, 0.60 m and 0.75 m. The inlet ceiling jet temperature rises, T_0, used in the parameter study are 100˚C, 200˚C, 300˚C and 400˚C. Velocities using equation (5) corresponding to these inlet depths and temperature increases are given in Table 1.

Boundary Conditions - all other surfaces

For each case, a non-slip velocity boundary condition was imposed at all solid boundaries. Adiabatic thermal boundary conditions were imposed at the walls to simulate no heat transfer to wall surfaces. A vertical symmetry plane along the centerline of the corridor was used to reduce the number of grids, thereby improving the resolution. An open boundary condition was imposed at the far end of the corridor.

Table 1: Inlet Velocity as a function of Inlet Temperature and Depth

	Temperature Excess (˚C)			
Depth (m)	+100	+200	+300	+400
0.15	0.50	0.71	0.87	1.00
0.30	0.71	1.00	1.22	1.41
0.45	0.87	1.22	1.50	1.73
0.60	1.00	1.41	1.73	2.00
0.75	1.12	1.58	1.94	2.24

The simulated corridor had dimensions of 10 m x 2.4 m x 2.4 m. Each grid cell had dimensions of approximately 10 cm x 5 cm x 2:5 cm, where the longest grid dimension occurred along the length of the corridor. Approximately 220,000 grid cells were used to model the corridor; 24 across the width of the corridor and 96 along both the height and length of the corridor. For most cases, a Reynold's number of 9200 (approximately 962) was used to resolve the small-scale flow features.

A coarser grid with dimensions 10 cm x 5 cm x 5 cm was used initially. It was found that the vertical grid dimension, 5 cm was not sufficiently small to resolve the thin, 0:15m ceiling jet cases.

Qualitative numerical corridor flow experiments

A parameter study was performed in order to study the quantitative behavior of the ceiling jet by varying the inlet ceiling jet depth and temperature rise.

As can be seen from Figures 1 and 2, a ceiling jet modeled in an enclosure with adiabatic walls travels farther and faster than a ceiling jet modeled with cold walls. Figure 3 shows shaded temperature contours in a vertical plane along the centerline of a 10 m corridor at 10 and 20

seconds. The temperature distribution at these two times is about the same. Even though an individual portion of smoke has moved up to 10 m, the peak temperature (edge of darkest contour) has only shifted by about one meter, from 5 m to 4 m.

Similarly, Figure 4 shows shaded velocity contours in a vertical plane along the centerline of a 10 m corridor at 20 and 40 seconds. The velocity distribution does not change much between the two times. Because of this, we assume that the walls do not heat up and that the temperature and velocity distributions quickly reach steady state.

Reducing the Data

Estimating Zone Fire Modeling Quantities from Field Modeling Results: The computational fluid dynamic or field model, LES3D, calculates temperatures, pressures and velocities at many points in a 3-D rectangular grid. The zone fire model, CFAST, on the other hand calculates pressure at the floor, temperatures in the lower and upper layer and a layer interface height. In this section, a procedure is presented for reducing the data from a field model to a form consistent with a zone fire model. For each vertical plane along the length of a corridor, a layer interface height is estimated by using the distance above the floor where the temperature gradient is greatest. An upper layer temperature is calculated by averaging all temperatures in the slice above the estimated layer height.

The simulation of these cases resulted in an extensive set of velocity, temperature and pressure predictions. This data is reduced to a more manageable size by noting that the inlet high-temperature ceiling jet flow stratifies the corridor gases into two regions; an upper region of hot, fast flowing air and a lower region of relatively cool quiescent air. An average upper layer temperature and layer height is estimated for each vertical slice along the length of the corridor. The temperature rise above ambient for each slice is given by $\Delta T(i) = T_U(i)-T_{amb}$. These temperature rises are scaled by the inlet temperature rise, T_0, and transformed using $\log(\Delta T/\Delta T_0)$. The resulting data are presented in Figure 5. Note that each plot is nearly linear and that all plots (except for the $d_0 = 0.15$m group) lie within a single group. This implies that the relative temperature falloff is independent of the inlet temperature rise and depth (assuming that the inlet depth is sufficiently thick). The temperature curves presented in Figure 5 were approximated by straight lines using a linear least squares curve fitting procedure.

Summary of Results - The numerical implementation into CFAST.

Ceiling Jet Temperatures

The line that fits the temperature fall off data in a least squares sense is given for the plots in Figure 5. This fit is given in the form of

$$\log\left(\frac{\Delta T}{\Delta T_0}\right) = a + bx. \qquad (6)$$

This is equivalent to

$$\frac{\Delta T}{\Delta T_0} = C_1 10^{bx} \rightarrow C_1 \left(\frac{1}{2}\right)^{x/h_{1/2}} \qquad (7)$$

where C1 = 10^a and $h_{1/2}$= - log(2)/b. The parameter $h_{1/2}$ in equation (7) has a physical interpretation. It is the distance down the corridor where the temperature rise ΔT , falls off to 50 per cent of its original value or equivalently, T (x + $h_{1/2}$) = 0.5 T (x).

The half-distance, $h_{1/2}$, can be approximated by $h_{1/2}$= log(2)/0.018 ≈ 16.7 where b = -0.018 is given in Figure 5. Similarly, the coefficients C_1 is approximated by $C_1 = 10^a = 10^{+0.003}$ ≈1 where a is also given in Figure 5. Therefore the temperature rise, ΔT , may be approximated by

$$\Delta T = \Delta T_0 \left(\frac{1}{2}\right)^{\frac{x}{16.7}} \qquad (8)$$

Ceiling Jet Arrival Times

Numerical thermocouples were placed 0.15 m (6 in) below the ceiling every 0.5 m along the center line of the corridor for all cases except for the d_0 = 0.15m cases where they were placed 0.075 m below the ceiling. Ceiling jet arrival times were recorded by noting when the temperatures rose 1OC. The arrival time for each case was scaled by the ceiling jet velocity, U_0, at the left entry vent. These reduced data are displayed in Figure 6. Relative temperature fall off data for all ceiling jets are displayed in Figure 4. Note that most arrival time curves lie within approximately the same region. A group of curves, corresponding to the inlet depth of d_0=0.15m, are separate from the main group. This is because the 0.15m ceiling jets are weaker than the rest. They lose their driving potential resulting in lower velocities and hence greater arrival times. The arrival time of the ceiling jet head may be approximated by t = x=U_0 for all d_0 except for d_0=0.15m . As stated before, the d_0=0.15m ceiling jets are not strong enough to sustain a well defined flow for the length of the corridor.

Conclusions

The numerical experiments with LES3D demonstrated that for the cases simulated, ceiling jet characteristics depend on the relative inlet temperature rise and not the inlet depth. Flow in long corridors (greater than 10 m) need to be better characterized due to the flow stagnation which may occur because of the ceiling jet's temperature decay.

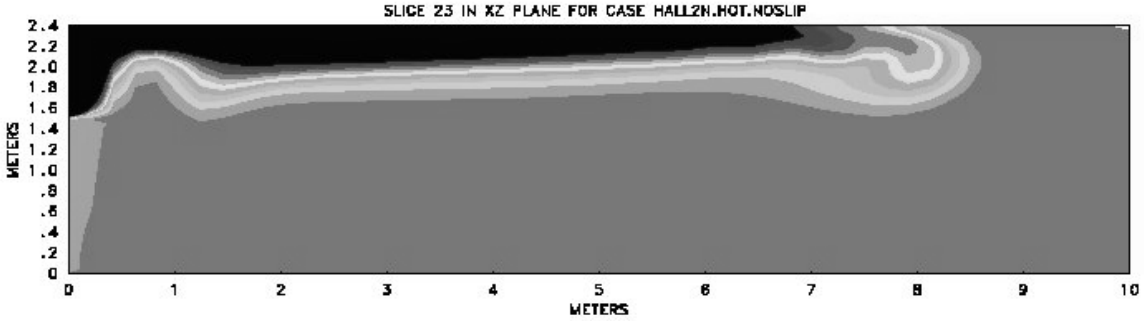

(a) Adiabatic walls

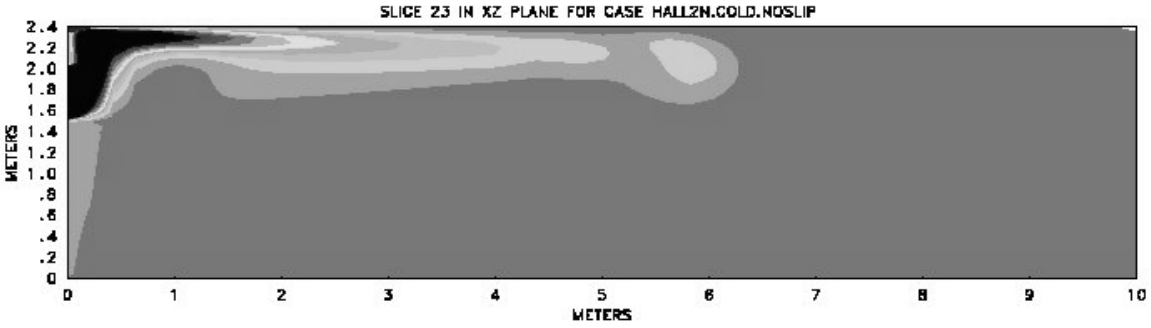

(b) Cold walls

Figure 1. Temperature contours along the corridor centerline for two temperature boundary conditions. The inlet flow has a depth of 0.6 m, a velocity of 1.0 m/s and a temperature rise of 300 ^{o}C above ambient. A no-slip boundary condition is imposed at all wall surfaces.

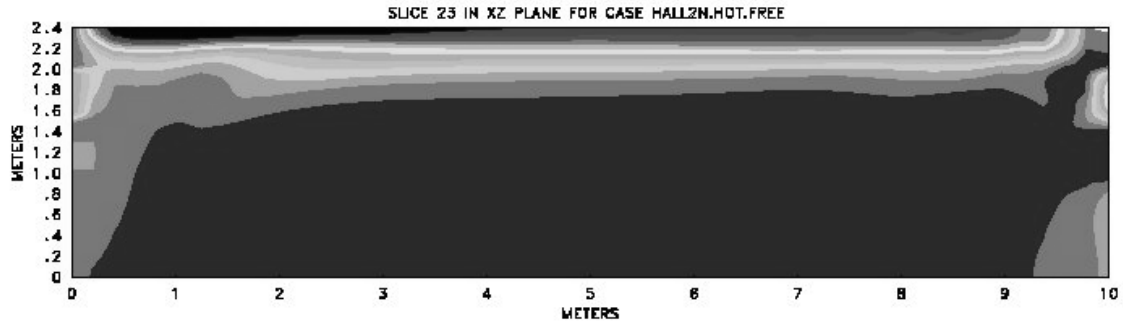

(a) free-slip, adiabatic

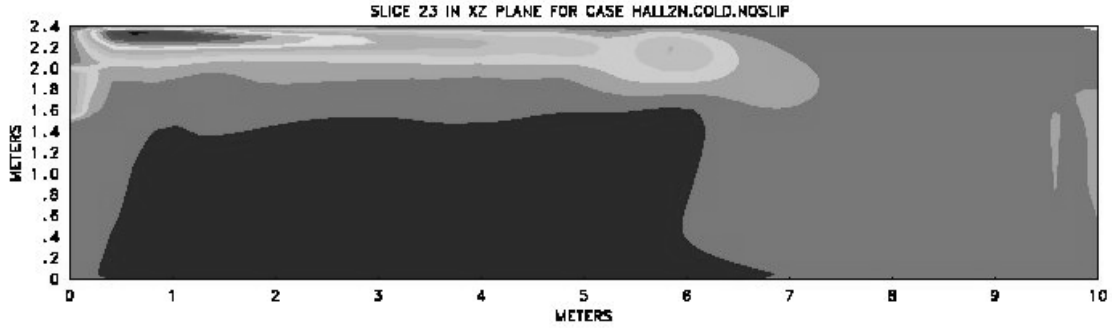

(b) no-slip, cold walls

Figure 2. Shaded velocity contours along the corridor centerline for two different boundary condistion. The inlet flow has a depth of 0.6 m, a velocity of 1.0 m/s and a temperature rise of 300 ^{o}C above ambient.

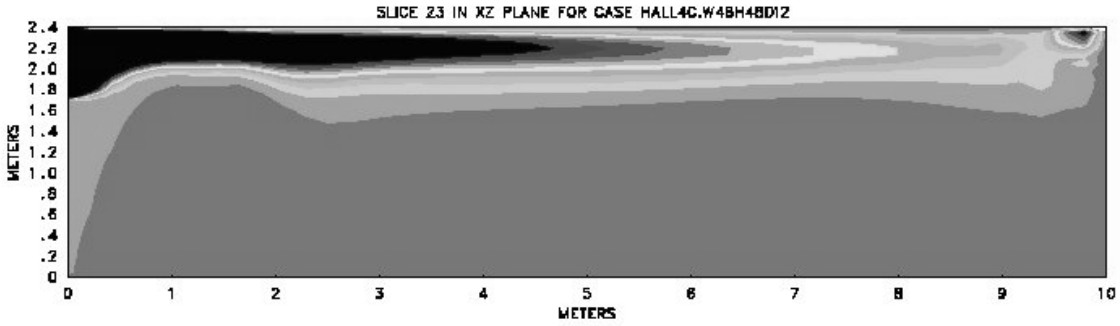

(a) 10 seconds

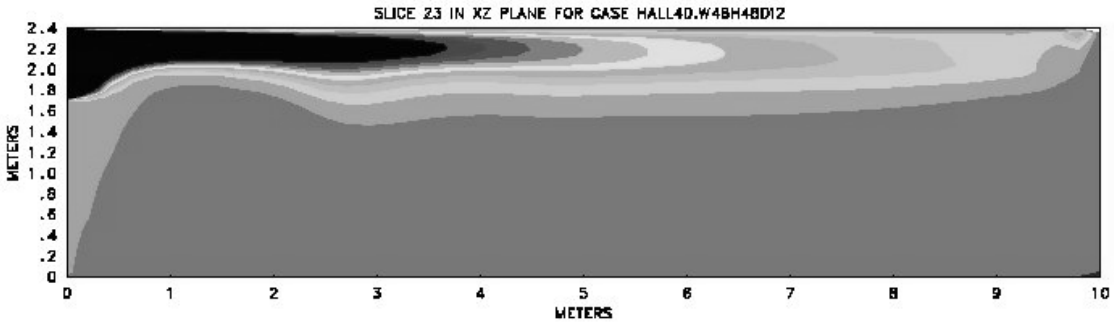

(b) 20 seconds

Figure 3. Shaded temperature contours along the corridor centerline at two different times during the simulation. The inlet flow has a depth of 0.6 m, a velocity of 1.0 m/s and a temperature rise of 300 ^{o}C above ambient.

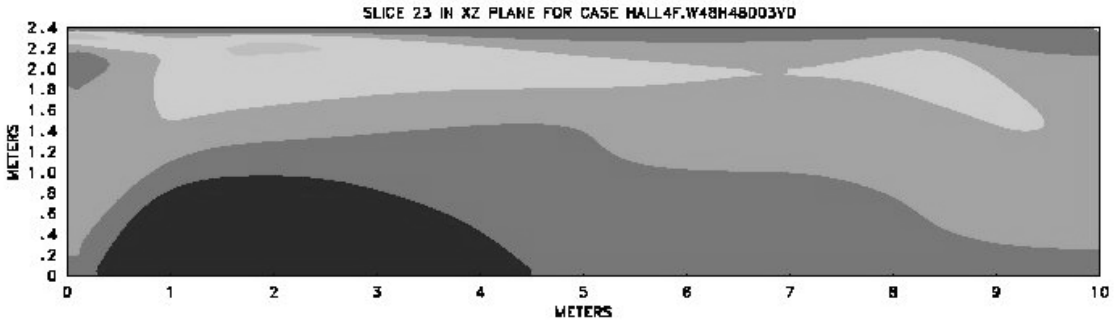

(a) 20 seconds

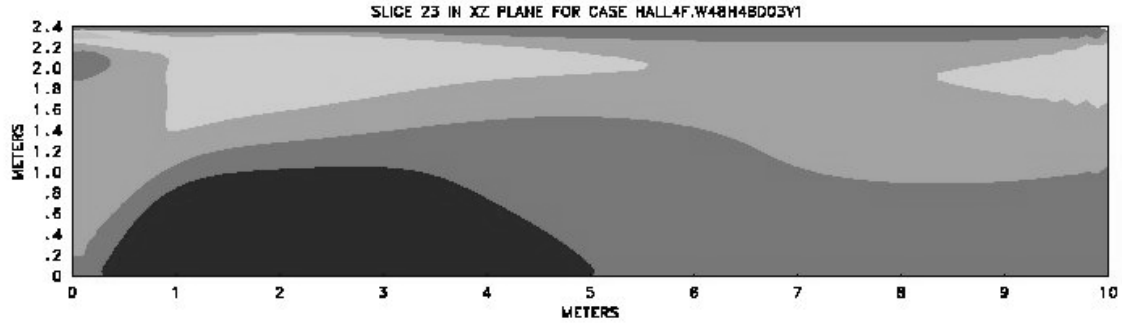

(b) 40 seconds

Figure 4. Shaded velocity contours along the corridor centerline at two different times during the simulation. The inlet flow has a depth of 0.6 m, a velocity of 1.0 m/s and a temperature rise of 312 oC above ambient.

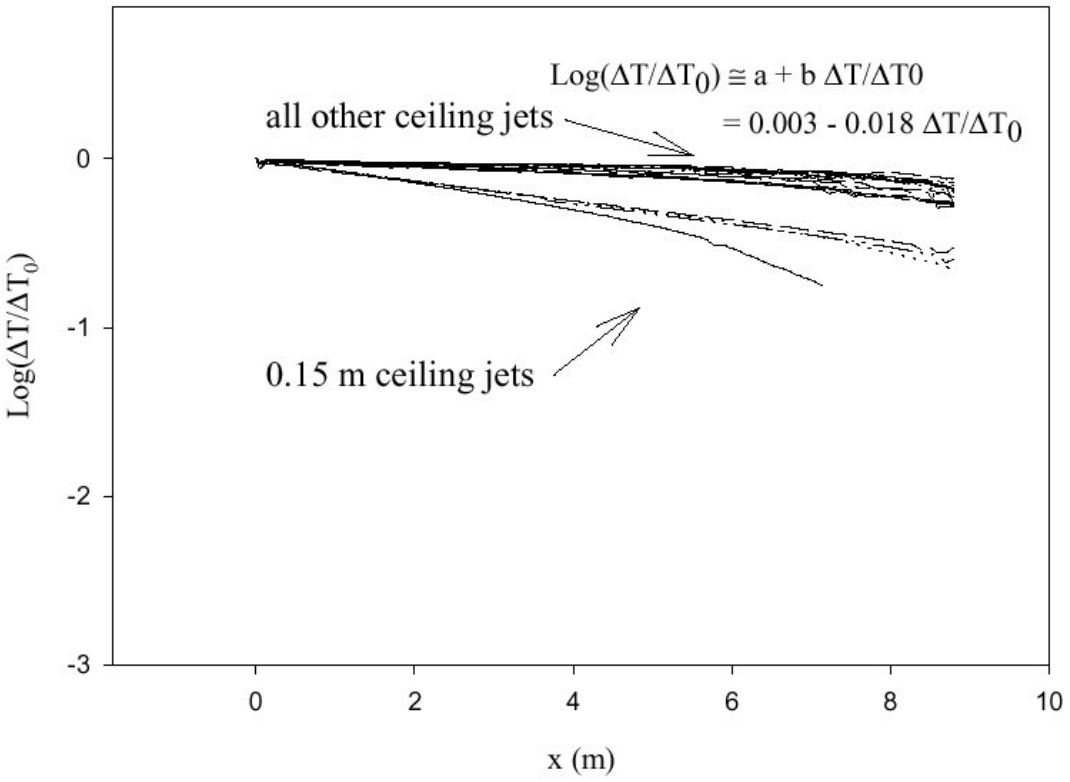

Figure 5. Log_{10} of the relative temperature excess downstream in a corridor using an adiabatic temperature boundary condition for several inlet depths and inlet temperature boundary condition for several inlet depths and inlet temperature rises. The inlet velocity, U_0, is given by equation (4).

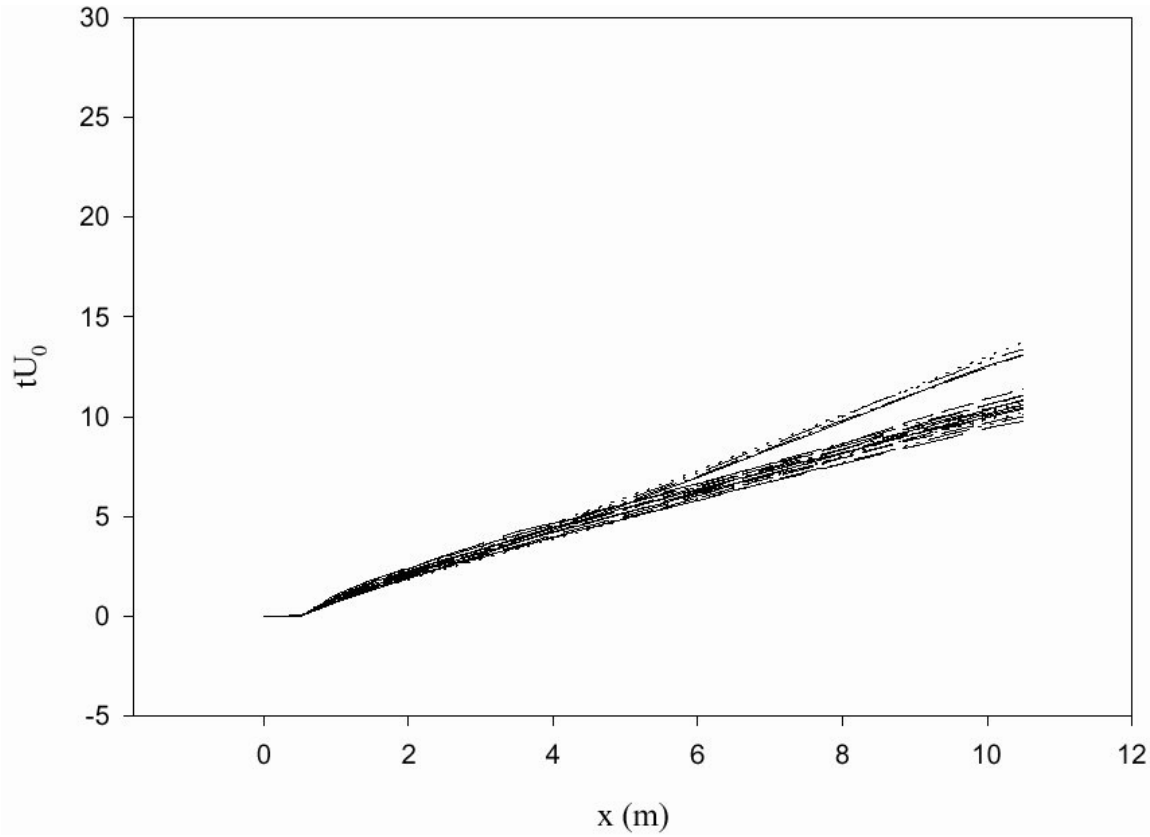

Figure 6. Ceiling jet arrival time as a function of distance down the corridor scaled by the initial ceiling jet velocity, U_0, for several initial inlet depths, d_0, and temperatures rises, T_0. The walls are adiabatic. The inlet velocity, U_0, is given by equation (4). The ceiling jet's arrival time is measure by noting when the temperature rises 1 ^oC above ambient at a given distance downstream from the inlet.

References

[1] David D. Evans. Ceiling jet flows. In Phillip J. DiNenno et al., editors, SFPE Handbook of Fire Protection Engineering, chapter I-9. McGraw-Hill Book Company, New York, first edition, 1989.

[2] Leonard Y. Cooper. Fire-plume-generated ceiling jet characteristics and convective heat transfer to ceiling and wall surfaces in a two-layer zone-type fire environment: Uniform temperature and walls. Technical Report 4705, National Institute of Standards and Technology, 1991.

[3] Richard D. Peacock, Glenn P. Forney, Paul Reneke, Rebecca Portier, and Walter W. Jones. CFAST, the consolidated model of fire growth and smoke transport. Technical Note 1299, National Institute of Standards and Technology, 1993.

[4] John E. Simpson. Gravity Currents In the Environment and the Laboratory. Halstead Press, New York, 1987.

[5] Kevin McGrattan, Ronald Rehm, and Howard Baum. Fire-driven flows in enclosures. J. Comp. Phys., 110(2):285-291, 1994.

Appendix B - Total Gas Layer Absorption

B.1 Theoretical Considerations

Absorption is known to be a function of several parameters, including the concentrations of various gases (primarily carbon dioxide and water vapor), the particle size distribution of the soot, the temperature of the radiation source and the temperature of the absorbing gas-soot mixture. The complexity of the relationship is indicated by

$$A = function(CO_2, H_2O, soot, T, \ldots) \tag{B1}$$

Given a volume filled with gases and suspended particulates, radiation traversing that volume will be transmitted, absorbed or scattered in accordance with,

$$1 = T + A + S \tag{B2}$$

where *T*, *A*, and *S* represent the energy fractions which are transmitted, absorbed and scattered, respectively. For our purposes, we will ignore the scattered component, because: (a) scattering would add considerable complexity (computational time) to the model; and (b) meaningful scattering calculations require a detailed knowledge of the particulate size distribution and of the optical properties of individual particles.

As a reasonable approximation, we assume exponential attenuation, so transmittance is

$$T = e^{-\alpha C L} \tag{B3}$$

where α is the specific absorption coefficient, C is the concentration of the absorbing species and L is the path length. The unit of α is in units of $(CL)^{-1}$, in our case, kg/m^2.

In general, the specific absorption coefficient is a function of wavelength, so we should calculate total transmittance by integrating the weighted spectral transmittance over the entire wavelength region of interest. Because that calculation is computationally expensive, we use the approximation that a constant, average value of α is valid for the entire wavelength region. This is a reasonable approximation for black- or gray body absorbers, such as soot, which have continuous absorption spectra. We also assume that absorption is only due to soot, H_2O and CO_2.

Applying eq. (B3) to soot, the transmittance becomes

$$Ts = e^{(-o_S C_S L)} \tag{B4}$$

where o_S is the effective soot specific absorption coefficient and C_S is the soot concentration.

Making the assumption that absorption is additive, except for a correction for band overlap, the gas absorbance will be

$$A_G = A_{H_2O} + A_{CO_2} - C \tag{B5}$$

For typical fire conditions, the overlap amounts to about half of the CO_2 absorbance [[B] so the gas transmittance is

$$T_G = 1 - A_{H_2O} - 0.5 A_{CO_2} \tag{B6}$$

Due to the band structure of gas absorption spectra, the assumption of continuous absorption is not a good approximation. Instead, the gas absorbance terms were estimated from graphs of detailed band absorbance calculations [B2].

The total transmittance of a gas-soot mixture is the product of the gas and soot transmittances

$$T_T = T_S T_G \tag{B7}$$

Substitution of eqs. (B4) and (B6) into eq. (B7) yields

$$TT = e^{(-\alpha_S C_S L)} \left[1 - A_{H_2O} - 0.5 A_{CO_2}\right] \tag{B8}$$

The parameters α_S and C_S may be lumped together as κ, which, in the optically thin limit, is the Planck mean absorption coefficient and, in the optically thick limit, is the Rosseland mean absorption coefficient. For the entire range of optical thicknesses, Tien, *et. al.* [B3] report that a reasonable approximation is

$$\kappa = k f_v T \tag{B9}$$

where *k* is a constant which depends on the optical properties of the soot particles, f_v is the soot volume fraction and T is the soot temperature in Kelvin. Rather than attempt to calculate κ from first principals, we have taken a semi-empirical approach, using values of κ, f_v, and T, which have been tabulated by Hubbard and Tien [B4] for various fuel types. As seen in Figure B-1, κ is quite variable [mean: 14.2 m^{-1}; standard deviation: 13.5 (95%)], depending on the type of fuel. However, after normalizing for f_v and T, k is found to be nearly constant [mean: 1195.5 $m^{-1}T^{-1}$; standard deviation: 43.6 (4%)]. Therefore, the average value of k is taken to be a valid approximation for a wide range of fuels. The soot volume fraction, f_v, is calculated from the soot mass, soot density and layer volume and the soot is assumed to be in thermal equilibrium with the gas layer.

Equation (B8) was developed for the case of point-to-point transfer, in which the value of L is known. In the context of zone models, however, the distance is ambiguous since the source is

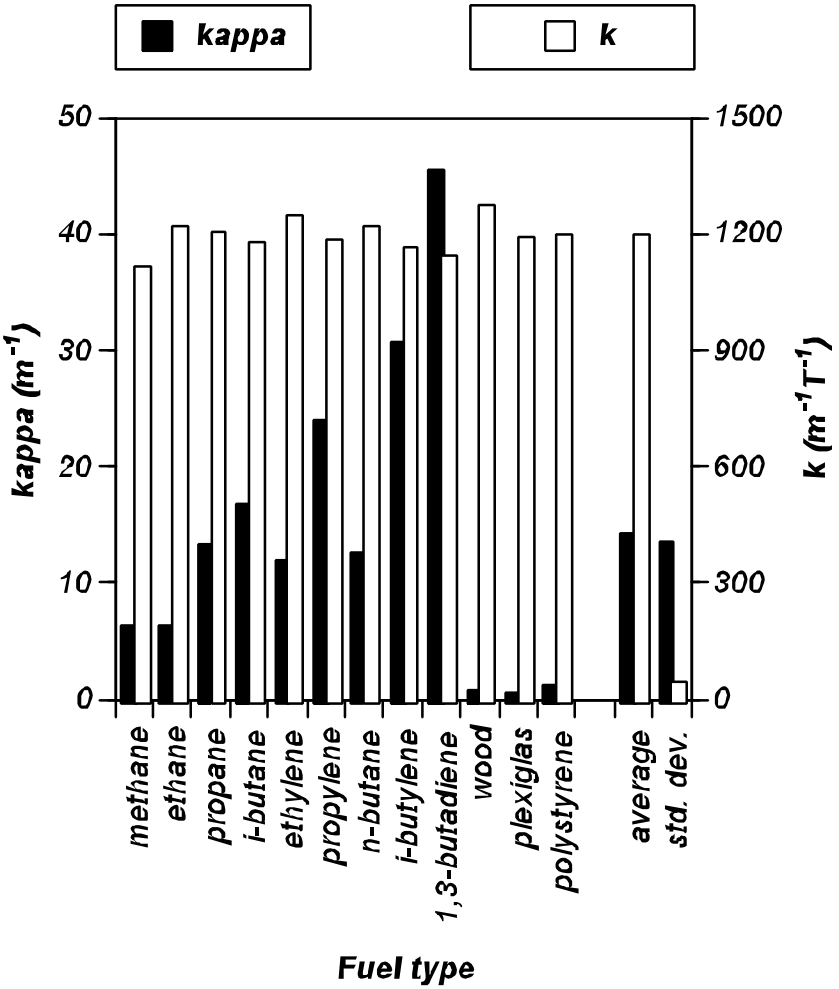

Figure B-1. Comparison of variability of κ and *k* for various fuels.

distributed over the volume of a layer and the destination is the surface area of the layer boundary. For this case, an effective path length must be calculated. The mean beam length concept treats an emitting volume as if it were a hemisphere of a radius such that the flux impinging on the center of the circular base is equal to the average boundary flux produced by the real volume. The value of this radius can be calculated for specific geometries but, for an arbitrary shape, Tien *et. al.* [B5] have found an approximate value to be

$$L = c\, 4\, V / A \qquad \text{(B10)}$$

where L is the mean beam length in meters, *c* is a constant (approximately 0.9, for typical geometries), V is the emitting gas volume (meter^3) and A is the surface area (meter^2) of the gas volume. The volume and surface area are calculated from the dimensions of the layer. Combining eq (B9) and (B10), we find the first term of eq (B8).

Edwards' [B2] absorbance data for H_2O and CO_2 are reported as log(emissivity) versus log(gas temperature), with log(gas concentration) as a parameter, where temperature is in Kelvin and gas concentrations is expressed a pressure-path length, in units of atmosphere-meters. For each gas, these data were incorporated into a look-up table, implemented as a two-dimensional array of log(emissivity) values, with indices based on temperature and gas concentration.

It should be noted that the literature usually reports the results of emission, rather than absorption, in experiments and calculations. However, for diffuse radiation impinging on gray bodies which are in thermal equilibrium with their surroundings, absorption and emission are equal. These are reasonable assumptions for the case of soot particles suspended in air, therefore the use of emission data to estimate absorbance parameters is valid for soot. The gray body approximation is not as good in the case of gases, but the alternative, a detailed absorbance band calculation, is computationally infeasible. Accordingly, we have assumed that absorbance and emissivity are equivalent.

The number of moles of each gas is found using the gas molecular weights and CFAST's estimated gas mass fractions and layer masses. The gas concentrations, in units of atmosphere-meters, are calculated from the number of moles, the universal gas constant, temperature, layer volume and effective optical path from eq (B10). For each gas, the log(absorbance) is estimated from the corresponding look-up table by linear interpolation in both the log(temperature) and log(concentration) domains. In the event that the required absorbance lies outside the temperature or concentration range of the look-up table, the nearest acceptable value is returned. Error flags are also returned, indicating whether each parameter was in or out of range and, in the latter case, whether it was high or low. Presently, these flags are only used to generate a warning message (sent to the default output device, unit 6) in the event that an out-of-range error occurs. In the future, they could be used for other purposes. For example, they might trigger a more complex extrapolation routine capable of providing better accuracy.

This entire process is carried out for both CO_2 and H_2O. Since the interpolated values are actually log(absorbance), rather than absorbance, antilogs are taken and gas absorbances are substituted into the second term of eq (B8) to calculate the total transmittance. Finally, the latter is converted to an effective absorption coefficient

$$\alpha_{EFF} = -\ln\left(T_T\right) / L \qquad \text{(B11)}$$

B.2 Results

Prior to the development of this algorithm, CFAST used constant absorbance coefficients of 0.5 for upper layers and 0.01 for lower layers. Those values are reasonable for the case of sooty upper layers and clean lower layers, but can lead to misleading predictions in other cases.

The interaction of radiative transport with walls, floor, ceiling and gas layers is very complex and the addition of variable absorbance coefficients makes the situation even more complicated. As a result of this complexity, it is not possible to make general statements regarding the effects

of a change in the absorbance coefficient. However, the effects of the new algorithm may readily be seen in specific cases.

To illustrate this point, we modeled full-scale fire tests using both the old and the new algorithms. The test involved four, vertically aligned compartments on the Navy's fire test ship, ex-USS SHADWELL, with a diesel spray fuel fire in compartment 1. For these tests, pilot fires were ignited at time zero and the main spray fires were ignited at +183 s. The configuration is illustrated in C-2; the double-headed arrows indicate vents between pairs of compartments or between a compartment and the exterior. A complete description of the test is given in Bailey and Tatem [B6].

Figure B-3 shows that the new absorption calculation had relatively little effect on the predicted upper layer temperature in the fire compartment. These were very sooty fires and, for that compartment, the absorption coefficient value assumed by the original algorithm was a good approximation. Both models closely predicted the observed air temperatures.

For comparison, we have included the results obtained with the new algorithm when soot generation is turned off (by setting CFAST's OD input parameter to zero). Compared with the case of a realistic amount of soot, CFAST predicts much higher upper layer temperatures when there is no soot. This effect may be qualitatively explained as follows:

The only source of energy in the fire compartment is the fire, modeled as a plume which injects the combustion products into the upper layer. Since the fire is constant for the two cases, the same amount of energy is delivered to the upper layer in both cases. The upper layer can only cool by radiation, convection or conduction of energy. The latter two are unaffected by any change in the absorbance, but the radiative losses will be lower due to decreased absorbance (recall that, for a gray body, the emissivity is the same as the absorptivity) when soot is eliminated. With smaller radiative losses, the gas will not cool as much, therefore the no-soot gas temperature will be higher than in the baseline case.

The situation in the upper layer of compartment 2 is different from that in the upper layer of the fire compartment. The primary energy source here is radiation from the hot deck so the temperature is directly related to layer absorbance. As seen in Figure B-4, the new algorithm reduces the predicted temperature and brings it into closer agreement with experimental values. For the no-soot case, absorbance is significantly reduced, resulting in much lower temperature predictions.

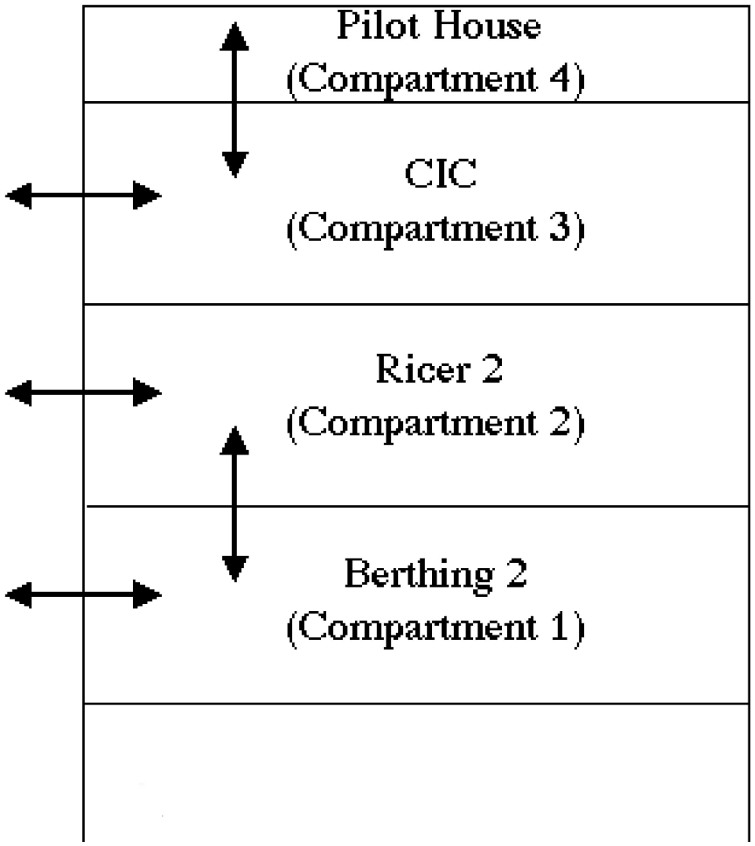

Figure B-2. Schematic of shipboard full-scale fire test area.

In this case, the vertical vent between compartments 1 and 2 was very small (0.002 m^2), which had two effects: (a) radiation from the hot deck was the dominant energy transport mechanism within compartment 2; and (b) very little soot was present in compartment 2. As a consequence, the original algorithm overestimated the absorbance of the upper layer and overpredicted the layer temperature. The new algorithm better accounts for the effects of the low soot concentration and comes closer to the actual temperatures. As we would expect, even less absorbance would occur if there were no soot, leading to lower-than-observed temperatures. This interpretation is consistent with the absorption coefficients shown in Figure B-5. The non-zero values for the no-soot case are due to the H_2O and CO_2 contributions.

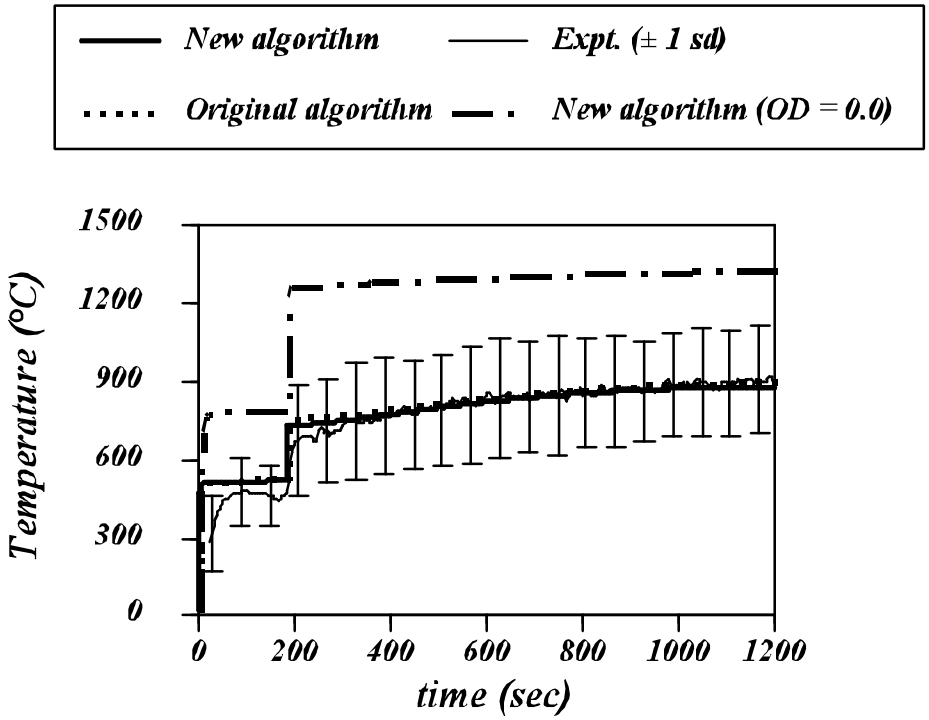

Figure B-3. Predicted and experimental upper layer air temperatures for compartment 1.

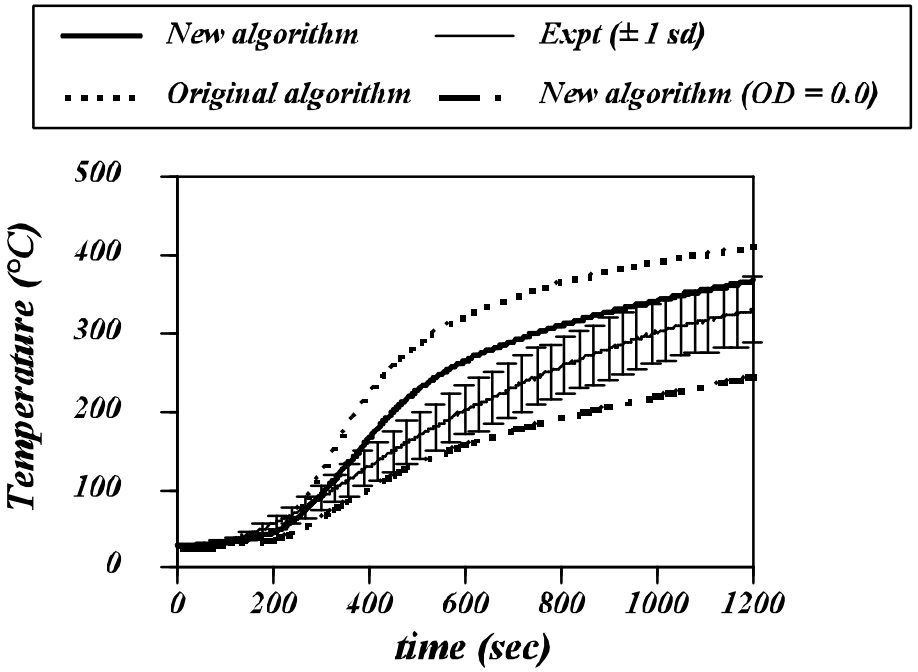

Figure B-4. Predicted and experimental upper layer air temperatures for compartment 2.

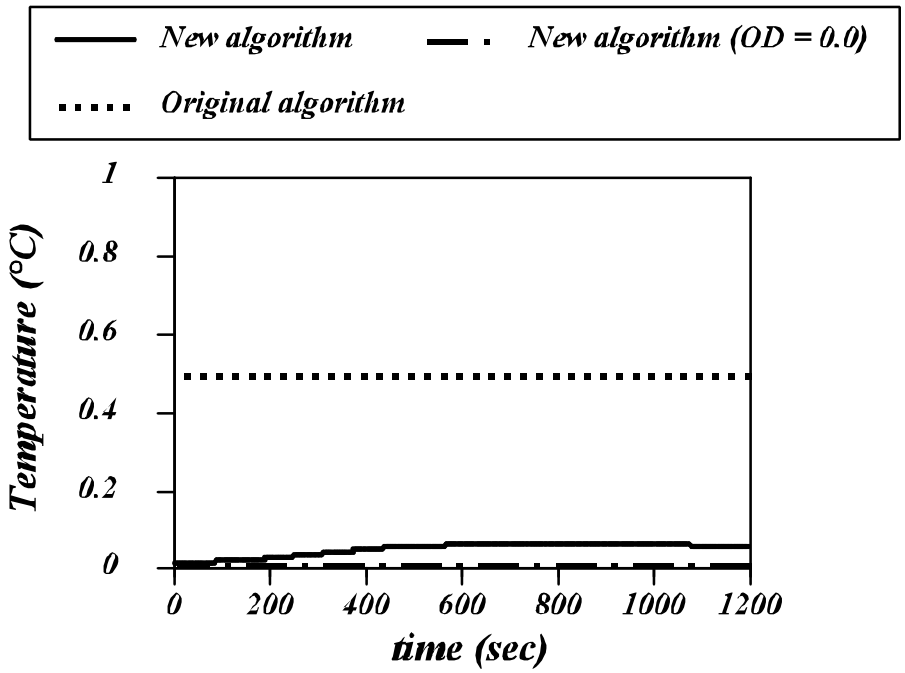

Figure B-5. Predicted upper layer absorption coefficient for compartment 2.

Symbol	Meaning	Units
Only symbols which differ from the main text are shown here		
A	Absorbance	dimensionless
α	Specific absorption coefficient	(meter-concentration)$^{-1}$
C	Concentration	unspecified
c	Mean beam length constant	dimensionless
f_V	Soot volume fraction	dimensionless
κ	Mean absorption coefficient	meter^{-1}
k	normalized κ	(meter-Kelvin)$^{-1}$
S	Scattering fraction	dimensionless
T	Transmittance	dimensionless

B.3 References

[B1] Tien *et. al.*, "Radiation Heat Transfer" in DiNenno, P.J. (Ed.) *The SFPE Handbook of Fire Protection Engineering*, 1st Ed., National Fire Protection Association, Eq. 34, p. 1-99 (1988).

[B2] Edwards, D.K., "Radiation Properties of Gases" In Rohsenow, W.M., *Handbook of Heat Transfer Fundamentals*, 2nd Ed., Chap. 14, Figures 2 and 3, pp. 74-75 (1985).

[B3] Tien, *et. al*., "Radiation Heat Transfer." in DiNenno, P.J. (Ed.) *The SFPE Handbook of Fire Protection Engineering*, 1st Ed., National Fire Protection Association, Eq. 39, p. 1-100 (1988).

[B4] Hubbard, G.L. and Tien, C.L. "Infrared Mean Absorption Coefficients of Luminous Flames and Smoke," *J. Hear Transfer*, **100**, p. 235 (1978).

[B5] Tien, *et. al*., "Radiation Heat Transfer." in DiNenno, P.J. (Ed.) *The SFPE Handbook of Fire Protection Engineering*, 1st Ed., National Fire Protection Association, Table 1-52, p. 1-98 (1988).

[B6] Bailey, J.L. and Tatem, P.A., "Validation of Fire/Smoke Spread Model (CFAST) Using Ex-USS SHADWELL Internal Ship Conflagration Control (ISCC) Fire Tests," US Naval Research Lab. Memo Report 6180-95-7781 (1995) [NTIS No. ADA300878].

Appendix C - Using Functional Analysis to Define a Metric of the Closeness of Two Time Series Curves.

C.1 Introduction

Functional analysis is a generalization of linear algebra, analysis, and geometry. It is a field of study that arose around 1900 from the work of Hilbert and others. Functional analysis is becoming of increasing importance in a number of fields including theoretical physics, economics, and engineering to answer questions on differential equations, numerical methods, approximation theory, and applied mathematical techniques. Its power lies in its ability to take different ideas and apply a unified symbolism and theory with a strongly geometric flavor to deal with the important central features of the problem. In practice, functional analysis allows problems to be described in vector notation and defines appropriate operations on these vectors to allow quantitative analysis of the properties of the underlying physical system. For this paper, the primary vector operations of interest are the norm, a measure of the length of a vector, and inner product, a measure of the angle between two vectors.

A simple sample of experimental data and a model prediction is shown in Figure C1. The question we wish to answer in comparing these two data sets: How close are the actual conditions to those predicted by the model? How to best quantify the comparison between model predictions and experiments (generally two time series) is not obvious. The necessary and

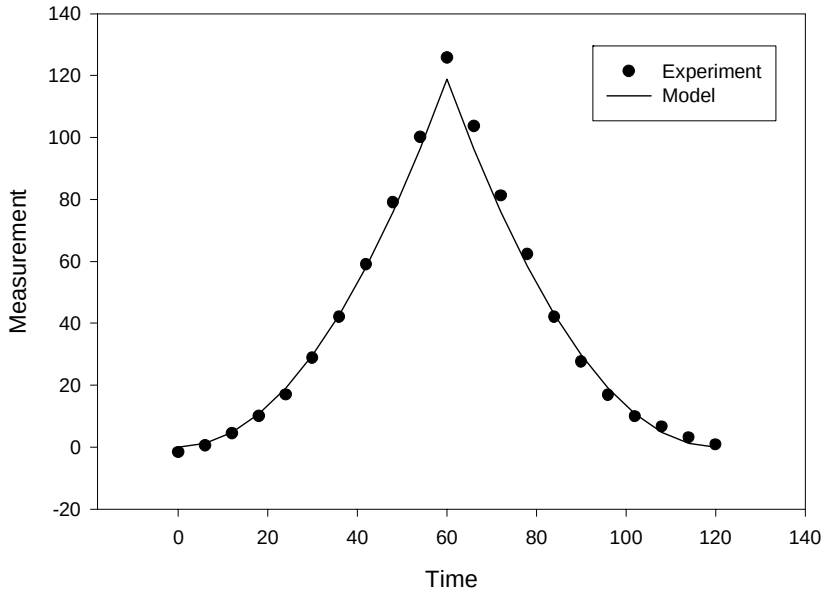

Figure C1. Simple example of experimental data with accompanying model prediction.

perceived level of agreement for any variable is dependent both upon the typical use of the

variable in a given simulation (for instance, the user may be interested in the time it takes to reach a certain temperature in the room), the nature of the experiment (peak temperatures would be of little interest in an experiment which quickly reached steady state), and the context of the comparison in relation to other comparisons being made (a true validation of a model would involve proper statistical treatment of many compared variables). For this simple example, a comparison of peak values would yields a difference of 6.9 or a relative difference, using the usual sum of squares of the difference between the experiment and model, (experiment – model) / experiment, of 0.055.

To obtain an overall comparison of the two curves, we can simply extend this single point comparison to multiple points. Each of these curves can be represented as a multi-dimensional vector, with each point in time defining an additional dimension. Using such a vector notation, a direct extension of the simple comparisons of maximums is the norm of the difference of the vectors of experimental and model data.

C.2 Finding the Length of a Vector, the Norm

The concept of a norm provides a definition of the length of a vector. The distance between two vectors is simply the length of the vector resulting from the difference of two vectors. The symbolic representation is written as $||\vec{x}||$ where $\vec{x}$ is the notation for the n-dimensional vector (x_1, x_2, …, x_{n-1}, x_n). For the above example in Figure C1, the comparison of peak values is called the sup norm, or a norm based on maximum absolute values. To extend the sup norm, all of the data can also be represented by a vector of values measured at each time point, $\vec{E}$. The model predictions at the same time points can be represented by a vector $\vec{m}$. The distance between these two vectors is the norm of the difference of the vectors, or $||\vec{E} - \vec{m}||$. It is convenient to normalize this as a relative difference to the experimental data as

$$\frac{||\vec{E} - \vec{m}||}{||\vec{E}||} \tag{1}$$

The difference vector is calculated just as it was for the simple example comparing the maximums of the two curves, taking the difference between the experiment and model at each time point. Initially, the Euclidean norm is most intuitive for computing length

$$||\vec{x}|| = \sqrt{\sum_i x_i^2} \tag{2}$$

As discussed later, other geometries can also be particularly useful for real-time comparisons. For the example in Figure C1, the distance between the two vectors, $||\vec{E} - \vec{m}||$, is 14.1 and the relative difference is 0.056. For the simple curves in Figure C52, the comparison of peak values provides a good measure of the overall agreement, nearly identical to the overall comparison

from eq. (1) since the two curves were chosen to differ only at the peak. For more complex curves, the comparison of maxima may not be as good an indicator.

C.3 Finding the Angle between Two Vectors, the Inner Product

While the difference, $||\vec{E} - \vec{m}||$, and the relative difference, $||\vec{E} - \vec{m}/||\vec{E}||$, provide measures of the difference between experimental data and model predictions, other calculations provide useful information on the source of the difference. When comparing vectors, there are basically two geometric components to consider: a difference in length between the two vectors and the (non-zero) angle between the two vectors. The inner product, $\langle \vec{x}, \vec{y} \rangle$, of two vectors is the product of the length of the two vectors and the cosine of the angle between them, or

$$\langle \vec{x}, \vec{y} \rangle = ||\vec{x}|| \cdot ||\vec{y}|| \cos\left(\angle (\vec{x}, \vec{y})\right) \tag{3}$$

or

$$\cos\left(\angle (\vec{x}, \vec{y})\right) = \frac{\langle \vec{x}, \vec{y} \rangle}{||\vec{x}|| \cdot ||\vec{y}||} \tag{4}$$

Choosing the inner product to be the standard dot product gives results consistent with typical Euclidean geometric perception

$$\langle \vec{x}, \vec{y} \rangle = \sum x_i y_i \tag{5}$$

For the example in Figure C1, $\cos\left(\angle \left(\vec{x}, \vec{y}\right)\right)$ = 0.99. Visually, this angle between the two vectors represents a measure of how well the shapes of the two vectors match. As the cosine of the angle approaches unity, the overall shape of the curves becomes identical.

C.4 Properties of Norms and Inner Product / Other Geometries

The form of the inner product and norm for Euclidean space is certainly not the only definition. In general, an inner product is simply a function that takes two vectors and returns a number. The number can be either real or complex – for our purposes, only real inner products will be considered. We will include three additional definitions, Hellinger, secant, and a hybrid of Euclidean and secant. For consistency, the norm can be defined in terms of the inner product. This ensures that appropriate, consistent definitions for the norm and inner product are used in calculations. Since the angle between a vector and itself is by definition zero, it follows from eq. (3) that

$$\langle \vec{x}, \vec{x} \rangle = ||\vec{x}||^2 \text{ or } ||\vec{x}|| = \sqrt{\langle \vec{x}, \vec{x} \rangle} \tag{6}$$

The Hellinger inner product for functions x such that $x(0)=0$ is defined based on the first derivative of the function:

$$\left\langle \vec{x},\vec{y}\right\rangle = \int_0^T x'(t)y'(t)dt \tag{7}$$

For discrete vectors, this can be approximated with first differences as:

$$\left\langle \vec{x},\vec{y}\right\rangle = \frac{\sum_{i=1}^{N}\left(x_i - x_{i-1}\right)\left(y_i - y_{i-1}\right)}{t_i - t_{i-1}} \tag{8}$$

Based on the first derivative or tangents to the curves, the Hellinger inner product and norm provide a sensitive measure of the comparison of the shape of two vectors. A variation of the Hellinger inner product can be defined based on the secant rather than tangent as

$$\left\langle \vec{x},\vec{y}\right\rangle = \int_{pT}^{T} \frac{\left(x(t) - x\left(t - pT\right)\right)\cdot\left(y(t) - y\left(t - pT\right)\right)}{\left(pT\right)^2} dt \tag{9}$$

where $0<p\leq 0.5$ defines the length of the secant. The limit of the secant inner product as $p\to 0$ is the Hellinger integral. For discrete vectors, this can be approximated analogous to the Hellinger geometry

$$\left\langle \vec{x},\vec{y}\right\rangle = \frac{\sum_{i=s}^{N}\left(x_i - x_{i-s}\right)\left(y_i - y_{i-s}\right)}{t_i - t_{i-1}} \tag{10}$$

When $s=1$, the secant definition is equivalent to the discrete Hellinger inner product. Depending on the value of p or s, the secant inner product and norm provide a level of smoothing of the data and thus better measures large-scale differences between vectors. For experimental data with inherent small-scale noise or model predictions with numerical instabilities, the secant provides a filter to compare the overall functional form of the curves without the underlying noise. Finally, a hybrid of the Euclidean and secant inner product provides a balance between the rank ordering of the Euclidean norm and the functional form comparison of the secant. From the axioms above, the sum of two inner products is also an inner product. For this paper, we will consider a simple weighted sum of the Euclidean inner product and secant inner product, or

$$\left\langle \vec{x},\vec{y}\right\rangle = \frac{1}{n}\sum_{i=1}^{N} x_i y_i + \frac{1}{n-s}\frac{\sum_{i=s}^{n}\left(x_i - x_{i-s}\right)\left(y_i - y_{i-s}\right)}{\left(i_i - t_{i-s}\right)} \tag{11}$$

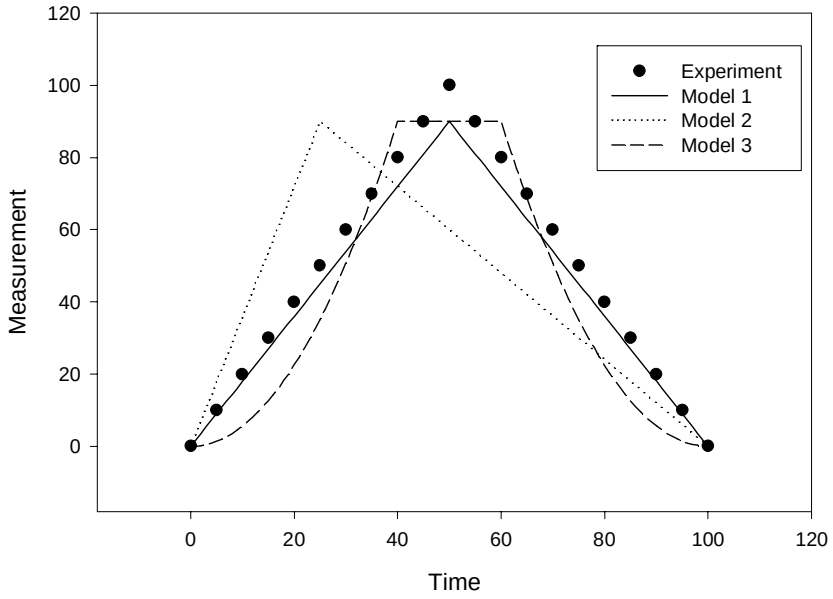

Figure C2. Three possible model predictions for a fictional example of experimental data.

The weighting factors equalize the contribution of the Euclidean inner product and the secant inner product to the combination. Figure C2 shows another simple example of fictitious experimental data compared with three model predictions. Model 1 is simply the experimental data multiplied by 0.9. Model 2 has the same peak value as model 1, but with the peak shifted -25 s. Model 3 has the same peak as Model 1 and Model 2, but with a 20 s plateau centered around the peak of the experimental data. The comparison only of maxima would show that all three models are identical with a relative difference of 0.1. Clearly this comparison fails to capture the differences between the three models. Table 1 shows the relative difference and cosine between the vectors of experimental data and model predictions for the three models using other definitions for the inner product and norm.

Table 1. Comparison of fictional experimental data with three model predictions using several different inner product definitions

Geometry	Model	Relative Difference	Cosine
Euclidean	1	0.10	1.00
	2	0.40	0.92
	3	0.20	0.98
Hellinger	1	0.10	1.00
	2	0.94	0.58
	3	0.74	0.77
Secant	1	0.10	1.00
	2	0.92	0.58
	3	0.66	0.83
Hybrid	1	0.10	1.00
	2	0.64	0.78
	3	0.43	0.91

All of the metrics rank the models in the same order, with Model 1 closest to the experimental data, followed by Models 2 and 3. The rank order matches a visual interpretation of the

comparisons. Model 1 is clearly the best, with the same functional form and a peak timed correctly but slightly lower than the experimental data. Conversely, Model 2, with its peak so offset from the experiment appears the worst. Although Model 3 does not have the correct type of peak (an elongated plateau rather than a sharp peak), it does have the right general form; changing to match the experiment.

The relative difference for Model 1 is the same for all of the metrics as it should be. By choice, the vector form of Model 1, $\vec{m}$, is simply $\vec{m} = 0.9 \cdot \vec{E}$. Thus, the relative difference, $||\vec{E} - \vec{m}|| / ||\vec{E}||$, regardless of the definition of the norm is just $||\vec{E} - 0.9\vec{E}|| / ||\vec{E}||$ or 0.1. Similarly, the cosine of the angle between Model 1 and the experiment is 1.0 for all of the comparisons.

While both the Euclidean relative difference and cosine have the appropriate ranking for all of the models, the cosine does not provide much differentiation between the model predictions. The Hellinger and secant values provide a wider range since they specifically compare the functional forms of the experiment and models. The hybrid equation combines the best features of these two.

Appendix D Annotated Bibliography of Experimental Comparison and Use of CFAST

CFAST is a widely used model of fire growth and smoke transport. A number of comparisons with experiments, other models and data from fire reconstructions have been done over the life time of the model. This section annotates the references based on the abstract from the papers which are available in the open literature. There are additional papers which are not available because of security restrictions and others which are part of legal proceedings. The conclusions of these latter are similar to those cited below.

There are two purposes for such a bibilography: to demonstrate the wide use of the model and to indicate the generally high accuracy of the model. Not all papers made direct model to experiment comparisons. Some uses were investigations and some were comparisons with other models. There are several papers which used the model to elicit hidden information, such as surrogate flashover criteria.

The abstract from the papers is included. There are both uses and comparison cited.

"A Short Note on Experimental Verification of Zone Models with an Electric Heater," G.C.H. Lui, and W.K. Chow, International Journal on Engineering Performance-Based Fire Codes *5*, 30 (2003).

> An electric heater with adjustable thermal power output was used to verify results predicted by CFAST. This gives better control on the thermal output of the hot object. Experiments were performend in a fire changer of length 4.0 m, width 2.8 m, and height 2.8 m.

"Modeling a Backdraft Incident: The 62 Watts Street (New York) Fire,' Bukowski, R. W. *Fire Engineers Journal, Vol. 56, No. 185, 14-17, November 1996*

> On March 28, 1994 the NYFD responded to the report of smoke and sparks issuing from the chimney at a three story apartment building in Manhattan. Upon arrival, a team of three firefighters was killed due to a backdraft condition occurring when the well-sealed apartment was forced open. At the request of the NYFD, NIST was given the task of modeling the fire with the hope of understanding the factors leading to and resulting from the backdraft condition. The CFAST model was able to (very accurately) reproduce the observable conditions and supported the theory as to how the fire began.

"Use of a Zone Model in Predicting Fire and Smoke Propagation in Tunnels," M.S. Altinakar, A. Weatherill, P.H. Nasch, *BHR Group Vehicle Tunnels. Proceedings. 623-639 pp, 1997.*

> This paper investigates the applicability of a modified version of CFAST in predicting fire development and smoke propagation in vehicle or railroad tunnels. The model is tested by simulating several full-scale tests carried out at memorial Tunnel Ventilation

Test Program in West Virginia, US, and the Offeneg Tunnel in Switzerland. The article compares simulated values (temperature, opacity and similar sensible quantities) with measured values and discusses the limits of the applicability of zone models for simulating fire and smoke propagation in vehicle and railroad tunnels. The two major modifications made to the model dealt with mixing between the upper and lower layers and friction losses along the tunnel.

"Comparison of CFAST Predictions to USCG Real-Scale Fire Tests," Reneke, P. A.; Peatross, M. J.; Jones, W. W.; Beyler, C. L.; Richards, R. *Journal of Fire Protection Engineering, Vol. 11, No. 1, 43-68, February 2001.*

In this report, CFAST was used to make predictions of single room pre-flashover fire tests conducted in steel enclosures. These results were then compared with previously published measurements obtained from fire tests. These tests include diesel pool fires, polyurethane slab fires, and wood crib fires. With the exception of heat release rates, all CFAST inputs were selected without knowledge of the experimental results. Key variables compared include the upper layer temperature, the hot layer interface location, and ceiling temperatures. Overall, predictions made by CFAST were in good agreement with the data. There was, however, a general tendency to over predict the hot gas layer temperature and the boundary surface temperature. Most of the difference vanishes when the experimental results are corrected for radiation from thermocouples.

"Systematic Experiments of Room and Corridor Smoke Filling for Use in Calibration of Zone and CFD Fire Models," Matsuyama, K.; Wakamatsu, T.; Harada, K. NISTIR 6588; November 2000.

It was the contention of Matsuyama that in the smoke control design process, smoke propagation is generally calculated using zone models, such as CFAST. He acknowledges that these models have been extensively validated by experiments carried out using steady heat release rate (HRR). The purpose of his paper is to question whether the models are as valid for t^2-fires. In this study, a series of full-scale experiments were carried out using t^2-fires. Fire room and corridor smoke filling process was measured. The size of the corridors and arrangements of smoke curtains were varied in several patterns. Comparisons were then made between the experimental results and those predicted by CFAST. The author concludes that while the model does a good job of predicting experimental results, there are systematic differences which could be reduced with some revision to zone type equations to include this effect.

"Evaluation of the HDR Fire Test Data and Accompanying Computational Activities With Conclusion From Present Code Capabilities. Volume 3. Test Series Description and CFAST Validation for HDR T51 Wood Crib Fire Test Series,"Floyd, J. E.; Wolf, L. NIST GCR 99-778; 120 p. September 1999.

Between 1984 and 1992 four major tests series were preformed in the HDR containment encompassing various fuels and three different axial positions in the high-rise, multi-

level, multi-compartment facility. These four test series consisted of gas, oil, cable, and wood crib fire tests. At the time these test were carried out, each test series was accompanied by extensive efforts to evaluate the predictive capabilities of a variety of fire models and codes developed in different countries by both blind pre-test and open-test computations. CFAST was one of these models. The report lists numerous accomplishments and suggests improvements for the CFAST model.

Predictability of Flashover by Zone Models, " Chow, W. K. Journal of Fire Sciences, Vol. 16, No. 5, 335-350, September/October 1998.

From a study identifying the chaotic behavior of fires in compartment fires, two additional flashover inspection criteria were established. It was during this study that phase space diagrams on fire temperatures and their time rates of change were analyzed. The proposal was applied to whether flashover can be predicted by the two-layer zone model, CFAST. It was concluded by the author that the current flashover criteria based on gas temperature near the ceiling, heat flux at the floor level and flames coming out of the openings, the rate of change of fire temperature should be used as an additional criterion when estimating flashover in compartment fires.

"Application of CFAST to Shipboard Fire Modeling. Part 3. Guidelines for Users. Final Report. 1998-2000." Hoover, J. B.; Tatem, P. A. NRL/MR/6180-01-8550; 104 p. April 23, 2001.

In January 1996, the US Navy began testing how the CFAST model would perform when tasked with predicting shipboard fires. Due the differences between shipboard fires and building type fires, the Navy has funded improvements in the CFAST model. These improvements were aimed at making the model more applicable to shipboard conditions. These conditions include mass transport through vertical vents (representing hatches and scuttles), energy transport via conduction through decks and improvement to the radiation transport sub model. The purpose of this study was to identify CFAST limitations and develop methods for circumnavigating these problems. The approach taken was to apply CFAST to the modeling of a full-scale shipboard fire test and then compare to model conditions. A retired ship representing the forward half of a USS LOS ANGELES class submarine was used during this test.

"Benchmark Analysis With CFAST and FDS. Appendix B," Dey, M. K. NISTIR 6872; June 2002. International Collaborative Project to Evaluate Fire Models for Nuclear Power Plant Applications. Evaluation of Fire Models for Nuclear Power Plant Applications: Cable Tray Fires. International Panel Report. Appendix B: Benchmark Analysis With CFAST and FDS, B/1-20 pp, 2002.

This appendix to 'Evaluation of Fire Models for Nuclear Power Plant applications: Cable Tray Fires', presents analyses conducted with CFAST for an international benchmark exercise aimed at evaluating the capability of current fire models to simulate cable tray fires of redundant safety systems in nuclear power plants. The exercise involved simulating fires scenarios in a large nuclear power plant compartment with cable trays as

targets in varying ventilation conditions. The analyses demonstrated that CFAST was able to provide an accurate description of most physical phenomena in the scenarios analyzed.

“Simulations Using JASMINE and CFAST. Benchmark Analysis With JASMINE and CFAST. Appendix G.” Miles, S NISTIR 6872; June 2002. International Collaborative Project to Evaluate Fire Models for Nuclear Power Plant Applications. Evaluation of Fire Models for Nuclear Power Plant Applications: Cable Tray Fires. International Panel Report. Appendix G: Benchmark Analysis With JASMINE and CFAST, G/1-24 pp, 2002.

As part of its participation in the International Collaborative Project to Evaluate Fire models for Nuclear Power Plant Applications, BRE has made numerous predictions for cable tray fires of redundant safety trains. For this particular analysis, trash bag and cable tray fires inside a switchgear room were modeled. The main objective was to ascertain the likelihood of thermal damage to a ‘target’ cable at various distances from the fire source. The CFAST model was one of two models being reviewed. The researchers reported that the models presented difficulty in modeling nearly sealed rooms. This condition showed the most noticeable differences between the outputs of the two models.

“Simulation of a Three-Story Wooden Apartment Building with CFAST 1.5.0,” Gautier, F. Centre Scientifique et Technique du Batiment, Cedex, France ; 81 p. October 1991/May 1992.

On December 4, 1992 a large fire experiment was carried out at the Building Research Institute near Tokyo, Japan. A three-story building was submitted to vibrations similar to those of an earthquake. A fire was then initiated in an attempt to test the buildings resistance. Upon completion of this experiment CFAST was used to simulate the large experiment. Although the experimenters encountered some difficulties, overall, the model provided accurate results.

“Experimental Evaluation of the Zone Models CFAST, FAST and CCFM.VENTS,” Chow, W. K.,Journal of Applied Fire Science, Vol. 2, No. 4, 307-332, 1992-1993.

Three zone models, one of which was CFAST, were evaluated experimentally using a small fire chamber. Liquid fires were chosen for having better control on the mass loss rate. The results on the development of smoke layer and the hot gas temperature predicted by the three models were compared with those measured experimentally. Fairly good agreement was found if the input parameters were chosen properly.

“Modeling the Impact of Post-Flashover shipboard fires on adjacent spaces”
White, D.a, Beyler, C.L, Scheffey, J.L, and Williams, F.W. Journal of Fire Protection Engineering, Vol 10, No. 4, 2000.

This paper looks at post-flashover fires in shipboard spaces and there pronounced effects on adjacent spaces due to highly conductive boundaries. Experimental data provided the input function for the hot wall. The CFAST model predictions for the gas temperature

and the cold wall temperature were compared with experimental data. The comparisons between the model and experimental data show conservative predictions. The author attributes this to an overestimation of the average hot wall temperature and an underestimation of external convective losses due to wind effects.

“Validation of Fire/Smoke Spread Model (CFAST) Using Ex-USS SHADWELL Internal Ship Conflagration Control (ISCC) Fire Tests.” Bailey, J. L.; Tatem, P. A. NRL/MR/6180-95-7781; 51 p. September 28, 1995.

This report describes some features of CFAST and compares predictions to data from real scale fire tests conducted onboard ex-USS SHADWELL, the Navy’s R&D damage control platform. The phenomenon of particular interest in this validation is the conduction of heat in the vertical direction, which was recently added to CFAST in an attempt to make the model more suitable for Navy applications. The model compared reasonably well with experimental results the fire compartment as well as for the compartment and deck directly above it. The model did, however, over predict the temperatures of the compartments and decks not directly adjacent to the fire compartment.

“Fire in a Residential Building: Comparisons Between Experimental Data and a Fire Zone Model.” Collier, P. C. R. Fire Technology, Vol. 32, No. 3, 195-218, August/September 1996.

In an attempt to quantify the fire hazards associated with a typical New Zealand dwelling, a series of experiments were conducted. These tests, done in a three-bedroom dwelling, included both a nonflashover and a flashover fire. A selection of experimental results was analyzed to determine smoke and gas movement together with temperature rises in the various rooms. These results were compared to the predictions of the CFAST fire and smoke transport computer model. The predictions were consistent (and compare favorably) with the experiments within the uncertainty of each.

“Compartment Fire Experiments: Comparison With Models.” Dembsey, N. A.; Pagni, P. J.; Williamson, R. B. Fire Safety Journal, Vol. 25, No. 3, 187-227, 1995.

Twenty compartment fire experiments suitable for model comparisons were conducted in a compartment that is similar in size, geometry, and construction to the standard fire test compartment specified in the Uniform Building Code. Ceiling jet temperatures, surface heat fluxes and heat transfer coefficients are all discussed. Data from 330 kW, 630 kW,and 980kW fires is used to compare with CFAST’s predicted values.

“Uncertainty in Smoke Transport Models.” Lundin, J. LUTVDG/TVBB-3086-SE; 77 p. July 1997.

For this report, data from full-scale experiments was collected and organized in a database. A statistical method was then developed to evaluate the uncertainty in predictions of smoke transport models. The method is based on regression analysis of

measured and predicted data. The computer program CFAST was evaluated to exemplify the statistical method. Uncertainty is quantified with a regression coefficient and the residual variance. With the model's uncertainty quantified, it is possible to adjust the model predictions for the model error. The uncertainty in CFAST's predictions of smoke gas temperature and position of interference is investigated for a number of different scenarios.

"Uncertainty Analysis of Zone Fire Models." Walker, A. M. Fire Engineering Research Report 97/8; 172 p. May 1997.

This report discusses the uncertainties in components of zone models and shows how uncertainty within user-supplied data affects the results obtained. Using the second version of CFAST, a numerical uncertainty analysis is performed, utilizing sensitivity factors as the basis of the analysis. The objective being to make fire engineers aware of the degree of uncertainty associated with zone fire models. These uncertainties discussed are those which exist within the model, and are not indicative of the uncertainties corresponding to comparisons of the model with reality. Experimental uncertainty and bias would require a similar study.

"Smoke Spread Experiment in a Multi-Storey Building and Computer Modeling"He, Y.; Beck, V. Fire Safety Journal, Vol. 28, No. 2, 139-164, March 1997.

This paper describes a series of full-scale fire experiments that were designed to investigate the validity of two zone models, CFAST being one. The experiments, involving steady state burning rates and a number of ventilation conditions were conducted in a four-story building. Temperature, pressure, flow velocity, smoke density and species concentrations were measured in various parts of the building. The chimney effect and its influence on temperature distribution in a stair shaft were observed. Comparisons were then made between the experimental results and the model predictions. In general the model predictions agreed well with the experimental measurements within the uncertain in both.

"Modeling the Fire Resistance of Wood-Frame Office Buildings." Lin, E. C. Y.; Mahaffey, J. R. Journal of Fire Sciences, Vol. 15, No. 4, 308-338, July/August 1997.

A fire safety engineering analysis has been undertaken to determine the fire resistance of gypsum protected wood stud walls in six simulated office fire scenarios. Each scenario consists of an office furnishing fire in an unsprinklered compartment with windows shut and doors closed at the initiation of fire. CFAST was used to calculate temperature throughout the compartment, heat transfer from the fire to the walls, and the structural degradation. The time to failure of the windows and doors were also determined. It was determined that CFAST could be employed to deliver performance-based design for fire resistance of wood frame buildings.

"Application of Field Model and Two-Zone Model to Flashover Fires in a Full-Scale Multi-

Room Single Level Building." Luo, M.; He, Y.; Beck, V. Fire Safety Journal, Vol. 29, No. 1, 1-25, July 1997.

> This paper presents a comparison of the results from CFAST against a comprehensive set of data obtained from one flashover fire experiment. The experimental results were obtained from a full-scale prototype apartment building under flashover conditions. Three polyurethane mattresses were used as fuel. The mass release rate, gas temperature, radiation heat flux and gas compositions were measured. It was found that the predicted temperatures from the CFAST fire model agreed well with the experimental results in most areas. However, the CFAST model under-predicted the temperature in the lower layer of the room of fire origin and the concentration of CO in most areas. These discrepencies disappear when radiation corrections are applied to the thermocouple data.

"Evaluation of the HDR Fire Test Data and Accompanying Computational Activities With Conclusion From Present Code Capabilities. Volume 2. CFAST Validation for T51 Gas Fire Test Series." Floyd, J. E.; Wolf, L.; Krawiec, J. NIST GCR 97-731; 79 p. November 1997.

> This report documents efforts to model the HDR T51 Gas Fire Test Series using the CFAST zone model. Four gas fires were used for the modeling effort. Three tests, a 229kW, 716kW, and 1011kW fire, were selected as they span the range of firepowers used in the T51 series. One additional test was used to examine the effects of changing the fire room ventilation during the test. For each selected test, three different models of increasing geometric complexity were developed, run, and compared with the respective data. The 229kW test further was used to look at the effects of input data uncertainties on CFAST results. While the agreement between prediction and measurement is good, the model is sensitive to input (particularly the measurement of the fire) and these values need to be choosen carefully. What is clear, however, is that some model such as CFAST will be required in a performance-based code system. Hand calculations are not going to have the precision to analyze an entire structure, and CFD methods are currently computationally too expensive to model multiple fire scenarios in large structures for long periods of time or to model very large, complex, structures in their entirety. Because of this, it can be concluded that CFAST should undergo further development and validation directed toward the goal of using it in a performance-based code system.

"Comparison of Existing Fire Model Predictions With Experimental Results From Real Fire Scenarios." Luo, M.; He, Y.; Beck, V. Journal of Applied Fire Science, Vol. 6, No. 4, 357-382, 1996/1997.

> This article presents a series of experimental results for flaming fires, obtained using realistic fires in a prototype apartment building. Fuel configurations in the fire test include horizontal plain polyurethane slab, mock-up chair (polyurethane slabs plus a cotton linen cover), and commercial chair. The predictions from the CFAST zone model were found to be in reasonable agreement with experimental results in all cases when the measured mass release rates were used.

“Application of Computer Modelling to Real Fire Incidents.” Chitty, R.; Foster, J. Interscience Communications Ltd.; International Interflam Conference, 9th Proceedings. Volume 2. September 17-19, 2001, Edinburgh, Scotland.

> This paper examines the use of computer modeling of two real fire incidents identifying the information needed to model these incidents and the assumptions made when using them. The first fire incident was a fire in a two-story concrete and steel school building. The second was a flat on the ninth floor of a 19story residential tower block. The authors concluded that by using a combination of modeling techniques, beginning with the simplest and progressing to more complicated ones, one could efficiently guide an investigator to a realistic portrayal of the incident.

“Development and Validation of Corridor Flow Submodel for CFAST.” Bailey, J. L.; Forney, G. P.; Tatem, P. A.; Jones, W. W. Journal of Fire Protection Engineering, Vol. 12, No. 3, 139-161, August 2002.

> This paper discusses the CFAST zone model and its recent addition, referred to as the Corridor Flow Submodel. Prior to the addition of this sub model CFAST assumed that smoke traveled instantly from one side of a compartment to another. This new addition more accurately predicts the flow of smoke down a corridor. This enhanced version of CFAST (4.0.1) is used to model a real-scale experiment conducted onboard the ex-USS SHADWELL, the Navy’s R&D Damage Control platform. It was found that this new addition to CFAST, greatly, enhanced its predictive capabilities.

“Comparison of CFAST and FDS for Fire Simulation With the HDR T51 and T52 Tests.” Floyd, J. E. NISTIR 6866; 111 p. March 2002.

> This work examines the predictive capabilities of three methods: hand calculations; CFAST; and the FDS fire simulator. The simulation results are compared against test data from two fire experiments performed in the HDR test facility, the containment building from a decommissioned German nuclear reactor. The first experiment is a gas fire which involves a 1Mw propane gas fire low in the containment building. The second experiment is an oil pool fire that was a 3MW oil fire high in the containment building.

“Prototype Model for Simulating Barrier Fire Performance: CFAST.GYPST - For Evaluating the Thermal Response of Gypsum-Panel/Steel-Stud Wall Systems.” Cooper, L. Y.; Reneke, P.A. NISTIR 6482; 70 p. February 2000.

> This paper looks at the validation of CFAST using previously acquired experimental data from ASTEM E119 furnace tests of two different, full-scale wall-system designs. In real-fire-type simulations that are relatively severe, CFAST is used to calculate the fire environment and associated wall response for each wall system for a room geometry and fire energy release history that is related to that of a newly developing ASTM room fire test standard. For these simulations, the thermal responses of the two wall systems are predicted and then evaluated relative to respective expected fire resistance.

“Numerical Study of Atrium Fires Using Deterministic Models.” Rho, J. S.; Ryou, H. S. Fire Safety Journal, Vol. 33, No. 3, 213-229, October 1999.

> This article is focused on finding out the smoke movement and temperature distribution in atrium spaces. Three types of atrium are looked at for this paper. A computational method for predicting velocity and temperature distribution in fire-induced flow is based on the solution of three-dimensional Navier-Stokes conservation equations for mass, momentum, energy, species etc. using a finite volume method and non-staggered grid system. This numerical calculation was then compared to CFAST’s predictions. CFAST’s predictions were similar to the results obtained from the calculation for the smoke layer temperature and the smoke layer interface heights.

“Quantifying Fire Model Evaluation Using Functional Analysis.” Peacock, R. D.; Reneke, P. A.; Davis, W. D.; Jones, W.W. Fire Safety Journal, Vol. 33, 167-184, 1999.

> Much of the work to validate fire models has been largely qualitative. Treating these time series curves as infinite-dimensional vectors, a branch of mathematics called functional analysis, defines geometrically meaningful operations on the curves. This allows lengths, angles, and distance between two arbitrary curves to be defined and quantified. This report gives an introduction to the theory and tools provided by this functional analysis. Examples of the application of these tools to CFAST evaluation are presented, allowing for a quantitative comparison between model and experiment. The conclusion is that it is now possible to quanfity the difference between modeld and experiment. For the examples choosen, CFAST predicts the measured values quite well; the values for both agreement and shape are close to unity.

“Comparison of Algorithms to Calculate Plume Centerline Temperature and Ceiling Jet Temperature With Experiments.” Davis, W. D.Journal of Fire Protection Engineering, Vol. 12, No. 1, 9-29, 2002.

> In this paper, the predictive capability of two algorithms, designed to calculate plume centerline temperature and maximum ceiling jet temperature in the presence of a hot upper layer, are compared to measurements from experiments and to predictions using CFAST’s ceiling jet algorithm. The experiments include ceiling heights of .58m to 22m and heat release rates of .62kW to 33MW. When compared to the experimental results CFAST’s ceiling jet algorithm tended to over-predict the temperature by 20%. With a proper adjustment for radiation effects of the termocouple measurements, this difference should disappear.

“Fire Growth Rates in Structural Fires.” Poole, G. M.; Weckman, E. J.; Strong, A. B. NISTIR 5499; September 1994.

> The work reported in this paper represents one aspect of a cooperative project between the city of Kitchener Fire Department and the University of Waterloo aimed at developing design criteria for the construction of a fire fighter training facility. One

particular criterion is that realistic training with respect to temperature, heat release and stratification be provided in such a facility. It is the purpose of this paper to compare existing analytical heat release and upper and lower gas temperature rise correlations and models with data from actual structures which were instrumented and burned in collaboration with the Kitchener Fire Department. The CFAST model was used successfully to predict these conditions.

"Verification of a Model of Fire and Smoke Transport." Peacock, R. D.; Jones, W. W.; Bukowski, R. W. Fire Safety Journal, Vol. 21, No. 2, 89-129, 1993.

This paper looks at a set of comparisons between CFAST predictions and a range of real-scale fire experiments. The model predicts the evolution of a fire in a room and the subsequent transport of the smoke and toxic gasses which result from the fire. These comparisons serve to determine, within limits, the accuracy of the predictions and to highlight the strengths and weaknesses of the underlying algorithms in the model. This is done to aid in future improvements to both CFAST and other fire models. Although differences between the model and the experiments were clear, they can, according to the author, be explained by limitations of the model and experiments.

"Studies on Closed Chamber Fires." Chow, W. K. Journal of Fire Sciences, Vol. 13, No. 2, 89-103, March/April 1995.

In this paper, closed chamber fires are studied by burning four types of organic liquids, namely ethanol, N-heptane, thinner and kerosene. The burning behavior of the liquids was observed, and the hot gas temperature measured. These behaviors along with the transient variations of the temperature were then compared with those predicted by the CFAST model.

"Use of Zone Models on Simulating Compartmental Fires With Forced Ventilation." Chow, W. K. Fire and Materials, Vol. 19, No. 3, 101-108, 1995.

The performance of CFAST along with two other zone models in simulating forced ventilation fires with low heat release and high ventilation rates were studied experimentally. A fire chamber of length 4.0m, width 3.0m and height 2.8m with adjustable ventilation rates was used. Burning tests were carried out with wood cribs and methanol to study the preflashover stage of a compartmental fire and the effect of ventilation. The mass loss rate of fuel, temperature distribution of the compartment and the air intake rate were measured. The heat release rates of the fuel were calculated and the smoke temperature was used as a validation parameter. A scoring system was proposed to compare the results predicted by the three models. CFAST does particularly well, though there are some differences which can be attributed to the zone model approach.

"Multi-Cell Concept for Simulating Fires in Big Enclosures Using a Zone Model." Chow, W. K. Jounal of Fire Sciences, Vol. 14, No. 3, 186-198, May/June 1996.

The multi-cell concept is applied to simulate fire in a big compartment with the zone model CFAST. The predicted physical properties of the smoke layer are used to justify the results, including the smoke layer temperature, smoke layer thickness and flows between each cell. Microscopic pictures of the flow pattern and smoke temperature distribution similar to the results predicted by the model can be obtained. The author recommends this idea to study fires in big enclosures.

"Prediction of Fire Environment in Apartments Using Zone Models." Chow, W. K. Journal of Fire Sciences, Vol. 14, No. 4, 263-312, July/August 1996.

Two fire zone models, CFAST and BRI2T, are applied to simulate fires in multi-level apartments. Apartments with different levels and several compartments, including a staircase, are taken as examples. Smoke control designs, including ceiling vents and smoke extraction systems, installed in the staircase are considered with their performance evaluated. Experimental results reported in the literature are used to compare with the predicted results. The comparison shows good agreement.

"Comparison of the Use of Fire Zone and Field Models for Simulating Atrium Smoke-Filling Processes." Chow, W. K. Fire Safety Journal, Vol. 25, No. 4, 337-353, November 1995.

This paper looks to compare the use of fire zone and field models for simulating the atrium smoke filling process for three types of atrium spaces. Three zone models, one of which is CFAST, are compared to the authors self-developed field model. The results predicted by the two approaches are very similar. The author concludes that simulation using field models requires much more computing time compared with the use of a zone model.

"Comparison of CFAST Predictions to Real Scale Fire Tests." Jones, W. W.; Bailey, J. L.; Tatem, P. A.; Forney, G. P. Institut de Securite. Fire Safety Conference on Performance Based Concepts. Proceedings. October 15-17, 1996, Zurich, Switzerland, 25/1-14 pp, 1996.

This paper describes the the CFAST model and compares it to data from real scale fire tests conducted onboard the ex-USS SHADWELL, the Navy's R&D Damage Control Platform. The phenomenon modeled in this work is the conduction of heat in the vertical direction. The work focuses on the four compartments of the ship that are vertically aligned. The temperatures of three of the compartments and decks between them were compared with model predictions. Predictions compared very closely with the experimental results for all compartments, although the temperature rise in the topmost compartment was barely above ambient.

"Performance of Sprinkler in Atria." Chow, W. K. Journal of Fire Sciences, Vol. 14, 466-488, November/December 1996.

This paper evaluates the performance of a sprinkler installed in an atrium roof. There were three main points being considered: the possibility of activating the sprinkler,

thermal response, and water requirement. The zone model CFAST was used to analyze the possibility of activating of the sprinkler head. Results derived from CFAST proved to be accurate (good agreement with experimental measurements).

“One Zone or Two Zones in the Room of Fire Origin During Fires? The Effects of the Air-Handling System.” Luo, M. Journal of Fire Sciences, Vol. 15, No. 3, 240-260, May/June 1997.

A two-zone model, CFAST, has been widely used in the fire research community. However, this study indicates that the CFAST model generally over predicts the upper layer temperature in the burn room because the zonal assumption is likely to break down in the burn room. It was found that the room –averaged temperatures obtained from CFAST were in good overall agreement with the experimental results. The discrepencies can be attributed to the correction needed for thermocouple measurments. The CO concentration, however, was inconsistent. CFAST tended to overestimate CO concentration when the air handling system was in operation. This is probably due to incosistencies in what is measured (point measurements) and predicted (global measurements). The under estimate CO when the system was off is lack of good CO generation data in fires.

“Preliminary Studies of a Large Fire in Hong Kong.” Chow, W. K. Journal of Applied Fire Science, Vol. 6, No. 3, 243-268, 1996/1997.

Aspects of a recent fire in a high-rise building in Hong Kong are discussed in this article. A general description is given and several points of concern are considered in this article. A point of primary interest is the long duration for which the fire burned. A second point of interest is the fire environment inside the building. CFAST simulations were performed to help understand the probable fire environment under different conditions. Three simulations were performed to study the consequences of a fire starting in the lift shaft. Possibilities for large fires in offices at several floor levels are discussed and further aspects of the investigation are identified.

“Approach for Evaluating Fire Zone Models.” Chow, W. K. Journal of Fire Sciences, Vol. 16, No. 1, 25-31, January/February 1998.

In this article an evaluation of zone models is proposed by checking the relationship between input heat release rate of a steady burning fire and the out flowing rates of smoke through the vertical openings. The zone model, CFAST, was tested by carrying out numerical studies in a small compartment. It was found that for preflashover fires with a heat release rate less than the flashover values, results predicted by the model are reasonable. However, care must be taken in using the models when the heat release rate of the fire exceeds the flashover rate.

“Development of a Method for Representing Complex Geometries in a Fire Model. Interim Report 1998-1999.” Hoover, J. B.; Tatem, P. A. NRL/NR/6180-99-8367; 70 p. April 12, 1999.

This report documents the design and development of a prototype software system capable of representing complex geometries for use in an advanced zone fire model. The authors discuss, what they refer to as, the geometric limitations of CFAST when applied to a real world Navy problem and illustrate those shortcomings using a case study. An alternative approach to representing complex geometries is proposed and a prototype implementation of the concept is presented.

"Atrium Smoke Filling Process in Shopping Malls of Hong Kong." Chow, W. K. Journal of Fire Protection Engineering, Vol. 9, No. 4, 18-30, 1999.

The smoke filling process in the atria of shopping malls in Hong Kong is studied. The atrium is located adjacent to a shop, assumed to have a fire. Atria classified into seven different shapes with volumes varying from 2500 to 3500m^3 were considered. The smoke filing time was simulated using the CFAST zone model. The effects of a ventilation system were also studied using CFAST.

Appendix E General Model Limitations

There are limitations in fire models in general, and zone modeling in particular which users should be aware of in order to make good and useful predictions. The following are issues which need to be kept in mind, though they do not fit neatly into the development of the theory.

E.1 Zone Model Assumption

The basic assumption of all zone fire models is that each compartment can be divided into a small number of control volumes, each of which is internally uniform in temperature and composition. In CFAST all compartments have two zones except for the fire room which has an additional zone for the plume. Since a real upper/lower interface is not as sharp as this, one has a spatial error of about 10% in determining the height of the layer, and consequently when the hot gases interact with occupants and building components.

The zone model concept best applies for an enclosure in which the height, width and length are not too different.

If the horizontal dimensions of the room differ too much (i.e. the room looks like a corridor), the flow pattern in the room may become nonsymmetrical. Therefore, an upper limit may be set on the ratio of the length (L) and width (W).

If the enclosure is too shallow, the temperature may have significant radial differences. Therefore, an upper limit may be set to the ratio of the length (L) and height (H).

The width of the plume may at some height become equal to the width of the room. Therefore, the assumptions fail in a tall and narrow enclosure and, consequently, a lower limit may be set on the ratio of the width (W) and the height of the room.

If the aspect ratio (length/width) is over about10, the corridor flow algorithm should be used. This provides the appropriate filling time. Similarly, for tall shafts (elevators and stairways), a single zone approximation is more appropriate. It was found experimentally (see Plaza reference) that the mixing between a plume and lower layer caused by interaction with the walls of the shaft, caused complete mixing. The is the flip side of the corridor problem and occurs at a ratio of the height to characteristic floor length of about 10.

The following quantitative limits may be recommended:

	Acceptable	Special consideration required	Need specific algorithm
$(L/W)_{max}$	L/W<3	3<L/W<5	L/W>5
$(L/H)_{max}$	L/H<3	3<L/H<6	L/H>6
$(W/H)_{min}$	W/H>0.4	0.2<W/H<0.4	W/H<0.2

E.2 Fires

CFAST depends on pyrolysis data for the source term for a fire. The usual way to obtain this data is a large-scale calorimeter. Generally, a product (e.g., chair, table, bookcase) is placed under a large collection hood and ignited by a burner (~50 kW simulating a wastebasket) placed adjacent to the item. The combustion process then proceeds under assumed "free-burning" conditions, and the release rate data are measured. Potential sources of uncertainty include measurement errors related to the instrumentation and the degree to which "free-burning" conditions are not achieved (e.g., radiation from the gases under the hood or from the hood itself, and restrictions in the air entrained by the object causing locally reduced oxygen concentrations affecting the combustion chemistry). There are limited experimental data for upholstered furniture which suggest that prior to the onset of flashover in a compartment, the influence of the compartment on the burning behavior of the item is small. The differences obtained from the use of different types or locations of ignition sources have not been explored. These factors are discussed in reference [1].

Where small-scale calorimeter data are used, procedures are available to extrapolate to the behavior of a full-size item. These procedures are based on empirical correlations of data which exhibit significant scatter, thus limiting their accuracy. For example, for upholstered furniture, the peak heat release rates estimated by the "triangular approximation" method averaged 91 % (range 46 to 103 %) of values measured for a group of 26 chairs with noncombustible frames, but only 63 per cent (range 46 to 83 %) of values measured for a group of 11 chairs with combustible frames [2]. Also, the triangle neglects the "tails" of the curve; these are the initial time from ignition to significant burning of the item, and the region of burning of the combustible frame, after the fabric and filler are consumed.

The provided data and procedures only relate directly to burning of items initiated by relatively large flaming sources. Little data are currently available for release rates under smoldering combustion, or for the high external flux and low oxygen conditions characteristic of post-flashover burning. While the model allows multiple items burning simultaneously, it does not account for the synergy of such multiple fires. Thus, for other ignition scenarios, multiple items burning simultaneously (which exchange energy by radiation and convection), combustible

interior finish, and post-flashover conditions, the move can give estimates which are often nonconservative (the actual release rates would be *greater* than estimated). At present, the only sure way to account for all of these complex phenomena is to conduct a full-scale compartment burn and use the pyrolysis rates directly.

Burning can be constrained by the available oxygen. However, this "constrained fire" (a "type 2" fire, see page 15) is not subject to the influences of radiation to enhance its burning rate, but is influenced by the oxygen available in the compartment. If a large mass loss rate is entered, the model will follow this input until there is insufficient oxygen available for that quantity of fuel to burn in the compartment. The unburned fuel (sometimes called excess pyrolyzate) is tracked as it flows out in the door jet, where it can entrain more oxygen. If this mixture is within the user-specified flammable range, it burns in the door plume. If not, it will be tracked throughout the building until it eventually collects as unburned fuel or burns in a vent. The enthalpy released in the fire compartment and in each vent, as well as the total enthalpy released, is detailed in the output of the model. Since mass and enthalpy are conserved, the total will be correct. However, since combustion did not take place adjacent to the burning object, the actual mass burned could be lower than that specified by the user. The difference will be the unburned fuel.

An oxygen combustion chemistry scheme is employed only in constrained fires. Here user-specified hydrocarbon ratios and species yields are used by the model to predict concentrations. A balance among hydrogen, carbon, and oxygen molecules is maintained. Under some conditions, low oxygen can change the combustion chemistry, with a resulting increase in the yields of products of incomplete combustion such as CO. Guidance is provided on how to adjust the CO/CO_2 ratio. However, not enough is known about these chemical processes to build this relationship into the model at the present time. Some data exist in reports of full-scale experiments (e.g., reference [3]) which can assist in making such determinations.

E.3 Plumes

The entrainment coefficients are empirically determined values. Small errors in these values will have a small effect on the fire plume or the flow in the plume of gases exiting the door of that compartment. In a multi-compartment model such as CFAST, however, small errors in each door plume are multiplicative as the flow proceeds through many compartments, possibly resulting in a significant error in the furthest compartments. The data available from validation experiments [4] indicate that the values for entrainment coefficients currently used in most zone models produce good agreement for a three-compartment configuration. More data are needed for larger numbers of compartments to study this further.

In real fires, smoke and gases are introduced into the lower layer of each compartment primarily due to mixing at connections between compartments and from the downward flows along walls (where contact with the wall cools the gas and reduces its buoyancy). Doorway mixing has been included in CFAST, using the same empirically derived mixing coefficients as used for calculating fire plume entrainment. Downward wall flow has not been included. This could result in underestimates of lower layer temperatures and species concentration.

Entrainment at a vent (doors, windows, ...) yields mixing into the lower and upper layers. The latter has been studied more extensively than the former. The door jets are not symmetric for these mixing phenomena, however. We have constrained the phenomenon for CFAST to be in the range as predicted by Zukoski et al. in the thesis of Lim at Cal. Tech.

[1] Babrauskas, V., Lawson, J. R., Walton, W. D., Twilley, W. H., "Upholstered Furniture Heat Release Rates Measured with a Furniture Calorimeter," Natl. Bur. Stand. (U.S.), NBSIR 82-2604, 1982.

[2] Babrauskas, V. and Krasny, J. F., "Fire Behavior of Upholstered Furniture," Natl. Bur. Stand. (U.S.), Monogr. 173, 1985.

[3] Lee, B.T., "Effect of Ventilation on the Rates of Heat, Smoke, and Carbon Monoxide Production in a Typical Jail Cell Fire," Natl. Bur. Stand. (U.S.), NBSIR 82-2469, 1982.

[4] Peacock, R. D., Davis, S., Lee, B. T., "An Experimental Data Set for the Accuracy Assessment of Room Fire Models," Natl. Bur. Stand. (U.S.), NBSIR 88-3752, April 1988, p. 120.